AD A138575

ALTERNATE FUELS COMBUSTION RESEARCH
PHASE II

PRATT & WHITNEY CANADA
MISSISSAUGA, ONTARIO

October 1983

Interim Report for Period May 1980 - February 1983

DTIC
ELECTE
MAR 5 1984

B

AERO PROPULSION LABORATORY
AIR FORCE WRIGHT AERONAUTICAL LABORATORIES
AIR FORCE SYSTEMS COMMAND
WRIGHT-PATTERSON AIR FORCE BASE, OHIO 45433

DTIC FILE COPY

84 04 05

NOTICE

When Government drawings, specifications or other data are used for any purpose other than in connection with a definitely related Government procurement operation, the United States Government thereby incurs no responsibility nor any obligation whatsoever; and the fact that the government may have formulated, furnished, or in any way supplied the said drawings, specifications, or other data, is not to be regarded by implication or otherwise as in any manner licensing the holder or any other person or corporation, or conveying any rights or permission to manufacture use, or sell any patented invention that may in any way be related thereto.

This report has been reviewed by the Office of Public Affairs (ASD/PA) and is releasable to the National Technical Information Service (NTIS). At NTIS, it will be available to the general public, including foreign nations.

This technical report has been reviewed and is approved for publication.
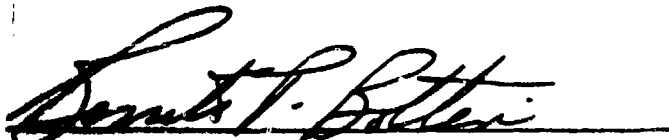
ROYCE P. BRADLEY, Prog Mgr
Fuels Branch
Fuels and Lubrication Division

ARTHUR V. CHURCHILL, Chief
Fuels Branch
Fuels and Lubrication Division

FOR THE COMMANDER

BENITO P. BOTTERI, Assistant Chief
Fuels and Lubrication Division
Aero Propulsion Laboratory

REPORT DOCUMENTATION PAGE

	READ INSTRUCTIONS BEFORE COMPLETING FORM

1. REPORT NUMBER	2. GOVT ACCESSION NO.	3. RECIPIENT'S CATALOG NUMBER
AFWAL-TR-83-2057	AD-A138 575	

4. TITLE (and Subtitle)	5. TYPE OF REPORT & PERIOD COVERED
Alternate Fuels Combustion Research Phase II	Interim Report for Period May 80 - Feb 83
	6. PERFORMING ORG. REPORT NUMBER

7. AUTHOR(s)	8. CONTRACT OR GRANT NUMBER(s)
M. GRATTON, P. SAMPATH	F33615-80-C-2002

9. PERFORMING ORGANIZATION NAME AND ADDRESS	10. PROGRAM ELEMENT, PROJECT, TASK AREA & WORK UNIT NUMBERS
PRATT & WHITNEY CANADA Mississauga, Ontario	P.E. 62203F 3048-05-06

11. CONTROLLING OFFICE NAME AND ADDRESS	12. REPORT DATE
Aero Propulsion Laboratory (AFWAL/POSF) Air Force Wright Aeronautical Laboratories (AFSC)	October 1983
	13. NUMBER OF PAGES
Wright Patterson Air Force Base, Ohio 45433	196

14. MONITORING AGENCY NAME & ADDRESS(if different from Controlling Office)	15. SECURITY CLASS. (of this report)
	UNCLASSIFIED
	15a. DECLASSIFICATION/DOWNGRADING SCHEDULE

16. DISTRIBUTION STATEMENT (of this Report)

Approved for Public Release; Distribution Unlimited.

17. DISTRIBUTION STATEMENT (of the abstract entered in Block 20, if different from Report)

18. SUPPLEMENTARY NOTES

19. KEY WORDS (Continue on reverse side if necessary and identify by block number)

FUELS
ALTERNATE FUELS
GAS TURBINE COMBUSTION
EXHAUST EMISSIONS

20. ABSTRACT (Continue on reverse side if necessary and identify by block number)

This report presents the results of the Can Combustor Test Phase (Phase II) of the Alternate Fuels Combustion Research Program. The effects of variations in fuel properties on the performance characteristics of a small can combustion system were determined. Fifteen different fuels were used, encompassing a wide range of chemical and physical properties. The tests covered current specification, broadened specification and alternate source (shale and tar sands derived) fuels.

DD FORM 1473 EDITION OF 1 NOV 65 IS OBSOLETE   UNCLASSIFIED
1 JAN 73

Combustor rig tests were performed to determine the effects of fuel properties on stability, low temperature light-offs, gaseous emissions, smoke emissions, metal temperatures and radiation heat loads. Attempts were also made to characterize fuel nozzle contamination and carbon formation, but these tests were somewhat inconclusive.

Lean blow-out stability limits were strongly influenced by fuel hydrogen content and spray quality, and to a lesser extent by fuel volatility; cold start tests showed good correlation with properties affecting fuel atomization. Steady state tests indicated CO, THC and smoke emissions were strongly influenced by fuel hydrogen content; fuel effects on take-off NO_x emissions were small, but significant at idle due to changes in combustion efficiency. Radiation heat loads and liner temperatures were strongly influenced by hydrogen content and by properties affecting fuel atomization characteristics.

Based on test results from can combustor tests, a test plan was formulated for testing PT6 and JT15D reverse-flow annular combustors.

FOREWORD

This report presents the results of the Can Combustor Test Phase (Phase II) of the Alternate Fuels Combustion Research Program. The test program was comprised of over a thousand tests with fifteen different test fuels. The work was conducted under contract No. F33615-80-C-2002. Program sponsorship was provided by the United States Air Force Wright Aeronautical Laboratories (AFWAL), the Canadian Departments of National Defence (CDND) and Regional Industrial Expansion (DRIE). Messrs. R. Bradley, AFWAL, and J. Coleman, CDND, were the project administrators.

Test fuel analysis was sponsored by CDND; results presented in Section III are based largely on inputs from Mr. J. Coleman and Mr. L.D. Gallop of CDND. Fuel nozzle hardware for the program was supplied by Delavan Manufacturing Co. (Duplex) and Ex-Cell-O Corporation (Airblast). The cooperation of these organizations is appreciated. Test fuels were supplied by AFWAL, CDND and P&WC. Blending material for Jet A-1 and JP4 were supplied by AFWAL.

Authors of this report wish to thank the following P&WC personnel for their contributions to this program: Messrs. J.A. Saintsbury, J. Allan, and M. Somji of Aerodynamics Engineering, Messrs. Y. Bergeron, R. Cyr and R. Ouelette of Experimental Engineering, Mr. S. Monaghan, R & D Support, and Mr. W. Sidorenko of Contracts Administration.

This report covers work conducted from 19 May 1980 through 20 February 1983.

Accession For

NTIS GRA&I	✓
DTIC TAB	☐
Unannounced	☐
Justification	

By
Distribution/
Availability Codes

| Dist | Avail and/or Special |

A-1

TABLE OF CONTENTS

TABLE OF CONTENTS CONT'D

LIST OF ILLUSTRATIONS

LIST OF TABLES

LIST OF SYMBOLS AND SUBSCRIPTS

SYMBOL	DESCRIPTION	UNITS
A	Area	cm^2, m^2
CO	Carbon Monoxide	—
CO_2	Carbon Dioxide	—
EI	Pollutant Emission Index	g pollutant/kg f
FN	Flow Number	PPH/$\sqrt{PSI}$
H	Fuel Hydrogen Content (mass fraction)	%
HC	Hydrocarbon (calculated as CH_4)	—
M	Mach Number	—
$\bar{M}$	Air Velocity Parameter	—
JFTOT	Jet Fuel Thermal Oxidation Tester	—
NO_x	Total Oxides of Nitrogen (=NO+NO_2) Calculated as NO_2	—
P	Pressure	Pa
Q	Heat of Combustion (net)	MJ/kg
SMD	Sauter Mean Diameter	micron
SN	Smoke Number	—
T	Temperature	K
V	Volume	m^3
W	Mass Flow Rate	kg/s
far	Fuel-Air Ratio	g fuel/g air
h	Absolute Humidity	g H_2O/kg air
k	Constant	—
Q	Heat Flux	W/m^2
x	Independent Variable	—
y	Dependent Variable	—
α	Carbon-to-Hydrogen Atoms Ratio	—
ΔP	Pressure Drop	Pa
ΔT	Temperature Rise	K
η	Combustion Efficiency	%
ν	Kinematic Viscosity	centistokes
Ω	Air Loading Parameter	—
ρ	Density	kg/m^3
σ	Surface Tension	dynes/cm

SUBSCRIPT	DESCRIPTION
3	Compressor Exit Station
4	Combustor Exit Station
c	Combustor
f	Fuel
r	Reference
st	Stoichiometric
L	Liner (skin)
TC	Thermocouple
aver	Average
max	Maximum

SECTION I

INTRODUCTION

Almost all projections during the past decade forecasted reduced avail-
ability and increased cost of petroleum crudes. There have recently
been some surpluses in oil supply and reductions in oil prices, but the
long term scenarios still appear valid. Only a limited amount of crude
oil can be converted into aviation kerosine according to present speci-
fications and there is also competition for middle distillate fuels from
other product requirements. To insure continued availability of jet
fuels, there is a need to consider broadened specification fuels and
fuels derived from new sources such as oil shales and tar sands.
Several investigations have already been carried out, or are under way,
to establish effects of fuel property changes on performance of gas tur-
bine systems. Many of the studies have involved commercial and military
aviation power plants, which generally use straight through highly
loaded annular combustion systems. However, most small aviation turbine
engines used for helicopters, business jets, general aviation and auxil-
iary power units (APU), use reverse-flow annular combustion systems of
moderate loadings and relatively high surface to volume ratios. The aim
of the present program is to evaluate and identify potential problems
resulting from the use of relaxed specification fuels and fuels derived
from unconventional sources in small engines with reverse-flow annular
combustion systems. Specifically, the objectives of the program are the
following:

- Determine relationships between specific fuel properties and com-
  bustor performance, combustor durability, emissions, fuel system
  performance and durability, and fuel pumpability. The combustor
  and fuel systems shall correspond to requirements of small gas tur-
  bine engines of the type used in small utility and training air-
  craft, business jets, general aviation, and APU's.

- Determine the effects of fuel properties on the performance of
  single and dual-orifice pressure atomizing nozzles, air-blast
  nozzles, and vaporizing nozzles. Examine the interrelationships
  among fuel properties, fuel nozzle types, engine combustor types
  and performance.

- Provide conclusions and recommendations concerning fuel specifica-
  tion limits for existing, conventional combustor and fuel nozzle
  designs, and for more advanced combustor and fuel nozzle designs
  which employ state-of-the-art concepts.

The program consists of combustor rig and gas generator testing to
evaluate effects of fuel property variations on performance of three
small gas turbine combustion systems. These are:

i)   Can combustion system - Phase II.

ii) Turboprop reverse-flow annular combustion system - Phase III.

iii) Turbofan reverse-flow annular combustion system - Phase III.

This report describes the results of investigations with the can combustion system. The experimental program was comprised of tests with 15 different fuels covering a range of fuel property variations, as well as shale and tar sand sources. Four different fuel spray/atomizing nozzle types were considered - single orifice pressure, dual orifice pressure, airblast and vaporizing nozzles. Combustor performance, exhaust emissions, flame radiation, combustor wall temperatures, ignition characteristics and similar data were obtained and analyzed. Detailed correlations were made relating selected fuel properties to the performance and durability parameters of the combustion system.

TEST PLAN

Phase I of the program formulated a detailed test plan[1] for the can combustor tests (Phase II), and a preliminary test plan for reverse-flow-annular combustor tests (Phase III). A 850 point test matrix was proposed for the can combustor tests, which was approved by AFWAL and CDND. The rationale for the can combustor test program and the description of the test matrix are given below.

2.1 RELATED STUDIES

Several investigations have been undertaken to evaluate fuel property effects on performance and durability of both military and commercial gas turbine engines, and others are still under way. Jackson[2] has summarized the investigations sponsored by AFWAL for the J-79, F-100, F-101, TF-41, J-57, J-85 and TF-39 combustion systems. In these programs the primary fuel properties varied were aromatics (single ring and multi ring), hydrogen content (12% to 14.5% by weight), distillation range (JP-4, JP-8 and diesel fuel), and distillation end point (535-616K). Experimental shale oil derived fuels were also included in some of the more recent programs.

Tables 2.1 and 2.2 summarize the parameters studied in the different programs sponsored by AFWAL. The J-79 program[3] showed a strong effect of hydrogen content on smoke, carbon deposition, liner temperature, flame temperature and a moderate effect on NOx emissions; fuel volatility and viscosity effects were evident only in the low power operating range, while aromatic type and final boiling range produced no direct effect on emissions or combustor performance. The F-101[4] program found similar trends, although the effect of hydrogen content on smoke was somewhat less severe, see Figure 2.1, which is thought to be due to the more advanced form of fuel preparation (airblast) in the F-101 combustor.

An in-house program by AFWAL[5] tested a T-56 single can combustor with a broad range of fuels, and these verified the strong effect of hydrogen content on combustor liner wall temperature. On the basis of extensive tests, a second order correlation was proposed between the fuel hydrogen content and combustor wall temperature:

$$T.P. = \frac{T_L - T_{LO}}{T_{LO} - T_3} = C_o + C_1(H) + C_2(H)^2$$

Where T.P. = temperature parameter
T_L = liner temperature
T_{LO} = liner temperature with baseline fuel
T_3 = combustor inlet temperature
H = hydrogen content %

The coefficients derived for JP4 fuels, with 14.5% hydrogen as the baseline, were: $T.P. = -.098 + .138H - .009H^2$

The tests also showed that irrespective of the hydrocarbon structure of the fuel blending component, combustor liner temperature varied primarily with fuel hydrogen content.

NASA Lewis Research center has sponsored a number of studies evaluating the impact of broadened specification fuels on commercial aircraft engine combustors. These have examined the Experimental Referee Broadened Specification (ERBS) fuel. Table 2.3 shows a comparison of specifications of Jet A and ERBS fuels. Significant property differences are the allowable aromatic/hydrogen content and the increase in allowable distillation temperatures. The increase in distillation temperature also necessitates a higher freeze point and increased viscosity, thus impacting atomization in the starting regime. The decrease in the minimum allowable breakpoint temperature implies that the thermal stability of ERBS fuel will be poorer than that of Jet A.

An analytical study of the impact of ERBS fuel on high bypass ratio commercial turbofan engines[6] concluded that the use of ERBS fuel will have the following major consequences:

- Increased radiant heat load produced by ERBS will cause substantial deterioration in the life of the combustion liner and adverse effects on the durability of turbine aerofoils.

- Increased CO and THC emissions at low power, although use of improved fuel injector concepts may reduce the sensitivity of low power emissions to higher fuel viscosity.

- Increased smoke emissions. Since smoke formation is strongly dependent on detailed composition of fuel including cyclic and non-cyclic compounds, use of hydrogen content may not be an adequate parameter for characterizing fuel composition in this regard. This conclusion is at some variance with results of other studies[5].

- Increased NO_x emissions due to higher adiabatic flame temperatures.

- No alteration will be required to the basic aerothermal definition of the combustors studied, although changes to better optimize the overall performance may be necessary.

2.2 SMALL ENGINE REQUIREMENTS

Small aviation turbine engines are largely used in small utility and training aircraft, auxiliary power units, cruise missiles and helicopters. Some of these typically have configurations as shown in Figure 2.2. The low pressure axial compressor stages and the high pressure centrifugal compressor stages are driven by an axial turbine. A separate power turbine provides output for turboprop or turboshaft applications. The combustor geometry most compatible with the geometric constraints of small engine flow path is the reverse-flow annular configuration, although straight-flow annular and can combustors are found in some models. Advantages of the reverse-flow configuration are the

ability to make use of the available combustion volume, relatively low combustor loading and simpler maintenance due to accessibility of fuel injectors. The principal disadvantage, however, is its comparatively high surface-to-volume ratio inherent in the reverse-flow shape which makes liner cooling a difficult problem. The other difference is the relatively larger pitching of fuel injectors which may affect exit temperature distribution. The relatively low fuel flow per injector results in small orifice sizes of pressure atomizers which may be prone to blockage and malfunction with usage of inferior fuels.

The overall aim of the test program is to examine effects of fuel properties on the performance of reverse-flow annular combustors used in the PWC family of turboprop and turbofan (PT6 and JT15D) engines. The advantage of can combustor testing was that it permitted quick and cost effective parametric investigations over a broad range of parameters from which a final test plan could be developed for investigation of reverse-flow annular combustion systems.

The JT15D family of turbofan engines has take-off ratings in the range of 2200-2500 lb thrust. The JT15D-1 engine with a take-off rating of 2200 lb thrust, has a bypass ratio of 3.3:1, pressure ratio of 9.7:1, and a total mass flow of 34 kg/sec (75 lb/sec). With the JT15D-4 engine, the thrust increase to 2500 lb has been achieved by the addition of an axial boost stage compressor. While the total airflow remains at 34 kg/sec (75 lb/sec), the overall pressure ratio is raised to 10.2:1, and the bypass ratio lowered to 2.68:1. Cross-sections of the JT15D-1 and the D-4 are shown in Figure 2.3.

The PT6 family of gas turbine engines, with applications on both fixed wing aircraft and helicopters, has rated SHP in the range of 550 to 1375. Table 2.4 shows performance ratings of PT6 turboprop engines. While the basic engine envelope has remained largely the same, the increase in power has been achieved by successive increases in air mass flow, incorporation of cooled turbine vanes, and the addition of a second power turbine stage. Figure 2.4 shows a cross-section of the PT6 engine, the operation of which will be simulated during combustion testing, along with that of the JT15D combustion system.

Figures 2.5 and 2.6 show the range of engine pressure ratio and turbine inlet temperature vs engine power level[8] for small gas turbine engines currently in use. For small aircraft propulsion engines, pressure ratios range from 6:1 to 17:1 and turbine inlet temperatures range from 1200K to 1530K (2160R to 2760R). The engines chosen for the study are PT6A and JT15D with the following sea level take-off parameters:

PT6A-41 (850 SHP) : Pressure ratio 8.2:1, TIT 1212K (2182R)
PT6A-65 (1300 SHP) : Pressure ratio 10:1, TIT 1309K (2357R)
JT15D-4 (2500 lb) : Pressure ratio 10.2:1, TIT 1280K (2304R)
JT15D-5 (2900 lb) : Pressure ratio 12.1:1, TIT 1254 (2257R)

Thus the combustion system/engines chosen for the program are representative of small gas turbine power plants.

- 5 -

Both PT6 and JT15D engines use reverse-flow annular combustors. The JT15D series of engines have axial fuel injection - 12 dual orifice pressure jets of Flow Number 4.65 $PPH/\sqrt{PSI}$. (Flow Number $= W_f/\sqrt{\Delta P}$). The PT6 series of engines utilize 14 single orifice pressure jets spraying tangentially. The Flow Number of the PT6A-41 fuel nozzle is 1.55 $PPH/\sqrt{PSI}$.

2.3 COMBUSTOR PERFORMANCE CRITERIA

Based on the anticipated effects of fuel properties, the following combustor parameters were chosen for investigation with the can combustor system during Phase II.

• Emissions - CO, THC, NO_x, smoke

• Combustion efficiency

• Flame luminosity and wall temperatures

• Carbon formation

• Ignition characteristics / cold starts

• Stability / lean limit performance

• Atomization - Pressure, airblast & vaporizing nozzles

Tests were categorized under the following headings:

i) Thermal paint tests

ii) Thrust level tests (JT15D-4 simulation)

iii) Power level tests (PT6A-41 simulation)

iv) Parametric tests

v) Lean limit tests

vi) Cold start tests

2.4 BASIS OF AIR FLOW DEFINITION

In the thermal paint, thrust and power level tests, all conditions are related directly to engine operating performance data. In the parametric, cold start and lean limit tests, all conditions are bracketed around a point that is directly related to engine operating performance data.

Since performance data are available only at certain measurement stations in the engine, whereas the can combustor rig simulated only the combustor liner, some processing of these data is required to yield the air mass flow through the engine combustor liner.

- 6 -

Figure 2.7 illustrates schematically the combustor assembly in the JT15D-4 engine and Figure 2.8 the combustor rig. Station 3 is the measurement station at the engine compressor diffuser exit or the rig air supply pipe, in both Figures 2.7 and 2.8 represented as the entrance to the combustor casing. Performance data give the air mass flow (W_3) at this station in the engine. For the JT15D-4 W_3 is the total compressor flow less some small bleeds to the bearings; for the PT6A-41 an interstage bleed is also subtracted that is quite large at low power levels.

In both engines, a significant part of W_3 goes into the combustor exit duct (turbine entrance duct) and a smaller fraction is bled off for turbine cooling and other miscellaneous uses. The percentage going into the combustor liner is not measured but calculations based on flow resistance of all possible flow paths give this percentage as 88% for the JT15D-4 and 80% for the PT6A-41. Therefore we have a combustor liner air flow $W_c = .88W_3$ in the JT15D-4 and $W_c = .80W_3$ in the PT6A-41. In Figures 2.7 and 2.8 the location where W_c would occur is shown as station 4c.

To convert W_c in the engine to W_c in the can combustor rig, a method is used that emphasizes simulation of emissions at low power (thrust) and simulation of performance at high power (thrust). The emissions are correlated by the loading parameter while the general performance is correlated by the velocity parameter. These two modelling parameters are, respectively:

$$\text{"Air Loading Parameter" } \Omega_c = \frac{K_1 W_c}{P_3^{1.8} e^{T_3/K_2 V_c}}$$

$$\text{"Air Velocity Parameter" } \overline{M}_c = K_3 \frac{W_c \sqrt{T_3}}{P_3 A_c}$$

where:

	Units	
	FPS	SI
W_c = combustor liner air flow	lb/s	kg/s
P_3 = combustor inlet pressure	atm	MPa
T_3 = combustor inlet temperature	R	K
V_c = volume of combustor liner	ft^3	m^3
A_c = combustor liner flow area	ft^2	m^2
K_1 = units conversion constant	1	1.035×10^{-3}
K_2 = empirical constant	540	300
K_3 = units conversion constant	5.143×10^{-4}	1.433×10^{-5}

P_3 and T_3 are the same in the can combustor rig as in the engine. Therefore, the modelling method is as follows. At low power (thrust), W_c is set to render the same Ω_c in the rig as in the engine. This is just the engine W_c times the ratio of combustor liner volumes. At high power (thrust), W_c in the rig is set to yield the same $\bar{H}_c$ in the rig as in the engine. This is just the engine W_c times the ratio of combustor liner flow cross-section areas.

These two extremes are defined at the ground idle and take-off conditions. At power (thrust) levels between these points, the value of W_c in the rig is taken between the values that would be correct according to Ω_c and $\bar{H}_c$. The position of W_c between the values indicated by Ω_c and $\bar{H}_c$ is in proportion to the position of the power (thrust) level between ground idle and take-off. Figures 2.9 and 2.10 illustrate this graphically for the JT15D-4 and the PT6A-41 respectively.

2.5 BASIS OF FUEL FLOW DEFINITION

For all conditions directly related to engine operating performance data, the overall fuel-air ratio in the combustor liner should be the same in the rig as in the engine. Having obtained the combustion liner air flow W_c in the manner described above, the fuel-air ratio is then obtained as W_f/W_c (dimensionless) where W_f is the total fuel flow. W_f in the engine is determined for fuels other than Jet A1 as the fuel flow that would give the same ideal heat release rate H as Jet A1. Therefore, when referring to several fuels at one condition H/W_c is a convenient expression of the fuel-air ratio.

The numerical values for H, G and T_4 in the following sections are based on 43.04 MJ/kg (18520 BTU/lb), the average heating value of Jet A1.

2.6 FUEL NOZZLE-TEST FUEL COMBINATIONS

A simplex fuel nozzle was chosen as the primary type of atomizer for Phase II testing. This type is standard on PT6 turboprop engines and is the most common type of atomizer in small engines. All 15 fuels were evaluated with this nozzle, tests consisting of lean limit, thrust level, power level, and parametric variations. Furthermore, six of the fifteen fuels were chosen for tests with dual-orifice, airblast and vaporizing nozzles. These were Jet A1, Jet A1/B2, JP4, JP4/B2, ERBS-3 and Tar Sands L-H. Lean limit, thrust level and parametric tests were undertaken with these nozzles.

Thermal paint tests were undertaken on all nozzle types, since the objective was to observe the wall temperature patterns prior to choosing locations for thermocouples on the liner wall.

Cold start tests were undertaken for seven fuels with simplex and duplex fuel nozzles. The duplex tests were comprised of operation with the primary jet only, as is the normal practice in engines.

Table 2.5 summarizes the combinations of fuel nozzles, fuels and test types for a total of 866 test points.

Table 2.1: Fuel Mainburner/Turbine Effects Test Scope (GE) [2]

TEST VEHICLE	Combustor Dome and Liner Temperature	Smoke and Gaseous Emissions	Combustor Exit Temp. Distribution	Combustor Stability at Idle	Cold Day Ground Start	Altitude Relight and Stability	Fuel Nozzle Plugging	Carbon Deposition	Transient Response	Turbine Material Erosion	Turbine Stator Heat Load	Fuels Tested
J79 Single Combustor High Pressure Rig	X	X					X					3
J85 Full Annular Combustor High/low Pressure Rig	X	X	X	X	X		X					6
TF39 Full Annular Combustor Atmospheric-Pressure Rig	X	X	X									3
TF39 36° Sector Combustor High Pressure Rig							X					6
TF39 36° Sector Combustor Low Pressure Rig				X	X							6
J79/J85/TF39 Fuel Nozzle Fouling Rig						X						2
J79/J85/TF39 Turbine Material Erosion Rig									X			1
J79 Engine	X	X						X		X		2
J85 Engine	X	X					X	X		X		6
TF39 Engine	X	X						X		X		2

- 10 -

Table 2.2: Fuel Mainburner/Turbine Effects Tests Scope (PWA) (2)

TEST VEHICLE	Combustor Dome and Liner Temperature	Smoke and Gaseous Emissions	Combustor Exit Temp. Distribution	Combustor Stability and Altitude Relight	Standard and Cold Day Ground Start	Carbon Deposition	Transient Response	Turbine Material Erosion
J57 (TF33) Single Can High Pressure Rig	6*	6			3	6		
J57 (TF33) Multiple Can Full Ann/Low Press Rig			6	6				
F100 90° Sector Rig	6	6	6	6	3	6	2	
Low Press Turbine Rig							2	

* Number of Test Fuels per Test

- 11 -

Table 2.3: Comparison of Specifications for Jet-A and ERBS Fuels[5]

	JET A	ERBS
Aromatic Content (% volume)	20 max.	-
Hydrogen Content (% weight)	*	12.8 ± .2
Sulphur Mercaptan (% weight) max.	0.003 max.	0.003
Sulphur Total (% weight)	0.3 max.	0.3 max.
Naphthalene Content (% volume)	3.0 max.	-
Distillation Temperature (K)		
10 Percent	500 max.	
90 Percent	-	
Final Boiling Point	561 max.	
Residue (% volume)	1.5 max.	
Loss (% volume)	1.5 max.	
Flashpoint (K)	311 min.	
Freezing Point (K)	233 max.	
Maximum Viscosity (cs)	8 @ 253 K	
Heat of Combustion (J/kg)	42.8×10^6 min.	
Thermal Stability:		
JFTOT Breakpoint Temperature (K)	533 min.	
Method	Visual	

* For comparison to ERBS, the smoke point and luminor
result in a minimum hydrogen content of approximatf

Table 2.4: Performance Ratings of PT6 Turboprops

Sea Level Static	Take-off/Max. Continuous			Max. Cruise			Weight lb.	Propeller RPM
	Thermodynamic Performance		Max SHP Performance	Thermodynamic Performance		Max SHP Performance		
	ESHP	SPC(1)	SHP	ESHP	SPC(1)	SHP		
PT6A-20 PT6A-20A	610	0.640	550 to 70°F	522	0.670	495 to 59°F	289	2200
PT6A-27	751	0.595	680 to 71°F	683	0.607	620 to 69°F	300	2200
PT6A-28	751	0.595	680 to 71°F	751	0.595	620 to 91°F	300	2200
PT6A-34	886	0.582	750 to 67°F	763	0.598	700 to 67°F	311	2200
PT6A-41	1089	0.558	850 to 106°F	1013	0.565	850 to 84°F	370	2000
PT6A-45	1179	0.557	1120 to 59°F	1004	0.578	956 to 59°F	423	1620 to 1700
PT6A-50	1174	0.560	1120 to 59°F	1017	0.578	900 to 74°F	545	1100 to 1210
PT6A-65	1375	0.517	1294 to 89°F	1022	0.522	956 to 80°F	464	1700

(1) lb/ESHP/hr

Table 2.5:   Nozzle/Fuel Combinations, Test Matrix

NUMBER OF TEST POINTS

NOZZLE TYPE:	SIMPLEX						DUPLEX						AIR-BLAST						VAPORIZER						TOTAL
*TEST TYPE:	L	C	T	P	K	S	L	C	T	P	K	S	L	C	T	P	K	S	L	C	T	P	K	S	
FUEL																									
Jet A-1	4	1	10	6	6	8	4	1	10		6	8	4	1	10		6		4	1	10		6	0	106
Jet A-1 mix (13% H)	4		10	6	6																				26
Jet A-1 mix (12% H)	4		10	6	6	8	4		10		6	8	4		10		6		4		10		6		102
Shale JP8	4		10	6	6																				26
JP-4	4		10	6	6	8	4		10		6	8	4		10		6		4		10		6		102
JP-4 mix (13% H)	4		10	6	6																				26
JP-4 mix (12% H)	4		10	6	6	8	4		10		6	8	4		10		6		4		10		6		102
JP-4/2040/DF	4		10	6	6																				26
ERBS 3	4		10	6	6	8	4		10		6	8	4		10		6		4		10		6		102
Diesel	4		10	6	6																				26
JP-10	4		10	6	6	8						8													42
Tar Sand (low B.P., high % H)	4		10	6	6	8	4		10		6	8	4		10		6		4		10		6		102
Tar Sand (low B.P., low % H)	4		10	6	6																				26
Tar Sand (high B.P., high % H)	4		10	6	6																				26
Tar Sand (high B.P., low % H)	4		10	6	6																				26
SUBTOTAL:	60	1	150	90	90	56	24	1	60	0	36	56	24	1	60	0	36	0	24	1	60	0	36	0	
			447						177						121						121				
TOTAL:																									866

* L = Lean-Limit Tests
C = Thermal Paint Tests
T = Thrust Level Tests
P = Power Level Tests
K = Parametric Tests
S = Cold Start Tests
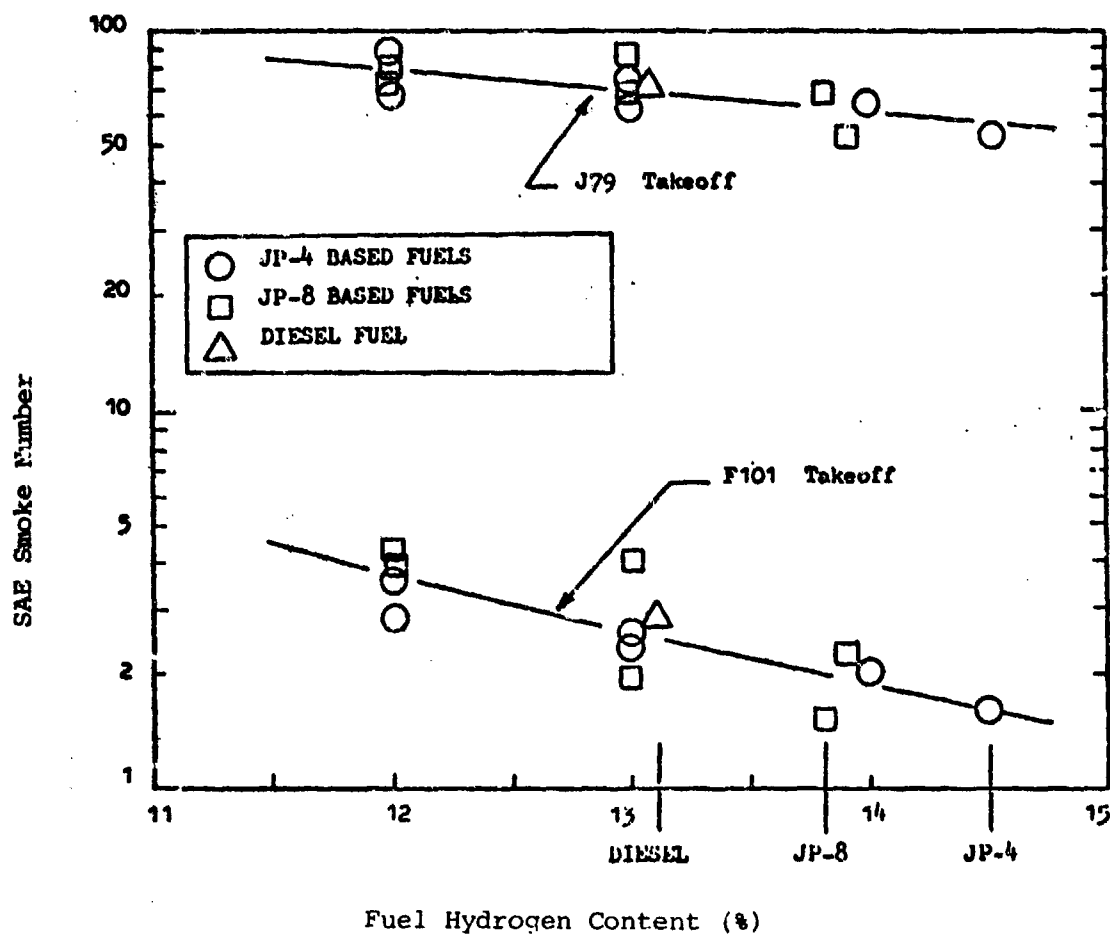
Figure 2.1: Effect of Fuel Type on Smoke Levels[2]
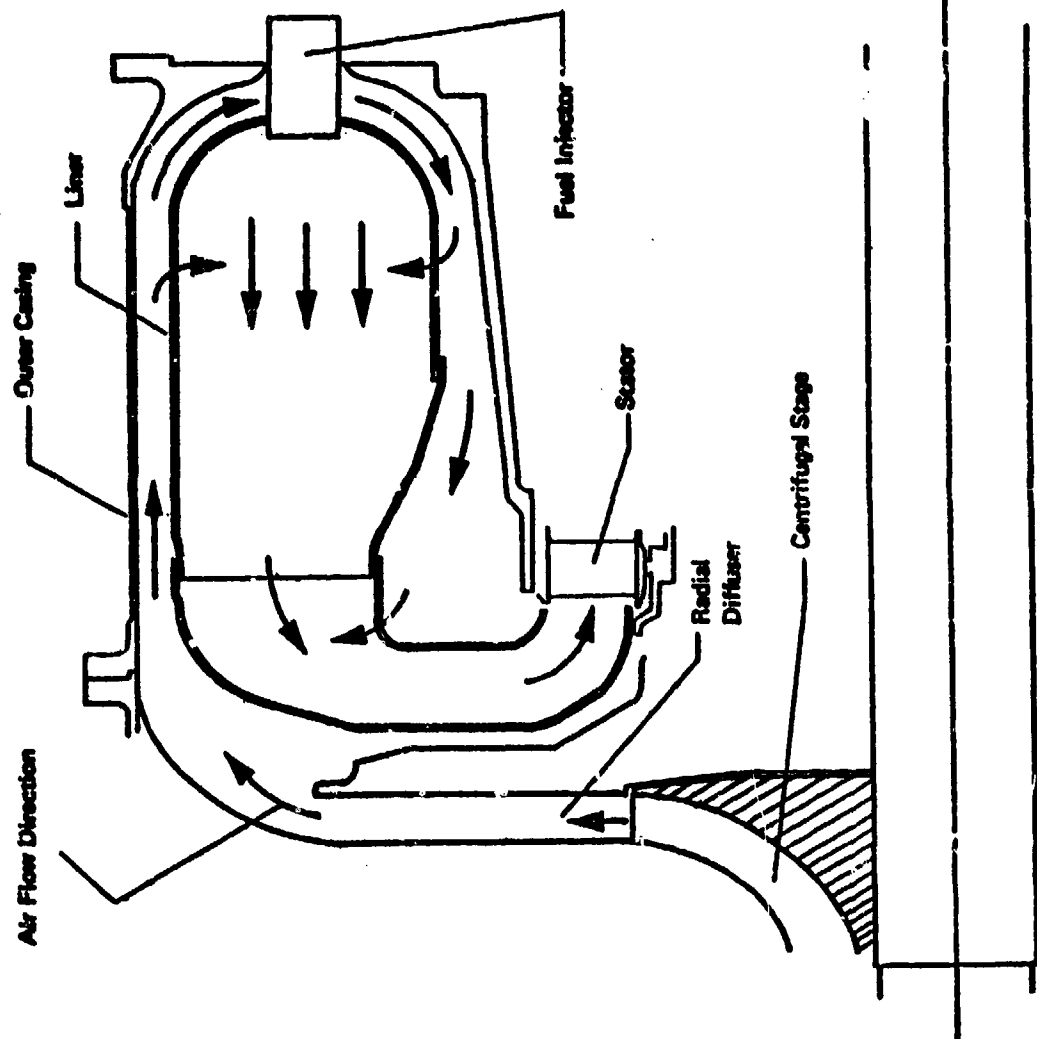
Figure 2.2: Illustration of a Reverse-Flow Annular Combustor

D—1

D—4
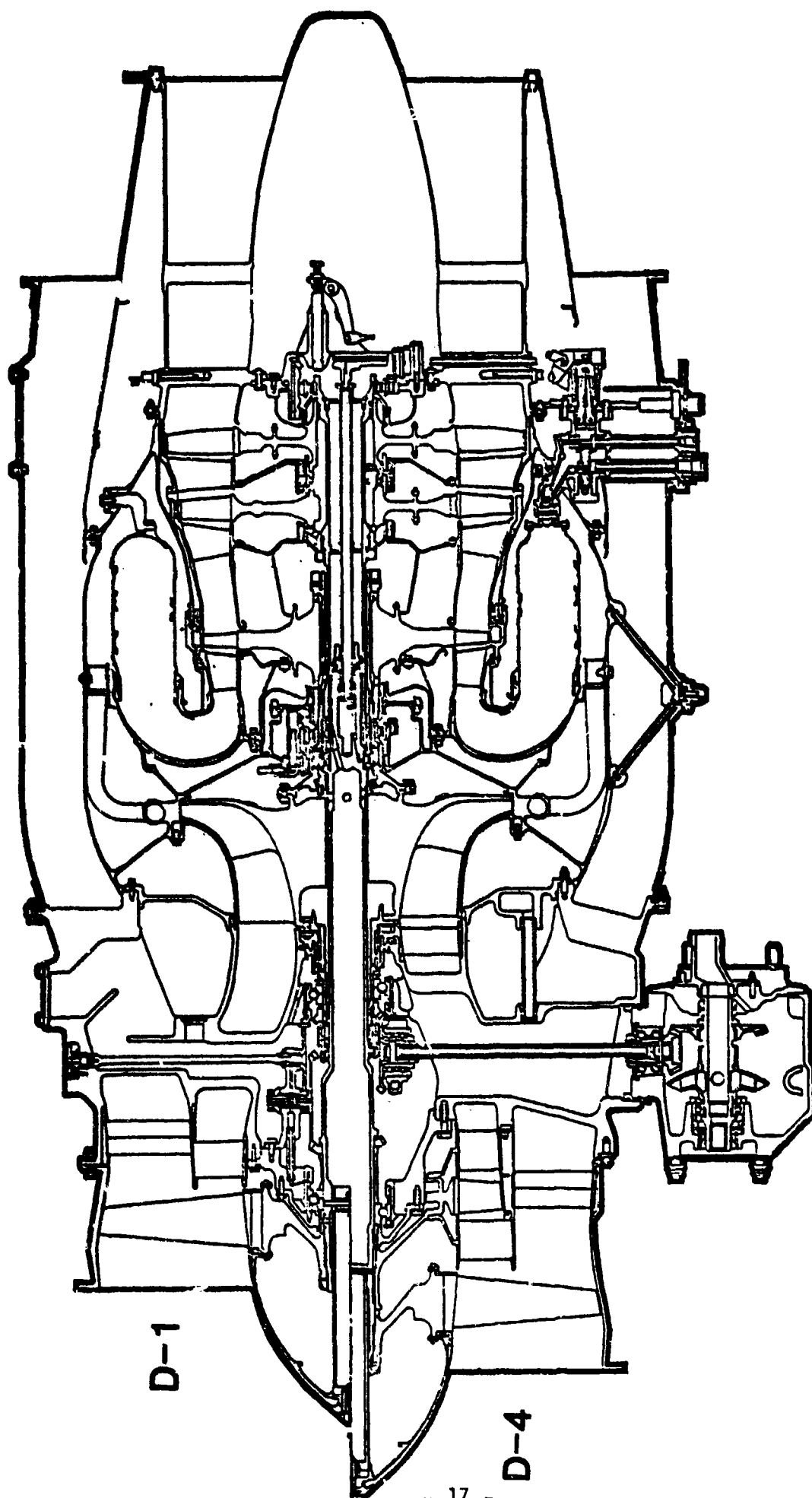
Figure 2.3:   JT15D Cross-Section
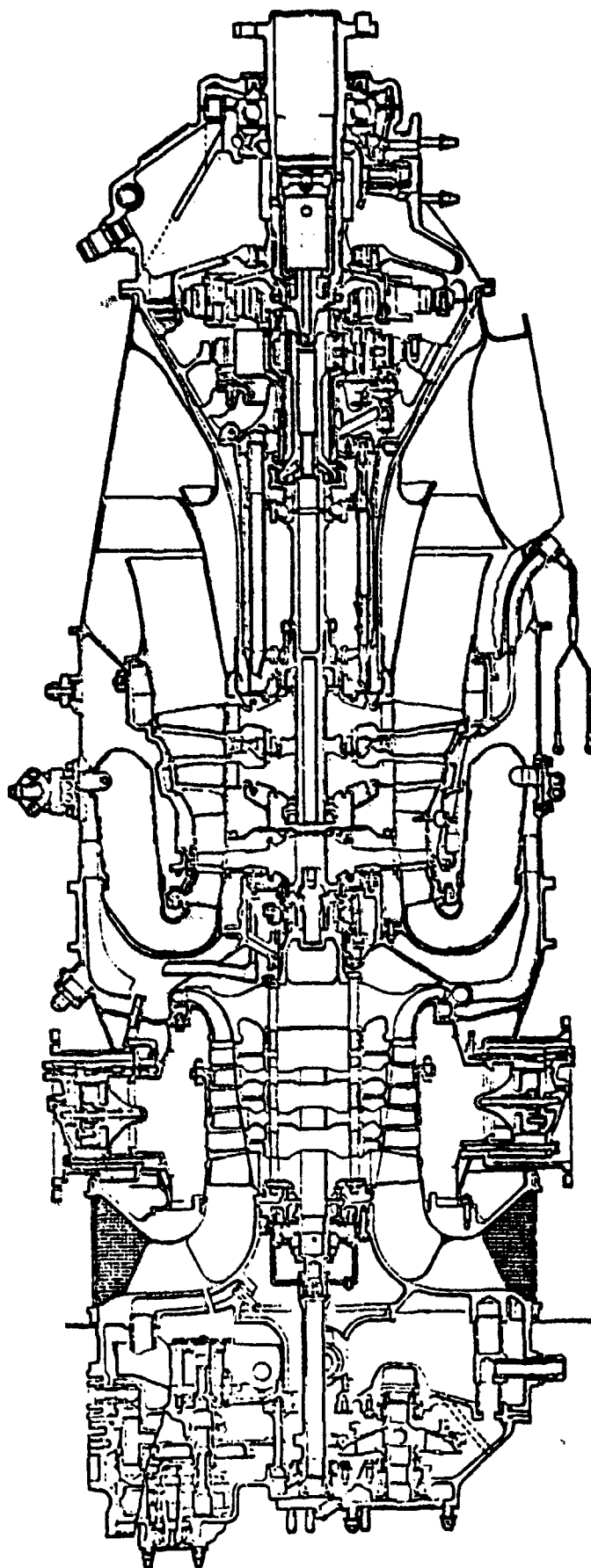
Figure 2.4: PT6A-41 Cross-Section
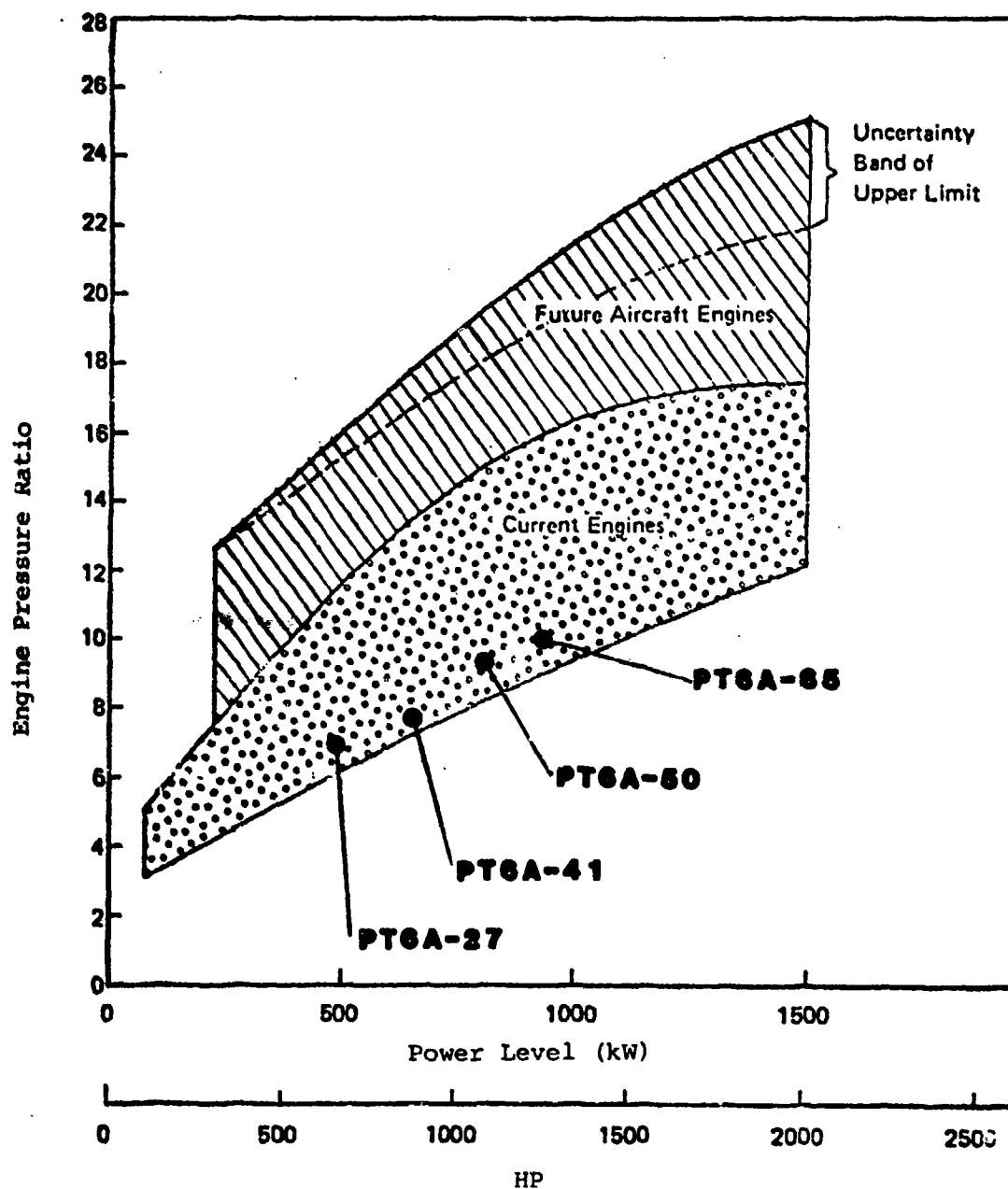
Figure 2.5: Projected Trends in Pressure Ratios
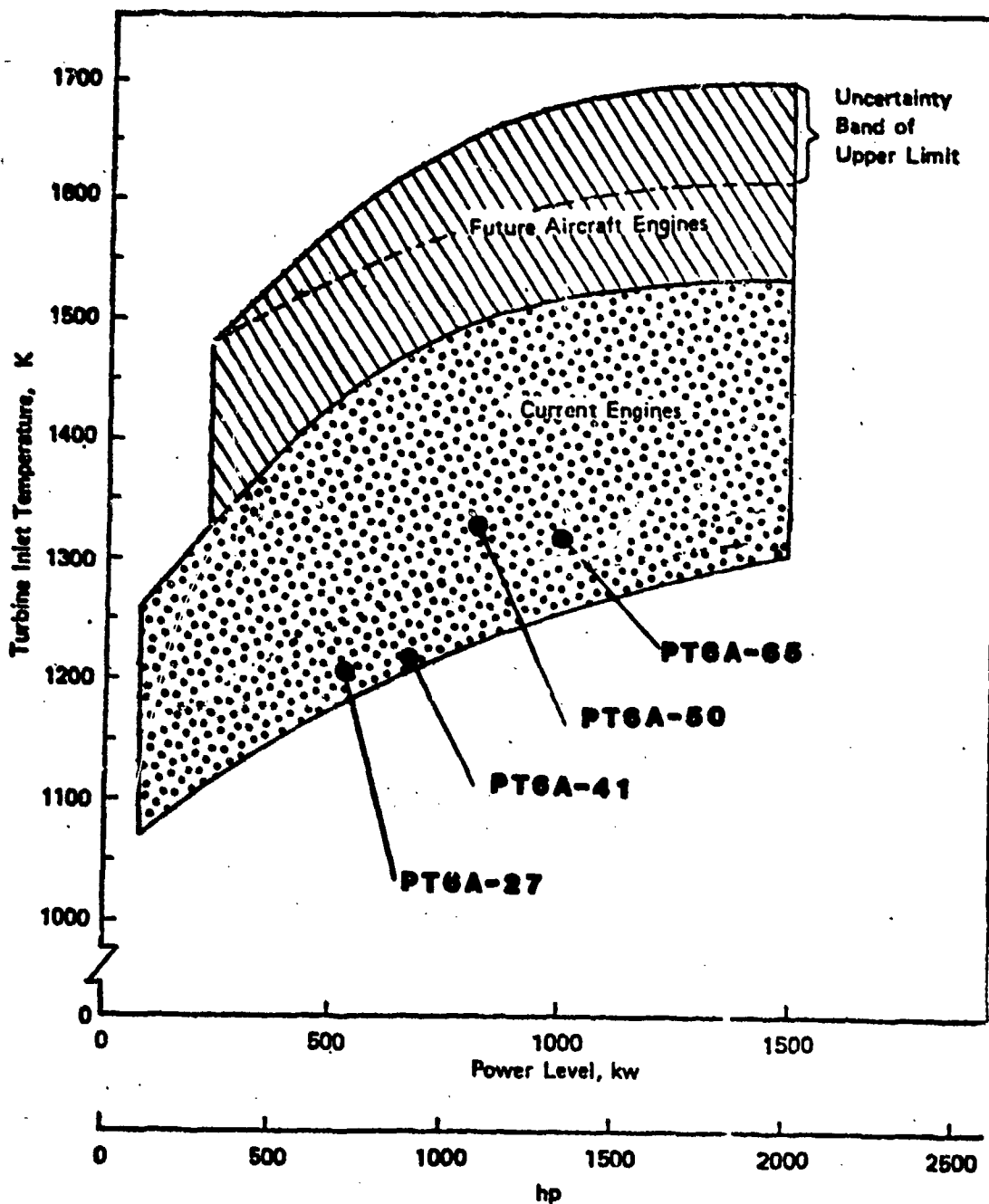
Figure 2.6: Projected Trends in Turbine Inlet Temperatures
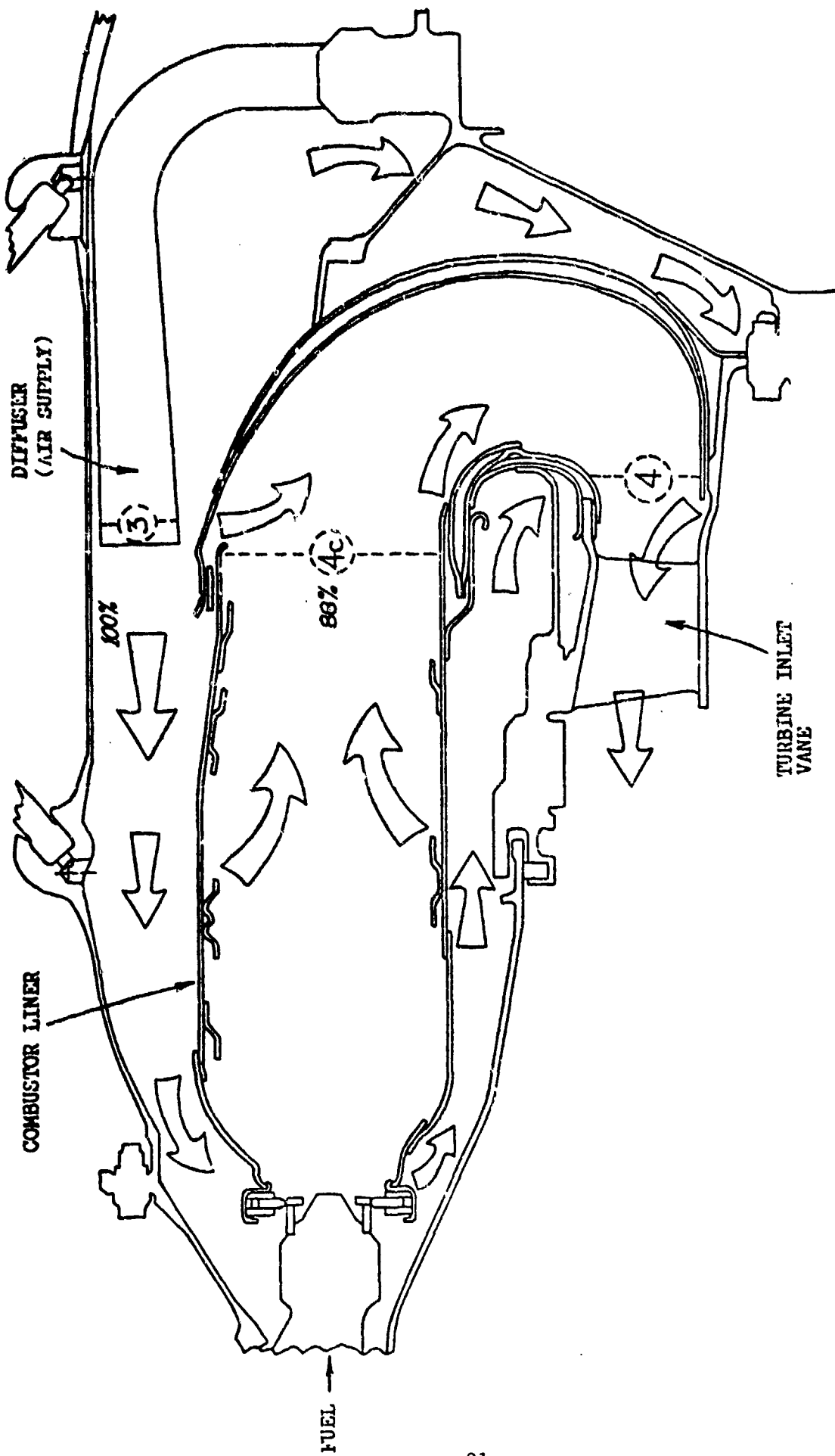
Figure 2.7: Schematic of JT15D-4 Combustion System

DIFFUSER
(AIR SUPPLY)

COMBUSTOR LINER

TURBINE INLET
VANE

FUEL

100%

80%

- 21 -
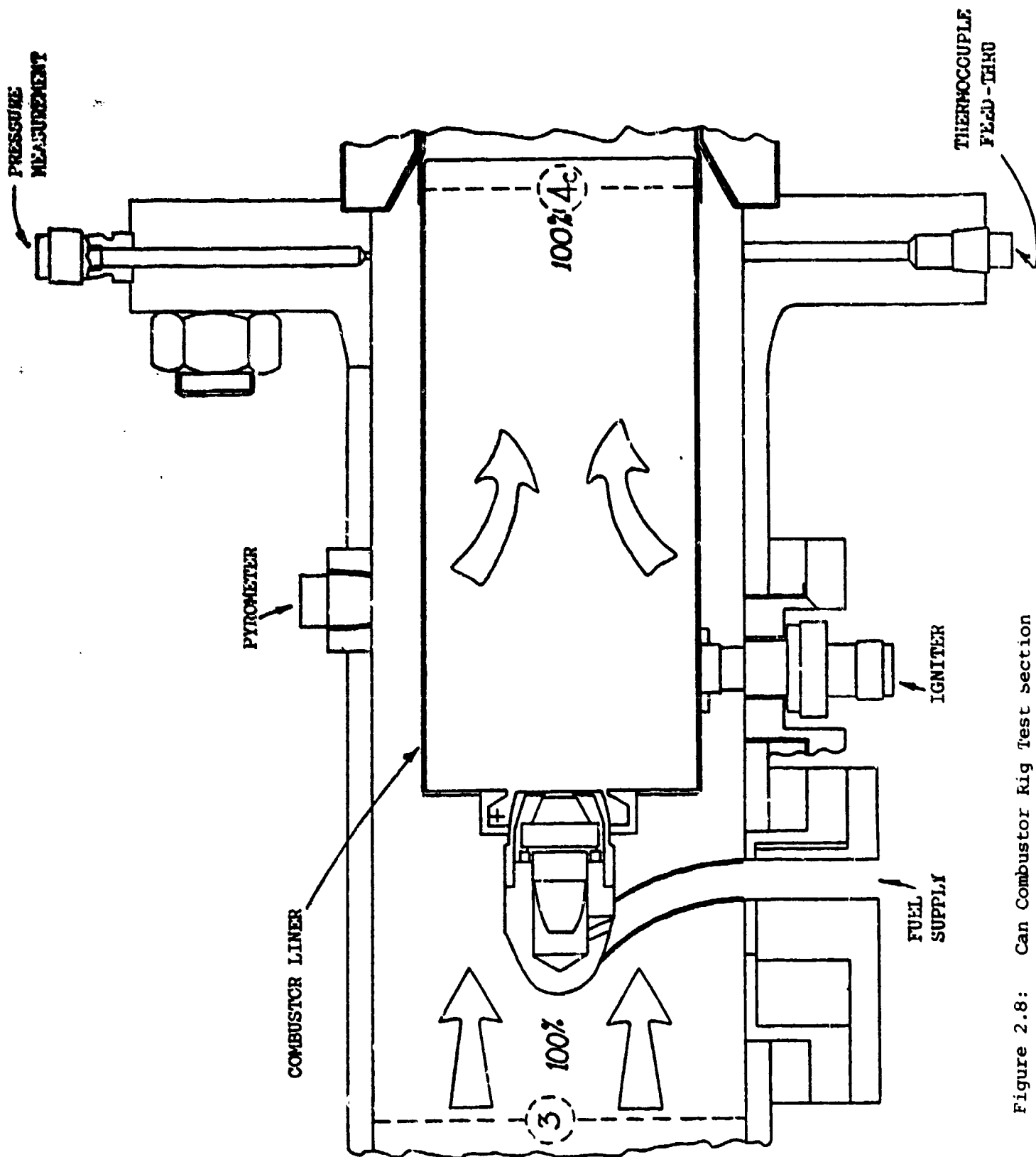
Figure 2.8: Can Combustor Rig Test section
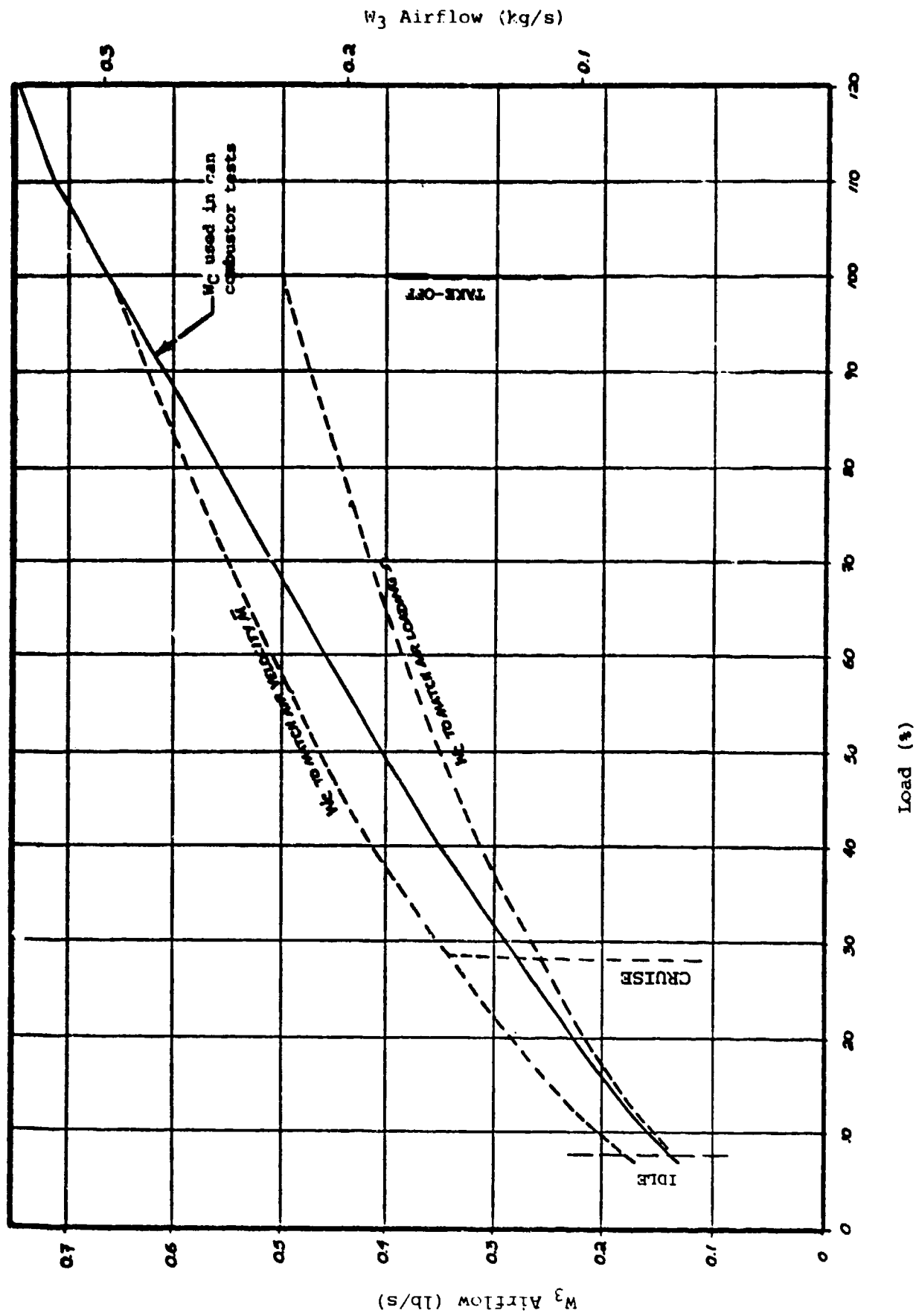
Figure 2.9: Can Combustor Airflow Simulating JT15D-4

- 23 -

W$_3$ Airflow (kg/s)

TAKE-OFF

W$_C$ used in can combustor rig

TO MATCH AIR LOADING W$_C$

TO MATCH AIR VELOCITY W$_C$

W$_C$

CRUISE

IDLE

Load (%)

W$_3$ Airflow (lb/s)
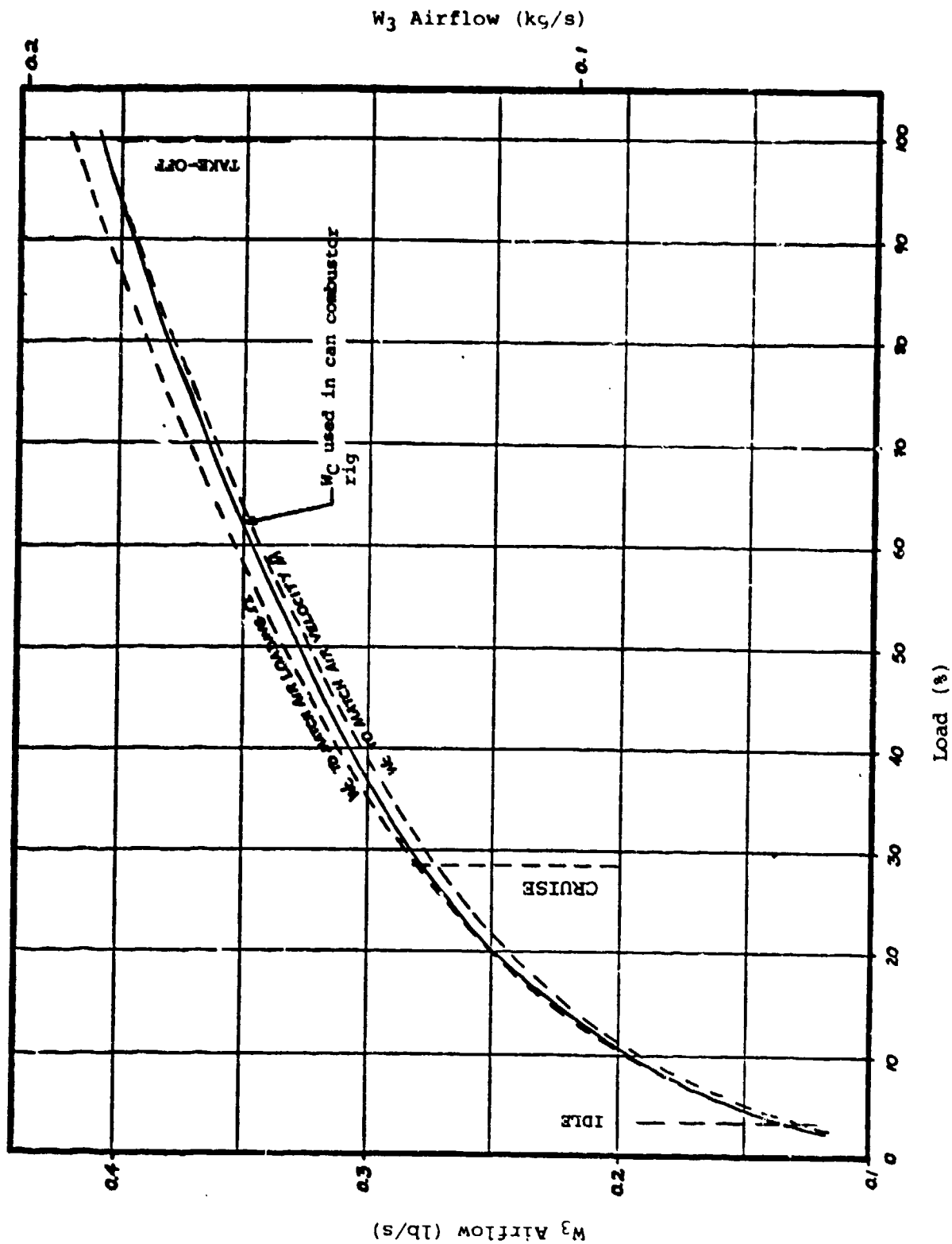
Figure 2.10: Can Combustor Airflow Simulating PT6A-41

SECTION III

TEST FUELS AND CHARACTERIZATION

3.1 TEST FUELS

Can combustor tests were conducted on 15 of 16 fuels categorized in Table 3.1. RJ6 fuel, although described in this Section, was not used in the can combustor tests but will be used in Phase III. Samples of the fuels collected during the period of the test program were sent to the CDND project manager for detailed analyses. Samples will also be sent to the AFWAL project manager when testing resumes under Phase III.

The specification fuels, a wide cut JP4 and a kerosene Jet Al, serve as baseline or reference fuels. The properties of the other fuels are varied systematically beyond the specification limits imposed on the reference fuels, principally in the direction of higher final boiling point and higher aromatics content, which correspond to lower hydrogen content. In addition, to this there are represented certain fuels of unconventional (non-petroleum) origin, and certain fuels not normally consumed in aircraft engines.

1. JP4 - a reference fuel, supplied by the contractor Pratt & Whitney.

2. JP4/B1

3. JP4/B2

   (2) and (3) are stocks of (1), JP4, to which two levels of an almost entirely aromatic solvent were added, with the object of reducing the hydrogen content to 13% and 12%, respectively. The 2040 solvent, supplied by AFWAL, has a boiling range approximately the same as that of typical kerosene gas turbine fuels.

4. Jet Al - a reference fuel supplied by the contractor.

5. Jet Al/B1

6. Jet Al/B2

   (5) and (6) are (4) (Jet Al), blended with 2040 solvent, with targeted final hydrogen contents of 13% and 12%.

7. JP4/2C40/DF2 - A fuel provided by AFWAL, consisting of JP4 to which 2040 solvent and No. 2 Diesel fuel had been added. The result is a fuel of 13% hydrogen by weight and an unusually wide boiling range.

8. Shale JP8 - A fuel prepared from oil shale and refined to meet Jet Al specifications.

9. Tar Sands L-H

10. Tar Sands H-M

11. Tar Sands L-M

12. Tar Sands L-L

The four tar sands fuels were prepared by the research department of Imperial Oil at Sarnia, Ontario. The initial L or H signifies a low or high final boiling point; the final L, M or H signifies a (relatively) low, medium and high hydrogen content. As starting materials two products were employed from Suncor's Athabaska operation, a kerocut, somewhat like JP5, with nominal boiling range of 473-573K, and aromatics level about 20%; and secondly a gas oil side stream of nominal boiling range 473-623K and considerably higher aromatics level, in excess of 40%.

(9), L-H is kerocut; (10), H-M is a blend of kerocut and gas oil side stream. For the remaining two fuels the gas oil side stream was distilled, and a fraction taken off of the same boiling range as the kerocut. Two blends of the kerocut and this topping were made to make fuels (11) and (12) of the same boiling range as the kerocut but successively higher aromatic levels.

13. No. 2 Diesel was procured locally by the contractor.

14. ERBS -3 (Experimental Referee Broadened Specification) Fuel - provided by AFWAL, who obtained the fuel from NASA. A fuel in some ways resembling No. 2 Diesel, with final boiling and aromatics level above specification for aviation fuels.

15. JP10 - hydrogenated dicyclopentadiene, a synthetic product supplied by AFWAL.

16. RJ6 - a blend of about 40% JP10 and 60% RJ5, which is a mixture of hydrogenated dimers of norbornadiene.

(15) and (16) are fuels of higher volumetric energy density, employed in cruise missiles and applications in which space is at a premium; they were both supplied by AFWAL.

3.2 FUEL CHARACTERIZATION

Fuel characterization was organized by CDND. Agencies involved in the analysis are listed in Table 3.2. Complete specification testing was undertaken as well as non-specification property determinations, viz - simulated distillation by gas chromatography; thermal stability breakpoint; density, specific heat, viscosity, surface tension and true vapor pressure, all as functions of temperature; heats of combustion; hydrogen content and detailed hydrocarbon compositional analysis.

3.3 TEST PROCEDURES

Nearly all of the fuel test procedures were ASTM test methods or modifications of them. There was some redundancy or overlap, the source data being provided by two different methods. When partial data were furnished by one source and complete data for the same measurement by another, the complete data have been used for reasons of consistency. When data were obtained by variant or dissimilar methods, they have both been reported and commented on, particularly if there were disagreements to resolve.

3.4 FUEL PROPERTIES

3.4.1 D86 DISTILLATION

Data are shown in Table 3.3.

3.4.2 D2887 SIMULATED DISTILLATIONS BY GAS CHROMATOGRAPHY (G.C.).

The results of G.C. are listed in Table 3.4 and are graphically illustrated in Figures 3.1 and 3.2.

These distillations were carried out in two lots, fuels 1, 2, 5-8, 13-15 being examined some months before 3, 4 and 9-12. This accounts for the difference in presentation (in degrees and tenths of a degree), and may also be responsible for the discrepancy between JP4/B1 and JP4/B2; one would expect the boiling point at any level of recovery to be higher, not lower for JP4/B2 (as is observed in the JET A1 blended fuels).

3.4.3 THERMAL STABILITY, Table 3.5.

Fuels were examined in the Jet Fuel Thermal Oxidation Tester (JFTOT) in two ways (Table 3.5). First, a pass or fail test was conducted according to ASTM D3241 at the generally adopted temperature of 260°C (533K). Fuels were recorded (row 1) as pass (P) or fail (F), by one of two criteria, a pressure build-up (row 2) of greater than 25 mm during the 2.5 hour course of the test; or (row 3) a visual rating of 3 assuming the normal (N) sequence of color development is observed (row 4). It is generally accepted that certain abnormal (A) color developments or observation of a series of interference colors - peacock (P) are cause for failure regardless of the color rating. Several abnormal and peacock observations are listed in row 4. It is seen that all fuels that failed based on visual ratings, except for No. 2 Diesel, also failed by pressure build-up.

In addition, some tubes were examined in the Tube Deposit Rater (TDR), which gives an alternative, and more objective measurement of color density by reflectance. Averaged observations along the length of the tube while it was rotated (spun) and determination of the individual point of maximum light absorption (spot) were recorded.

TDR readings for the two failures among the fuels so examined (JP4/B1 and No. 2 Diesel) are quite large, exceeding the TDR spot reading of 15 which has been proposed as a criterion of failure.

The concept of breakpoint was introduced a few years ago in an attempt to quantify fuel thermal stability by defining a temperature at which some observation made with JFTOT exceeds a critical value. The fuel is run in the JFTOT at several temperatures, and by interpolation of results, the lowest temperature is found at which either pressure build-up exceeds 25 mm or the color rating (assuming the normal sequence of color development) reaches 3.

Breakpoints and failure modes are listed in the lower half of Table 3.5. The determination is not precise, and an uncertainty of at least ±5°C is to be expected. In principle a fuel with a breakpoint below 260°C should fail the specification test. As can be see , JP4 which originally passed the specification test gave a breakpo nt of 239°C based on visual ratings. In addition JP4/B2, which failed the specification test on pressure was limited in breakpoint determination by color development. Several samplings of JP4 had been observed to contain sediments, and the testing agency reported extensive deposits of material on the prefiltering through Whatman filter paper that precedes JFTOT testing. The same agency reported a quite satisfactory breakpoint on the 2040 solvent (275-280°C, failure on color), so that blends of JP4 and 2040, even with the inherent uncertainty of the breakpoint method, are distinctly worse than either component alone. The most probable explanation of these irregular results is contamination of the stock of JP4, and variations in the method of subsequent sampling of JP4 and its blends.

Some thought has been given to the possible effects of this contamination on combustor test results. All fuels are filtered again before introduction to the combustor, therefore, blocked nozzles or distorted spray patterns due to gross contamination seems unlikely. As runs are at most several hours in duration, in power and thrust variation, with disassembly and examination of parts (e.g. for carbon buildup), the low thermal stability is not likely to have any effect, by deposition, during a run.

3.4.4 DENSITY

Densities at 288K were determined at QETE using ASTM D1298, and at four temperatures at Sherbrooke (Table 3.6, Figure 3.3). Sherbrooke tests used a Picker dynamic densimeter to determine density at the reference temperature of 298K. Thermal expansion coefficients were then measured for each fuel with high precision, and by an integration process densities at other temperatures could be calculated. QETE results fell quite satisfactorily on the curve obtained by plotting the Sherbrooke data.

The densities listed for RJ6 were calculated from data provided by AFWAL, a density measurement at 288K, and a curve relating density to temperature presumably of general validity for fuels of this type.

3.4.5 SPECIFIC HEAT

Specific heats as a function of temperature were determined at Sherbrooke, employing the Picker differential dynamic microcalorimeter (Table 3.6).

3.4.6 VISCOSITY

Viscosities for fifteen fuels were determined at QETE, by ASTM D445. The viscosity of RJ6 at 219K (394°R) was 423.90 cSt, which is higher than the specification limit of 400 cSt at that temperature (Table 3.6, Figure 3.4).

3.4.7 SURFACE TENSION

Surface tension (Laval) was determined by a capillary rise technique, employing benzene as a reference fluid (Table 3.6, Figure 3.5).

3.4.8 VAPOR PRESSURE

The method employed is a modification of the isoteniscopic procedure of ASTM D2879-75. For a mixture of many components such as a liquid fuel, the vapor pressure is not defined uniquely by temperature, but depends on the ratio of vapor to liquid volume. As this ratio approaches zero the contribution of the volatile components becomes increasingly important, and the vapor pressure approaches a limiting value. In the present work four isoteniscopes of V_v/V_l varying from 0.06 to 0.280 were used. These ratios are considerably smaller than those used in most previous work, and the results in consequence reflect more closely the limiting intrinsic value. Considerable manipulation of the experimental data is necessary in order to make correction for the air inevitably retained by the fuels. The original report[9] should be consulted for details of this data treatment. What is presented in Table 3-7 is a very small portion of the data generated, and is intended only to be representative of the information available in the report. Table 3-7 contains the experimental data at the two higher V_v/V_l ratios, 0.280 and 0.184, and the derived or corrected data at the highest V_v/V_l ratio (.280) and the limiting value $V_v/V_l = 0$. (The experimental data marked with an asterisk are derived by a short extrapolation from the experimental points in the original report).

The original report comments on the extreme difficulty in getting error-free results, and the fact that anomalies can occur even if meticulous care is exercised. An instance of this is found on comparing data for JP4/B1 and JP4/B2.

The latter fuel contains more 2040 solvent, and in view of the boiling ranges of JP4 and 2040 solvent, it should have under the same conditions a lower vapor pressure than JP4/B1, not higher, as observed. This anomaly occurs both in the experimental and the derived data. Again, the experimental vapor pressure data for tar sands fuel L-M appears abnormally high at $V_v/V_l = 0.280$, probably due to trapped air. The irregularity has disappeared in the corresponding derived data. JP10 is supposedly a pure compound, and one would expect to find its vapor pressure at any temperature independent of liquid-vapor ratio. Instead, some dependence similar to that of the other fuels is observed. This can be attributed either to residual air or to the presence of small amounts of light material not removed during production. The ASTM D2887 distillation of JP10 (Table 3.4) suggests that both light and heavy ends may be present.

3.4.9 SPECIFICATION PROPERTIES

Properties required by fuel specifications have been tabulated in Table 3.8.

<u>Flash Point</u> ASTM D56-11 fuels - (QETE), ASTM D3828 (Setaflash) - (NRC)

There is significant disagreement between the two methods in the case of the less volatile fuels.

Freeze Point ASTM D2386 (QETE) Setapoint (NRC)

ASTM D2386 (Figure 3.6) records the disappearance of the last wax crystals on rewarming; it has been reported that the Setapoint reflects rather the wax appearance point, so that Setapoint measurements tend to be systematically lower than ASTM D2386. This observation is in general supported by examination of the data (omitting JP10 as anomalous). For fuels containing middle distillate fractions (JP4/2040/DF2, tar sands fuels, No. 2 diesel, and ERBS-3) Setapoint measurements are from 2 to 6°C lower than D2386. For the lighter JP4 and Jet A1 based fuels, the two measurements coincide within a degree, with the single exception of JP4/B1, in which the Setapoint reading is 2°C higher.

Smoke Point ASTM (D1322) data were provided by QETE and Gulf; Gulf also provided luminometer data (ASTM D1840).

Heats of Combustion by ASTM D2382 were provided by EMR and, for comparison, calculated heats of combustion by ASTM D1405 (Table 3.8 and Figure 3.7) from aniline-gravity product were provided by QETE. This latter determination is included as a matter of interest, as the aniline-gravity estimation applies only to petroleum-based fuels that meet a recognized specification (aviation gasoline, JP4, Jet A, etc.). Taking the ASTM D2382 heat of combustion figures as correct, and examining the ASTM D1405 figures, significant disagreement is seen with JP4 and its blends, and with Jet A1/B2. Calculated heating values for tar sands fuels are surprisingly good.

3.4.10 FUEL COMPOSITION

Hydrogen content: The first two rows of Table 3.9 compare hydrogen content as determined by NMR (ASTM D3701) at NRC, and by microcombustion at EMR. The latter figures are typical of the best that can be achieved by classical methods. Figure 3.8 is a bar chart comparison of NMR measured fuel hydrogen content values.

It is seen that attempts to reach 13 and 12% hydrogen by addition of 2040 solvent to the two base fuels were not completely successful. The location of the test laboratory (NRC in Ottawa), being remote from the blending site, made it difficult to adjust blend ratios to the required levels. The hydrogen content of JP10 was calculated from its formula and for RJ6 from its composition (39.9% RJ5) supplied by AFWAL.

Aromatics, Olefins and Paraffins: ASTM D1319 (Fluorescent indicator absorption) analysis provides a rough division into three fractions – aromatics, olefins and paraffins. Developed for gasoline and turbine fuel of petroleum origin, it provides an estimate of proportions. Results depend to some extent on operator techniques; only with considerable reservations can it be used for other fuels. The ASTM D1319 data provided by Imperial Oil for the four tar sands fuels are included with the QETE values, and show the kind of variation that can be expected.

- 30 -

<u>Naphthalenes</u>: This estimation by ASTM D1840 is made by light absorption in the near ultraviolet. For the JP4 and Jet Al blends with 2040 solvent, the naphthalene content can be calculated from the blend ratio, and the knowledge that 2040 solvent contains 57% naphthalenes. Results from ASTM D1840 come out in quite satisfactory agreement with these calculated values even though ASTM D1840 is a rather rough method of estimation.

<u>Hydrocarbon Compositional Analysis</u>: Detailed hydrocarbon compositional analysis was carried out by EMR, employing a modification of ASTM D2789 (ASTM D2789 is a gasoline analysis and this procedure was extended to include a mass spectrometric analysis of hydrocarbon composition). The original results were presented as paraffin; naphthenes in two categories; and aromatics broken into six categories. In this summary they have for purposes of comparison been reconsolidated into paraffins, naphthenes and aromatics (Table 3.9). The analytical program is so devised that olefins, low in any case, always appear as zero. Para-fins, naphthenes and aromatics add up to 100%, apart from rounding off errors. Again, naphthalenes are shown as a separate category.

Comparing the two sets of data from the two sources (ASTM D1319 and modified ASTM D2789), it appears that, in particular for high aromatic fuels, ASTM D2789 understates the aromatics level. In the case of one blend, Jet Al/B2, figures for both aromatic and naphthalene content are significantly lower than what may be called "true" values, calculated from the blend ratio and the composition of Jet Al and 2040. Much the same observation may be made about the four tar sands derived fuels. From the available data on the kerocut and gas oil side stream rough compositions for the blends can be worked out. Either of the two ASTM D1319 analyses, for all their uncertainty, is closer to this "true" value than the ASTM D2789 results. It is evident that with this latter method at high aromatic levels a saturation effect has led to a compression in the aromatic readings.

Data by either of the two methods may be taken as indicative of trends in composition and used for comparative purposes; however the ASTM D1319 data are closer to the actual composition.

<u>Sulfur and Nitrogen Content</u>: The last three determinations; total sulfur (ASTM D1266), mercaptan sulfur (ASTM D1323) and nitrogen (ASTM D3228) were performed at QETE. The sulfur determinations are all within specification for aviation turbine fuels. Nitrogen levels, for which no specifications exist, are in the range anticipated.

Table 3.1: Phase II Test Fuels

CURRENT SPEC.	BROADENED SPEC.	ALTERNATE FUELS
JP4/JET B	JP4/B$_1$ JP4/B$_2$	JP4/DF/2040
JP8/JET A$_1$	JET A$_1$/B$_1$ JET A$_1$/B$_2$	SHALE JP8
JP10 DIESEL 2 RJ6*	ERBS-3	TAR SANDS L-H TAR SANDS L-M TAR SANDS L-L TAR SANDS H-M

* Phase III Test Fuel

Table 3.2: Fuel Characterization Agencies

PROPERTY	SOURCE
SPECIFIC GRAVITY	P&WC
	CDND (QETE)
DISTILLATION	CDND (QETE/EMR)
FREEZING POINT	CDND (QETE)
SPECIFIC HEAT vs TEMP	CDND (SHERBROOKE)
CHARACTERIZATION FACTOR	P&WC (CALCULATED)
THERMAL OXIDATIVE STABILITY	CDND (QETE)
TOTAL AROMATICS	CDND (QETE)
VISCOSITY vs TEMPERATURE	CDND (QETE) (253 to 310K)
HYDROCARBON COMPOSITION	CDND (ERL-EMR)
SMOKE POINT	CDND (GULF)
LUMINOMETER NUMBER	CDND (GULF)
HEAT OF COMBUSTION	CDND (QETE)
FLASH POINT	CDND (QETE/LAVAL)

PROPERTY	SOURCE
STOICHIOMETRY	P&WC (CALCULATED)
TOTAL SULPHUR	CDND (QETE)
MERCAPTAN SULPHUR	CDND (QETE)
WEIGHT % HYDROGEN	CDND (NRC/ERL-EMR)
SURFACE TENSION	CDND (NRC/LAVAL)
TRUE VAPOR PRESSURE	CDND (LAVAL)

QETE = Quality Engineering Test Establishment (CDND)
LAVAL = Université Laval
SHERBROOKE = Université de Sherbrooke
CDND = Canadian Department of National Defense
NRC = National Research Council
P&WC = Pratt & Whitney of Canada

Table 3.3: Fuel Distillation Range (ASTM D86)

D86	1 JP4	2 JP4 B1	3 JP4 B2	4 JP4 2040 DF2	5 JET A1	6 JET A1 B1	7 JET A1 B2	8 JP8 SHALE	9 KEROSIN LN	10 KC-GOSS MN	11 KC-GOSS TOPPING LN	12 KC-GOSS TOPPING LL	13 DIESEL #2	14 ERBS-3	15 JP10	16 RJ6
I.B.P. °C	61	64	58	68.5	169	173	174	175	171	172	174	182	191	187	178	
5	88	92	91	99	177	180	183	184	197	192	194	197	223	197	181.5	
10	99	104	108	114	181	184	185.5	186	203	200	200	204	233	200	182	
20	117	126	131	141.5	186.5	191	192	189	211	214	210	213	246	208	182.5	
30	132.5	143	155	161	189.5	194	195	191	217	221	215	219	255	215	183	
40	147	160	173	194	193	197	200	195	223	227	223	225	263	220	183	
50	159	175	185	213	196	201	204	199	229	233	229	232	271	226.5	183	
60	166.5	185	197	220	200	206	210	204	234	240	236	238	280	235	183	
70	172	197	210	247	205	211	217	209	241	249	242	245	290	241	183	
80	187	209	223	265	210	218	224.5	217	249	259	249	254	301	260	183.5	
90	199.5	229	243	292	219	232	238	226	260	275	261	265	316	288	184	
95	210	248	258	319	229	245	253	235	270	296	271	278	334	309	184	
96	214	253	263	328	234	251	257	238	274	304	275	283	338	315	185	
E.P.	218.5	263	268	329.5	244	266.5	272	248	283	311	288	285	346	329	195.5	
RECOVERY %	97.5	98	97.6	97.0	97.5	98	98.5	98.5	98.0	97.7	98.3	97.3	98.0	98.5	98.5	
RESIDUE	1.4	1.1	1.4	1.6	1.4	1.2	1.2	1.5	1.8	1.9	1.5	2.4	1.7	1.5	1.0	
LOSS	1.1	0.9	1.0	1.4	1.1	0.8	0.3	-	0.2	0.4	0.2	0.3	0.3	-	0.5	

Table 3.4:   Fuel Distillation Range (ASTM D2887)

	1	2	3	4	5	6	7	8	9	10	11	12	13	14	15	16
	JP4	JP4 B1	JP4 B2	JP4 2C40 DF2	JET A1	JET A1 B1	JET A1 B2	JP8 SHALE	KEROCUT LH	KC+GOSS HM	KC+GOSS TOPPING LM	KC+GOSS TOPPING LL	CIESEL #2	ERBS-3	JP10	RJ6
D2887 0.5%	30	44	22.9	33.0	131	133	135	146	131.5	128.8	123.7	132.9	148	145	169	
5	64	85	67.8	72.4	157	159	161	162	167.5	171.0	169.0	171.8	201	170	170	
10	82	111	94.9	96.7	165	167	170	169	185.4	189.7	185.8	187.8	213	162	172	
20	105	143	122.0	133.4	175	176	183	177	202.5	205.8	203.8	204.2	239	197	176	
30	127	169	159.5	162.7	184	188	193	186	212.1	215.3	213.0	213.9	255	208	179	
40	145	191	175.8	197.0	193	195	200	194	220.3	225.7	222.8	224.2	270	216	181	
50	159	204	192.6	214.3	197	201	206	200	229.6	235.4	232.1	233.5	281	226	182	
60	169	217	204.1	230.9	203	207	212	208	238.8	245.9	241.2	243.2	293	237	184	
70	180	231	218.1	250.1	206	213	220	213	249.0	256.7	251.0	252.9	308	248	186	
80	194	249	229.8	272.1	214	221	227	223	259.7	270.4	262.0	264.3	322	270	187	
90	205	267	245.8	301.6	225	234	243	235	273.5	286.1	275.6	278.3	339	300	189	
95	213	280	255.9	326.2	235	246	256	246	283.3	305.2	285.8	289.6	353	326	190	
99.5	235	326	295.8	372.0	280	292	299	284	-	360.7	329.1	331.3	401	428	323	

Note: Fuels 3, 4, 9-12 were run at one time,
the balance at another time, by the same agency.

Table 3.5: Fuel Properties I

	1	2	3	4	5	6	7	8	9	10	11	12	13	14	15	16
	JP4	JP4 B1	JP4 B2	JP4 2040 CF?	JET A1	JET A1 B1	JET A1 B2	JP8 SHALE	KEROCUT LH	KC-GOSS HM	KC-GOSS TOPPING LM	KC-GOSS TOPPING LL	DIESEL #2	ERBS-3	JP10	RJ6
JFTOT D3241 AT 260°	P	F	F	F	P	P	P	P	F	F	F	F	F	P	P	
P mm Hg	2.5	>254	>254	>254	3	7.5	1.0	0.5	38	>254	>254	>254	2.5	2	2	
VISUAL	1 N	3-4 A	4 P	3-4 N	<1 N	<1 N	<1 N	<1 N	1 N	1 N	1 N	4 A	1 A	1 N	<1 N	
Δ TDR (a) SPUN (b) SPOT	3 4.5	43.5 45	- -	- -	<0 2	0 0	0 1	0 1	- -	- -	- -	- -	23.5 17.5	5 7	0 0	
BREAKPOINT °C	238	212	203	247	277	274	274	276	246	229	256	258	258	292	313	
P mm Hg	0	>25	1	>25	>25	6	5	>25	>25	>25	>25	>25	2	1	-	
VISUAL	3	1	3	2	1	3	3	1	1	1	1	1-2	3	3	-	

Table 3.6: Fuel Properties II

	1	2	3	4	5	6	7	8	9	10	11	12	13	14	15	16
	JP4	JP4 B1	JP4 B2	JP4 2040 DF2	JET A1	JET A1 B1	JET A1 B2	JP8 SHALE	KEROCUT LH	KC-GOSS MH	KC-GOSS TOPPING LH	KC-GOSS TOPPING LL	DIESEL F2	DMBS-3	JP10	RJ6
DENSITY Kg/L																
D1298 5°C	.77480	.81543	.84472	.82897	.81201	.83580	.84913	.81013	.84457	.85055	.84920	.85480	.85762	.84792	.94620	1.0245
15	.7668	.8078	.8359	.8215	.8048	.8299	.8518	.8033	.8380	.8436	.8434	.8481	.8509	.8417	.9377	1.0185
25	.75964	.80032	.82970	.81443	.79788	.82161	.84484	.79603	.83086	.83650	.83542	.84093	.84432	.83427	.93139	1.0100
45	.74447	.78520	.81362	.79287	.78372	.80740	.83053	.78192	.81714	.82244	.82163	.82074	.83100	.82061	.91657	.9955
65	.72920	.77008	.79767	.78532	.76957	.79318	.81623	.76781	.80342	.80838	.80784	.81315	.81769	.80696	.90175	.9315
SPECIFIC HEAT J/kg DIFFERENTIAL MICROCALORIMETRY																
5°C	1.9310	1.8498	-	1.8508	1.8913	1.8429	1.7983	1.9143	1.8246	1.8164	1.8168	1.8084	1.8488	1.8496	1.5185	...
25	2.0026	1.9186	-	1.9180	1.9600	1.9142	1.8625	1.9838	1.8992	1.8896	1.8906	1.8469	1.9193	1.9152	1.5999	...
45	2.0896	1.9963	1.9366	1.9991	2.0489	1.9873	1.9377	2.0650	1.9945	1.9724	1.9744	1.7630	1.9973	1.9922	1.6868	...
65	2.1816	2.0831	2.0212	2.0894	2.1465	2.0824	2.0208	2.1561	2.0985	2.0372	2.0632	2.0713	2.0883	2.0804	1.7965	...
VISCOSITY cSt D445 -20°C	1.85	2.15	2.52	4.05*	3.93	4.07	4.36	4.17	8.10	9.20	8.01	8.55	-	8.16	8.84	41.3
0°C (32°F)	1.29	1.45	1.66	2.35	2.39	2.46	2.56	2.52	4.15	4.55	4.08	4.31	8.63	4.19	5.05	15.9
21.1°C (70°F)	1.00	1.07	1.18	1.60	1.65	1.62	1.70	1.70	2.55	2.77	2.53	2.67	4.53	2.55	3.26	9.15
37.8°C (100°F)	0.730	.877	.955	1.26	1.28	1.27	1.30	1.35	1.85	1.96	1.82	1.89	3.03	1.85	2.37	7.05
SURFACE TENSION (dyne/cm) CAPILLARY 0°C	24.7	26.9	26.0	24.4	27.95	28.2	29.2	26.95	28.5	29.1	28.8	28.5	29.5	30.2	-	
25	22.5	24.1	23.9	23.4	25.35	26.2	26.95	25.1	26.4	26.8	26.6	26.2	26.3	27.2	32.1	
50	20.35	21.4	22.0	21.6	22.9	24.1	24.8	23.1	24.3	24.7	24.6	24.2	25.3	24.4	29.8	
75	18.2	18.7	20.0	19.5	20.3	22.3	22.45	21.5	22.1	22.5	22.5	21.9	23.2	21.5	27.4	

*interpolated

Table 3.7: Fuel Properties III

	1	2	3	4	5	6	7	8	9	10	11	12	13	14	15	16
	JP4	JP4 B1	JP4 B2	JP4 2040 DF2	JET A1	JET A1 B1	JET A1 B2	JP8 SHALE	KEROCUT LH	KC-GOSS HH	KC-GOSS TOPPING LH	KC-GOSS TOPPING LL	DIESEL F2	CHNS-3	JP10	RJ6
Vapour Pressure (mm Hg)																
D2879-75 Modified																
Experimental Data 0°C																
Vv/VL = 0.220 0	52*	39*	54*	30.5*	25.5*	33.5*	49*	30*	23*	17*	45.5*	22*	20.5*	25.6*	32*	
25	112	87	111	80	42.5	53	63	56	46	28	67	40	35.5	57	43	
50	220	172	211	173	62	77	87	88	83	42.5	92	77	52	84	62	
75	395	325	368	310	90	110	131	140	120	65	140	105	74	115	100	
Vv/VL = 0.184 0	73*	61*	77*	48*	33*	48*	67*	42.5*	78*	62*	61*	97*	37*	55*	42*	
25	158	120	151	121	66	68	85	73	130	91	90	145	61	120	61	
50	292	222	290	275	103	85	124	118	202	130	134	200	95	215	87	
75	510	410	530	480	150	118	180	180	253	160	195	250	139	350	132	
Derived Data																
Vv/VL = 0.220 0	34	29	45	26.5	12	22	7	23.5	23	10	10	15	-	23	-	
25	85	70	95	67.5	24	48	18	43.5	43	17.5	21	30.5	14	38.5	12	
50	187	153	184	152	43	61	39	76	75	32.5	48	57.5	30	61	29	
75	365	300	325	305	68	92	75	122	120	58	97	99	57	90	61	
Vv/VL = 0.0 0	74	94	152	70	73	164	60	78	217	44	87	198	93	207	25	
25	173	190	360	188	157	290	137	149	400	92	205	355	208	380	66	
50	380	370	770	445	310	478	290	268	675	175	435	610	425	650	155	
75	740	650	-	930	545	725	540	440	~1050	305	825	940	760	1000	320	

* Derived by short extrapolation from experimental points.

- 38 -

Table 3.8: Fuel Properties IV

	1	2	3	4	5	6	7	8	9	10	11	12	13	14	15	16
	JP4	JP4 B1	JP4 B2	JP4 2340 DF2	JET A1	JET A1 B1	JET A1 B2	JP8 SHALE	KEROOUT LH	KL-GOSS HH	KC-GOSS TOPPING LH	KC-GOSS TOPPING LL	DIESEL #2	EXSS-3	JP10	RJ5
FLASH POINT D56-TAG °C / D 3828-SETAFLASH °C	-18	-14	-13.5	-7.5	53.5 / 55.5	55.0 / 56.0	57.0 / 59.0	54.5 / 55.5	63.0 / 66.0	63.5 / 67.0	62.0 / 64.5	64.0 / 67.5	66.0 / 73.0	66.0 / 69.0	50.5 / 52.5	65.5
FREEZE POINT D 2386 °C / SETAPOINT °C	<73 / <70	-61 / -59	-47.5 / -47.5	-25 / -31	-60 / -59.5	-63 / -62	-53 / -54	-52 / -51	-48.5 / -50.5	-49 / -52.5	-48 / -53.5	-49 / -53.5	-13 / -15.5	-24 / -26.5	<-73 / <-70	
SMOKE POINT D 1322 mm	28.5	14.9	10.0	14.5	22.8	15.9	11.5	24.2	16.0	17.0	16.3	15.0	15.7	15.5	16.6	
SMOKE POINT D 1322 / LUMINOMETER NO D 174C	27 / 63	14 / 34	12 / 19	14 / 31	22 / 46	17 / 29	12 / 21	22 / 51	17 / 35	16 / 31	16 / 32	14 / 28	15 / 29	14 / 28	17 / 30	
HEAT OF COMBUSTION MJ/kg D 2382	43.82	43.16	41.90	42.80	43.04	42.99	43.52	43.30	42.87	42.66	42.80	42.80	43.21	43.67	42.81	41.99
ANILINE POINT °C D 611	52.5	35.8	22.4	46.1	56.1	44.4	31.8	56.9	55.4	52.8	50.0	45.9	62.5	53.3	(27)	
NET HEAT OF COMBUSTION (CALC) D 1405 MJ/kg	43.46	42.65	42.67	42.94	43.17	42.80	42.47	43.20	42.93	42.04	42.89	42.78	.	.	.	

Table 3.9: Fuel Compositions

	1	2	3	4	5	6	7	8	9	10	11	12	13	14	15	16
	JP4	JP4 B1	JP4 B2	JP4 2040 DF2	JET A1	JET A1 B1	JET A1 B2	JP8 SHALE	KEROOUT LH	KC-GOSS HH	KC-GOSS TOPPING LH	KC-GOSS TOPPING LL	DIESEL #2	ERBS-3	JP10	RJ6
HYDROGEN WT % D3701	14.25	12.86	11.93	13.01	13.76	12.88	12.04	13.82	13.38	13.21	13.17	13.03	13.05	12.96	11.88[1]	10.55[1]
MICROCOMBUSTION	14.2	12.9	12.09	12.89	13.9	13.0	12.4	14.0	13.21	13.09	13.03	12.83	12.9	13.2	12.0	-
D1319 COMPOSITION[2] PARAFFINS % V	84.6	69.1	56.7	70.8	78.9	68.5	57.4	77.0	69.1 (78)	65.4 (70)	61.0 (66)	56.4 (63)	64.9	69.6	98.5	..
AROMATICS	14.5	30.2	42.5	28.3	19.7	30.2	41.7	21.1	29.1 (20)	33.4 (28)	37.2 (32)	41.8 (36)	31.9	29.1	0	..
OLEFINS	0.9	0.7	0.3	0.9	1.4	1.3	0.9	1.9	1.8 (2)	1.2 (2)	1.8 (2)	1.8 (1)	3.2	1.3	1.5	..
D1840 NAPHTHALENES %V	0.3	11.0	17.6	10.7	0.7	9.2	17.3	0.6	1.0	1.7	1.3	1.6	7.8	12.5	0	-
D2789 MODIFIED PARAFFINS %V	49.3	43.8	41.9	47.6	48.7	43.8	43.0	51.6	39.2	38.1	38.0	36.6	43.6	43.6		..
NAPHTHENES	35.9	30.0	25.1	29.0	35.1	30.7	28.4	30.8	41.3	40.7	40.0	38.7	28.4	27.2		..
AROMATICS	14.8	25.3	33.0	23.4	16.2	25.5	28.6	17.6	19.6	21.3	22.0	24.2	28.0	29.2		..
NAPHTHALENES (FROM AROMATIC FRACTION IN D 2789)	1.1	10.1	16.2	8.9	1.3	9.0	11.7	1.2	1.0	1.3	1.4	1.5	4.9	7.5	-	-
D1266 TOTAL SULFUR % W/W	0.044	0.035	0.0034	0.085	0.004	0.005	0.003	0.003	0.003	0.024	0.019	0.024	0.241	0.050	0.002	
D484 MERCAPTAN % W/W	0.0012	0.00089	NEG	NEG	0.00058	0.00038	0.00035	0.00042	NEG	NEG	NEG	NEG	0.00065	0.00082	0.00059	
D3228 NITROGEN % W/W	0.0001	0.0001	0.0015	0.003	0.0020	0.0019	0.0019	0.0164	.0013	.007	0.018	0.021	0.0109	0.0000	0.0000	

1. Calculated from the chemical formula.
2. Bracketed data for the four tar sands fuels were supplied by Imperial Oil, who prepared the fuels.

- 40 -
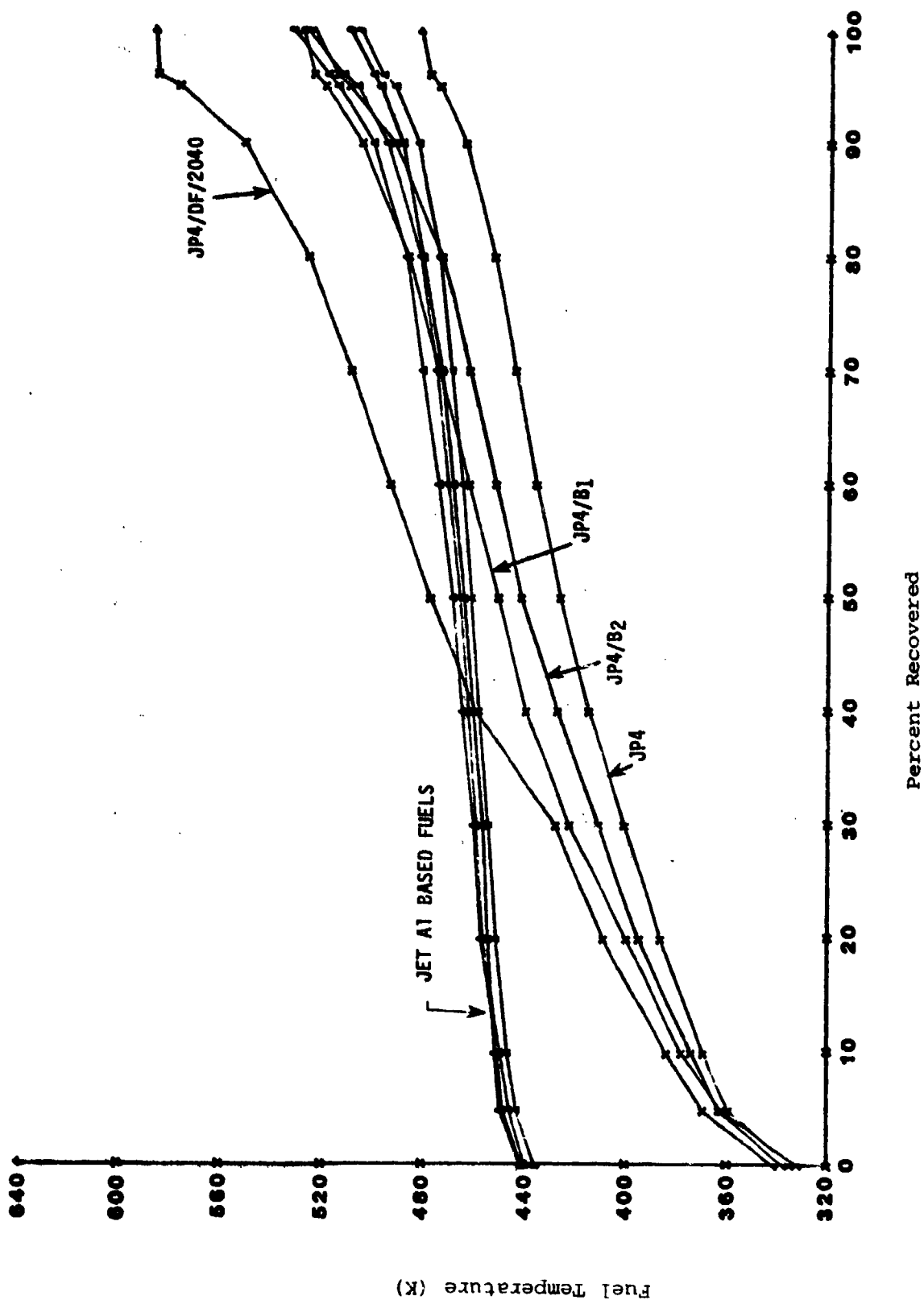
Figure 3.1: Fuel Distillation Ranges (ASTM D2887)
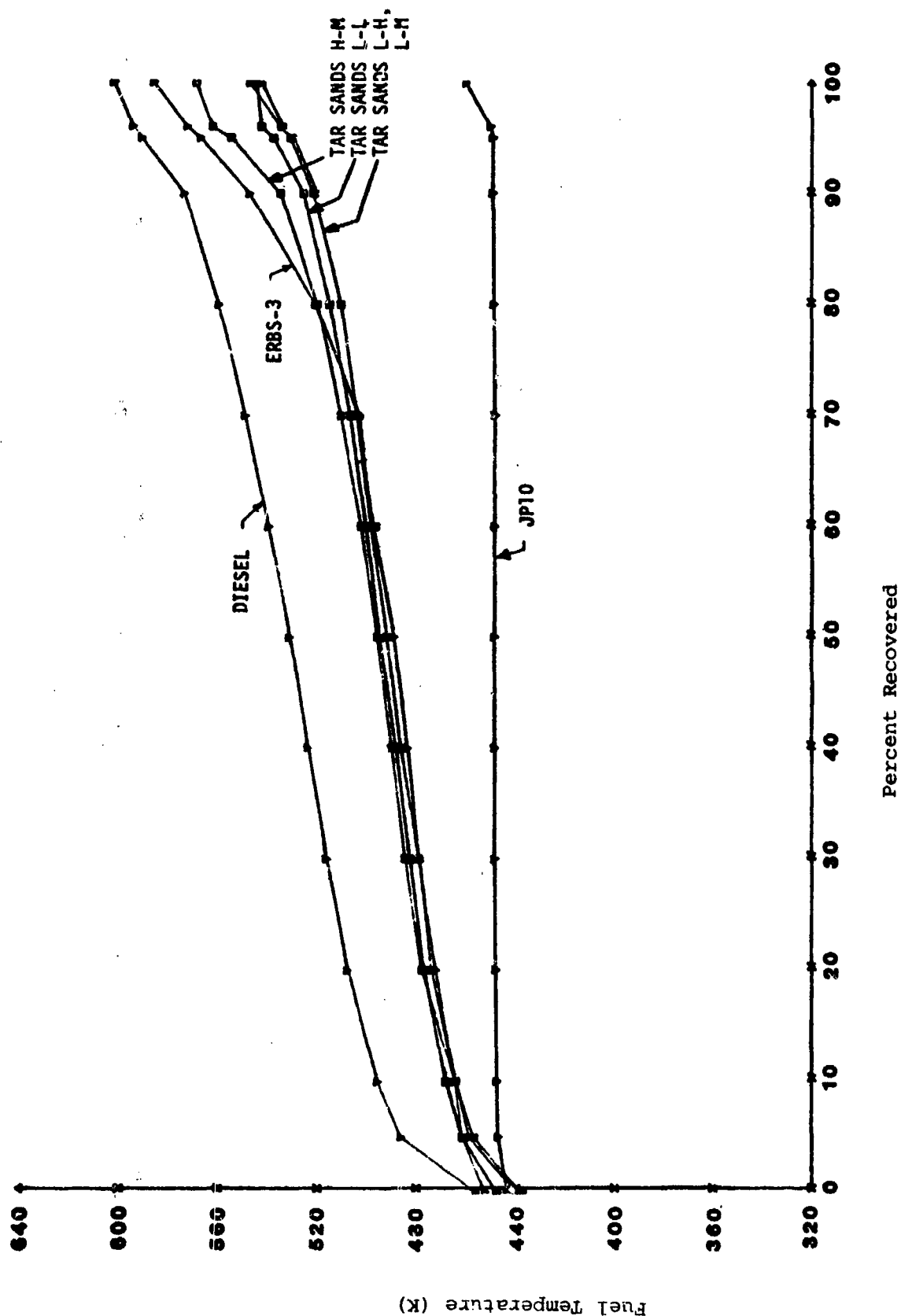
Figure 3 2: Fuel Distillation Ranges (ASTM D2887)

- 42 -

Figure 3.3: Effect of Temperature on Fuel Density   (ASTM D1298)

Figure 3.4: Effect of Temperature on Viscosity (ASTM D445)

Figure 3.5: Effect of Temperature on Surface Tension
(Capillary Rise Technique)

Figure 3.6:   Comparison of Fuel Freeze Points   (ASTM D2386)

Figure 3.7: Comparison of Fuel Heating Values (ASTM D1405)

Figure 3.8: Comparison of Fuel Hydrogen Contents (ASTM D3701)

SECTION IV

CAN COMBUSTION SYSTEM DESCRIPTION

4.1 ORIGINAL CONFIGURATION

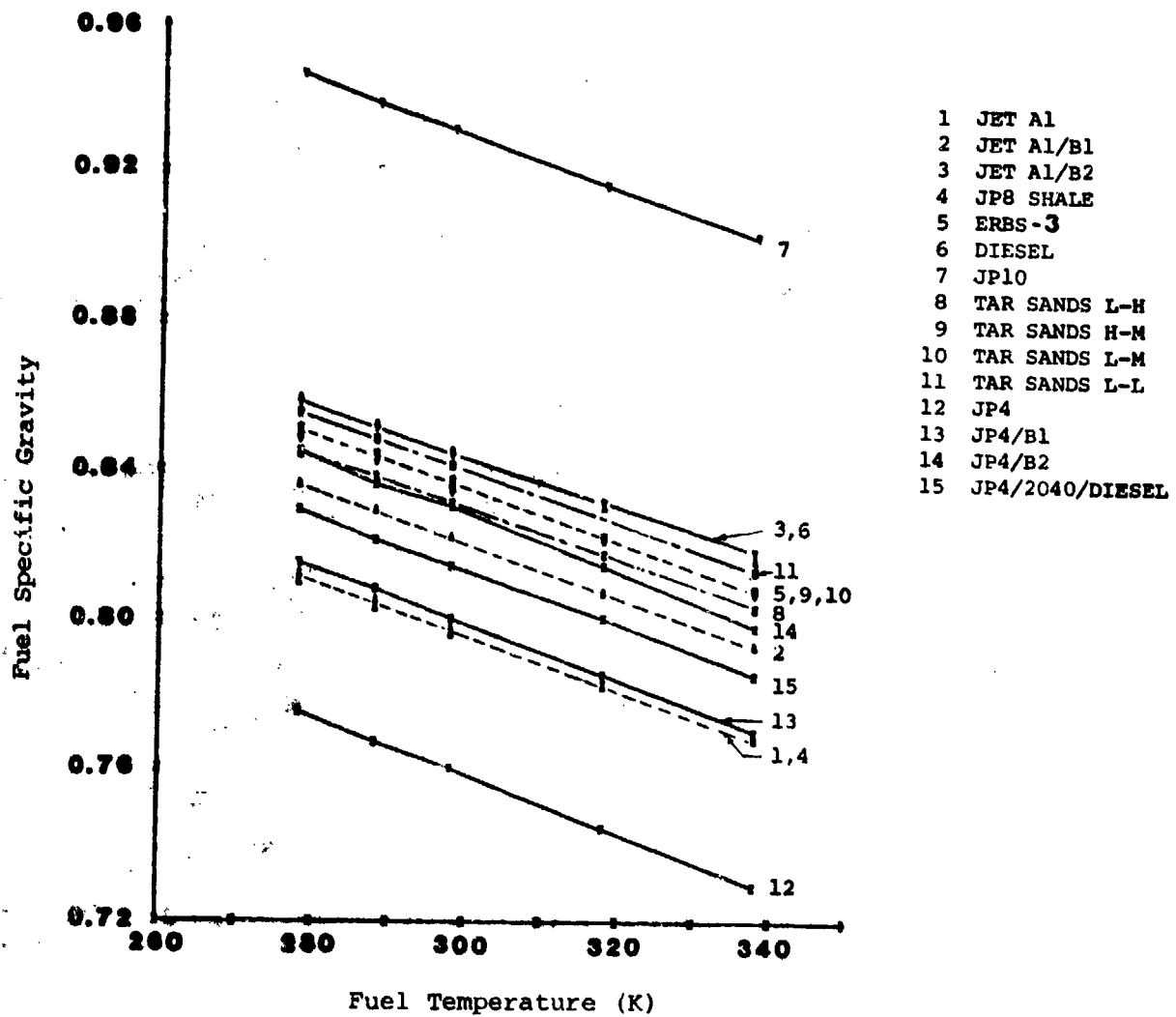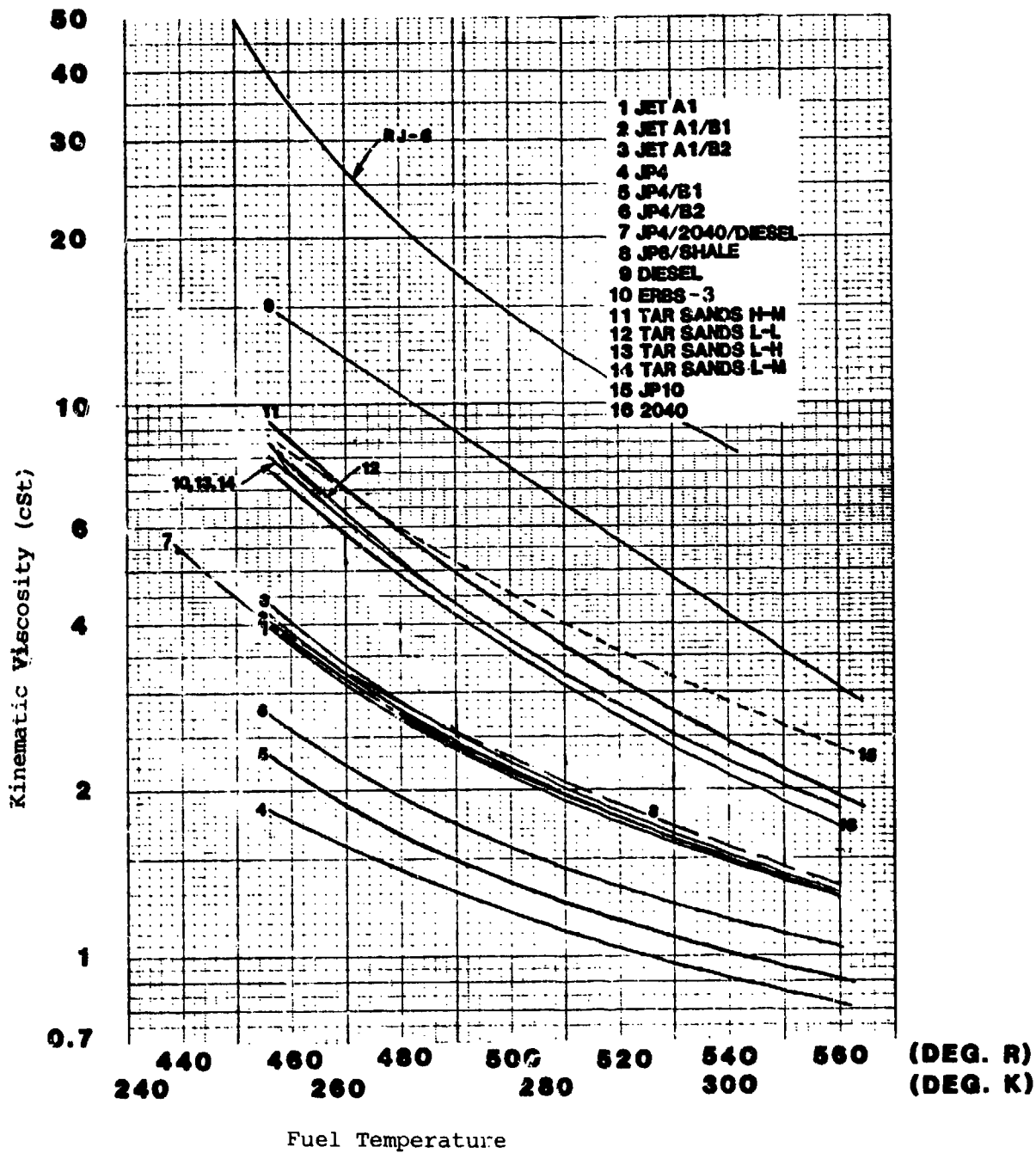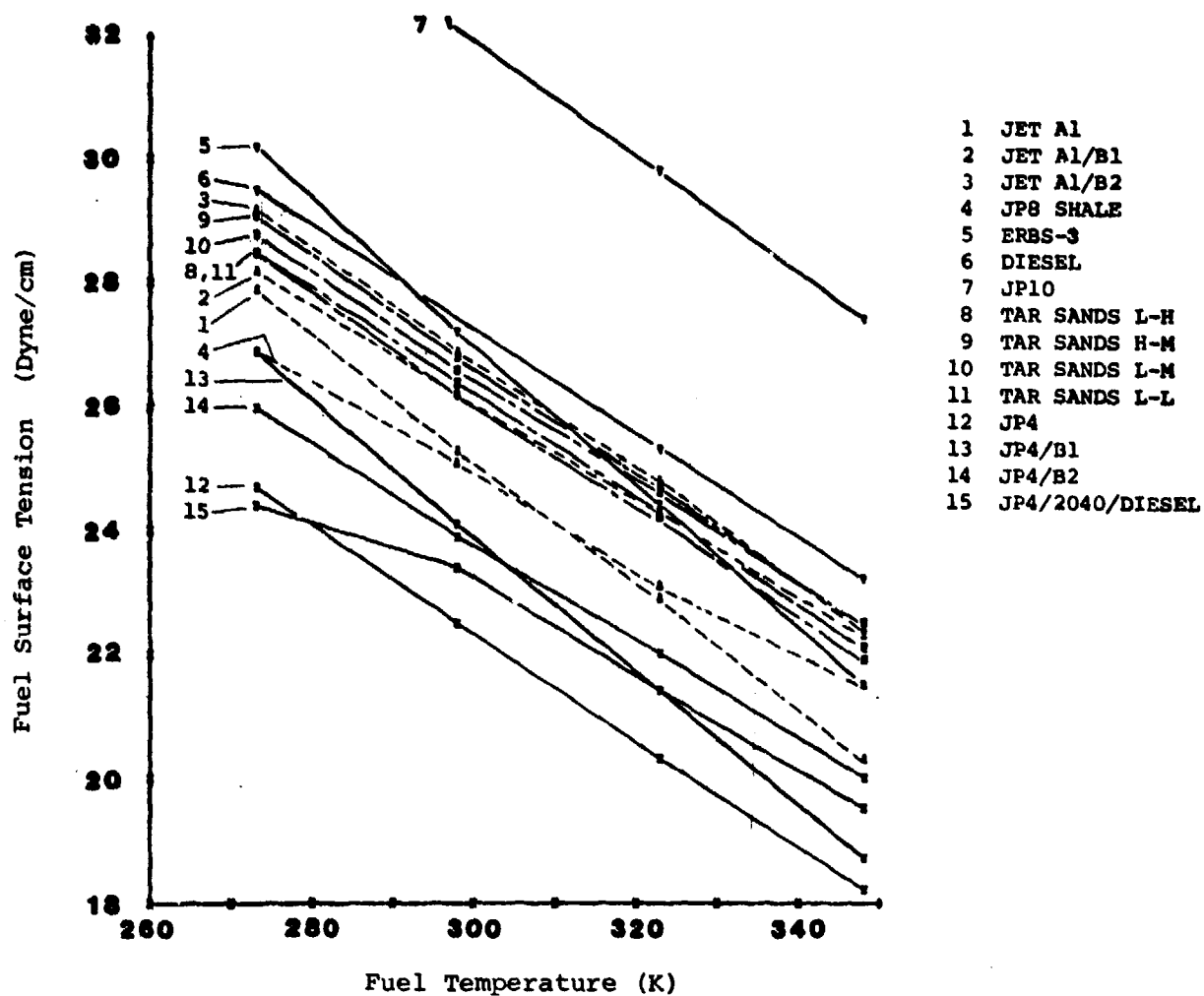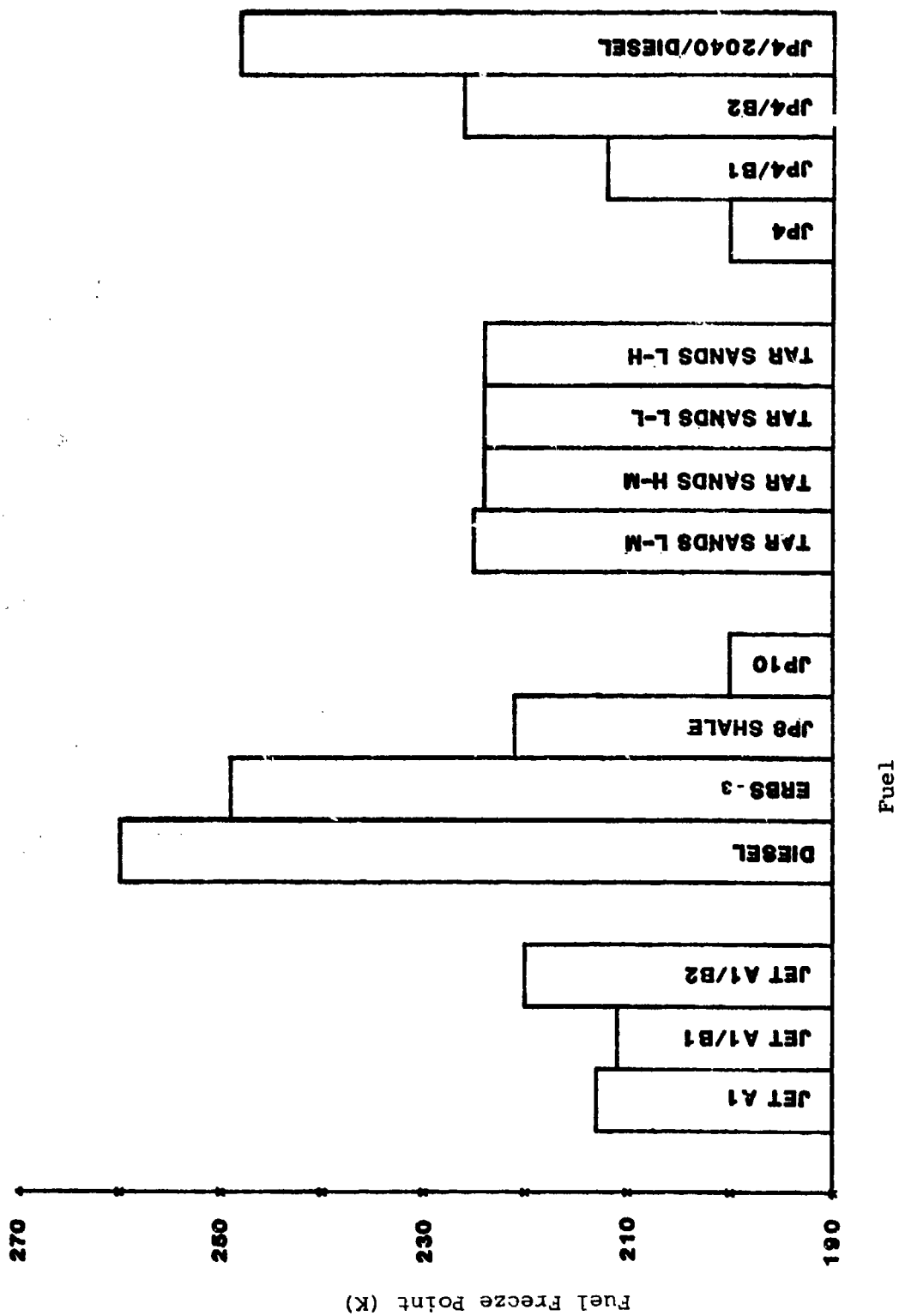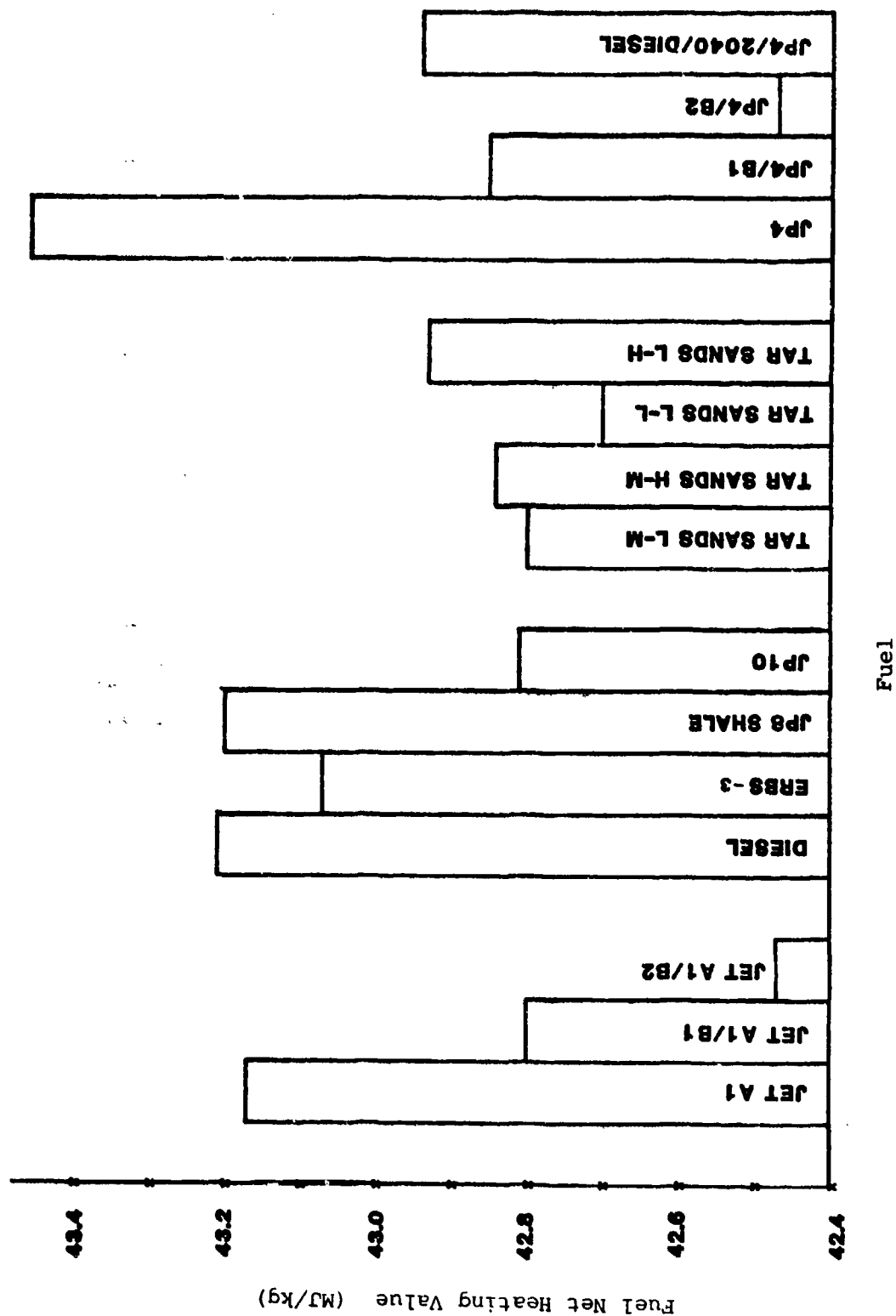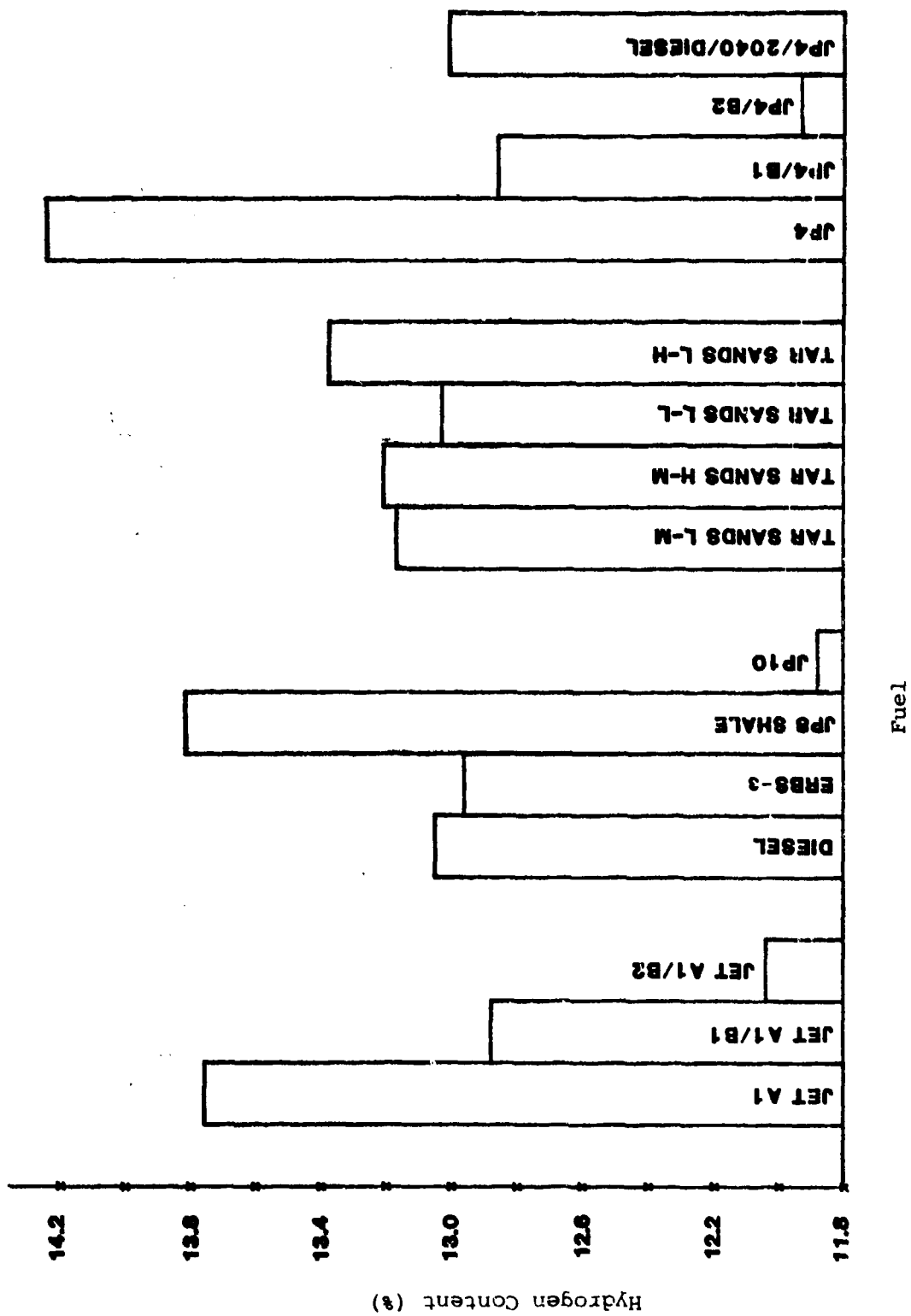In order to minimize costs, a can combustor developed under an EPA sponsored research program[7] was used. The design data for the original combustor is listed in Table 4.1. The combustor was designed such that it accepted any one of four different nozzles, described in a subsequent section.

4.2 CAN COMBUSTOR DEVELOPMENT

In order to test the durability of the can combustor, a thermal paint test was conducted at a condition simulating 100% thrust on the turbofan cycle. Results from the paint test demonstrated unacceptably high metal temperatures in the primary, intermediate, and dilution zones (Figure 4.1). These were attributed to fuel-rich mixture conditions in the primary zone and inadequate liner wall cooling. For this reason, a modification program aimed at increasing the combustor life expectancy was undertaken, using the following approaches:

i) Leaning out the primary zone.

ii) Adding an extra cooling louvre in the dilution zone.

iii) Increasing the amount of cooling air passing through all the cooling louvres.

iv) Relocating the dilution holes further upstream to reduce gas temperatures in the downstream sections.

Further paint tests were conducted simulating the 60% thrust condition to ascertain the integrity of the combustor during each step of the development. Tests with the final configuration were conducted simulating 100% thrust condition. Figures 4.2, 4.3 and 4.4 show temperature patterns for three types of fuel nozzles.

4.3 FINAL COMBUSTOR CONFIGURATION

A schematic representation of the final configuration is shown in Figure 4.5. The combustor performed well through the lean limit tests; however, post-test inspection after some running at full power revealed marginal durability in the primary zone immediately upstream of the igniter plane. It was therefore decided that combustor durability should be further improved by application of thermal barrier coating to the

liner inner wall (Table 4.2). A new can combustor with the thermal barrier coating, provided adequate durability over the balance of the program.

4.4 NOZZLE CONFIGURATIONS

As described earlier in Section II, four types of fuel nozzles were tested: simplex, duplex, airblast and vaporizer. The pressure atomizing nozzle assembly shown in Figure 4.6 is composed of three parts: fuel nozzle adapter (capable of accepting simplex or duplex pressure atomizers), the nozzle, and a swirler which enhances fuel air mixing. The airblast nozzle (Figure 4.7) works on the premise that relatively slow moving fuel is exposed to a high velocity airstream which shears the fuel into very small droplets. Swirler air, which is introduced close to the nozzle face provides for fuel-air mixing and flame stability. The vaporizing nozzle (Figures 4.8, 4.9) is comprised of a tube (exposed to hot primary zone gases) which transfers thermal energy to the incoming fuel and air, thus vaporizing the fuel. The rich mixture then passes through a small swirler before it exits via the mushroom-shaped outlet. Figure 4.10 shows the assembly of the can combustor with the simplex nozzle adapter.

In each case, depending on how much air was used for either atomizing or mixing, the flow splits within the can combustor varied. The amount of air available for wall cooling, primary zone mixing, and dilution depended on the type of nozzle being used. The combustor flow splits for the three fuel systems are shown in Tables 4.3, 4.4, and 4.5.

4.5 CAN COMBUSTOR INSTRUMENTATION

The final step in the combustor preparation was the determination of various thermocouple locations required for metal temperature measurements. Based on results of thermal paint tests, twelve thermocouple locations were chosen, in consultation with AFWAL and CDND program managers, Figure 4.11.

Table 4.1: Summary of Design Data for Original Simple Cycle Gas Turbine Combustor Used in Phase II Test Program

PARAMETERS			
Inlet pressure	MPa (atm)	1.2	(12)
Air flow rate	kg/sec (lbs per sec)	0.50	(1.1)
Fuel flow rate	kg/hr (lbs per hr)	35	(77)
Fuel air ratio	overall	0.0195	
Inlet air temp.	K (R)	700	(1260)
Outlet temp.	K (R)	1311	(2360)
Pressure drop	%	2.6	
Reference velocity annulus	m/sec (ft/sec)	23.3	(76.3)
Reference velocity - flametube	m/sec (ft/sec)	23.8	(78.1)
Number of fuel nozzles		1	
Fuel		JP4	
Liner diameter	cm (in)	6.6	(2.61)
Liner length	cm (in)	14	(5.56)
Liner length PZ	cm (in)	3.38	(1.33)
Liner length IZ	cm (in)	6.78	(2.67)
Liner length DZ	cm (in)	3.84	(1.56)
Liner cross sectional area	cm^2 (in^2)	34.6	(5.37)
Liner volume - total	cm^3 (ft^3)	480	(.0173)
Liner volume - PZ	cm^3 (ft^3)	116	(.0041)
Heat release rate,watts/m^3-Pa(MM BTU/hr.ft^3.atm) (based on total liner volume)		719	(6.95)
Heat release rate,watts/m^3-Pa(MM BTU/hr.ft^3.atm)		3012	(29.1)
Casing Diameter	cm (in)	9.0	(3.55)

Table 4.2: Specifications for Thermal Barrier Coating

TECHNICAL REQUIREMENTS

Coating Material: Shall be as follows:

Coating	Powder Specification	Coating Thickness
Bond	CPW 387 (Alumina)	.003-.005 inch (0.08-0.13 mm)
Surface	CPW 388 (Ytrium)	.010-.012 inch (0.25-0.31 mm)

Equipment: Shall consist of a plasma spray torch using argon, argon/helium, or argon/hydrogen as the powder carrier and/or arc gas. Purity of gas atmosphere shall be as agreed upon by P&WC and vendor.

Procedure: Unless otherwise specified, shall be as follows:

Preparation: Base metal surface to be initially coated shall be thoroughly cleaned free from any prior coating and from dirt, oil, grease, stains and other foreign materials; they shall be cleaned by vapor degreasing or by washing in petroleum solvent and dried. Surfaces to be coated shall be dry abrasive blasted with a suitable coarse non-metallic grit.

Base metal surfaces to be coated shall be preheated to remove moisture and, when desired, to control thermal expansion of the part with respect to coating. Preheat may be accomplished by controlling torch dwell time immediately prior to spraying or by other suitable means. Temperature of part during preheat and subsequent spraying shall be maintained sufficiently low to prevent discoloration, oxidation, distortion and other conditions detrimental to coating or base metal.

SCOPE:

Purpose: This specification covers the procedure for producing a multi-layered plasma spray coating and the properties of the deposited coating.

Application: Primarily to increase oxidation and hot corrosion resistance, and to provide a thermal barrier for combustion chambers and other sheet metal components.

Coating: Dry, free-flowing and thoroughly blended coating material of bond coat shall be deposited as soon as practicable after surface preparation, preferably within two hours.

The surface coating shall be deposited as soon as practicable after completion of bond coat, preferably within two hours of depositing bond coat.

Micro Examination: Coating shall be free from cracks, massive porosity and excessive oxides; it shall be essentially free from inclusions and contamination at the bond coating to base metal interface and the bond coating to surface coating interface. Microstructural standards for acceptance or rejection shall be as agreed upon between P&WC and the vendor.

QUALITY: Coating shall be adherent to base metal and shall have a uniform continuous surface free from spalling, chipping, cracking, crazing, staining or other objectionable imperfections.
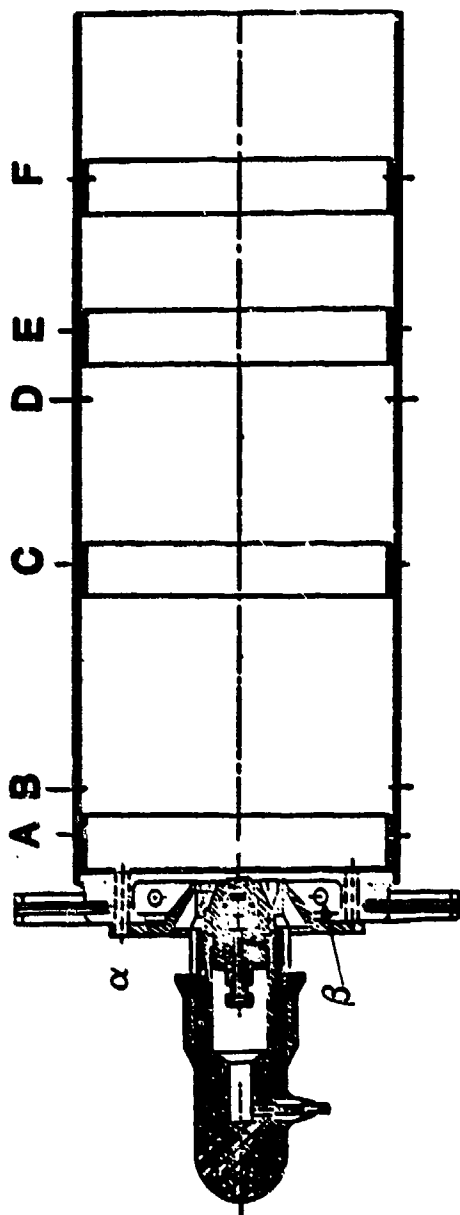
Table 4.3: Can Combustor Airflows (Simplex/Duplex Configuration)

STATION	DIA OF HOLES (IN)	NUMBER OF HOLES	% FLOW
A	.100	24	12.09
B	.089	24	9.58
C	.100	24	12.09
D	.228	16	41.87
E	.089	24	9.58
F	.057	24	3.93
J	.089	· 12	4.79
B	.129	6	5.03
NOZZLE FRONT FACE FLOW			1.04
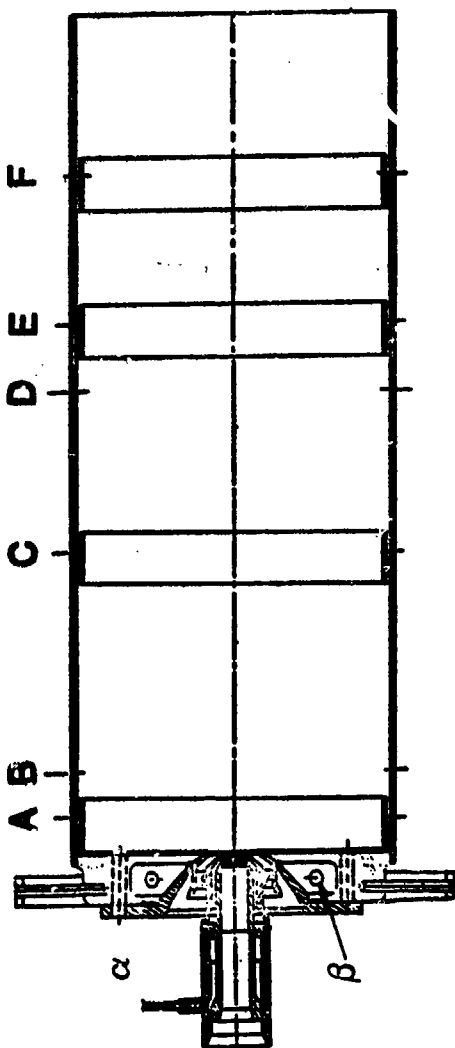
Table 4.4: Can Combustor Airflows (Airblast Configuration)

STATION	DIA OF HOLES (IN)	NUMBER OF HOLES	% FLOW
A	.100	24	11.34
B	.089	24	8.98
C	.100	24	11.34
D	.228	16	39.28
E	.089	24	8.98
F	.057	24	3.68
α	.089	12	4.49
β	.129	6	2.60
AIRBLAST SECONDARY FLOW			4.59
AIRBLAST PRIMARY FLOW			2.60
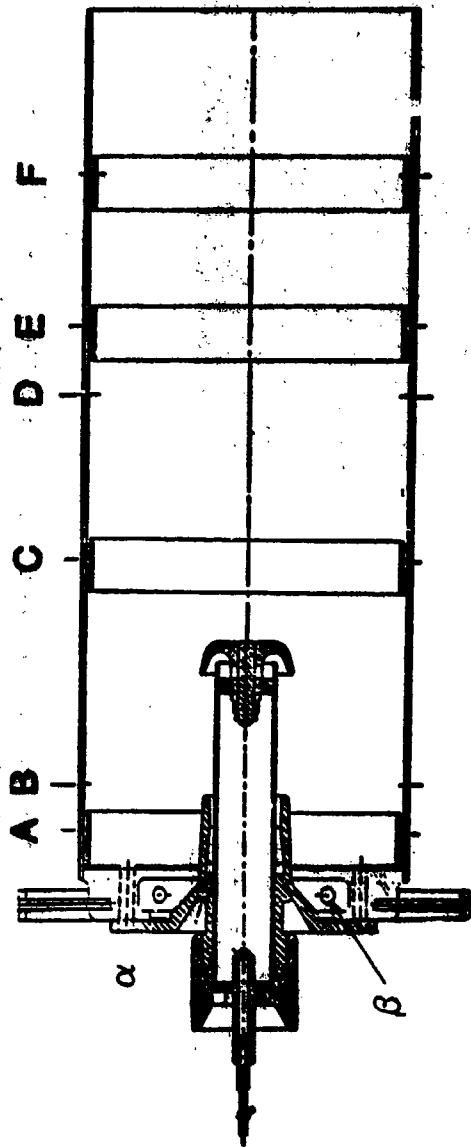
Table 4.5: Can Combustor Airflows (Vaporizer Configuration)

STATION	DIA OF HOLES (IN)	NUMBER OF HOLES	% FLOW
A	.100	24	11.24
B	.089	24	8.90
C	.100	24	11.24
D	.228	16	38.95
E	.089	24	8.90
F	.057	24	3.65
α	.089	12	4.45
β	.129	6	4.67
VAPORIZER SECONDARY FLOW			0.91
VAPORIZER PRIMARY FLOW			7.09

FRONT VIEW

>1550 °F

REAR VIEW

>1500 °F
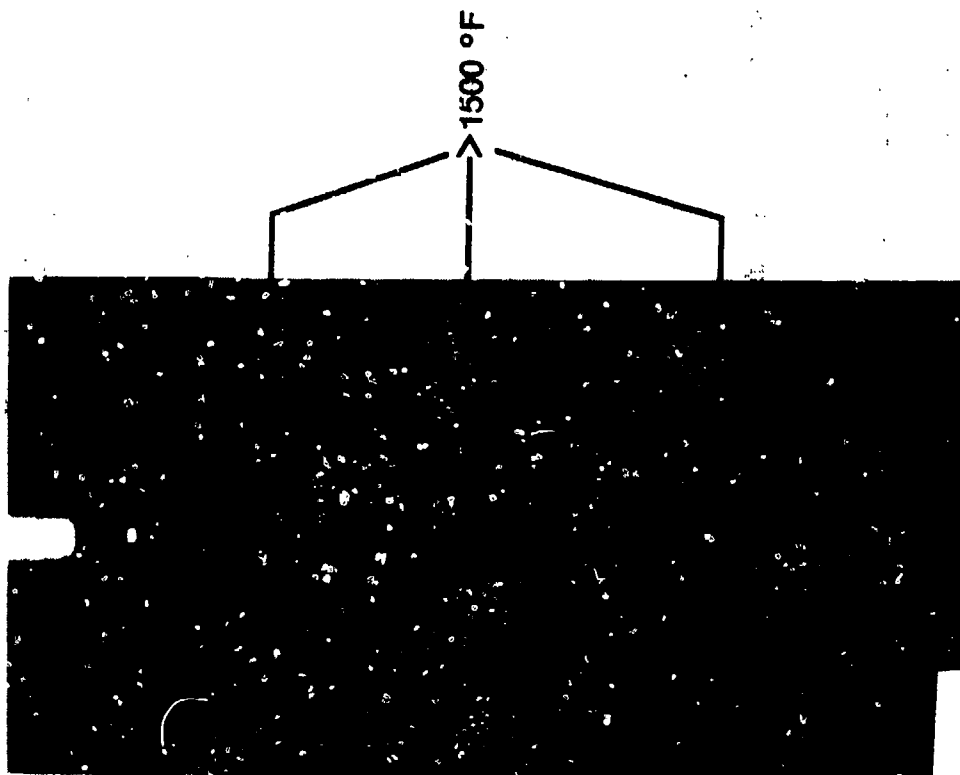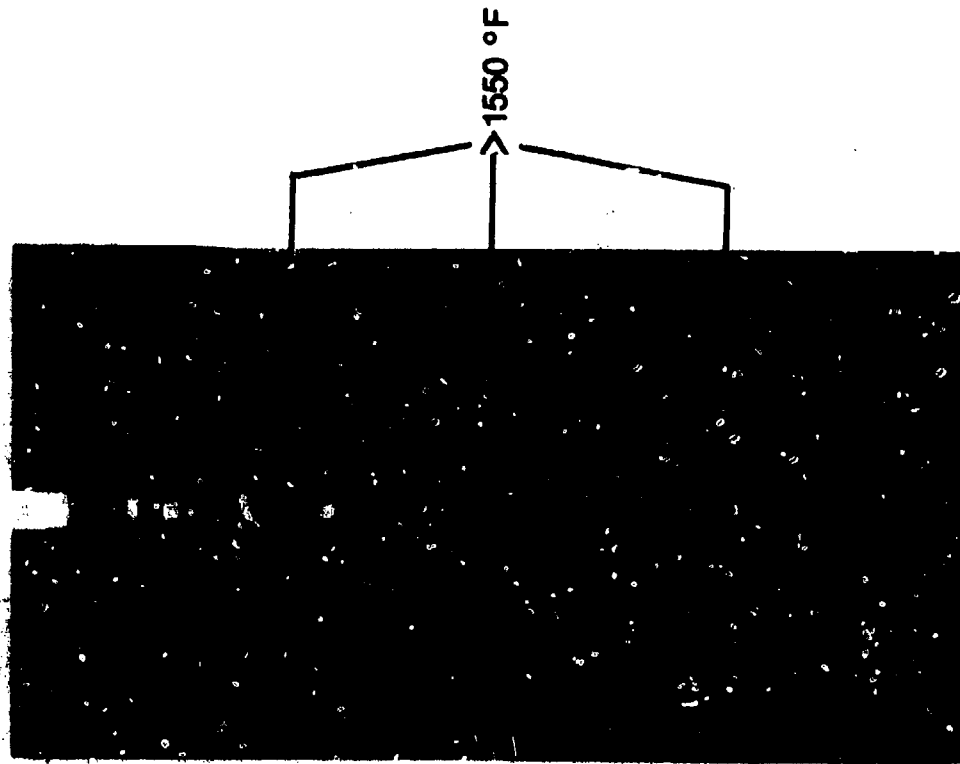
Figure 4.1: Can Combustor Test Simulating 100% Thrust Condition
(Simplex Pressure Atomizer, Original Version)

REAR VIEW

835-980 °F
<835 °F
980-1340 °F
>1340 °F
>1340 °F
>1550 °F
980-1340 °F

FRONT VIEW

835-980 °F
980-1340 °F
>1340 °F
980-1340 °F
>1340 °F
>1550 °F
980-1340 °F
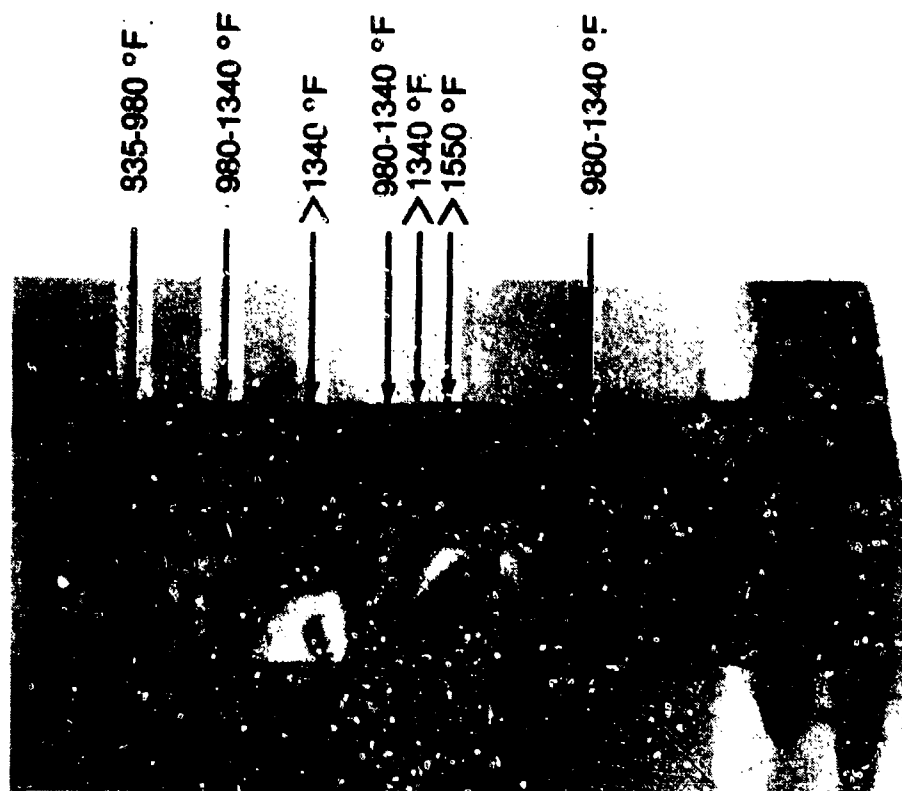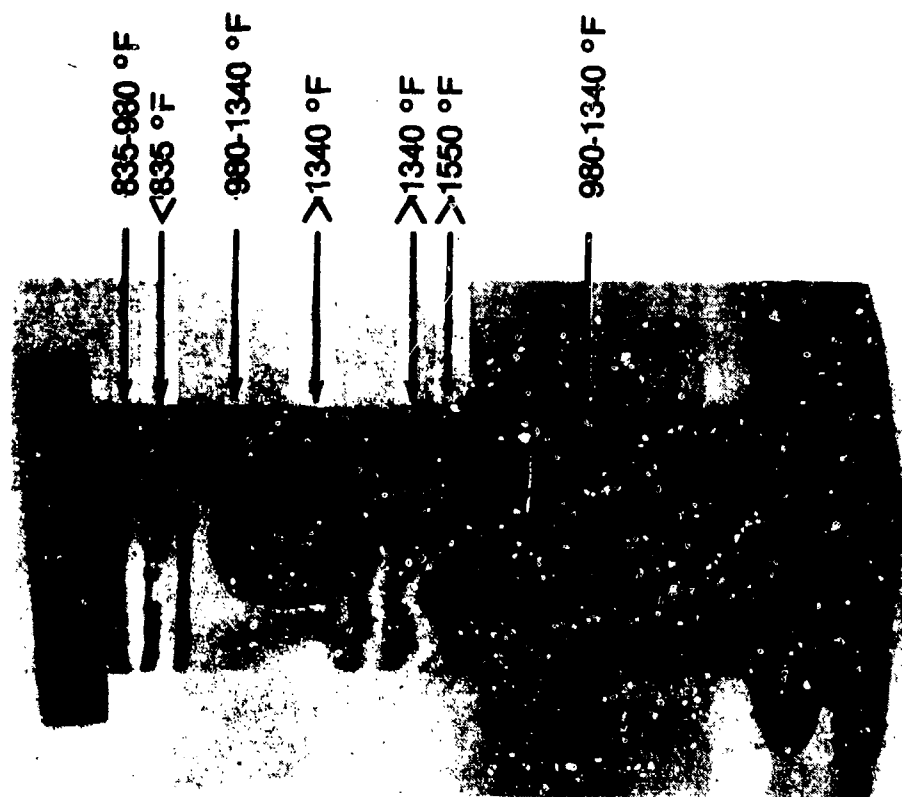
Figure 4.2: Can Combustor Test Simulating 100% Thrust Condition
(Simplex Pressure Atomizer)

- 57 -

REAR VIEW

835-980 °F

>1550 °F

980-1340 °F
>1550 °F
>1340 °F

980-1340 °F

FRONT VIEW

835-980 °F
980-1340 °F

>1550 °F

>1340 °F
>1550 °F

980-1340 °F
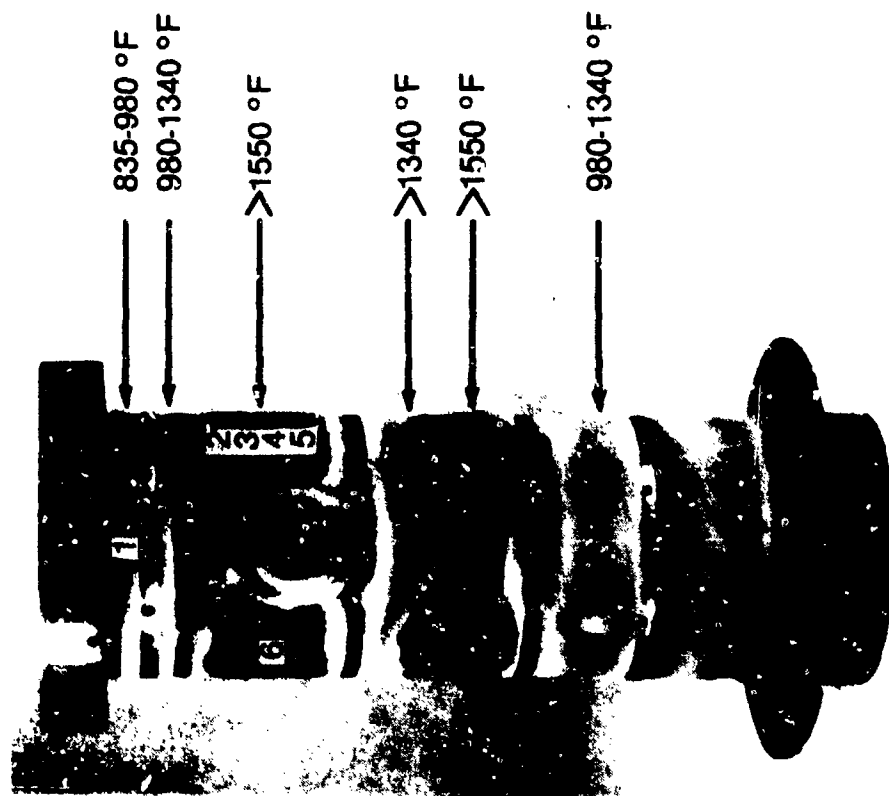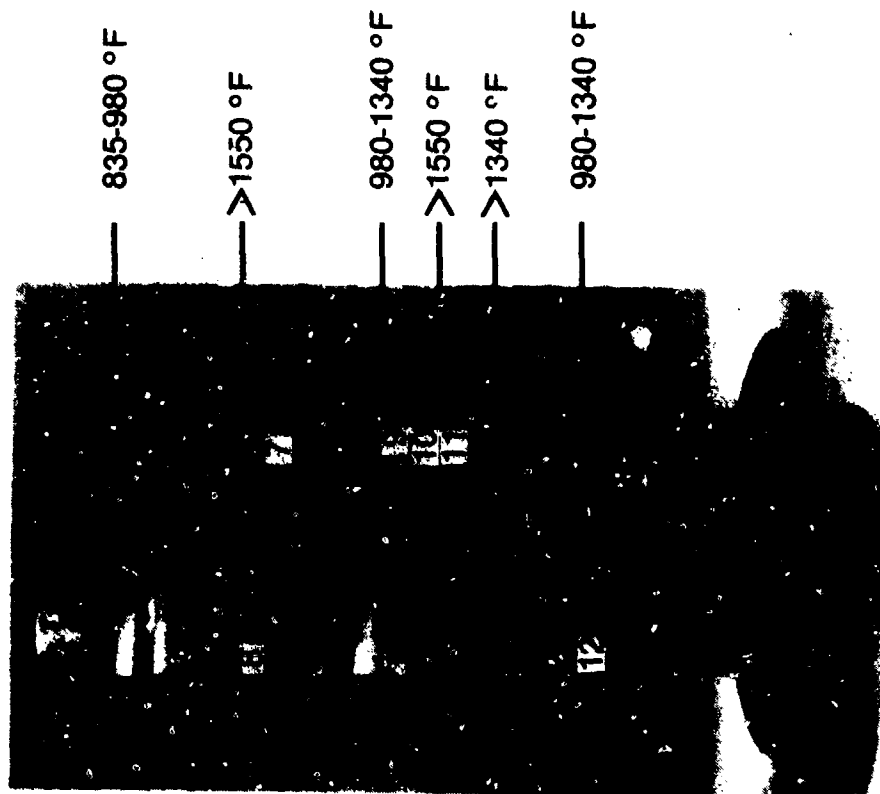
Figure 4.3: Can Combustor Test Simulating 100% Thrust Condition
(Duplex Pressure Atomizer)

- 58 -

REAR VIEW

>1340 °F
980-1340 °F
>1340 °F

>1550 °F

980-1340 °F

>1340 °F

980-1340 °F
>1550 °F

FRONT VIEW

>1340 °F

>1550 °F

>1340 °F

>1550 °F

980-1340 °F
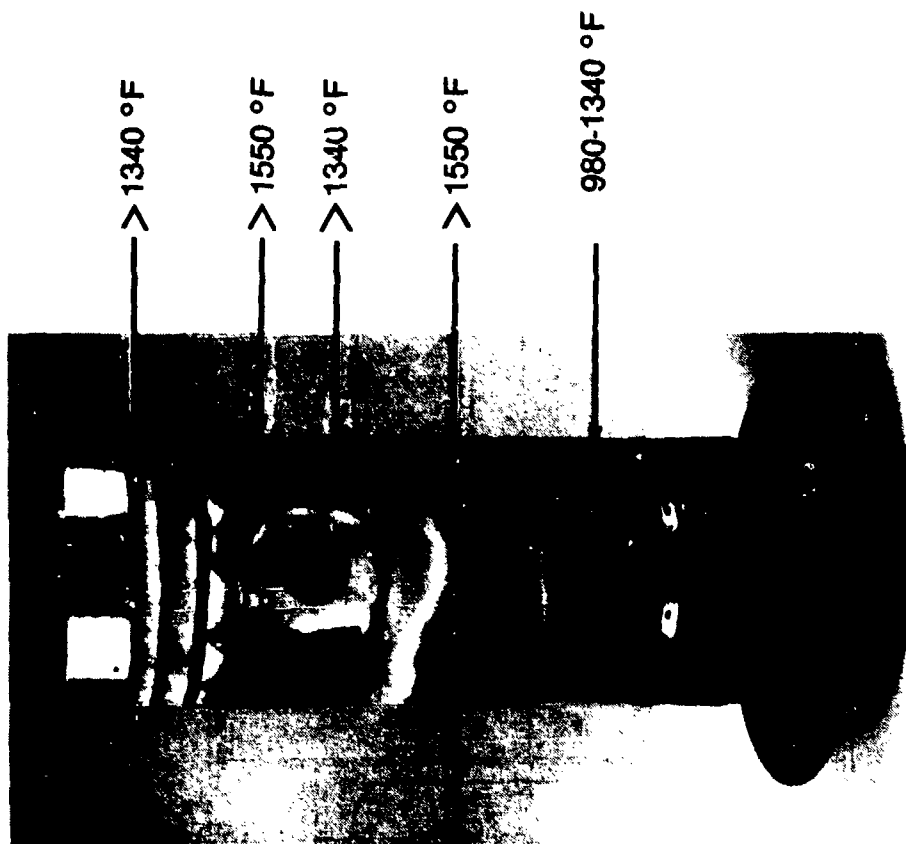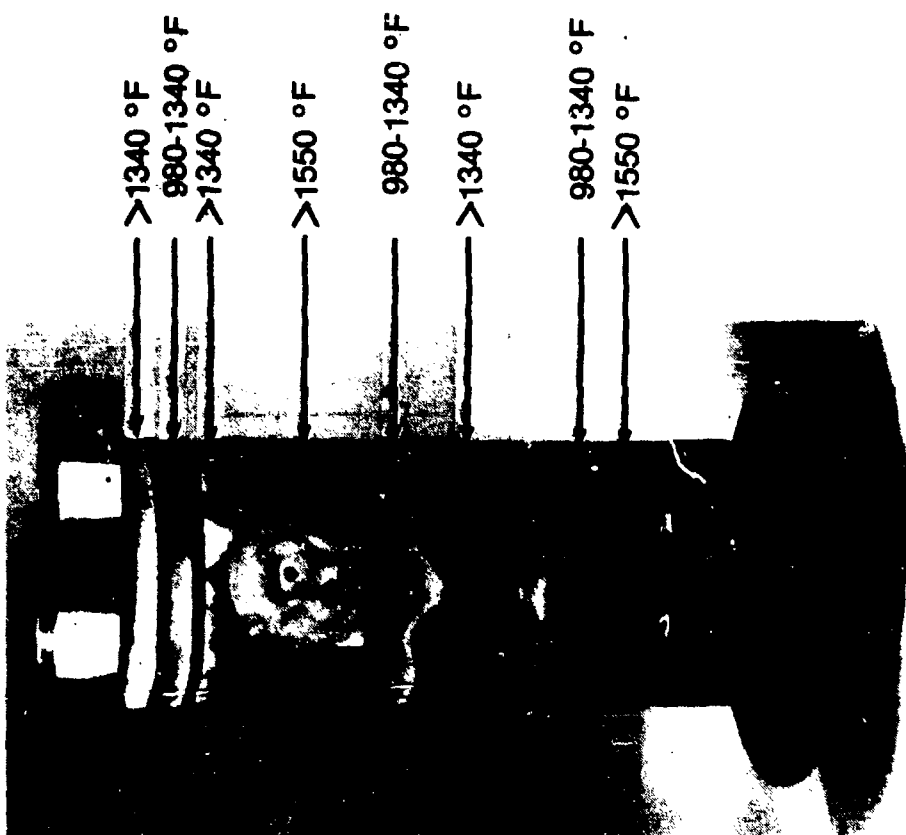
Figure 4.4: Can Combustor Test Simulating 100% Thrust Condition
(Airblast Atomizer)

- 59 -
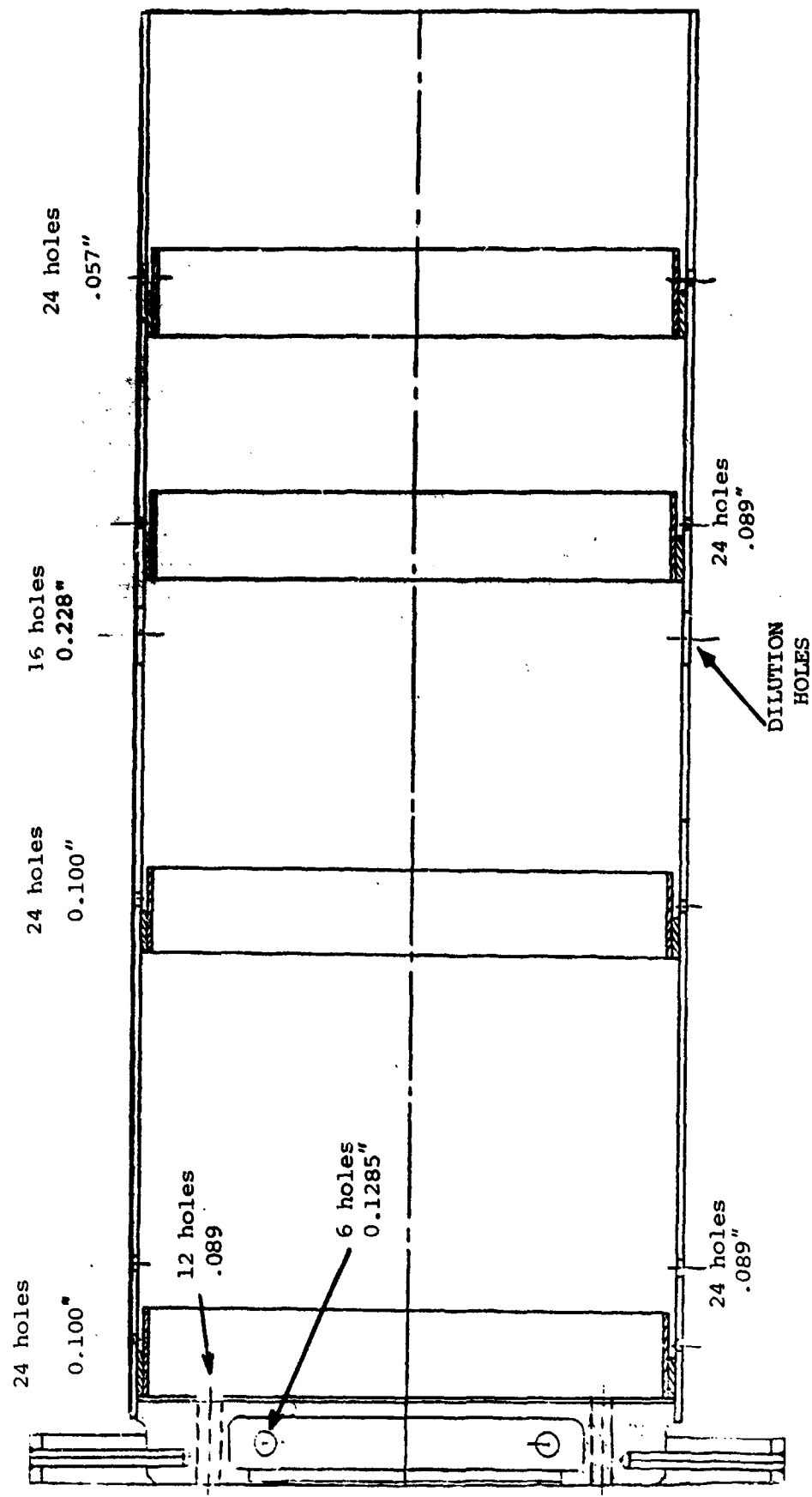
Figure 4.5: Final Configuration of Can Combustor

24 holes .057"

24 holes .089"

16 holes 0.228"

DILUTION HOLES

24 holes 0.100"

12 holes .089

6 holes 0.1285"

24 holes 0.100"

24 holes .089"
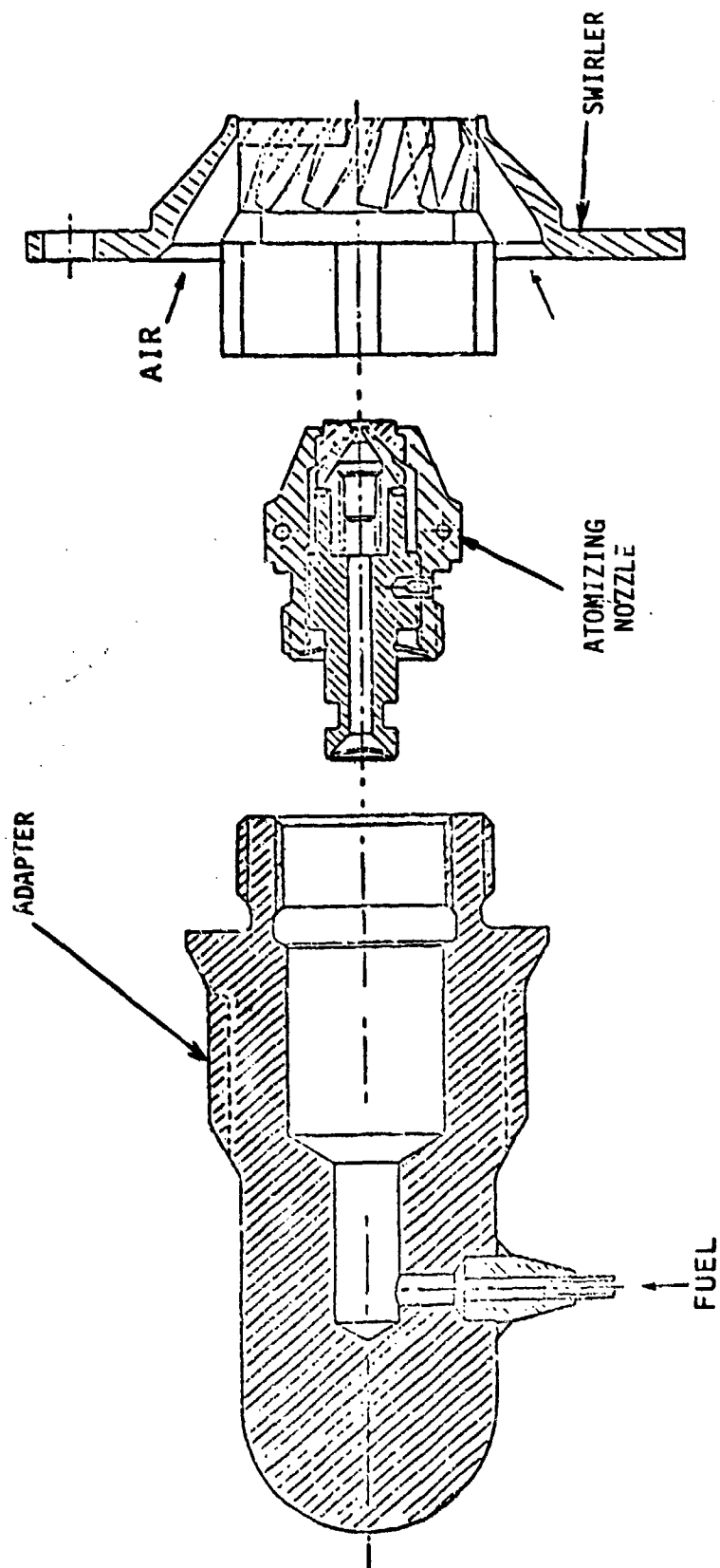
Figure 4.6: Pressure Atomizing Nozzle for Can Combustor Tests

FUEL →

AIR

AIR →
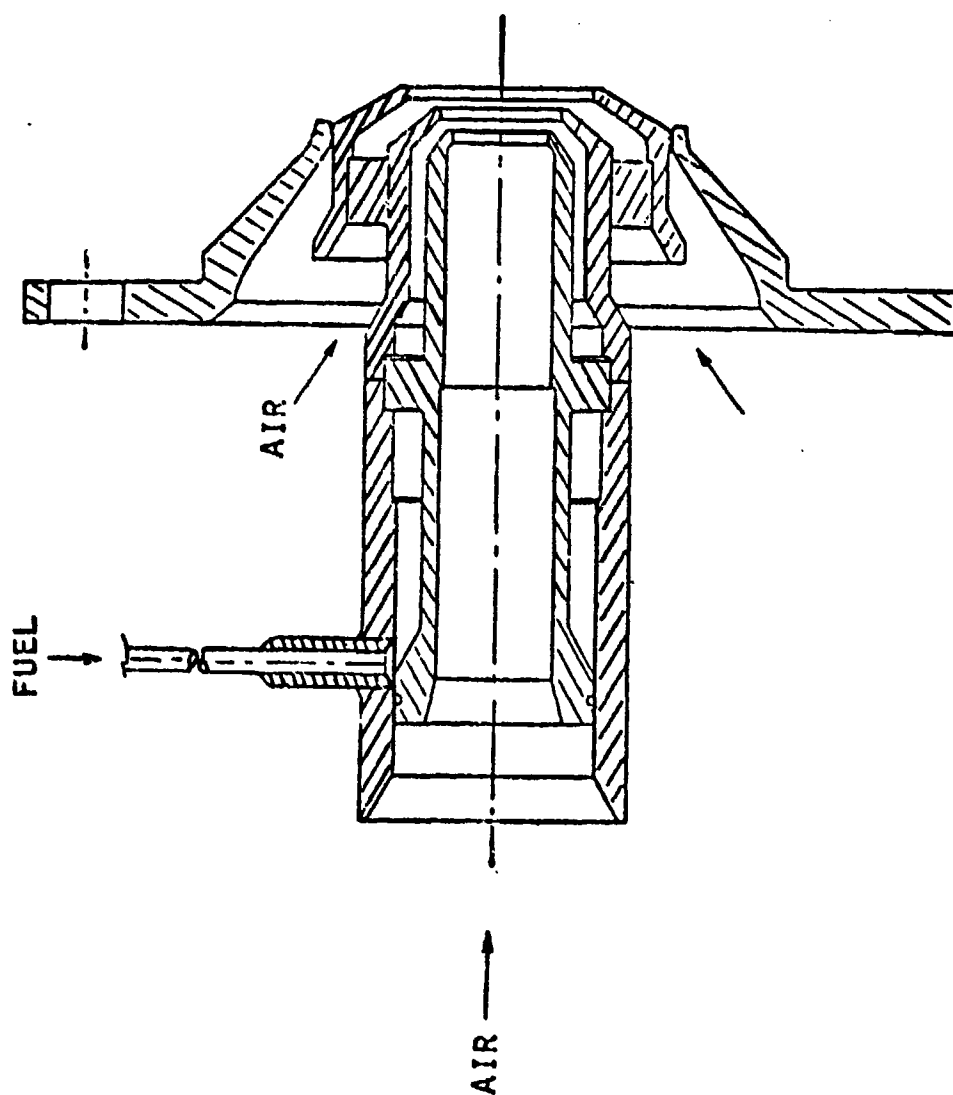
Figure 4.7: Airblast Nozzle for Can Combustor Tests.

Mushroom head with swirler

Air

Air

Air

Fuel

Air
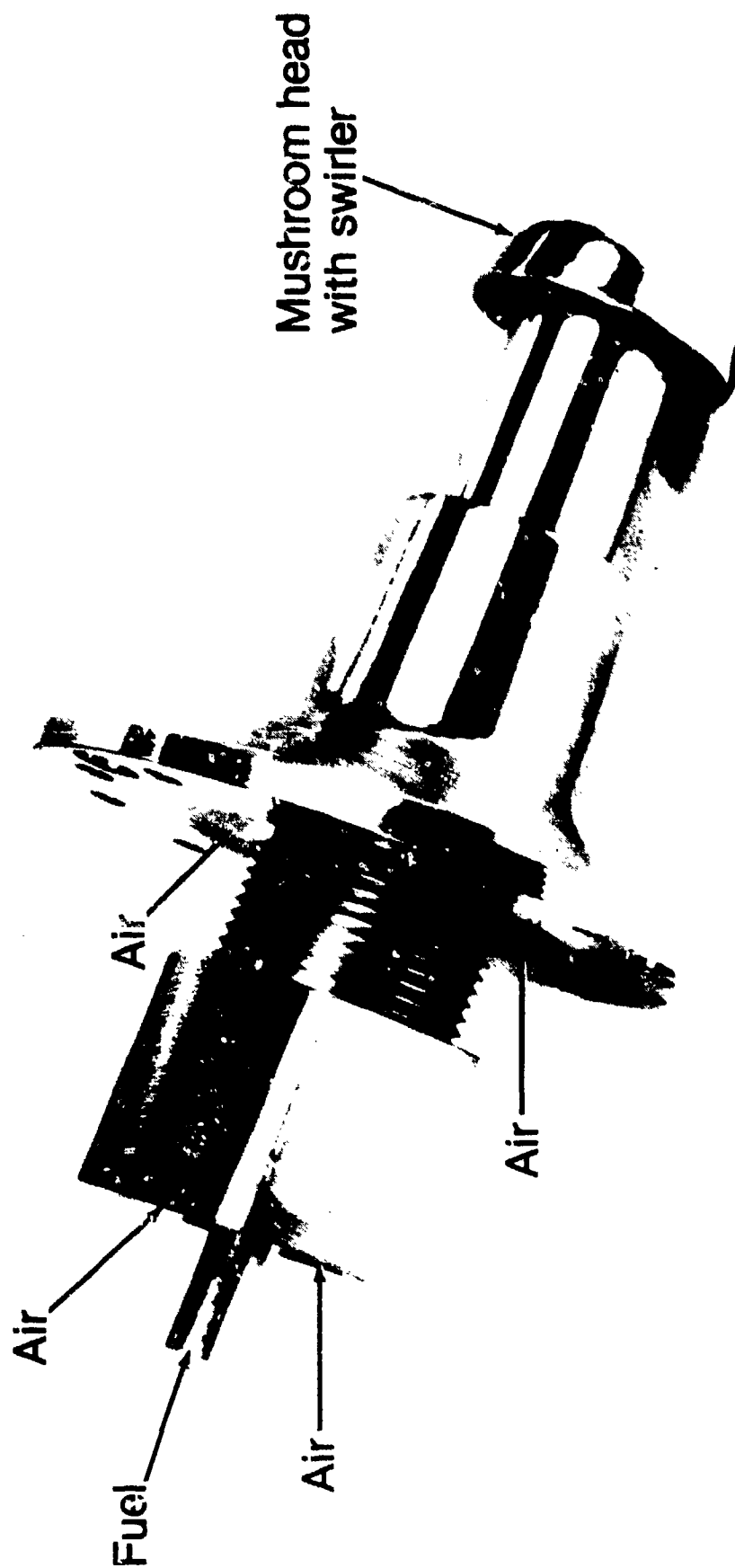
Figure 4.8: Vaporizing Nozzle

- 63 -
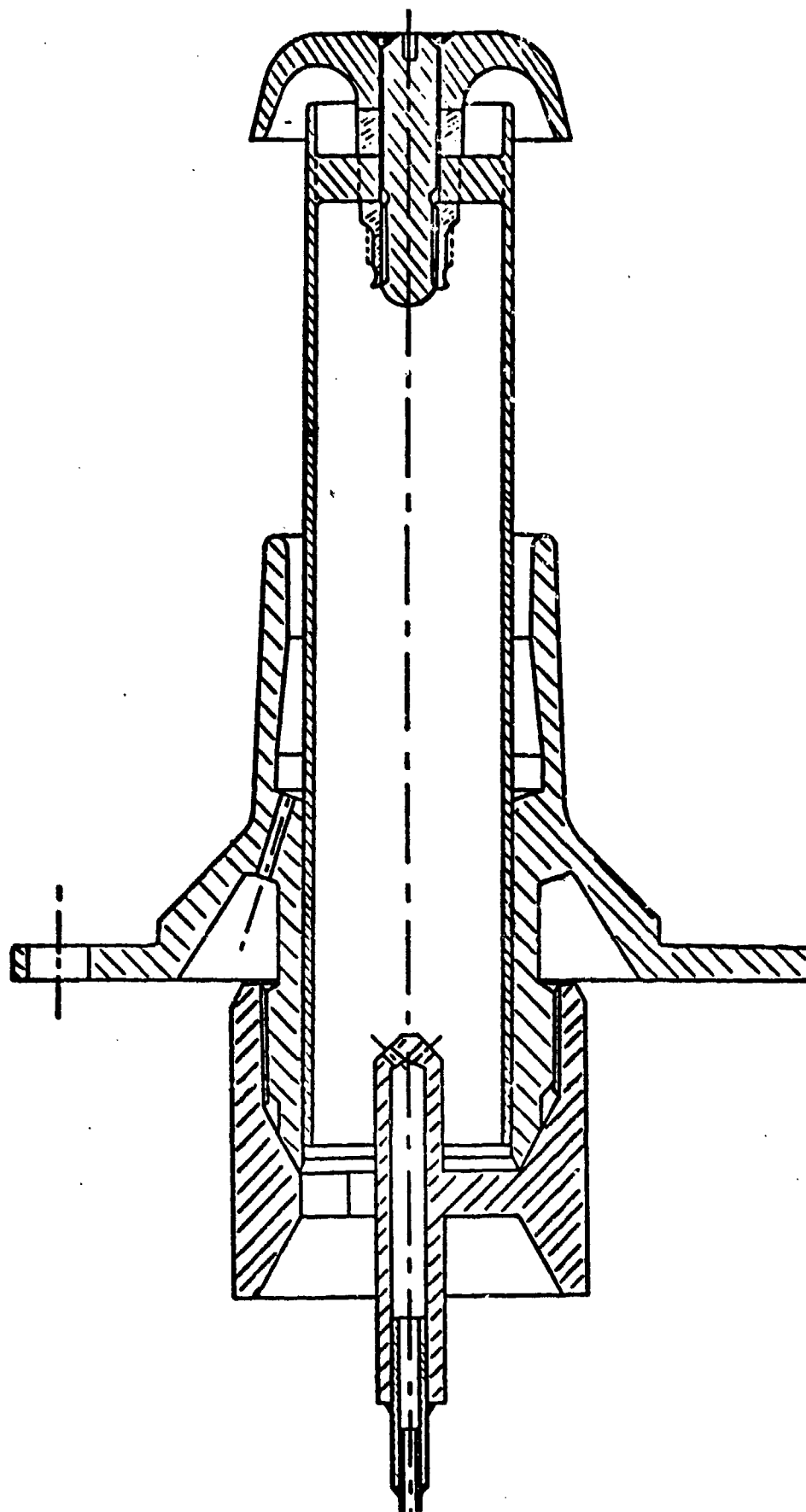
Figure 4.9: Vaporizing Nozzle for Can Combustor Tests
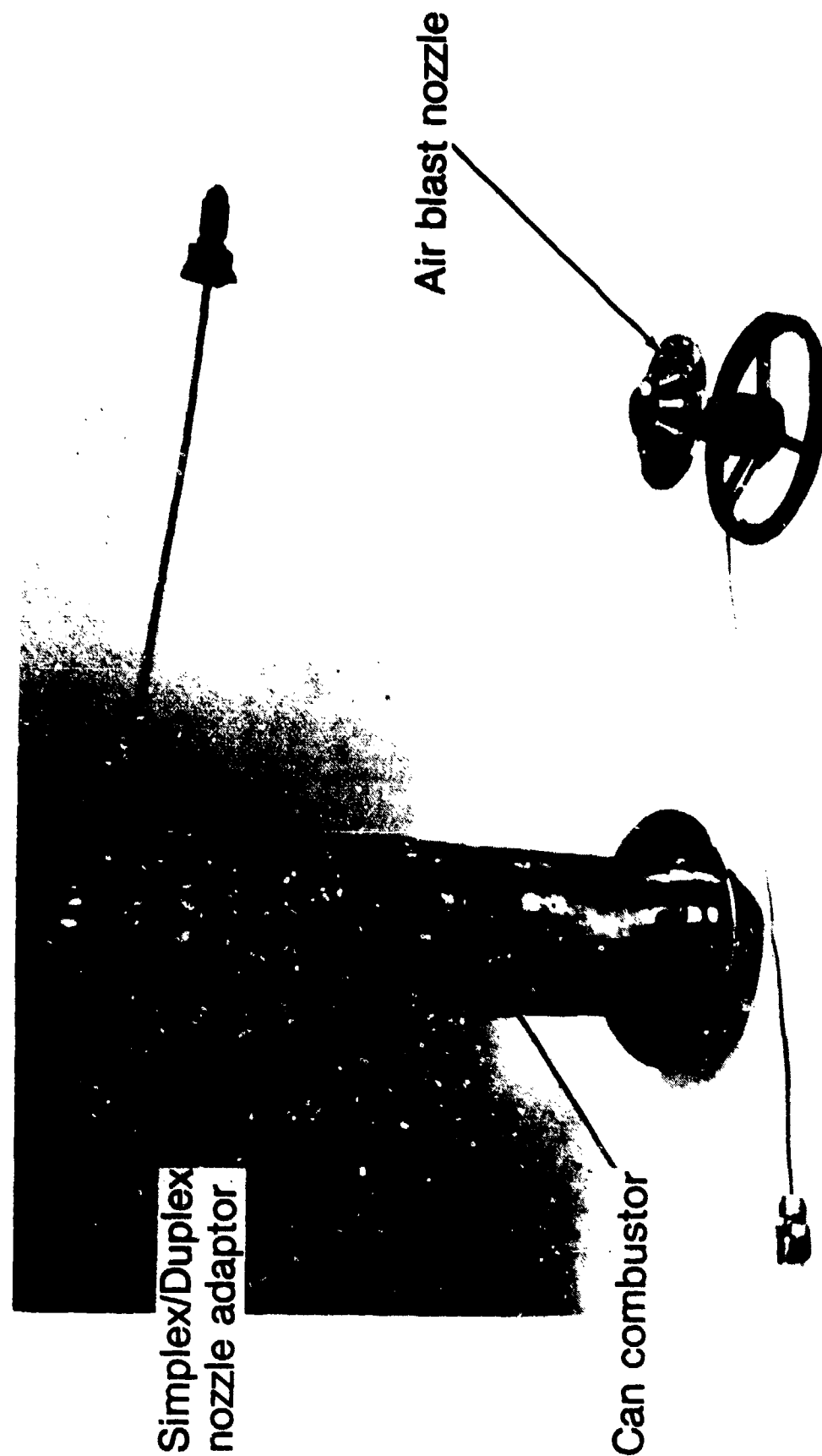
Figure 4.10: Combustor and Fuel Nozzle Configurations

Air blast nozzle

Simplex/Duplex nozzle adaptor
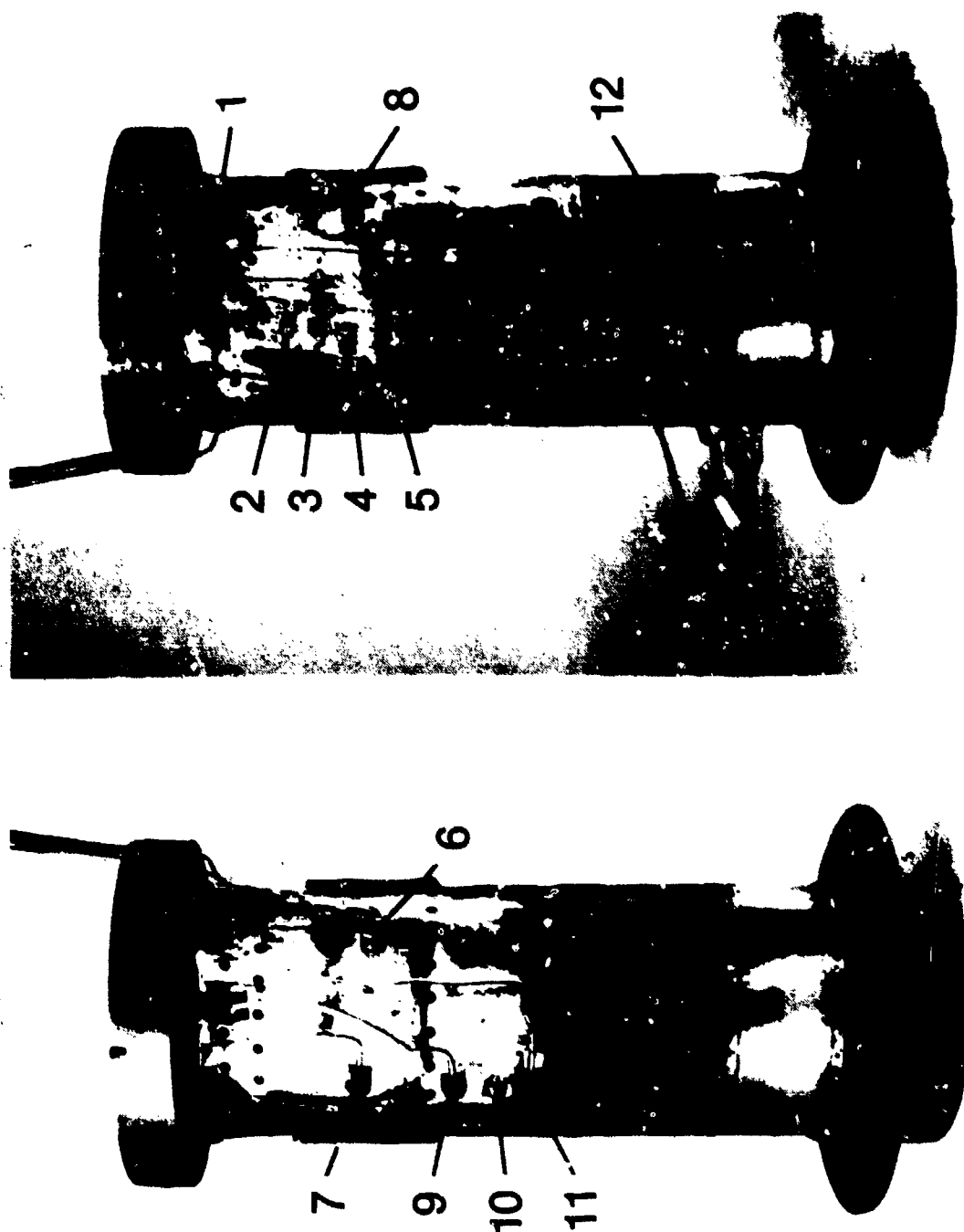
Can combustor

Figure 4.11: Can Combustor Showing Thermocouple Instrumentation

SECTION V

APPARATUS AND PROCEDURES

The test facilities and techniques used in evaluating fuel property effects on can combustor performance are described in the following paragraphs. Two rigs were used: steady-state and lean-limit tests were conducted in the high-pressure can-combustor rig located in P&WC's facilities in Longueuil, Quebec, while cold start tests were conducted in the atmospheric-pressure can-combustor rig located in Mississauga, Ontario.

5.1 HIGH PRESSURE COMBUSTOR RIG

5.1.1 GENERAL LAYOUT

The can combustor rig shown in Figures 5.1 & 5.2 was used for performance, lean limit, parametric, and carbon deposition tests. The air system (Figure 5.3) was fed by a 0.72 MPa (6.1 atm) shop air supply. Further compression to 1.68 MPa (15.6 atm) was achieved by way of a rotary boost compressor. The oil separator and sterling air filters served to remove oil, water and other foreign particles; however, should any blockage occur due to oil contamination, a differential pressure switch trips the compressor and heater. A separate shop air supply was available which feeds air downstream of the Sterling filters when pressures less than 0.72 MPa were required. A "coalescing type" air filter located downstream of the second shop air inlet ensured further oil removal and was equipped with an automatic drain valve which dumped the oil to a container. This container was equipped with a level switch which tripped the compressor and heater should a large volume of oil be accumulated.

The air was passed through an electrical heater which raised temperatures up to 700K (1260°R). A pneumatically operated bypass valve downstream of the heater ensured minimum heater flow requirements (0.23 kg/s). Air from the heater passed into the test section via a metering section which consisted of a standard ASME square-edged orifice and upstream and downstream pressure taps. Screens located downstream of the metering section served to straighten the flow before it reached the test section.

A schematic of the test section is shown in Figure 5.4. The instrumentation section downstream of the can combustor was water-cooled as were the radiation and emissions probes. A quartz window located on the instrumentation section permitted direct observation of the flame inside the combustor. A remotely operated butterfly valve back-pressured the entire air system and provided for pressure and flow rate control through the test section.

Combustor inlet and outlet pressures were measured using static pressure taps while temperatures were recorded from Type K thermocouples. Metal temperatures were measured using twelve Type K thermocouples as described earlier.

Fuel flow rates were measured with calibrated turbine flowmeters (low and high flow ranges) and with a wide range rotameter (corrected for specific gravity at test temperature).

5.1.2 GAS ANALYSIS AND SMOKE METER

Emission samples were collected using a five point multi-purpose exhaust probe (Figures 5.5 and 5.6) which was located 5.5 inches downstream of the combustor exit plane. Exhaust pressure and temperatures were also measured using this probe. The water cooled probe was mounted on an actuator which enabled probe retraction from the air stream during rig start-up. Emission gases were routed to a Beckman Emission Analy er through heated lines. The analyzer measured emissions with the follow instruments:

CO, CO_2 - Infrared Analyzers
THC   - Flame Ionization Detector
NO, NO_x - Chemiluminiscent Analyzer

Smoke samples were collected with a smoke meter conforming to EPA specifications [10]. Smoke samples were analyzed and converted to smoke numbers using a Photovolt reflection meter.

5.1.3 RADIOMETER PROBE

Flame radiation in the primary zone was measured using a P&WA developed transpiration radiometer probe (Figure 5.7). The probe was used to measure thermal radiation at the combustor liner without interference from convective or conductive heat transfers. The porous disc at the tip of the probe provided an outlet for the pressurized nitrogen purge gas. When the gas filtered through the porous disc, it served to destroy the hot boundary layer which would normally transfer heat through convection. At steady-state, the heat transferred from the porous disc to the nitrogen gas would be a measure of the heat radiated from the flame to the disc. To eliminate heat conduction between the porous disc and its support, a water-cooled sleeve was provided which prevented the edge supports from becoming too hot. Differentially connected thermocouples measured the net temperature difference between the nitrogen gas just upstream of the disc and the disc itself. If the gas flow rate was known, it would be possible to undertake an energy balance and obtain a net radiative heat flux. A careful calibration of the probe provided empirical constants required to make the energy balance. All relevant parameters were recorded using an automated data quisition system which batched the input to the main computer for analysis. Flame radiation was measured for selected parametric test points only, as described in paragraph 5.1.6.

5.1.4 LEAN LIMIT TEST PROCEDURES

The lean limit tests for each fuel covered four airflows at a combustor inlet temper ure corresponding to a JT15D-4 idle condition (375K). Inlet pressures during the tests were kept constant at 4 atmospheres

while the airflow range was 0.1 to 0.23 kg/s. The top end of the airflow range corresponded to a simulation of the ground idle condition of the turbofan engine cycle (based on air loading parameter). Set-up conditions are listed in Table 5.1.

The procedure for lean limit tests was quite simple. For each airflow, a steady operating condition was first set up corresponding to a fuel-air ratio of 0.015. The fuel flow was then gradually reduced until flame-out and the corresponding flow rates were recorded. The test was then repeated until a consistent lean limit fuel-air ratio was established. The duration of each test was kept nearly constant, of the order of 3 minutes. All fifteen fuels were tested with the simplex nozzle, while six fuels were tested with duplex, airblast, and vaporizing nozzles, resulting in a total of 33 fuel/nozzle combinations (Table 2.5).

5.1.5 STEADY STATE PERFORMANCE TESTS

Steady state performance tests were undertaken simulating both turbofan and turboprop operating cycles. The following performance parameters were measured - combustor metal temperatures, combustion efficiency, gaseous emissions, smoke emissions, carbon formation, fuel nozzle fouling and liner pressure drop. Fuel nozzle effects were evaluated by undertaking turbofan cycle tests on all four nozzle types - simplex, duplex, airblast and vaporizer. Turboprop cycle tests were done with simplex nozzles only (see Table 2.5).

Thrust level tests simulated the following operating conditions of JT15D-4 turbofan engines. Idle, 30%, 60%, 90% and 100% thrust. Rig set-up (air & fuel flow) conditions were determined from the modelling parameters discussed in Section II. Set up parameters are listed in in Table 5.2

The schedule for thrust level tests was to operate for 30 minutes at each of conditions 1, 2 and 3 and 15 minutes at conditions 4 and 5. After reaching condition 5, the conditions were repeated in the descending mode, i.e. 15 minutes at condition 4 and 30 minutes in conditions 3, 2 and 1. These represented a total of 3.7 hours of continuous running to establish any trends in carbon formation and fuel nozzle fouling. Carbon tests were performed for all fuels with the simplex nozzle, and for six fuels with the other nozzles.

Power level tests simulated the following operating conditions of PT6A-41 turboprop engine - idle, 60% and 100% power. Rig set-up (air and fuel flow) conditions were determined from modelling parameters discussed in Section II. Set-up parameters are listed in Table 5.3.

A schedule similar to thrust level tests was used on the power cycle. The 2.5 hour continuous running was comprised of 30-minute segments at idle, 60%, 100%, in the ascending mode and 30-minute segments at 60% and idle in the descending mode. Comparison of performance on the power cycle was made for the simplex nozzle with 15 fuels.

5.1.6 PARAMETRIC TEST PROCEDURE

In order to study the effects of varying inlet pressure (P_3) and fuel-air ratio, parametric tests were conducted. To provide the most relevance to other tests simulating engine operation, these parametric tests were bracketed around a condition simulating a medium thrust level, namely the JT15D-4 cruise at an altitude of 30,000 feet and a speed of 0.7M.

Three tests were done varying P_3 alone, both upward and downward, while keeping everything else constant. Three more tests were conducted while varying the fuel-air ratio up and down. At each of the six conditions, emissions (CO, THC, NO, NO_x), smoke, metal temperatures, and primary zone radiation measurements were taken. The test parameters are listed in Table 5.4. Fifteen fuels were tested with simplex nozzle while six fuels were tested with duplex, airblast and vaporizing nozzles for a total of 33 fuel/nozzle combinations.

5.1.7 CARBON DEPOSITION AND FUEL NOZZLE TEST PROCEDURE

In order to obtain data on carbon deposition, certain steps were taken to measure the carbon thickness on various parts of the can combustor. In addition, checks were also made on the spray condition of the fuel nozzles. As mentioned previously, continuous running periods of 3.7 and 2.5 hours were accomplished during the thrust level and power level tests respectively. After each run, the rig was split and the following steps were taken:

a. carefully disassemble fuel nozzle assembly
b. pump fuel through nozzle and make visual check for fuel spray streaks
c. make visual carbon checks on can combustor liner
d. measure maximum carbon thickness, if any, on front face of fuel nozzle using a vernier
e. take photographs of carbon accumulation

Carbon deposition checks were done for all fifteen fuels with simplex nozzle and six fuels with duplex , airblast and vaporizing nozzles.

5.2 ATMOSPHERIC PRESSURE COLD START TESTS

Cold start tests were conducted using the can combustor to establish starting capabilities of seven fuels. The purpose was to determine the minimum light-off fuel-air ratio at several temperatures in the range of 242K (435°R) to 289K (520°R).

Cold start tests were conducted in P&WC's facilities in Mississauga. Air and fuel temperatures down to 242K (435°R) were required for these tests, and the equipment, instrumentation and procedures used are described in the following sections.

5.2.1 EQUIPMENT AND LAYOUT

A layout of the cold start rig is shown in Figure 5.8. Ambient air was drawn through the test section by means of an ejector located in the exhaust stack, which operated off a 11 atm. (150 psig) air supply. The air was cooled through a refrigerator as well as a secondary heat exchanger which used dry ice/alcohol as the coolant. Temperatures down to 242K (435°R) were obtained with this facility for combustor airflows up to 0.08 kg/s. The airflow was metered by an ASME standard orifice located upstream of the test section. A pictorial view of the cold start test facility is shown in Figure 5.9. A quartz window in the exhaust elbow was used for flame visualization and start-up detection.

The fuel system used for cold start tests was "custom made" for the task. Figure 5.10 illustrates the flow path: test fuel was pumped from the tank through a filter and through two recirculation loops which both returned to the tank. The first loop circulated fuel from the tank to the fuel cooler and back to the tank, thus accomplishing the bulk of the heat transfer. The coolant used in the fuel cooler was the same dry ice and alcohol mixture used for the secondary air heat exchanger described earlier. While the fuel circulated through this primary loop, fuel was also circulated through the secondary loop, flowing from the tank through the secondary heat exchanger, a flowmeter, and a metering valve back to the tank. The secondary heat exhanger used shop air to make finer adjustments to the fuel temperature. Once the flow rate and temperature were set, two solenoid cut-off valves redirected the fuel flow to the test section. A bypass nozzle in the tank return port assured similar resistances in the bypass and test modes to minimize changes in fuel flow rate when transition occurred.

The combustor configuration for cold start tests was the same as that used in the high pressure can combustor rig. Originally, both simplex and airblast nozzles were to be tested; however it was found that the airblast nozzle was impossible to light at the low airflows and pressures used during the tests. It was therefore decided that two simplex pressure atomizers with 0.9 and 3.0 flow numbers would be tested, thus evaluating the effect of fuel droplet size on ignition performance (0.9 FN corresponded to the primary of a duplex nozzle while 3.0 FN corresponded to a simplex fuel nozzle).

- 71 -

The igniter used for these tests was a standard PT6A-65 igniter which was mounted flush with the inner combustor wall. The spark energy for this type of igniter is approximately 2 joules, at one spark per second.

5.2.2 COLD START RIG INSTRUMENTATION

Cold start tests, as opposed to steady state tests, require accurate measurements of transient conditions. The instrumentation schedule is thus very important. A schematic of the cold start instrumentation is shown in Figure 5.11.

The air mass flow rate was measured using a standard ASME orifice plate. The static upstream and downstream pressure taps were connected differentially to a water manometer.

A strip chart recorder was used to measure transients such as inlet air and fuel temperatures, fuel flow rates, fuel pressure, and exhaust temperature. The calibrated turbine flowmeter provided accurate fuel flow rates in the range of 4.5 to 41 kg/hr (10 to 90 pph). The chart recorder gave accurate measurements of time to light.

A video and audio record was made for each test. The video camera was oriented such that excellent flame pictures were produced. In addition, during light-up tests, the test engineer called out the test number, fuel flow and time to light. These were recorded, along with the video image, on video tape.

A complete log of all relevant information was made by the rig operator. These parameters included fuel and air inlet temperatures and pressures, air and fuel flows, exhaust temperature, and time to light.

5.2.3 COLD START TEST PROCEDURE

A special procedure was devised for undertaking the cold start tests, Table 5.6. The procedure described is the final version arrived after several trial runs with the cold start rig. It was designed to produce minimal set-up times and accurate, repeatable results. Seven fuels were tested: Jet A1, Jet A1/B2, JP4, JP4/B2, ERBS-3, Tar Sands L-H, and JP10. Furthermore, two nozzles were tested with each fuel: 0.9 and 3.0 flow number.

The purpose of these tests was to establish the minimum fuel air-ratio (far) that permits ignition at 3.9K (7°R) intervals between 289K (520°R) and 242K (435°R). A maximum fuel flow was chosen as 5.4 kg/h (12 pph)corresponding to a far of 0.065. If light-up did not occur at maximum fuel flow, a "no-light" condition was assumed for that specific temperature. The idea was to pinpoint the lowest temperature at which light-up would occur without exceeding the maximum allowable fuel flow. The test parameters are listed in Table 5.5.

5.3 FUEL HANDLING PROCEDURES

In order to prevent contamination of test fuels, certain procedures had to be adopted for handling and transferring. The following fuels were stored in 45 gal. drums: JET A1, ERBS-3, JP8 Shale, Diesel, Tar Sands, JP10, JP4/2040/DF, RJ6. The remaining fuels, JET A1/B1, JET A1/B2, JP4, JP4/B1, and JP4/B2, were stored in underground tanks. The samples used for analysis were taken using specially lined funnels and cans. These were always rinsed first with petroleum ether and then with the fuel itself to avoid any contamination. In order to avoid any fuel mix-up, all drums and tanks were identified with a letter code, i.e each fuel was assigned a letter.

For each fuel tested. a standard flushing procedure was adopted. First, all fuel lines were drained using compressed air. Then all fuel filters were replaced by "flushing filters" (these filters were only used for flushing). The lines were then flushed using the new fuel, then drained once again. The appropriate filters were then installed (each fuel was assigned a specific set of filters). Finally, the entire system was flushed using the new fuel.

A schematic of the blending area fuel system is shown in Figure 5.12. This system enabled direct hook-up of some fuels to the test cell.

5.4 DATA ANALYSIS PROCEDURE

5.4.1 COMBUSTION EFFICIENCY CALCULATIONS

The measured emissions (ppm) were converted to emission indices using an in-house data reduction computer program. Wet concentrations of CO, HC, and CO_2 were used to compute sample fuel-air ratios based on the following relationships:

$$far = \left[\frac{M_C + \alpha M_H}{M_{AIR}}\right]\left[\frac{(1 + h) \, [10^{-4}(CO) + (CO_2) + 10^{-4}(THC)]}{100 - 0.25\alpha \, [10^{-4}(CO) + (CO_2) + 10^{-4}(THC)]}\right]$$

where: h = humidity of air, moles of water per mole of dry inlet air

α = Carbon/Hydrogen ratio

M_C = Carbon molecular weight

M_{AIR} = Air molecular weight

M_H = Hydrogen molecular weight

- 73 -

Combustion efficiency and emission indices are computed using the following relationships:

$$\eta = 100 - \left[0.0232 \ EI_{CO} + 0.0908 \ EI_{THC} \right]$$

$$EI_{CO} = \left[\frac{(CO)}{10^{-4}(CO) + (CO_2) + 10^{-4}(THC)} \right] \left[\frac{M_{CO}}{10(M_C + \alpha \ M_H)} \right]$$

$$EI_{HC} = \left[\frac{(THC)}{10^{-4}(CO) + (CO_2) + 10^{-4}(THC)} \right] \left[\frac{M_{HC}}{10(M_C + \alpha \ M_H)} \right]$$

$$EI_{NO_X} = \left[\frac{(NO_X)}{10^{-4}(CO) + (CO_2) + 10^{-4}(THC)} \right] \left[\frac{M_{NO_2}}{10(M_C + \alpha \ M_H)} \right]$$

The program was modified to calculate a net temperature rise for each set condition. The temperature rise is from a kinetics routine which uses all relevant fuel properties (C-H ratio, heat of combustion, specific gravity, sulphur content, enthalpy of evaporation, etc.) and calculates an ideal temperature rise. The previously calculated combustion efficiency is then applied to the ideal temperature rise to arrive at an actual gas exit temperature. This information was used in NO_X vs T_4 correlations which will be discussed in the chapter dealing with test results.

5.4.2 FUEL PROPERTY CORRELATIONS

The main thrust in the data analysis was to try to correlate such performance parameters as emissions, liner temperatures, flame radiation, and combustion efficiency to such fuel properties as hydrogen content, mean droplet size, volatility, etc. A central data base was therefore established which would permit comparisons between any two parametric sets of data (smoke emissions and fuel hydrogen content, for example). A computer program was then set up to plot any combinations of these data sets on an X-Y plotter. This greatly accelerated the task of trying to draw correlations from the data. Ir most cases, a straight line was drawn through data points using a linear regression technique.

These lines were meant only as trend indicators and were not meant to dictate the type of correlation (linear, 2nd order, etc) present. The plotting capability proved to be a valuable tool in the data analysis.

Table 5.1: Lean Limit Test Parameters

Condition No.	P3 MPa (atm)	T3 K (R)	W_c kg/s (lb/s)	Air Loading Parameter Ω
1	0.41 (4.0)	375 (675)	.100 (.230)	.314
2	0.41 (4.0)	375 (675)	.143 (.323)	.441
3	0.41 (4.0)	375 (675)	.187 (.417)	.569
4	0.41 (4.0)	375 (675)	.231 (.510)	.696

Table 5.2: Thrust Level Test Parameters

Condition No.	Thrust Level %	P₃ MPa (atm)	T₃ K (R)	W_c kg/s (lb/s)	T₄ (ideal) K (R)
1	6.8	.365 (3.61)	375 (675)	.186 (.41)	835 (1503)
2	30	.446 (4.4)	500 (900)	.130 (.287)	1030 (1854)
3	60	.689 (6.8)	569 (1025)	.208 (.458)	1192 (2146)
4	90	.907 (8.95)	617 (1110)	.277 (.611)	1331 (2396)
5	100	.988 (9.75)	631 (1136)	.295 (.65)	1367 (2460)

Table 5.3: Power Level Test Parameters

Condition No.	Power Level %	P₃ MPa (atm)	T₃ K (R)	W_c kg/s (lb/s)	T₄ (ideal) K (R)
1	3	0.354 (3.49)	366 (658)	0.155 (.344)	907 (1633)
2	60	0.664 (6.55)	.540 (972)	0.155 (.344)	1089 (1961)
3	100	0.837 (8.26)	574 (1034)	0.185 (.407)	1202 (2163)

Table 5.4: Parametric Test Parameters

Condition No.	P_3 MPa (atm)	T_3 K (R)	W_c kg/s (lb/s)	F/A (for JET Al)
1	1.621 (16.0)	586 (1054)	.291 (.64)	.0205
2	1.013 (10.0)	586 (1054)	.291 (.64)	.0205
3	0.492 (4.86)	586 (1054)	.291 (.64)	.0179
4	0.613 (6.05)	586 (1054)	.291 (.64)	.0205
5	0.492 (4.86)	586 (1054)	.291 (.64)	.0205
6	0.492 (4.86)	586 (1054)	.291 (.64)	.0225

Table 5.5: Cold Start Test Parameters

W_c air mass flow	.0231 kg/s	(.0511 lb/s)
W_f fuel maximum flow	5.44 kg/h	(12 lb/hr)
P_3 air inlet pressure	0.10 MP$_a$	(1.0 atm)
T_3 air inlet temperature	241-289 K	(434-520R)
T_f fuel inlet temperature	241-289 K	(434-520R)

Table 5.6: Cold Start Testing Procedure

1. **Flushing the fuel system**

   - drain tank, lines, and filter housing
   - change filter
   - add 2 quarts of new fuel
   - run pump for 5 minutes alternating between bypass & test modes
   - drain tank, lines, and filter housing
   - replace filter
   - add 2 gallons of new fuel

2. **Regulating fuel & air temperatures**

   - fill fuel cooler with about 5 gallons of alcohol
   - add dry ice piece by piece until one whole block has been immersed
   - close cover & connect vent
   - before starting the fuel pump, close micrometer valve and open cooler valve
   - set fuel circuit to bypass mode

   - start fuel pump & close cooler valve until about 100 psi is indicated on the cooler gauge
   - open micrometer valve to desired fuel flow
   - start main air and switch on the refrigeration unit
   - allow both the fuel and air systems to reach steady state conditions
   - adjust fuel heat exchanger to the desired temperature
   - set air flow temperature to within 3°F of fuel temperature using the hot-air bleed
   - when both temperatures are close enough and appear to be reasonably steady, a light-up may be attempted

3. **Lighting-up Procedure**

   Two light-up attempts will be made at each temperature regardless of whether or not light-up occurs on the first trial. The following procedure should be adhered to as closely as possible to ensure consistent results.

   - prior to test, record ambient conditions and applicable data: date, fuel types, ambient temperature, dew point temperature, barometric pressure, etc.
   - prior to light-up, record set-up conditions: Test No., video counter reading, fuel temperature, fuel flow and pressure (bypass), orifice P, upstream pressure, T_3, T_4, T_1, downstream T.
   - start strip chart recorder and inscribe Test No., and video counter reading
   - start video and narrate REF #, and air temperature
   - switch on igniter 5 seconds prior to fuel flow & mark strip chart
   - switch fuel "on", mark strip chart & say "fuel on" into microphone
   - allow maximum 30 seconds for light-up and describe what is happening into the microphone
   - if no light-up:

     * turn off fuel, igniter, video, and strip chart
     * allow one minute for fuel to drain
     * turn on strip chart and video & say "repeat previous test"
     * repeat light-up attempt
     * if still no light-up, drain fuel and proceed to next test point

   - If light-up:

     * record fuel flow at light-up
     * allow combustion for 5 seconds
     * record T_4 prior to shut-down
     * shut-off fuel
     * say "fuel off" into microphone & switch off video and strip chart
     * allow two minutes for cool-down
     * repeat test

   - once both trials have been done, regardless of whether or not they were successful, set air and fuel to next conditions.

- 4 -
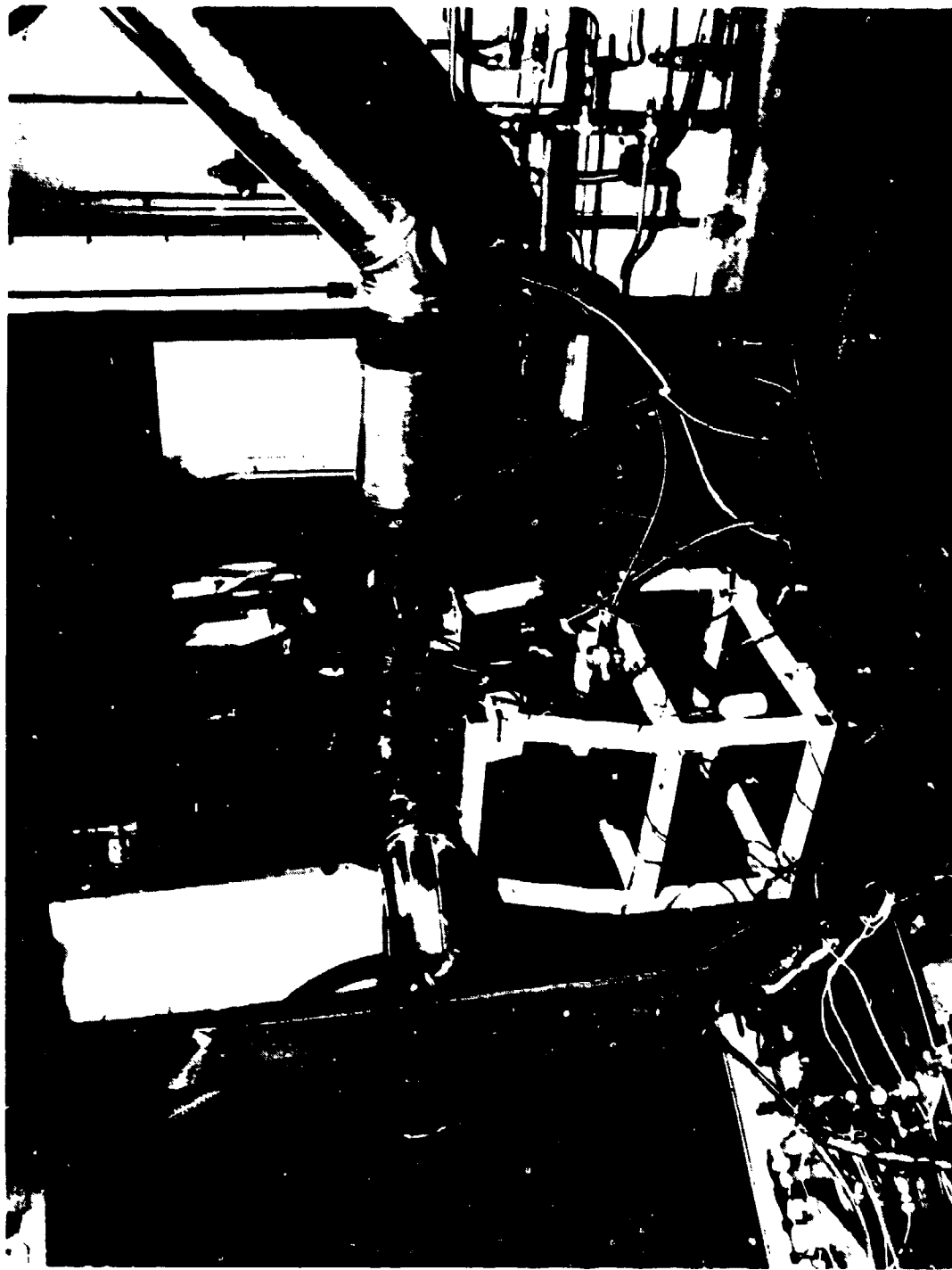
Figure 5.1: General View of Can Combustor Rig

Multipoint exh. probe

Water cooled Instrumentation section

Combustor test section

Radiometer probe boss

Back pressure valve
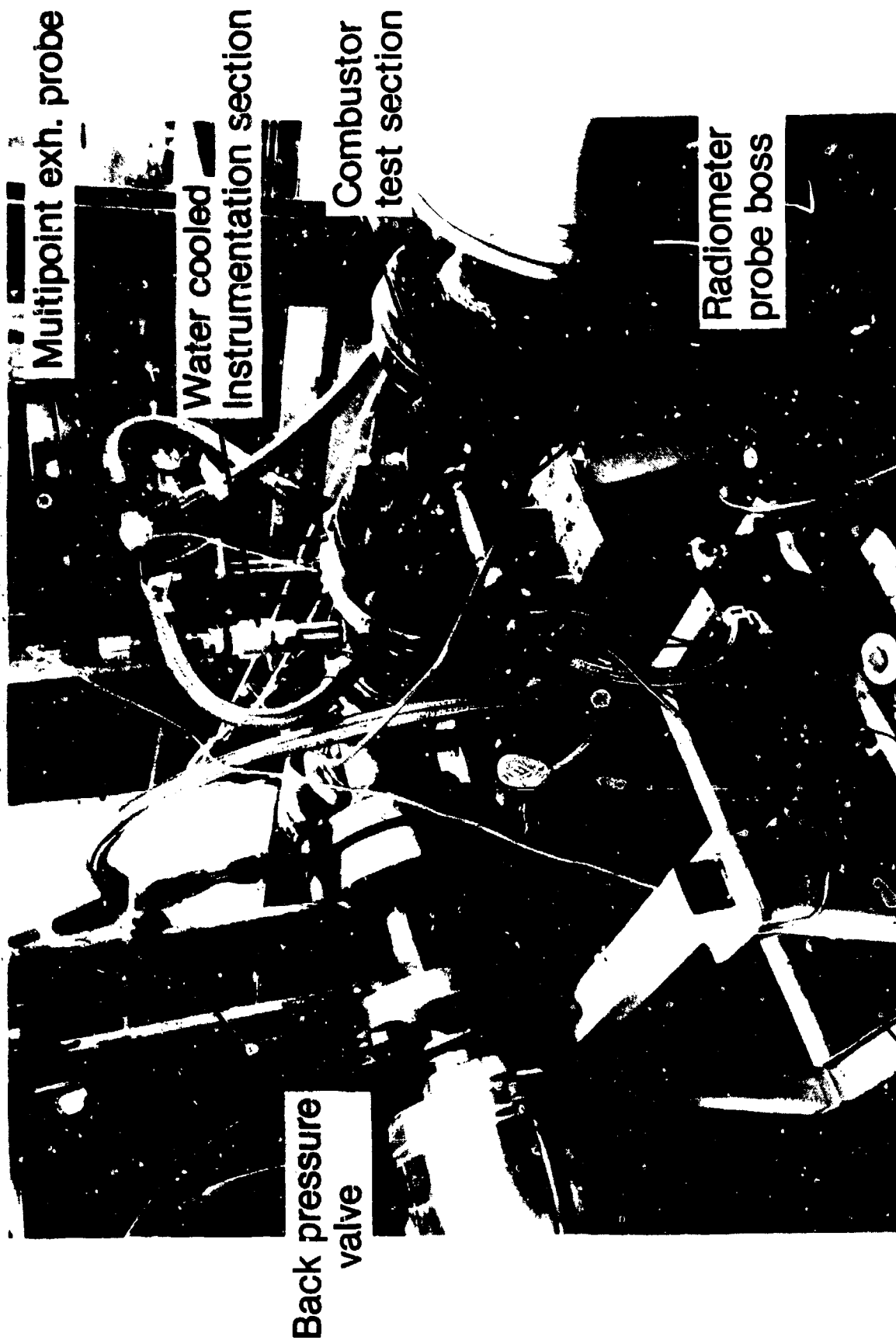
Figure 5.2: Can Combustor Rig
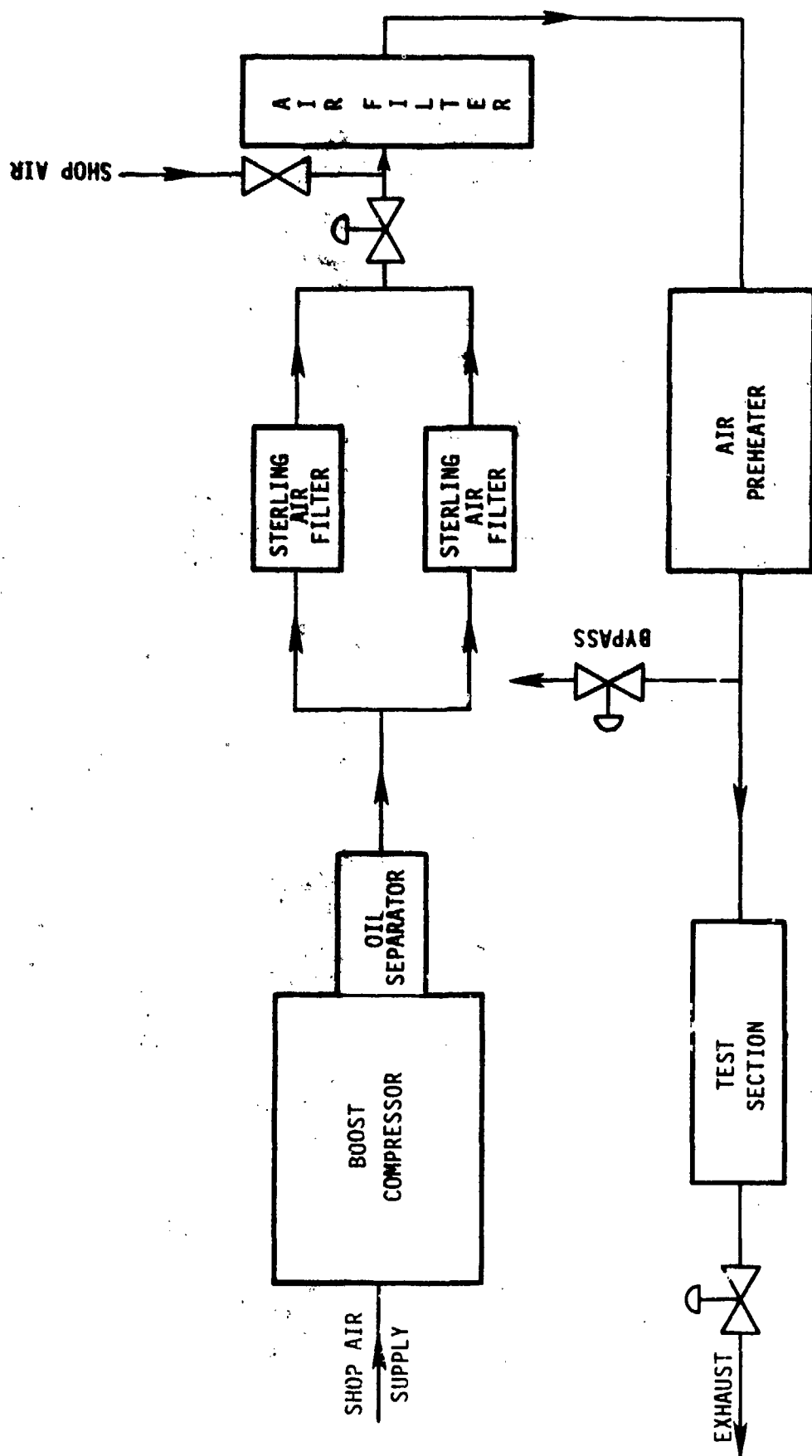
Figure 5.3: Schematic of Can Combustor Rig Air Path
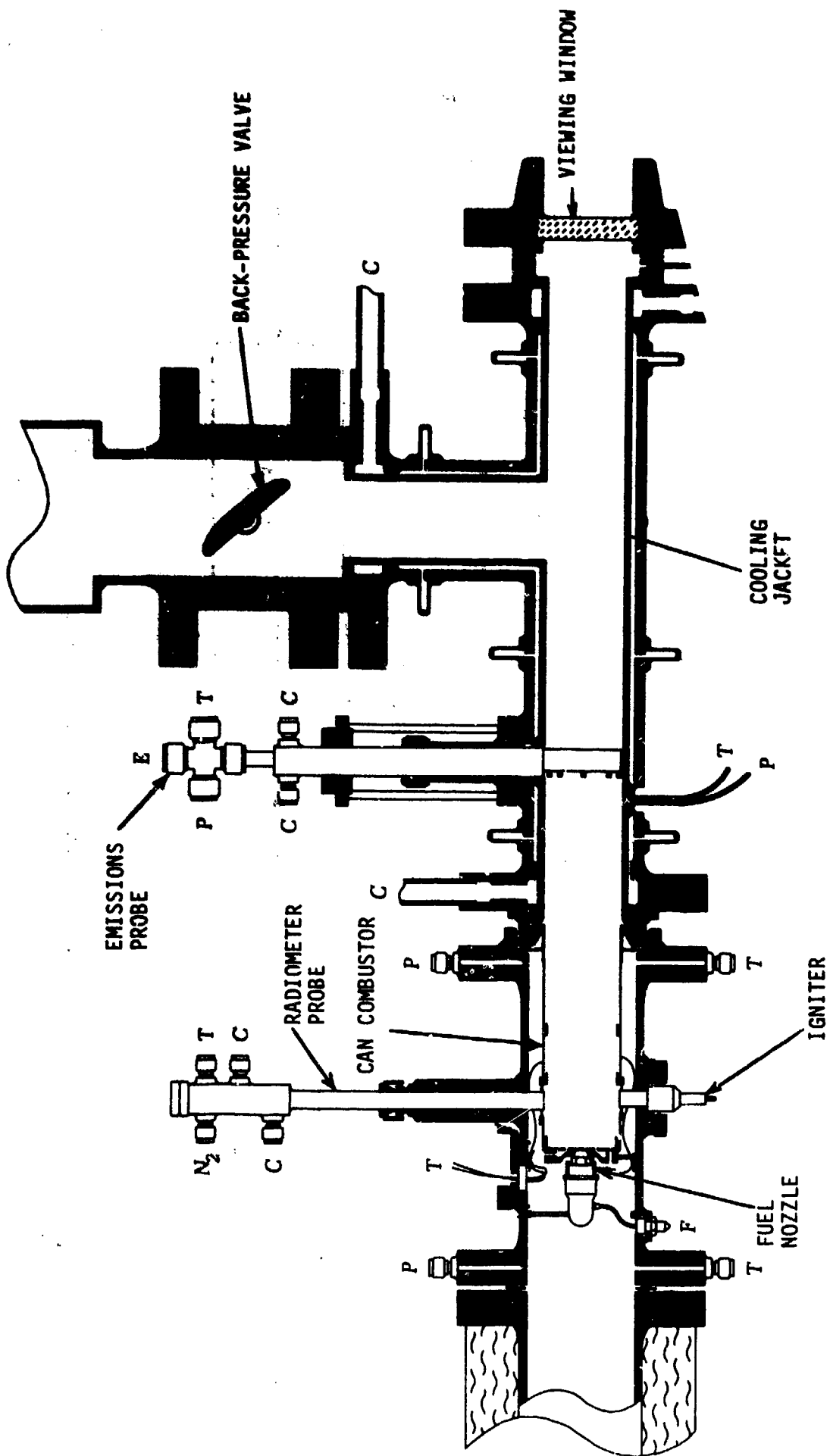
Figure 5.4: Can Combustor Rig Cross Section
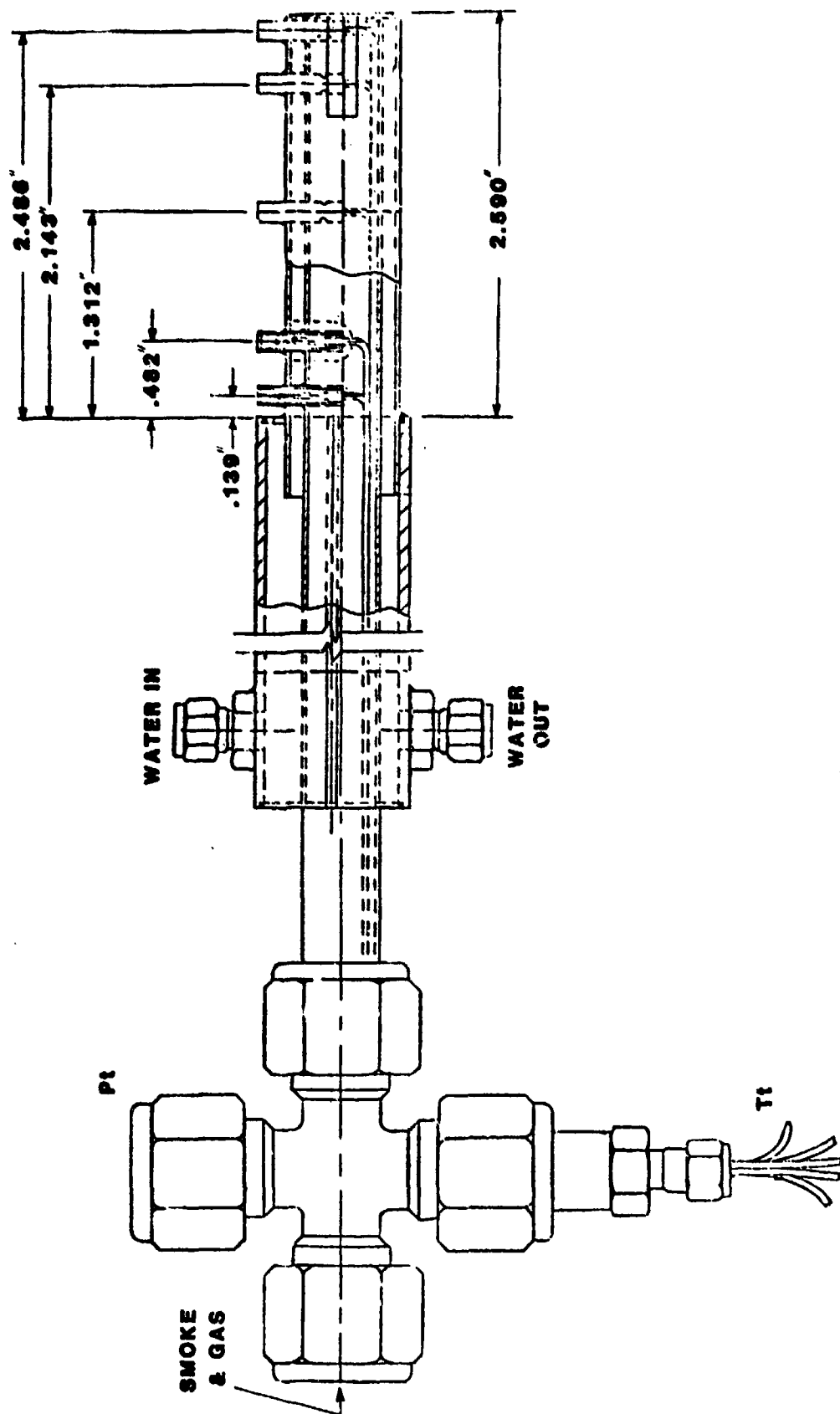
Figure 5.5: Schematic of Multi-Purpose Exhaust Probe
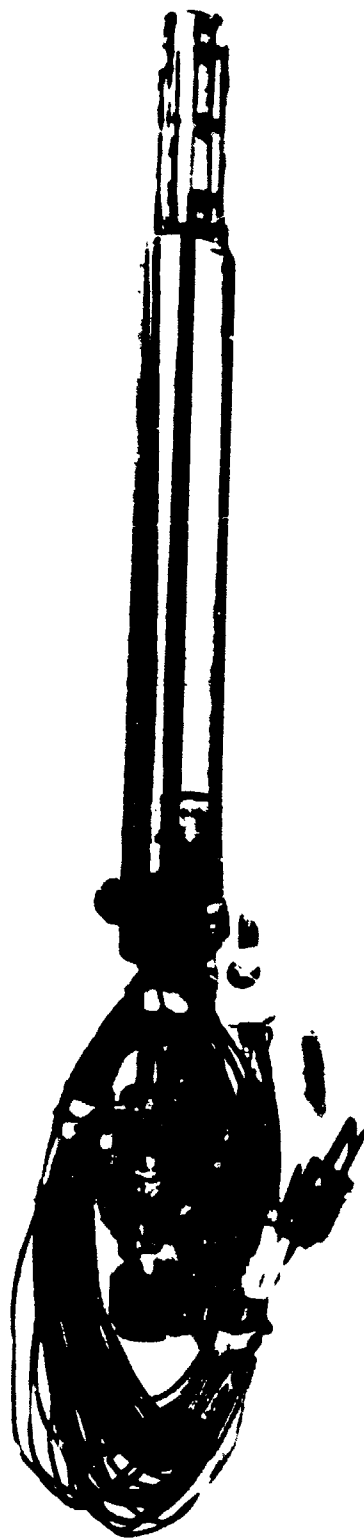
Figure 5.6: Multi Point Temperature, Pressure and Emissions Probe

WATER OUT

GAS IN

WATER IN

DIFFERENTIALLY CONNECTED THERMOCOUPLES

POROUS DISK

WATER COOLED HEAD
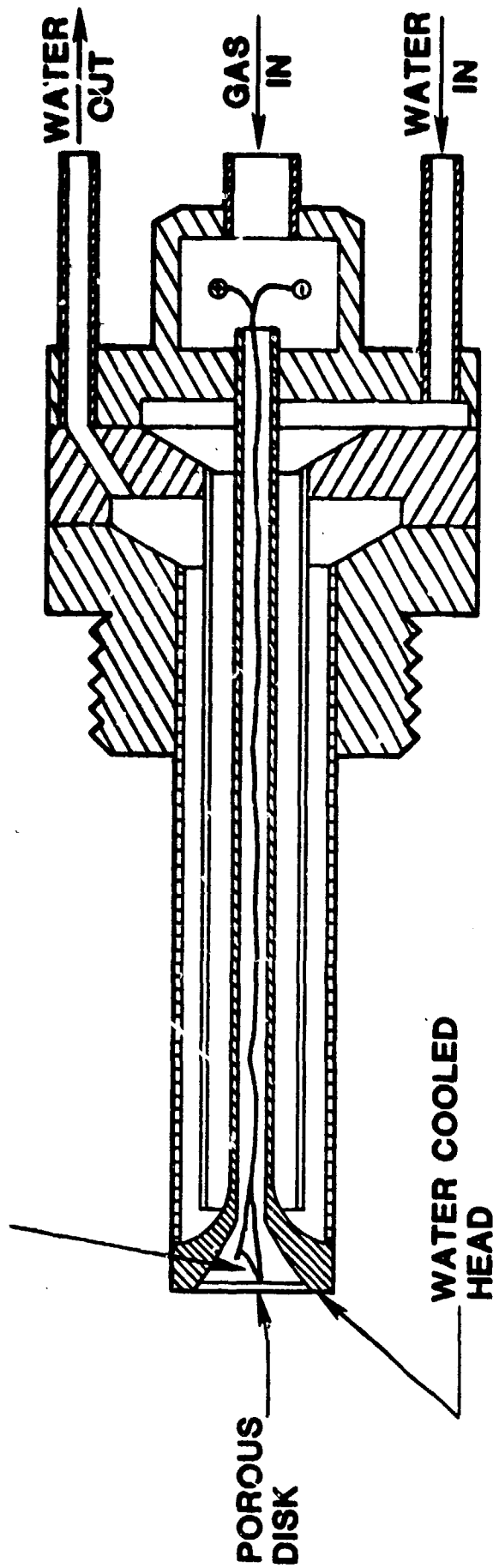
Figure 5.7: Schematic of Transpiration Radiometer Probe
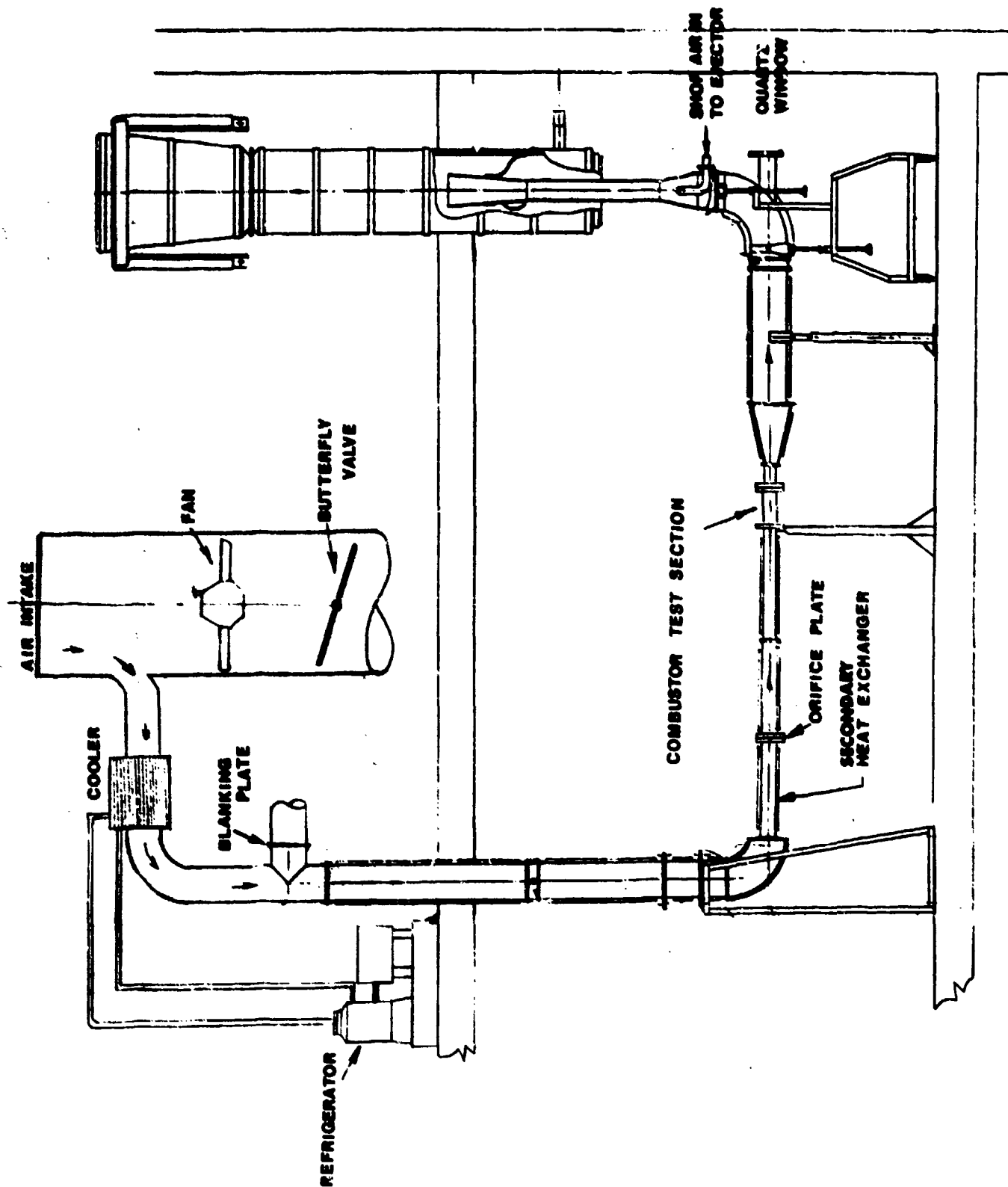
Figure 5.8: Schematic of Cold Start Rig Layout

AIR INTAKE

FAN

BUTTERFLY VALVE

COOLER

BLANKING PLATE

REFRIGERATOR

COMBUSTOR TEST SECTION

ORIFICE PLATE

SECONDARY HEAT EXCHANGER

SHROUD AIR IN TO EJECTOR

QUARTZ WINDOW

- 88 -
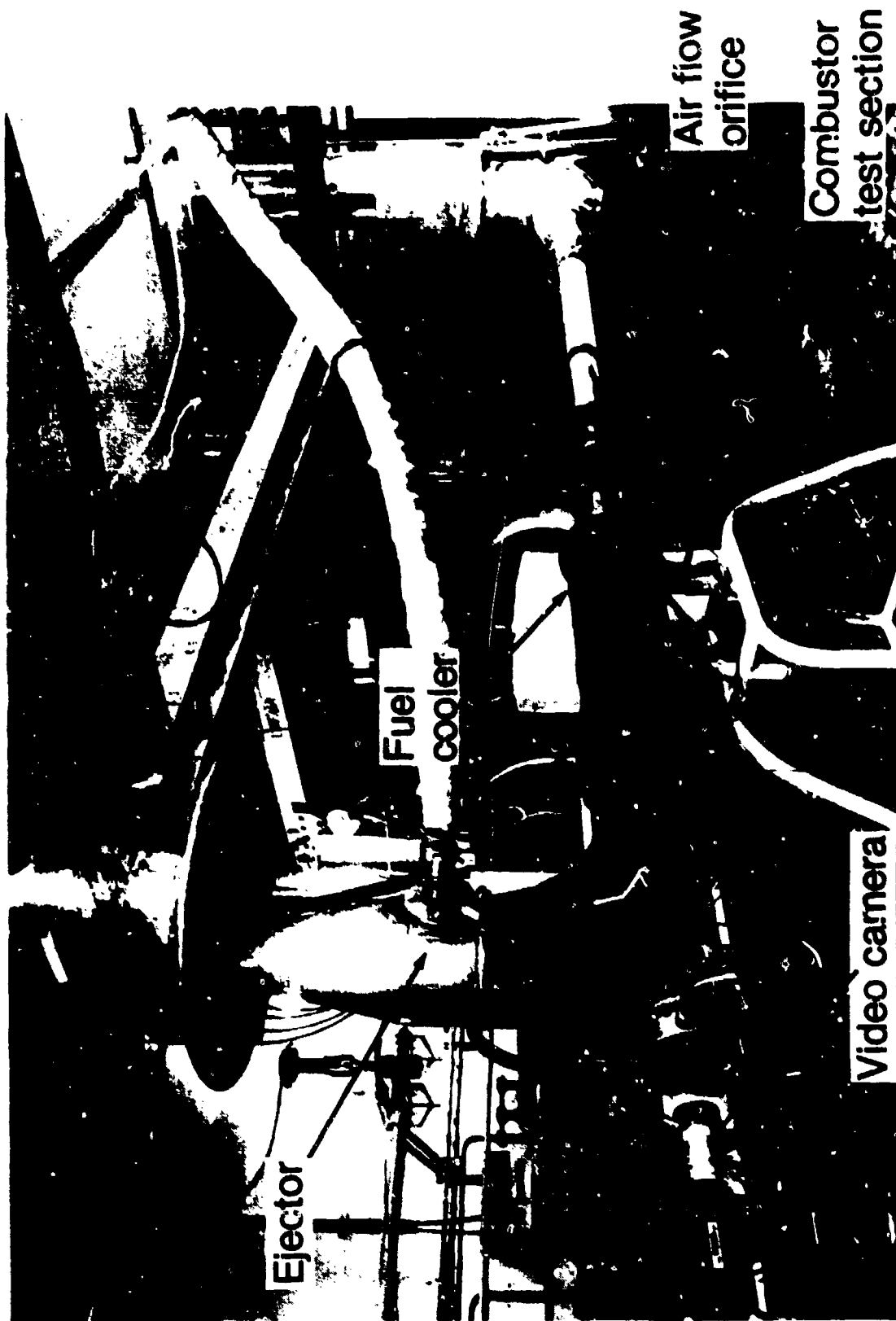
Figure 5.9: Cold Start Test Facility
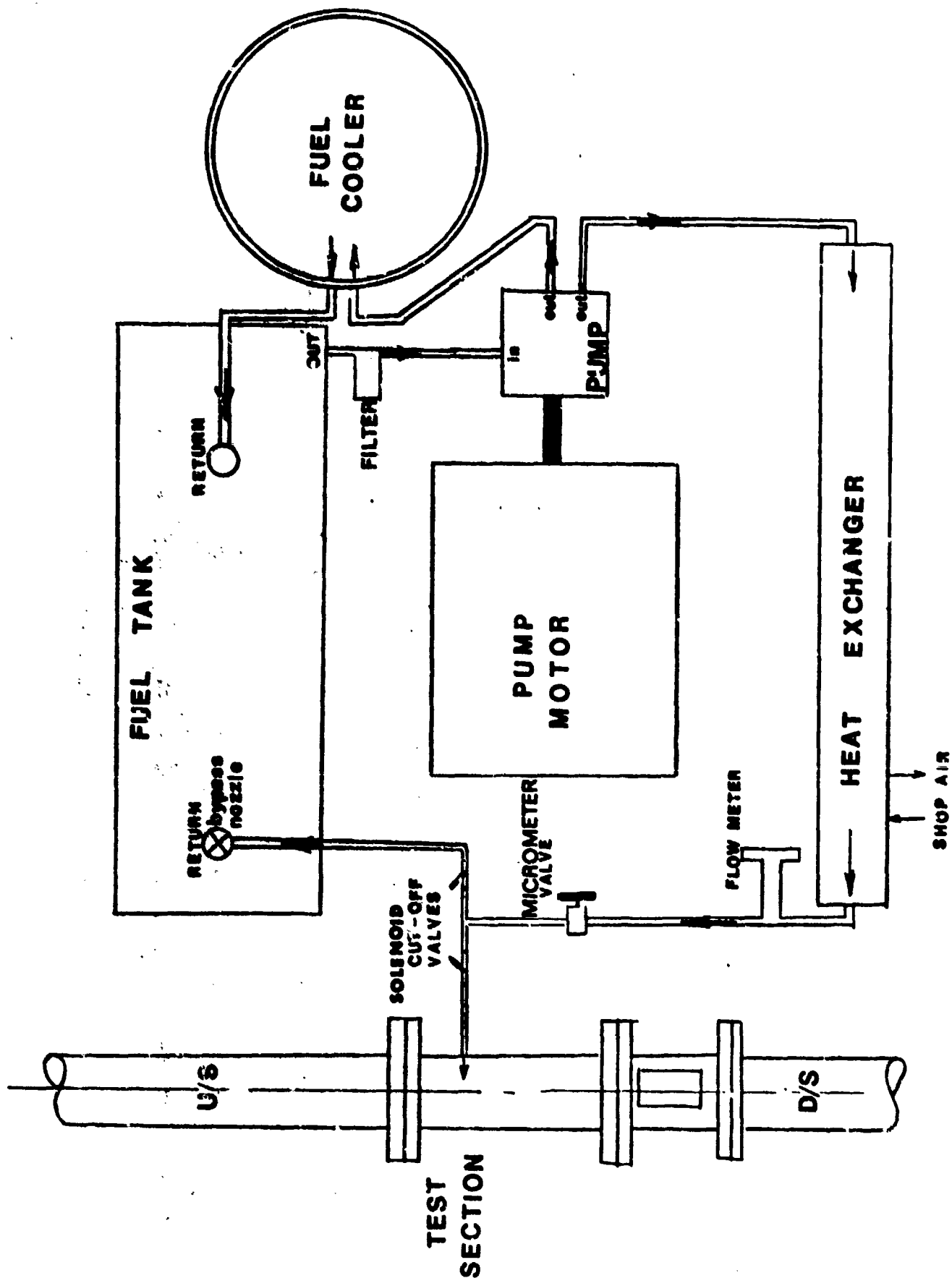
Figure 5.10:   Schematic of Cold Start Rig Fuel System
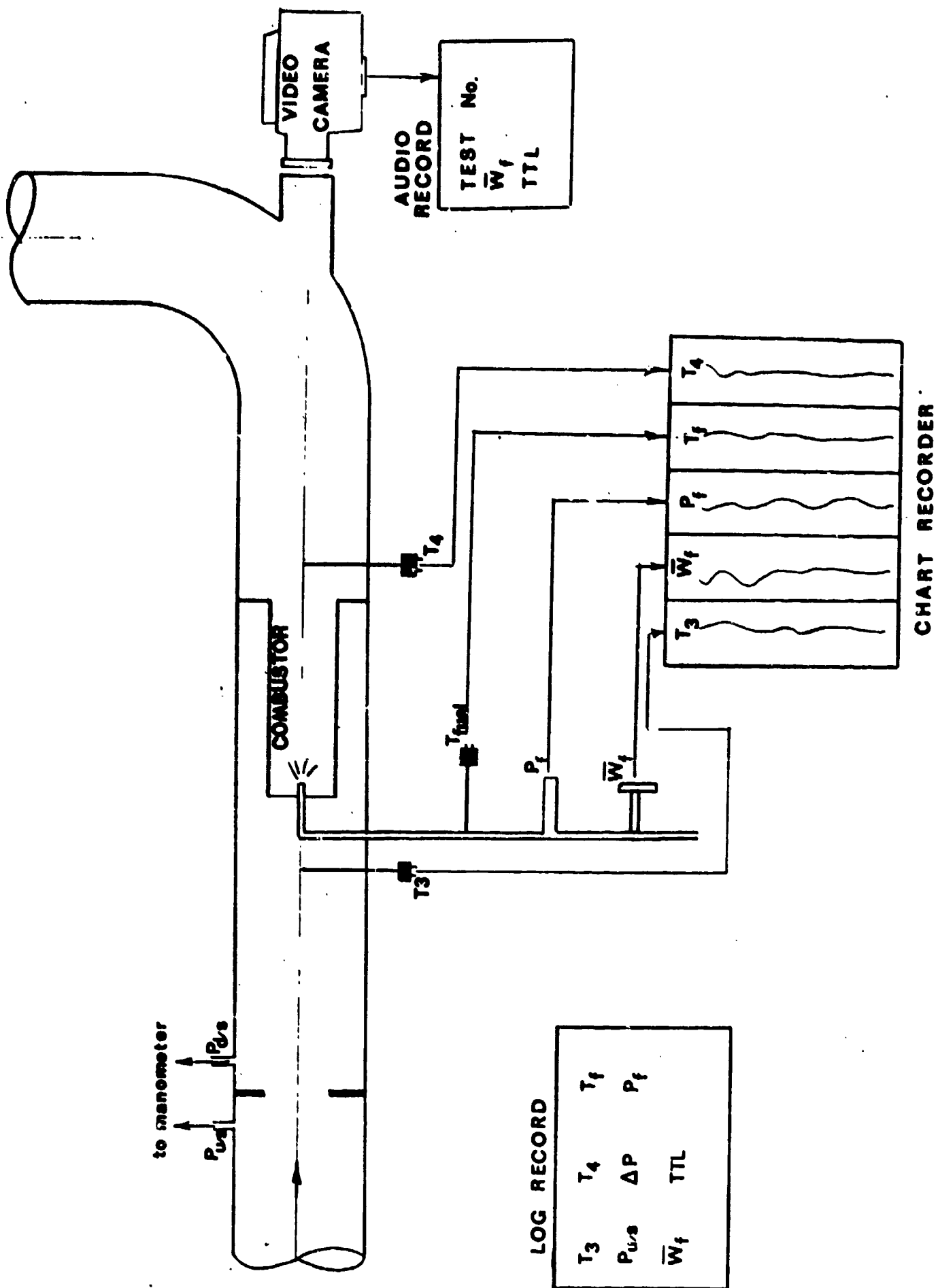
Figure 5.11: Schematic of Cold Start Rig Instrumentation

Figure 5.12: Schematic of Blending Area Fuel System
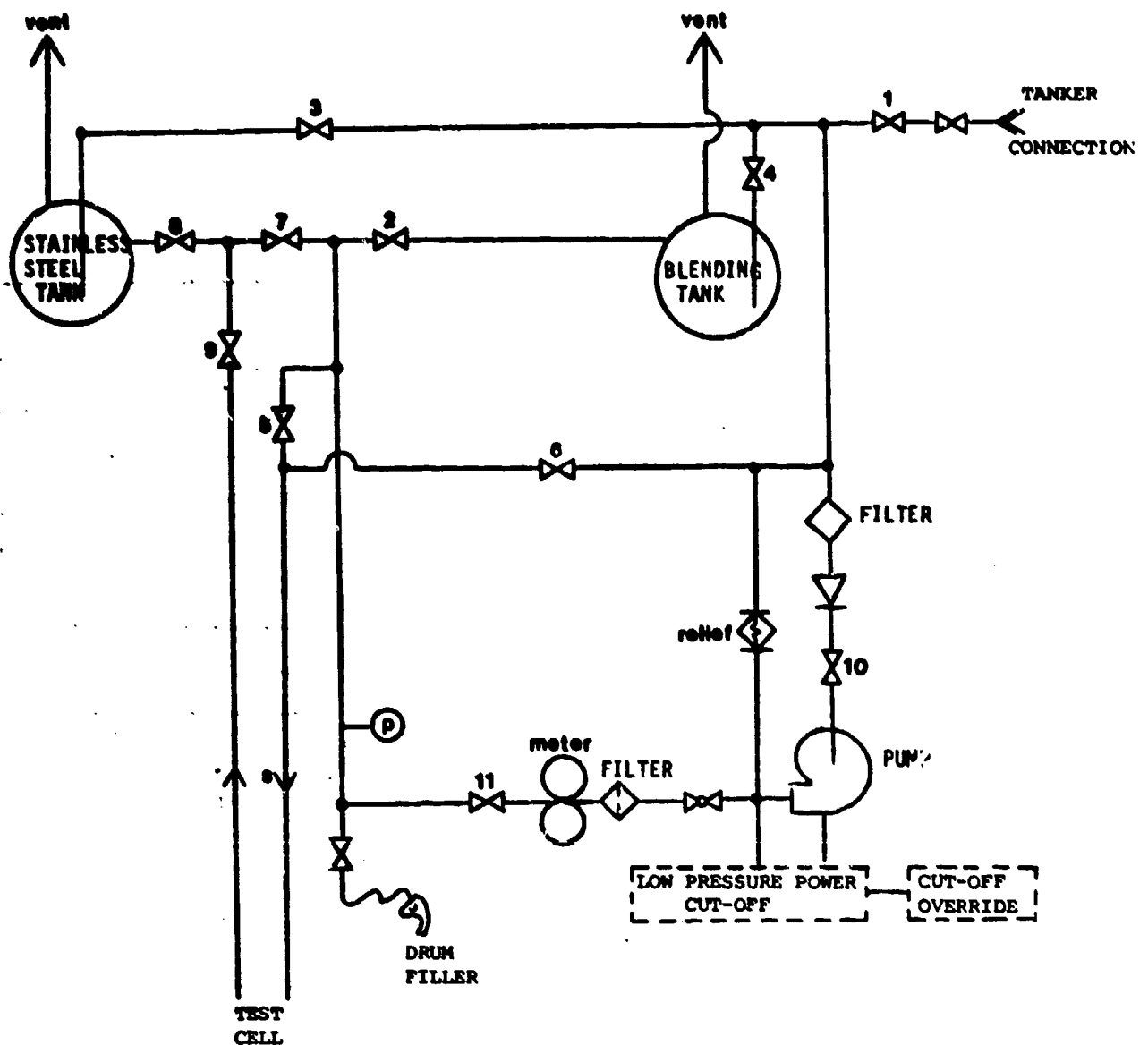
OPEN VALVES

1, 10, 11, 2	TO FILL BT FROM TANKER
3, 10, 11, 2	TO FILL BT FROM SS
4, 10, 11, 7, 8	TO FILL SS FROM BT
4, 10, 11, 2	TO CIRCULATE BT
4, 10, 11, 5	TO TRANSFER FROM BT TO UNDERGROUND STORAGE
4, 6, 9, 7, 2	TO USE BT AS SUPPLY TO TEST CELL
4, 6, 9, 8	TO USE SS AS SUPPLY TO TEST CELL

SECTION VI

RESULTS AND DISCUSSION

All the tests described in the test plan (Section II) were completed with only minor modifications. The planned and achieved tests are shown below:

	Thermal Paint	Lean Limit	Cold Start	Power Level	Thrust Level	Parametric	Total
Test Plan	4	132	112	90	330	198	866
Actual	14	154	309	74	271	198	1020

In general, results were repeatable and the test results listed in Appendices A through F are discussed in detail in the following sections.

6.1 LEAN-LIMIT TEST RESULTS

Lean-limit fuel-air ratios (LLFAR) were obtained at four different air flows for each test fuel/fuel nozzle combination. All fifteen fuels were tested with the simplex pressure atomizing nozzle, and in general an increase in air flow resulted in an increase in lean-limit fuel-air ratios, Figures 6.1 and 6.2. As expected, Jet Al and JP8 showed very similar lean limit performance. The addition of 2040 solvent to JP4 and Jet Al fuels caused a marked increase in LLFAR. The tar sand fuels all showed similar stability performance except for the L-L blend which resulted in much poorer lean stability, especially at high air flows (Figure 6.2). JP-10 also showed a marked increase in LLFAR at high air flows, while Diesel and ERBS-3 fuels showed similar lean limit performance. In order to compare all fuels on an absolute basis, lean-limit fuel-air ratios were determined for two air flows. The first, 0.236 kg/sec (0.52 lb/s) corresponded to an air loading parameter Ω_c simulating idle (0.71) and the second air flow, 0.141 kg/sec (0.31 lb/s) to simulate Mach Number ($\overline{M}_c$) at idle (.027). Interpolated values of LLFAR at the two air flows (Table 6.1) were then correlated with fuel properties. These included fuel hydrogen content, fuel volatility expressed as 10% recovery temperature and the physical properties i.e. viscosity, surface tension and density. Best correlations with physical properties were achieved when expressed in terms of empirical parameters for mean droplet size. The relative droplet size was defined as the ratio of Sauter Mean Diameter (SMD) of the fuel in question and the SMD of JP4. The SMD of the spray produced by a pressure atomizing fuel nozzle is generally expressed in the form:

$$SMD = \frac{K \, W_f^{\,0.25} \, \nu_f^{\,0.20} \, \sigma_f^{\,0.60}}{\Delta P^{0.40}}$$

$$\text{and} \quad \Delta P = \frac{C \, (\rho_f \, W_f)^2}{(FN)^2}$$

where K and C = constants
SMD = Sauter Mean Diameter
P = Fuel Pressure Drop
FN = Fuel Nozzle Flow Number
W_f = Fuel Flow Rate
ν_f = Fuel Kinematic Viscosity
σ_f = Fuel Surface Tension
ρ_f = Fuel Density

Lean limit performance at the air flow rate of 0.236 kg/sec (Ω_c equivalent) correlated well with fuel hydrogen content (Figure 6.3) but poorly with relative fuel droplet size and fuel volatility. A different trend was observed at 0.141 kg/sec (Mach number equivalent) where relatively poor correlation resulted with fuel hydrogen content and good correlations with relative fuel droplet size and volatility (Figure 6.4). Linear regression analysis resulted in the following correlations:

LLFAR = 0.0409 - 0.0026 (H) for Ω_{idle}

LLFAR = 0.0247 - 0.0015 (H) for M_{idle}

LLFAR = 2.27×10^{-5} (K)-.0047 for M_{idle}

LLFAR = 0.0084 (RSMD) - 0.00495 for M_{idle}

where LLFAR = Lean Limit fuel-air ratio
H = Fuel Hydrogen Content
K = 10% Recovery Temperature, K
RSMD = SMD/SMD $_{JP4}$, relative fuel droplet size

Similar lean limit tests were conducted with duplex, airblast and vaporizer nozzles, using six test fuels in each case. Results showed similar lean stability trends between simplex and duplex pressure atomizers (Figures 6.5 and 6.6), increasing air flow rates resulting in higher lean-limit fuel-air ratios. The airblast nozzle however illustrated relatively small dependence on air flows, but in general, lean stability was worse than with pressure atomizers. Finally, the vaporizer nozzle showed the worst performance, with very poor stability at medium to high airflows. Similar overall trends were observed with all six test fuels (Figures 6.5 and 6.6).

6.2 COLD START TEST RESULTS

Start-up tests were conducted for seven fuels using two simplex nozzles (0.9 and 3.0 FN); the 0.9 FN nozzle was simulative of a 0.9 FN primary plus 2.1 FN secondary duplex system operating on primary only at light-off. For each condition, a minimum light-off fuel-air ratio was established. The results are illustrated in Figure 6.7. For the fine spray atomizer (0.9 FN), all fuels lit down to 242K (435°R). For the coarser nozzle (3.0 FN), JP4 fuel lit at 242K while other fuels had minimum light-off temperatures higher than 242K. JP10 did not light even at 289K (520°R) with this nozzle. A comparison of minimum light-up temperature for each fuel is shown in Figure 6.8. It is evident that addition of 2040 solvent to base fuels considerably worsens the start-up performance.

An attempt was made to correlate minimum light-off fuel-air ratio to fuel volatility (expressed as 10% recovery temperature). A good correlation exists between these two parameters (Figure 6.9) both at 289K (520°R) and 241K (434°R) indicating that the more volatile fuels have better start-up characteristics than the less volatile ones.

Minimum light-off fuel-air ratio also correlated well with relative fuel spray droplet size (Figure 6.10) reinforcing the premise that fuel droplet size is an important factor influencing start-up capabilities.

Hydrogen content was not a strong determinant of minimum light-off fuel air ratio and minimum light-off temperature (Figure 6.11) indicating that fuel properties other than H-content had a stronger influence.

Besides minimum light-off fuel-air ratio, attempts were also made to characterize the fuels according to temperature rise after light-off; however, results indicated that temperature rise was directly related to time to light (Figure 6.12). Therefore, time to light was plotted versus fuel 10% recovery temperature. The trend indicated that the more volatile fuels (JP4) generally took less time to light than the less volatile ones (Tar Sands, ERBS-3, etc).

Linear regression analysis of the test data resulted in the following correlations:

at 289K (520°R): $MLOFAR = 2.15 \times 10^{-4}$ (K) $-$ 0.037 for 3.0 FN
$MLOFAR = 6.84 \times 10^{-5}$ (K) $-$ 0.0073 for 0.9 FN
$MLOFAR = 0.115 - 0.00454$ (H) for 3.0 FN
$MLOFAR = 0.045 - 0.0015$ (H) for 0.9 FN
$TR = 180.8 + 4.54$ (TTL) for 0.9 FN; f.a.r. $=$ 0.0250
$TTL = 0.0733$(K) $-$ 16.92 for 0.9 FN; f.a.r. $=$ 0.0250

at 241K (434°R): $MLOFAR = 6.845 \times 10^{-5}$ (K) $-$ 0.00732 for 0.9 FN

at any temperature: $MLOFAR = 0.0417$ (RSMD) for 3.0 FN
$MLOFAR = 0.015 + 0.006$ (RSMD) for 0.9 FN

where: MLOFAR = Minimum light-off fuel-air ratio
TR = Temperature rise 5 seconds after light-off (K)

TTL = Time to light (sec)
K = Fuel 10% Recovery temperature (K)
H = Fuel Hydrogen content %

6.3 COMBUSTION INEFFICIENCY

Combustion inefficiencies were obtained from measurement of unburnt species in the exhaust, i.e. THC and CO. Measurements were made at idle, 60% and 100% power simulation on the turboprop cycle, and idle, 30%, 60%, 90% and 100% thrust simulation on the turbofan cycle. Thrust level simulation included all 15 fuels with simplex atomizer, and six fuels (Jet Al, Jet Al/B2, JP4, JP4/B2, ERBS-3 and Tar Sands L-H) with duplex, airblast and vaporizing nozzles. Power level simulation included all 15 fuels, but with the simplex nozzle only.

As discussed in Section II, a potentially significant parameter for correlating combustion inefficiency is the air loading parameter, expressed as follows:

$$\Omega_c = \frac{K_1 \, W_c}{P_3^{1.8} \, e^{\, T_3/K_2} \, V_c}$$

The expression represents a rough approximation of the extent to which the fuel combustion should have proceeded. Specifically,

$$\Omega_c \, \alpha \, \frac{1}{(\text{reaction rate}) \times (\text{residence time})}$$

Thus larger values of Ω_c mean that the product of the rate times the residence time is small, indicating that either the reaction rate or the residence time or both are small. High values of combustion inefficiency can then be expected. Conversely, smaller values of Ω_c indicate higher reaction rates and/or residence time which both contribute to low values of combustion inefficiency.

Figure 6.13 shows combustion inefficiency vs Ω_c plots for the various fuels operating on the thrust simulation cycle with simplex atomizer. Figure 6.14 shows similar plots with simplex atomizer when operating on the power simulation cycle. On both plots a high value of Ω_c corresponds to operation at low power simulations such as idle while low values of Ω_c correspond to operation at higher power levels. Figure 6.13(a) indicates the effect of 2040 solvent on Jet Al, higher combustion inefficiencies resulting over the entire simulated operating range. The effect of solvent on JP4 is similar except JP4/B1, having a lesser quantity of blend (i.e.; higher hydrogen content), and yet a higher combustion inefficiency than JP4/B2 (figure 6.13 (b)). The reasons for this inconsistency are not known. JP8 performance is similar to Jet Al, Figure 6.13(c), while Diesel and ERBS-3 are somewhat worse than Jet Al. Among Tar Sand fuels Figure 6.13(d), combustion inefficiency with L-H is similar to Jet Al; reducing the hydrogen content with H-M, L-M and L-L results in higher inefficiencies.

Figure 6.14 shows combustion efficiency performance on simulated turbo-prop cycle with simplex nozzle, the trends being similar to the thrust level tests.

Figure 6.15 shows performance comparison of different fuel nozzles with six of the test fuels. In all cases at low power levels the airblast nozzle had higher combustion inefficiencies than pressure atomizers, but performed as well as the pressure atomizers at high power levels with the more viscous fuels. The vaporizer nozzle performed very poorly at low and intermediate power levels.

Figure 6.16 shows the effect of H-content on idle combustion inefficiency. For each fuel, idle combustion inefficiency was interpolated for $\Omega_c = 0.71$ on the thrust cycle and $\Omega_c = 0.62$ on the power cycle for simplex nozzle. The trends indicate wide scatter, but generally display higher idle inefficiency as the hydrogen content is reduced. The plots also show similar trends for Jet A1 fuels, but with much less scatter than with other fuel types. The general correlations based on linear regression are as follows:

Inefficiency = 18.319 - 1.054 (H) for thrust level tests

Inefficiency = 11.136 - 0.565 (H) for power level tests

Figure 6.17 shows the effect of relative droplet size on idle combustion inefficiency. While there is a marked trend with RSMD, the wide scatter implies that factors other than RSMD have significant influence on the combustion process. Correlations with relative droplet size are as follows:

$$\text{Inefficiency} = 5.054 \left(\frac{SMD}{SMD_{JB4}}\right) - 1.48 \qquad \text{for thrust level tests}$$

$$\text{Inefficiency} = 9.101 \left(\frac{SMD}{SMD_{JP4}}\right) - 7.165 \qquad \text{for power level tests}$$

Figure 6.18 shows dependence of idle combustion inefficiencies on 10% recovery temperature (T_{10}), trends indicating the expected effect of higher idle combustion inefficiency with reduced volatility. The correlations are:

Inefficiency = 0.0173 (T_{10}) - 2.912 for thrust level tests

Inefficiency = 0.0235 (T_{10}) - 6.401 for power level tests

6.4 HYDROCARBON EMISSIONS

Data on THC emissions with the simplex pressure atomizing nozzle correlated very poorly with all three variables i.e.; hydrogen content and relative droplet size (Figures 6.19 and 6.20), and volatility. Correlations with hydrogen content were considerably better when examined separately for the Jet A1 or JP4 fuels and respective 2040 blends, Figures 6.21, 6.22.

- 97 -

The poor correlation of THC emissions with hydrogen content is consistent with reported data on other combustion systems[5]; however, the poor relationship with relative droplet size of the pressure atomizer is somewhat surprising. Figure 6.23 shows a comparison of different fuel atomizers at 60% thrust simulated conditions. The vaporizer nozzle shows much stronger influence of hydrogen content than other forms of fuel preparation.

Parametric tests showed no measurable THC emissions because of the representation of high-end operating conditions, so trends with P_3 and fuel-air ratio could not be evaluated.

6.5 CO EMISSIONS

The data on carbon monoxide emissions at idle generally correlated well with the hydrogen content of the fuel, as is evident from Figure 6.24. Thrust level simulation at idle showed stronger sensitivity of CO emissions to hydrogen content than power level simulation at idle. Take off simulation in both cases showed relative insensitivity to hydrogen content. Correlations with respect to hydrogen content are as follows:

At idle: $EI_{CO} = 236.4 - 11.18 (H)$ for thrust simulation
$EI_{CO} = 144.5 - 4.61 (H)$ for power simulation

At Take-off: $EI_{CO} = 33.69 - 1.92 (H)$ for thrust simulation
$EI_{CO} = 9.1$ for power simulation

CO emissions with a simplex pressure atomizer correlated poorly with relative droplet size and volatility, Figures 6.25 and 6.26, plots showing considerable data scatter. This relative insensitivity to fuel property variables is similar to reported data from J-79 combustors, (Figure 6.27), although stronger dependence at SMD ratios close to 1 and T_{10} in the 350-360K range were not repeated (probably due to insufficient data).

The effect of changing atomizers could not be evaluated at idle due to poor stability of airblast and vaporizer injectors at low power. Figure 6.28 shows comparison at 60% thrust simulation for the four atomizer types. Once again the vaporizing nozzle showed strongest influence of hydrogen content.

Parametric tests showed a reduced sensitivity to hydrogen content as the operating pressures were increased, Figure 6.29. No trends were observed with fuel-air ratio variation, (as is indicated by the scatter in Figure 6.29 (b)), but all the data were for operation at high combustor delivery temperatures representing low levels of CO emission.

6.6 NO$_x$ EMISSIONS

Figure 6.30 shows an attempted correlation of NO$_x$ emissions with fuel hydrogen content. For both simulated thrust and power level tests, take-off NO$_x$ emissions with a simplex pressure atomizer appear insensitive to hydrogen content. Idle NO$_x$ however decreases with reduction in hydrogen content which is probably the impact of lower primary zone gas temperature resulting from decreased combustion efficiencies at idle. Similar trends have been observed on other combustors, as shown in Figure 6.31 for TF39 engine. At high power, however, NO$_x$ emissions can be expected to increase with reduced hydrogen content because of increase in flame temperature. Relative insensitivity in this case indicates that changes in flame temperature are not of a sufficient magnitude to significantly influence NO$_x$ emmissions.

Data from other engines appear to indicate that the trends are dependent on combustor design. For example, the J85 combustion system with pressure atomizer appears to have only a poor dependence of NO$_x$ emissions with hydrogen content, whereas the F101 combustion system with airblast atomizer has a much stronger influence of hydrogen content, Figure 6.31. The TF39 combustion system showed an opposite trend, NO$_x$ emissions reducing with lower hydrogen content.

Comparison of fuel nozzles, Figure 6.32, shows stronger dependence between NO$_x$ emissions and hydrogen content for airblast and vaporizer systems. The increase of NO$_x$ emissions with reduction in hydrogen content possibly implies stronger influence of flame temperature changes for these fuel systems.

NO$_x$ emissions were also found to be insensitive to relative droplet size (of pressure atomizer) and volatility of fuel, Figure 6.33. Figures 6.34 and 6.35 show results of parametric tests with the simplex atomizer. For all fuels, strong dependence on operating pressures and marginal dependence on fuel-air ratios were observed.

6.7 SMOKE EMISSIONS

Figures 6.36 to 6.38 summarize results of smoke tests with the simplex pressure atomizer. Only data from thrust level tests were considered since a leak in the smoke sample collector was discovered halfway through the test program. Therefore the power level data were discarded and tests were repeated for take off simulation of thrust level with all fuels.

Figure 6.36 shows the variation of smoke with fuel hydrogen content, the general trend indicating an increase in smoke emissions as the fuel hydrogen content is reduced. Correlations based on linear regression are as follows:

$$SN = 146 - 8.33 \ (H) \ \text{at take off}$$
$$SN = 72.6 - 4.58 \ (H) \ \text{at idle}$$

The data also indicates considerable amount of scatter and inconsistent trends between take-off and idle. It may also be noted that JP-10

resulted in smoke levels generally lower than the trend line, the effect being particularly apparent at low power simulation (Figure 6.36).

Figure 6.37 shows smoke number as a function of hydrogen content for Jet Al and JP4 based fuels. Figure 6.38 shows smoke number at take-off plotted against aromatic content by volume and fuel naphthalene content. Figure 6.39 shows variations of aromatic and naphthalene contents of test fuels. With Jet Al and JP4 fuels, the addition of 2040 solvent increases both aromatic and naphthalene contents appreciably and results in a strong increase in smoke level. However fuels such as L-H, H-M, L-M have relatively lower naphthalene content accompanying moderately high aromatic content, and these fuels appear to have correspondingly lower smoke emissions. On the other hand, ERBS-3 with higher than average naphthalene content appears to have higher smoke emissions. These observations appear to indicate that the types as well as overall levels of aromatics are significant and that the presence of high concentrations of more complex multi-ring aromatics may increase the propensity for smoke formation.

Figure 6.40 shows the effect of relative droplet size for the pressure atomizer; once again the trend at idle appears inconsistent possibly due to wall quenching effects; however, take-off smoke increases marginally with increased fuel droplet size.

Figure 6.41 shows the effect of fuel preparation technique on smoke emissions. Airblast and vaporizer nozzles result not only in lower smoke emissions but also appear to be less sensitive to hydrogen contents. These trends are consistent with results from other programs, Figure 2.1, which have compared performances of airblast (F101) and pressure atomizing (J79) combustion systems.

6.8 CARBON AND FUEL SPRAY QUALITY

In order to obtain qualitative understanding of carbon deposition and fuel atomizer performance, checks of carbon build-up and fuel nozzle sprays were made after continuous running for 3.7 hours on the simulated turbofan cycle and 2.5 hours on the simulated turboprop cycle. There was no evidence of carbon formation on the main body of the liner with any of the test fuels. Airblast and vaporizer nozzles did not show any carbon or soot on either the air-fuel passages or on the swirler faces. There was however, depending on the fuel, soot and carbon formation on the front face of the pressure atomizer swirler sheath. Figures 6.42 to 6.45 show photographs of nozzle swirler front face, along with measured maximum thickness of carbon formation. With some of the fuels there was evidence of carbon shedding which made comparison with other fuels difficult. With Jet A based fuels for example, evidence from thrust cycle runs showed increased carbon build-up with reduced hydrogen content; however, on the power cycle, carbon shedding with Jet Al/Bl and Jet Al/B2 gave inconclusive results. Shale JP8 showed build-ups similar to Jet Al. JP4/B2 showed different carbon build-ups on the thrust and power cycles. On the power cycle, there were unexpectedly high carbon build-ups while on the thrust cycle, the carbon build-ups were lighter than both JP4 and JP4/Bl. However, in the latter case most of the carbon appeared to be of the soft type prone to easy shedding, which may

explain the low measured build-up. Diesel resulted in heavy build-up on the power cycle, Figure 6.45, while L-M tar sands showed heavy build-ups on both thrust and power cycles. Low hydrogen tar sands blends (L-L) showed marginally heavier build-ups than the high hydrogen blends (L-H). JP-10 resulted in moderate carbon build-up on the turboprop cycle and much lighter build-up on the turbofan cycle.

Table 6.2 shows measured carbon build-up with the various fuels. Because of carbon shedding with some of the fuels, only qualitative comparison is possible. In general, reduced hydrogen appears to increase carbon forming tendencies; heavy carbon build-up was observed with JP4/B2, L-M tar sands and Diesel fuels. Surprisingly ERBS-3, compared with Diesel, showed very little carbon build-up on both thrust and power cycle operations.

Changes in fuel composition can alter the thermal stability of the fuel and lead to changes in the propensity for deposit formation on the surface of fuel passages in injectors and manifolds. However, the thrust and power level tests showed no apparent deposit formation in the fuel passages which affected the quality of the fuel spray in a visual sense. The other possibility is carbon deposition on hot fuel nozzle faces and combustor components due to the early cracking of the fuel. Attempts were made to correlate the maximum measured carbon deposits with fuel breakpoint temperatures (shown in Table 3.5). A wide degree of scatter was observed preventing correlation of thermal stability to carbon deposition rates on fuel nozzle surfaces.

6.9 LINER METAL TEMPERATURES

Liner temperature measurements were obtained with 12 thermocouples located on the cold side of the liner. As described in Section IV, the thermocouples were located in the primary, intermediate and dilution zones of the combustor. The liner temperatures, in general, showed wide variations from test to test, apparently in a random manner. For example, while some liner temperatures appeared to increase with decreasing hydrogen content at some power settings, at other settings the reverse occured. These effects are thought to be the result of local fuel-air ratios and flame fronts being influenced by fuel properties. As well, three of the thermocouples were erratic and one failed midway through the test program. For purposes of analysis, data from the eight thermocouples shown in Figure 6.46 were considered.

Figure 6.47 shows average liner delta T's(T_L - T_3) at simulated take off thrust condition as a function of fuel hydrogen content, for the simplex fuel nozzle. While the data shows considerable scatter, the general trend indicates higher metal temperatures corresponding to reduced hydrogen content. Less scatter may be observed for individual groups of fuels such as Jet A1 and JP4. Figure 6.48 shows the same effect when expressed as Liner Temperature Parameter, which is based on average liner temperature relative to the baseline JP4 fuel. The relationship between Liner Temperature Parameter and fuel hydrogen content can be expressed as follows:

$$\frac{T_L - T_{L_{JP4}}}{T_{L_{JP4}} - T_3} = 0.336 - 0.0189 \, (H)$$

Also shown for comparative purposes are the engine correlations by Blazowski [11], the dashed lines encompassing data from five combustors.

Figure 6.49 shows the data plotted against fuel aromatic content. Increases in the aromatic content of the fuel can have substantial impact on the radiant heat transfer to the combustion liner, because of the increased concentrations of highly luminous carbon particulates in the combustion gases. Radiation effects are likely to be most significant in the primary combustion zone where the local fuel-air ratios and gas temperatures are the highest. JP10, being a synthetic fuel shows high temperature levels, in spite of the absence of aromatics.

To evaluate the effect of fuel properties on radiation, measurements of radiant heat flux were made at two pressure levels using a transpiration radiometer (Section 5.1.3). Figure 6.50(a) shows radiant heat flux as a function of fuel hydrogen content, data at both pressure levels showing good correlations according to:

$$Q_r = 3828 - 184.6(H) \text{ at } P_3 = 10 \text{ atm}$$

$$Q_r = 2620 - 166.7(H) \text{ at } P_3 = 4.8 \text{ atm}$$

Stronger trends were apparent at higher pressure levels, larger droplet size resulting in higher radiant heat loads (Figure 6.50(b)). Correlations for droplet size are as follows:

$$Q_r = 547 + 733(RSMD) \text{ at } P_3 = 10 \text{ atm}$$

$$Q_r = 165 + 244(RSMD) \text{ at } P_3 = 4.8 \text{ atm}$$

Figure 6.51 is a plot of Liner Temperature Parameter against Relative Radiation Flux defined as (Q_r/Q_{rJP4}). It appears that much of the increased liner temperatures associated with reduced hydrogen content is due to increased radiation loads on the liner walls; however the data scatter also indicates that other parameters may be influencing the liner temperatures. Also, liner temperatures are averaged over the entire combustor, whereas radiation measurements were made in the primary zone only.

Figure 6.52 shows the relative effect of fuel atomizers on liner temperatures. Airblast and vaporizer nozzles appear to be less sensitive to hydrogen content than pressure atomizing nozzles, which augurs well for advanced combustion systems which use these techniques for fuel preparation.

Figures 6.53 through 6.55 show results of parametric tests on average liner metal temperatures. Increasing operating pressures result in higher liner temperatures. While the effects on Jet A1, Tar Sand and Diesel groups are similar, there is considerable variation among JP4 based fuels. Fuel-air ratio effects, Figure 6.54, also show inconsistent trends with JP4 based fuels. Figure 6.55 shows liner temperature data at two of the parametric test conditions. The relative effect of using different fuel nozzles was similar to trends observed at 100% thrust simulation (Figure 6.52). The lower liner temperatures with the vaporizing nozzle may be the result of lower radiation and direction of fuel-air mixture toward the dome of the combustor.

- 102 -

Fuel	LL FAR for Ω_{idle} *	LL FAR for M_{idle} **
JET A1	0.0048	.0041
JET A1/B1	0.0069	.0043
JET A1/B2	0.0066	.0049
JP8 Shale	0.0045	.0040
JP4	0.0056	.0034
JP4/B1	0.0054	.0039
JP4/B2	0.1050	.0042
JP4/2040/diesel	0.0070	.0045
ERBS	0.0064	.0064
Diesel	0.0063	.0079
JP10	0.1300	.0070
Tar Sands L-N	0.0051	.0054
Tar Sands N-N	0.0051	.0054
Tar Sands L-M	0.0051	.0054
Tar Sands L-L	0.0087	.0063

* $W_c = 0.236$ kg/s (0.52 lb/s)
$P3 = 0.41$ MPa (4.0 atm)
$T3 = 375$ K
Simplex Nozzle

** $W_c = 0.141$ kg/s (0.31 lb/s)
$P3 = 0.41$ MPa (4.0 atm)
$T3 = 375$ K (675°R)
Simplex Nozzle

Table 6.2: Summary of Nozzle Face Carbon Accumulations

	TEST FUELS										TAR SANDS				
	JET A1	JET A1 B1	JET A1 B2	SHALE JP-8	ERBS	JP4	JP4 B1	JP4 B2	JP4/ 2040/ DF	DIESEL	L-N	L-M	L-L	N-N	JP-10
Thrust Level Tests (4.5 hour cycle) Simplex Nozzle	.76	.94	1.2	.64	0*	.79	1.1	.15	1.1	0*	.99	3.2	1.2	0*	.28
Power Level Tests (3.5 hour cycle) Simplex Nozzle	.79	.28	.25	1.4	0*	.25	0*	22.9	.64	2.1	.84	21.5	1.3	.76	1.5
Thrust Level Tests (4.5 hour cycle) Duplex Nozzle	1.1	✕	1.7	✕	4.4	1.3	✕	.64	✕	✕	.69	✕	✕	✕	✕

dimensions are in mm.

* No carbon, but stains indicate possible shedding
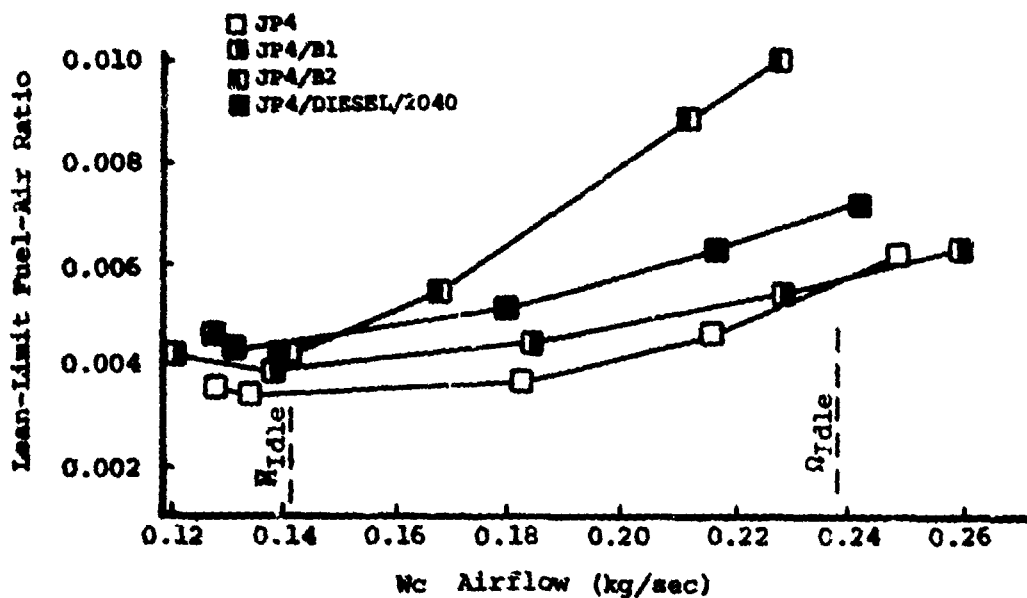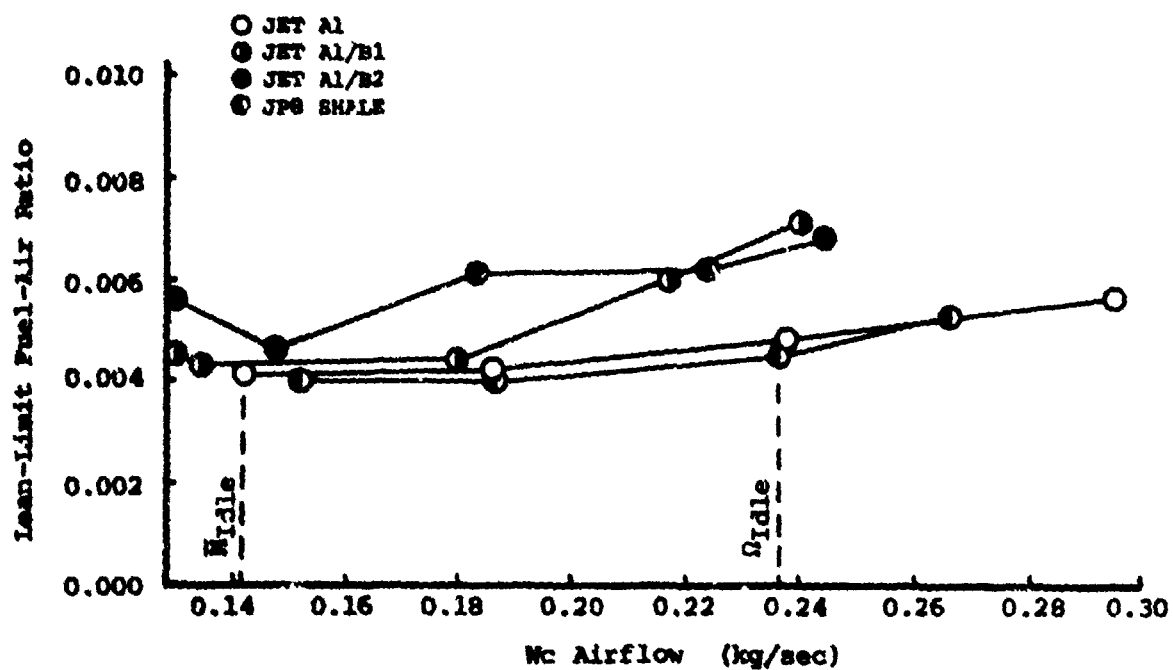
Figure 6.1: Effect of Airflow on Lean-Limit Fuel-Air Ratio
(Jet A1 and JP4 Based Fuels, Simplex Nozzle)
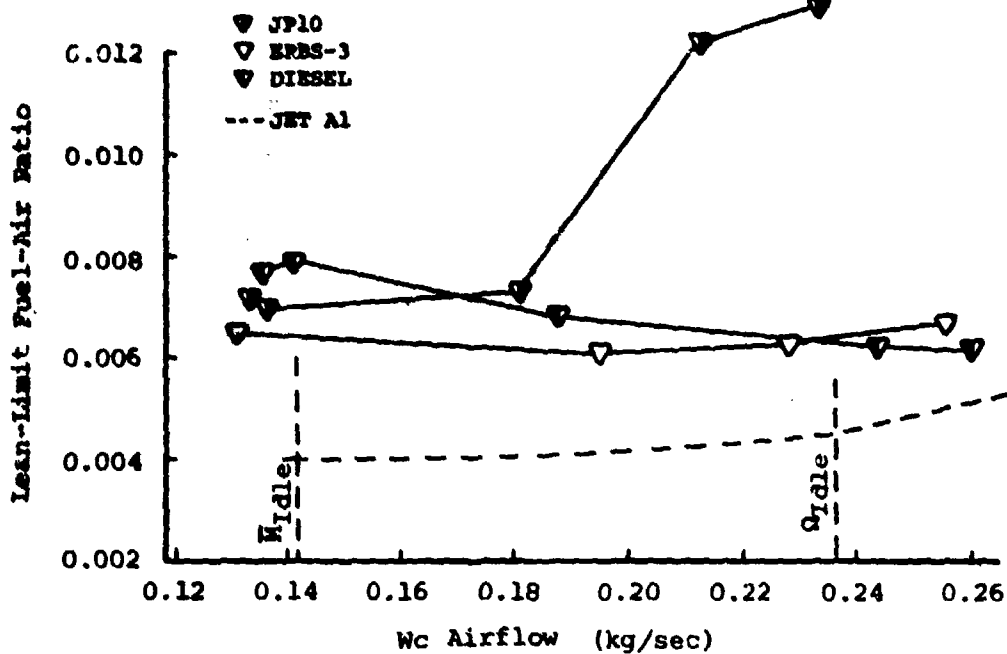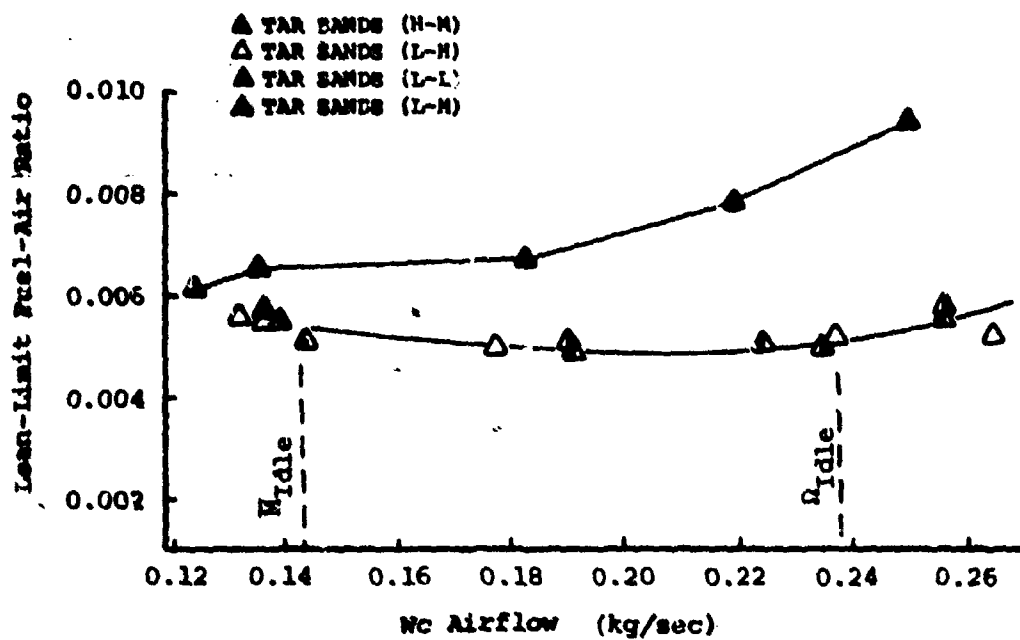
Figure 6.2: Effect of Airflow on Lean-Limit Fuel-Air Ratio (Tar Sands and Diesel, ERBS-3 and JP10 Fuels)
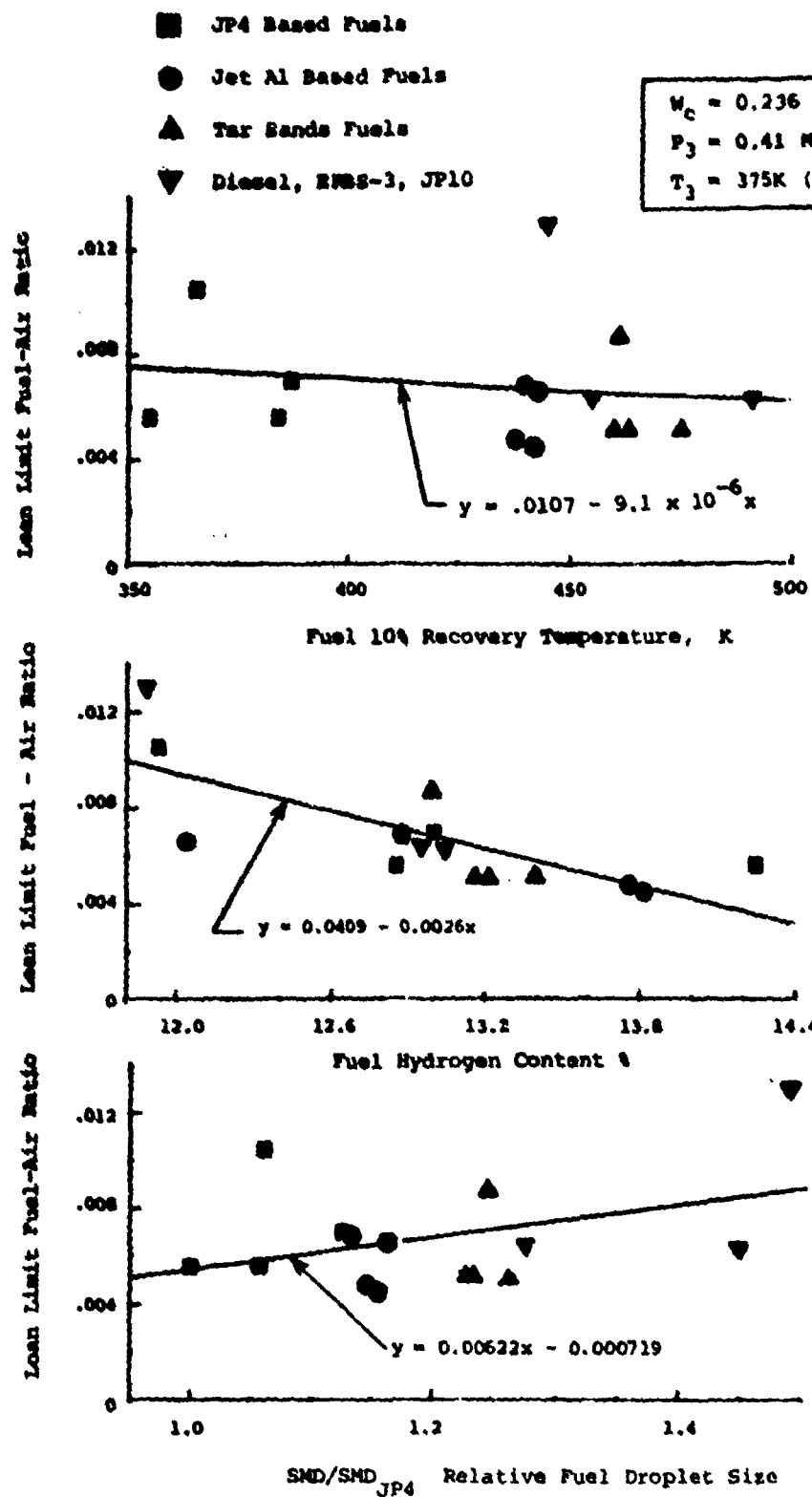
Figure 6.3: Effect of Fuel Properties on Lean Limit Fuel-Air Ratio
(Based on Ω_{IDLE} Simulation, Simplex Nozzle)
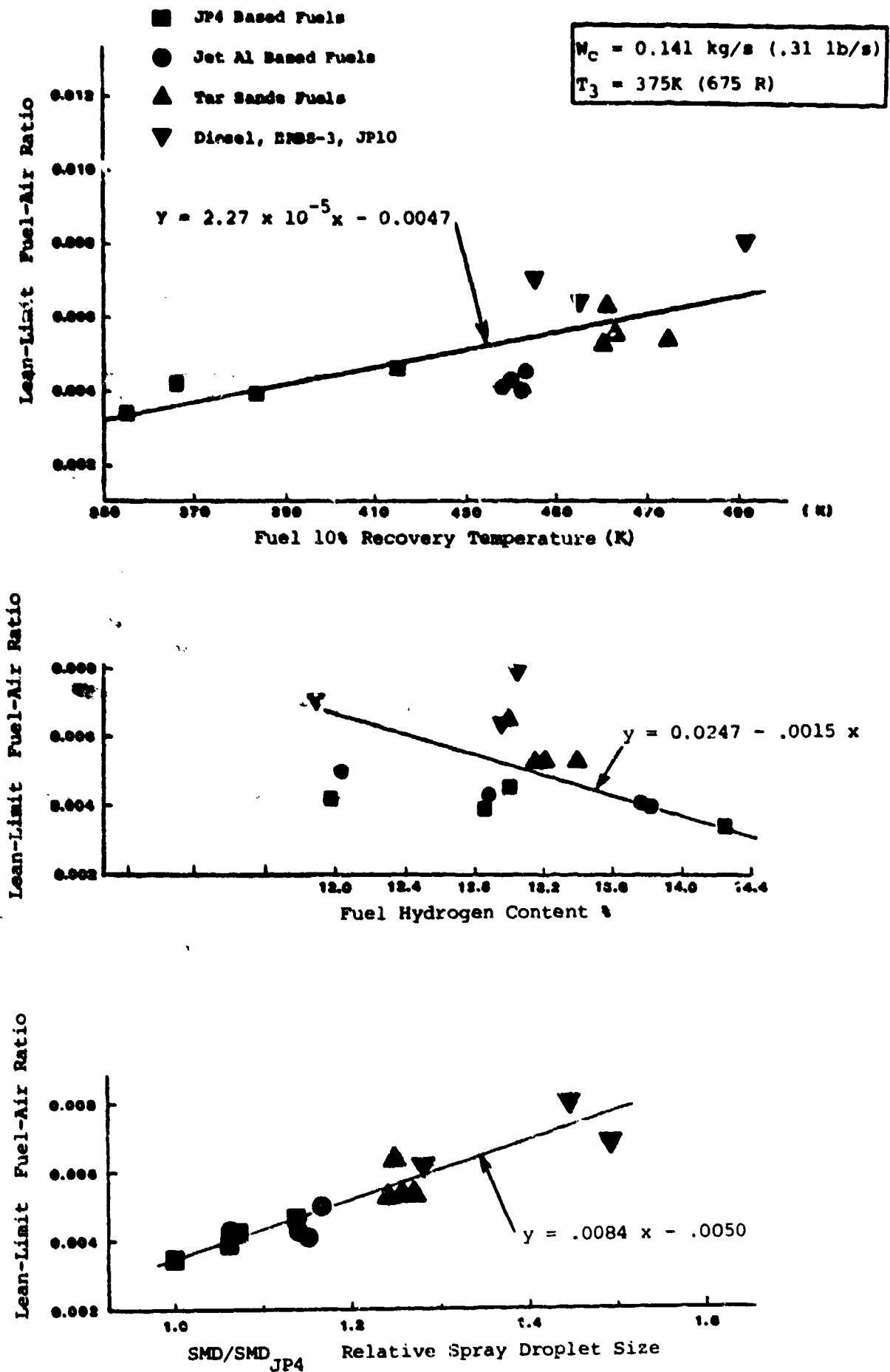
Figure 6.4: Effect of Fuel Properties on Lean Limit Fuel-Air Ratios
(Based on H Simulation, Simplex Nozzle)
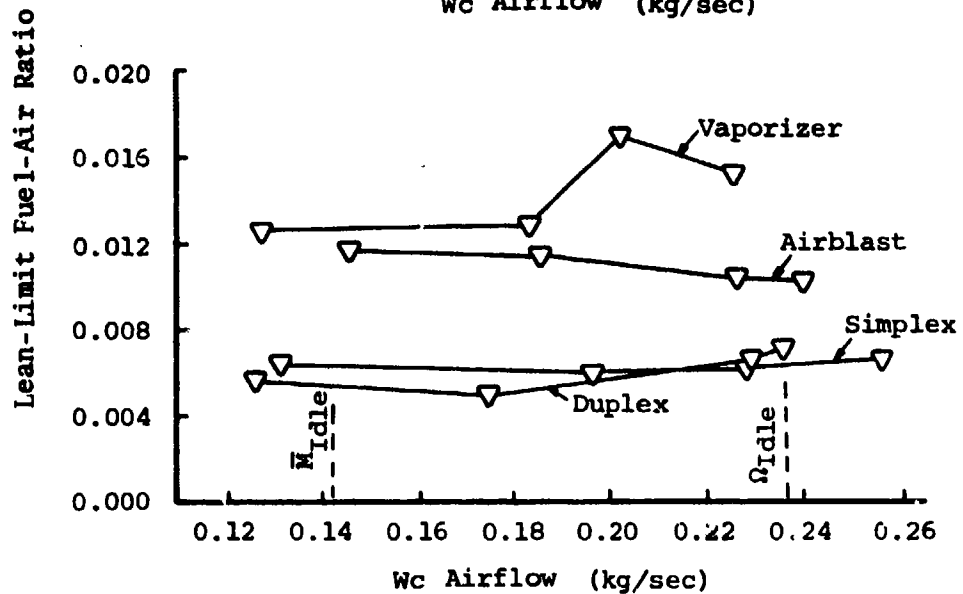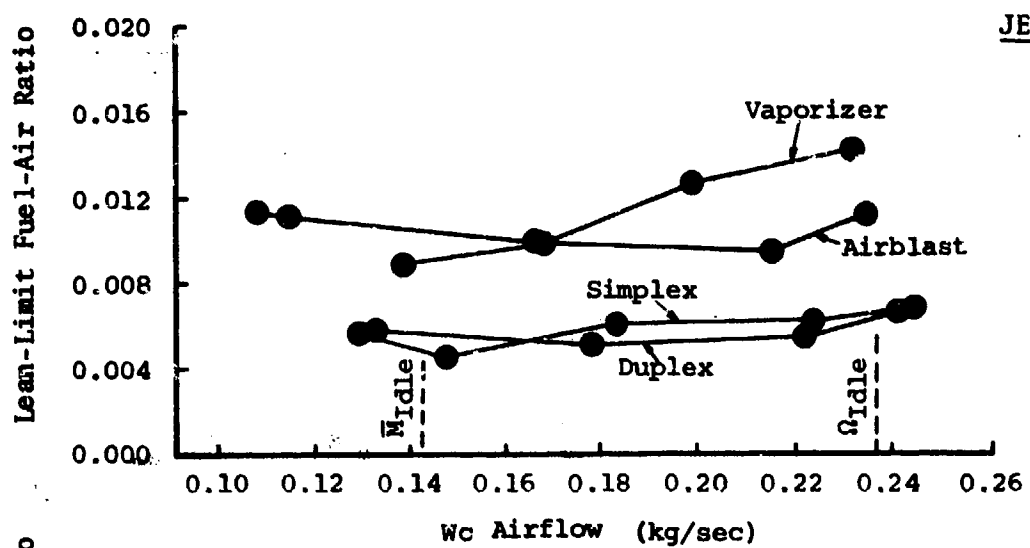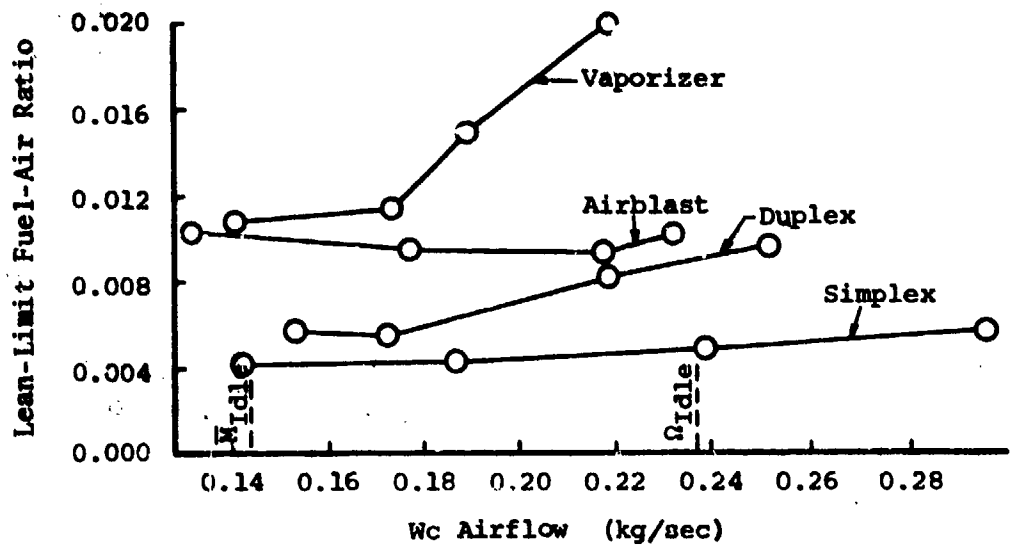
Figure 6.5: Effect of Airflow on Lean-Limit Fuel-Air Ratio (Nozzle Comparison)
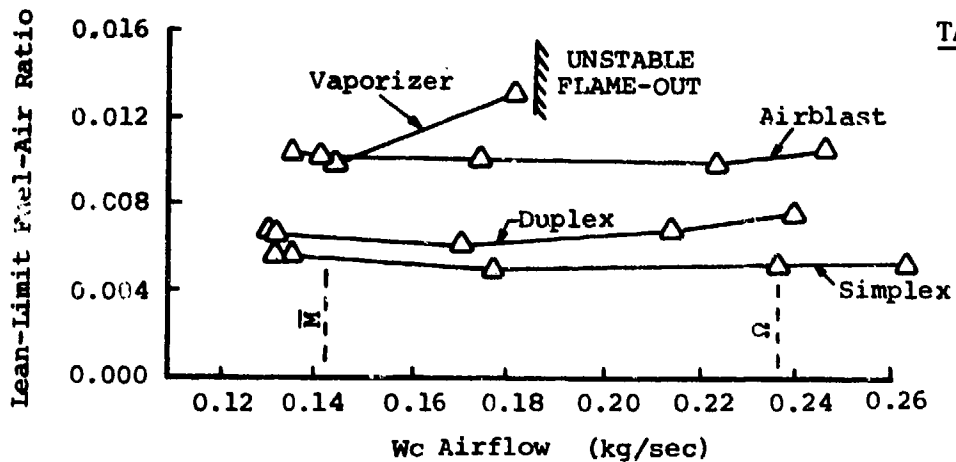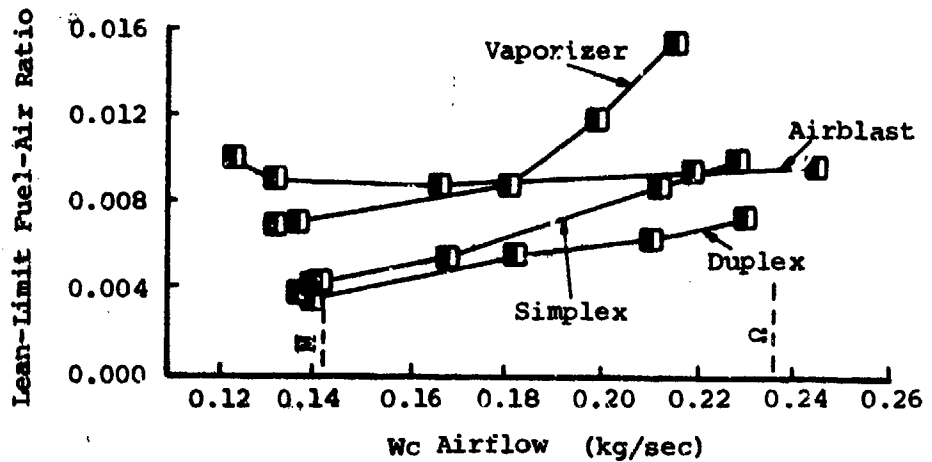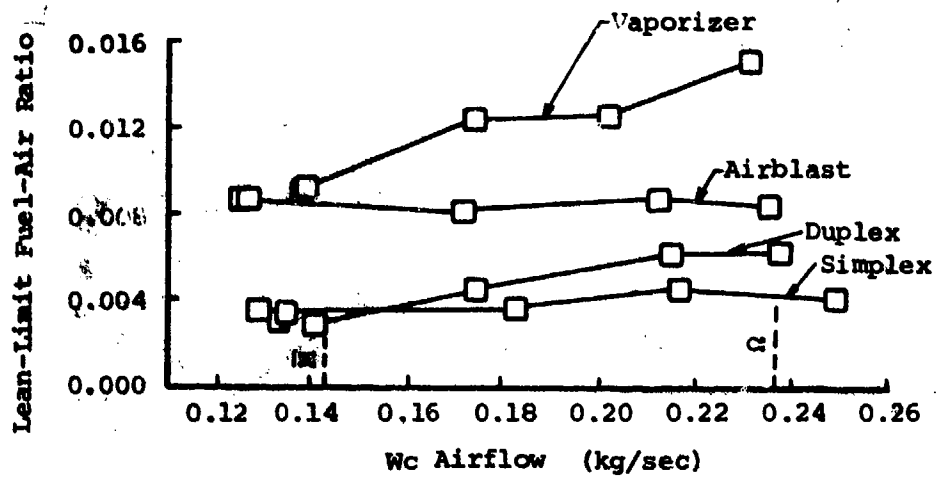
Figure 6.6: Effect of Airflow on Lean-Limit Fuel-Air Ratio
(Nozzle Comparison)
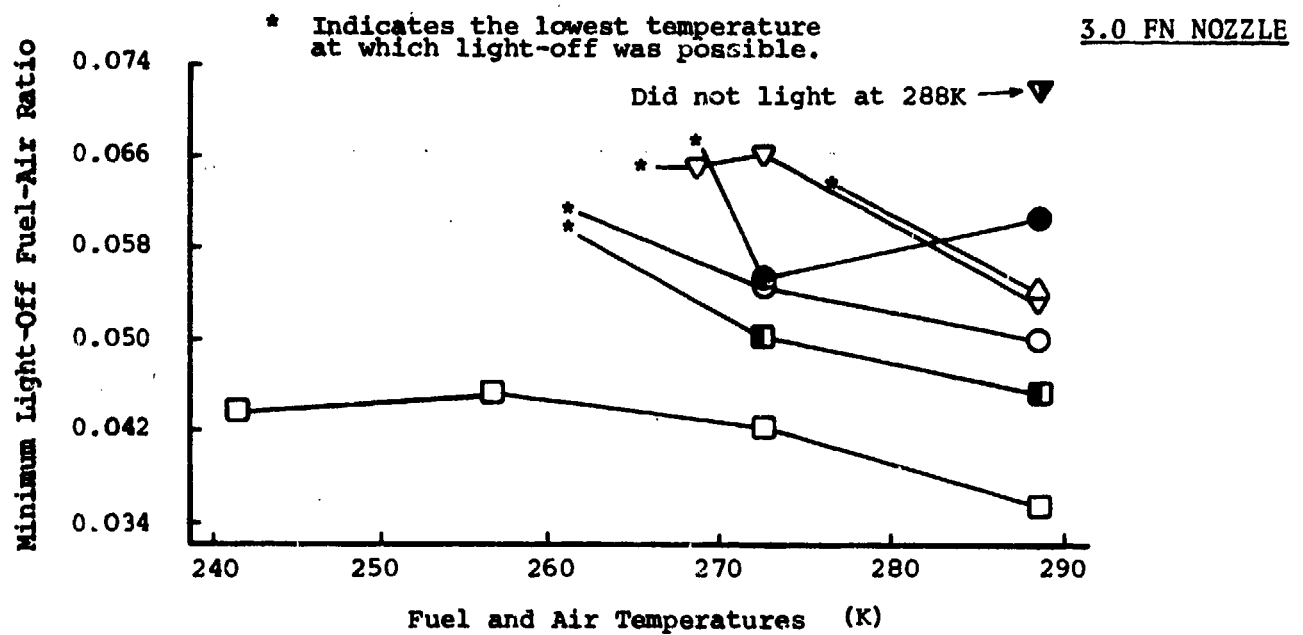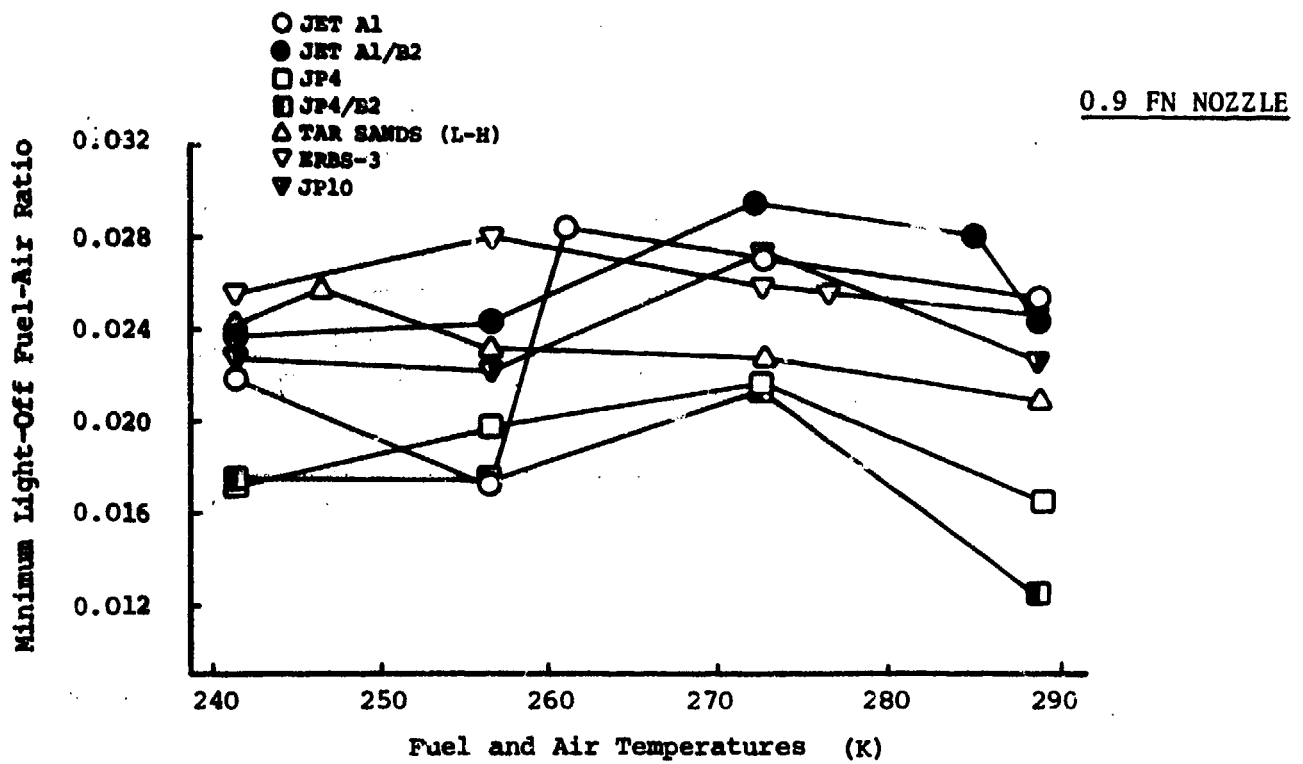
Figure 6.7: Effect of Fuel and Air Temperatures on Minimum Light-Off
Fuel-Air Ratio
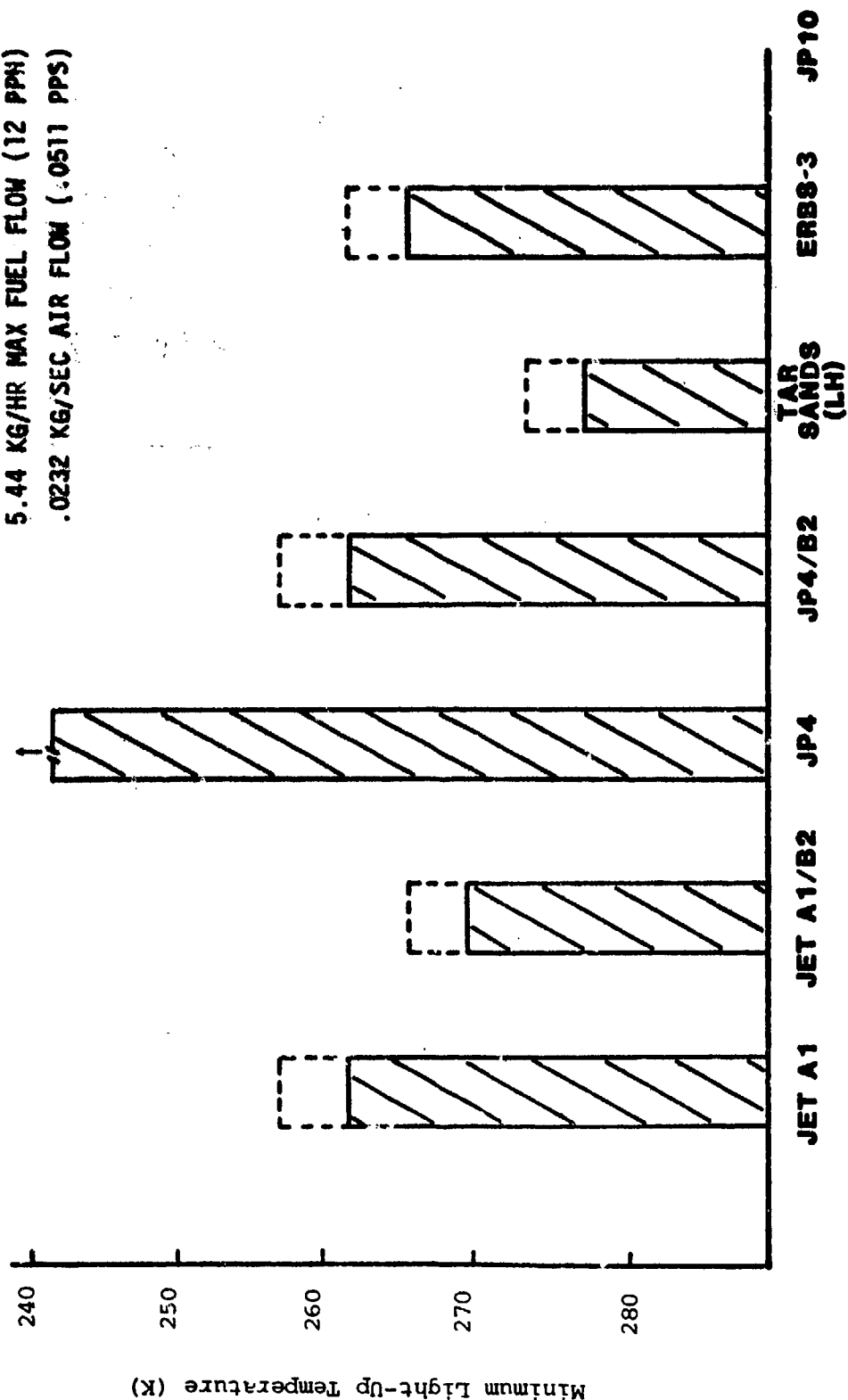
Figure 6.8: Comparison of Light-Off Performance for Different Fuels
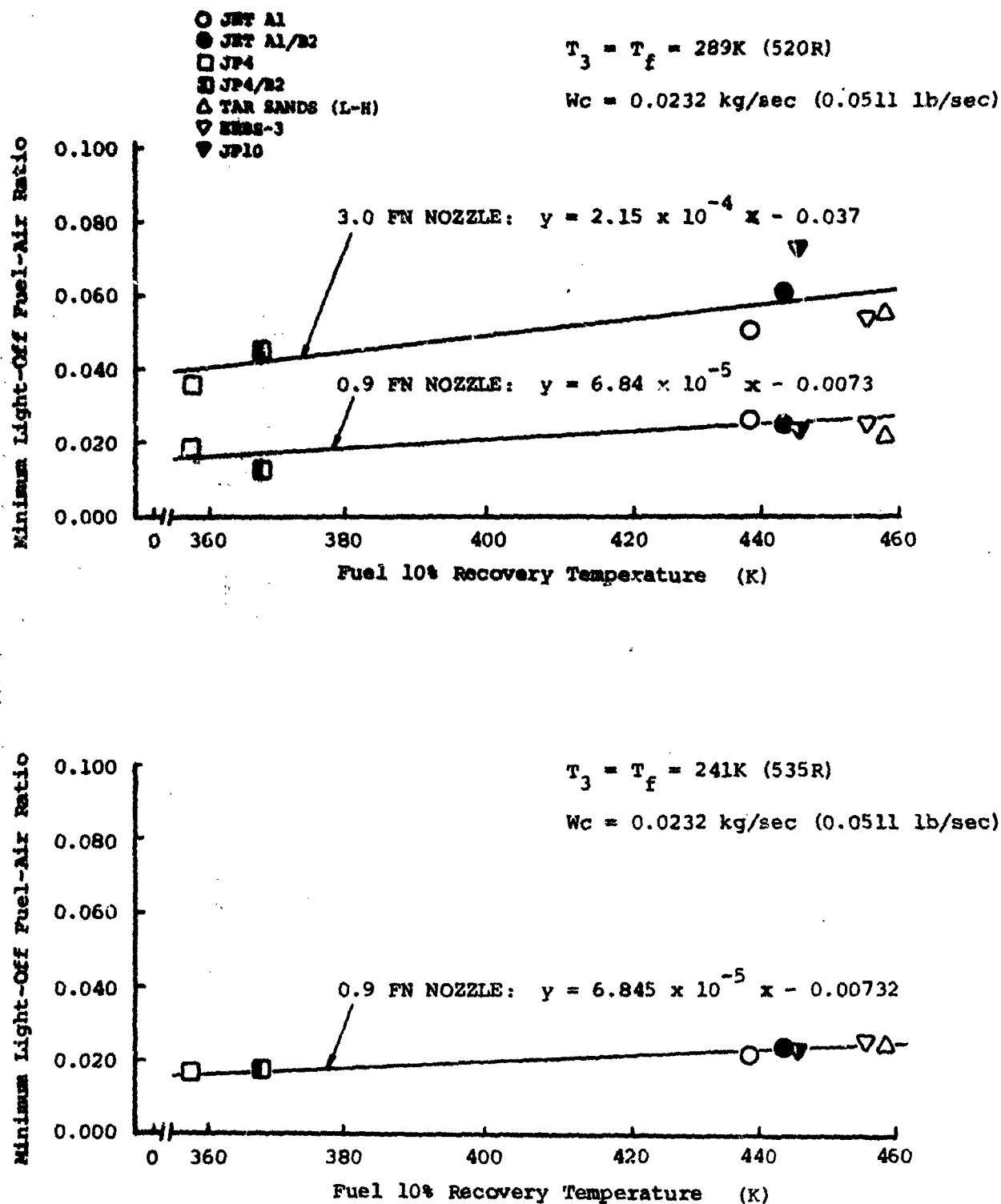
Figure 6.9: Effect of Fuel Volatility on Start-up Performance

SMD/SMD$_{JP4}$ Relative Spray Droplet Size at Test Temperature
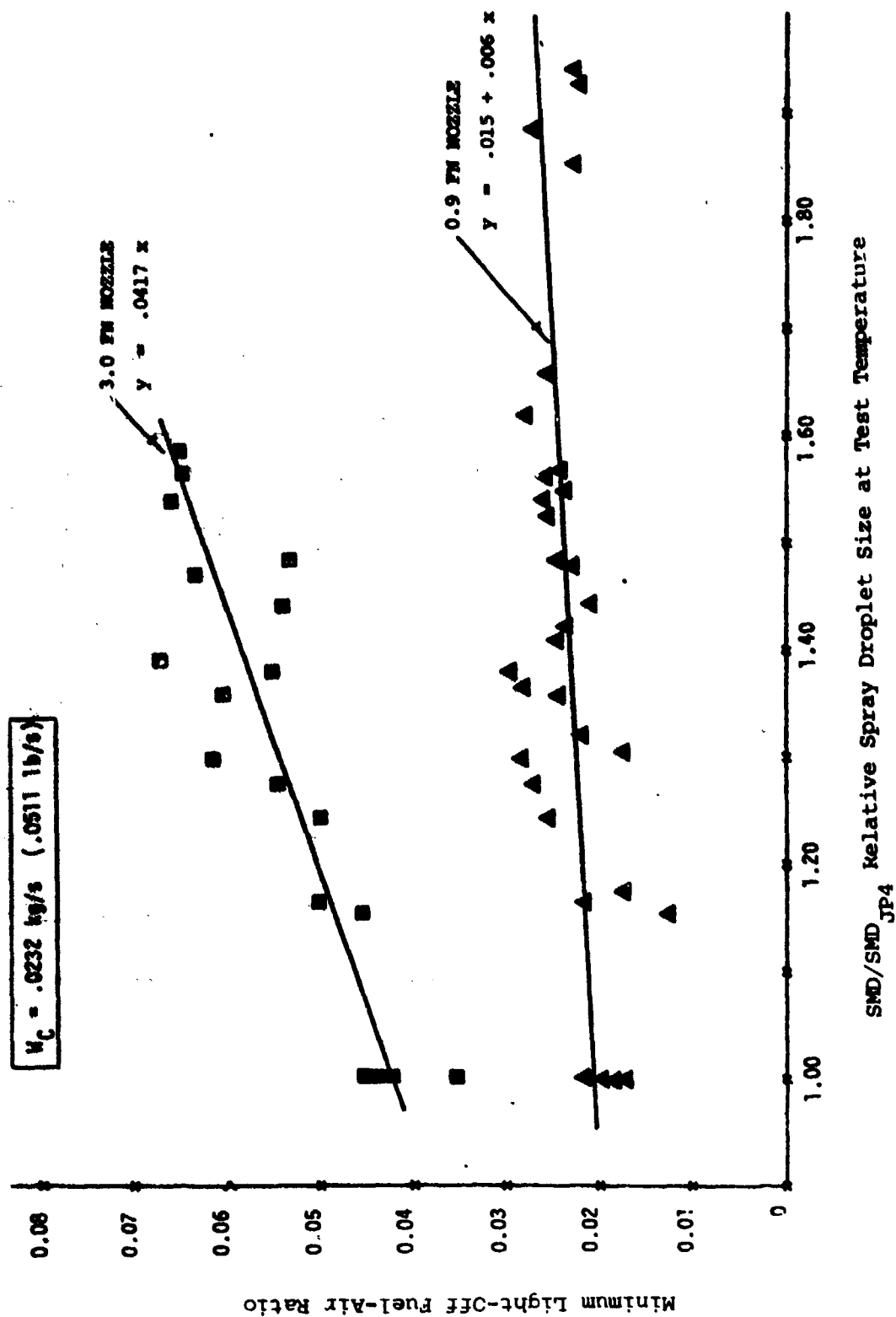
Figure 6.10: Effect of Fuel Atomizing Characteristics on Light-Up Performance
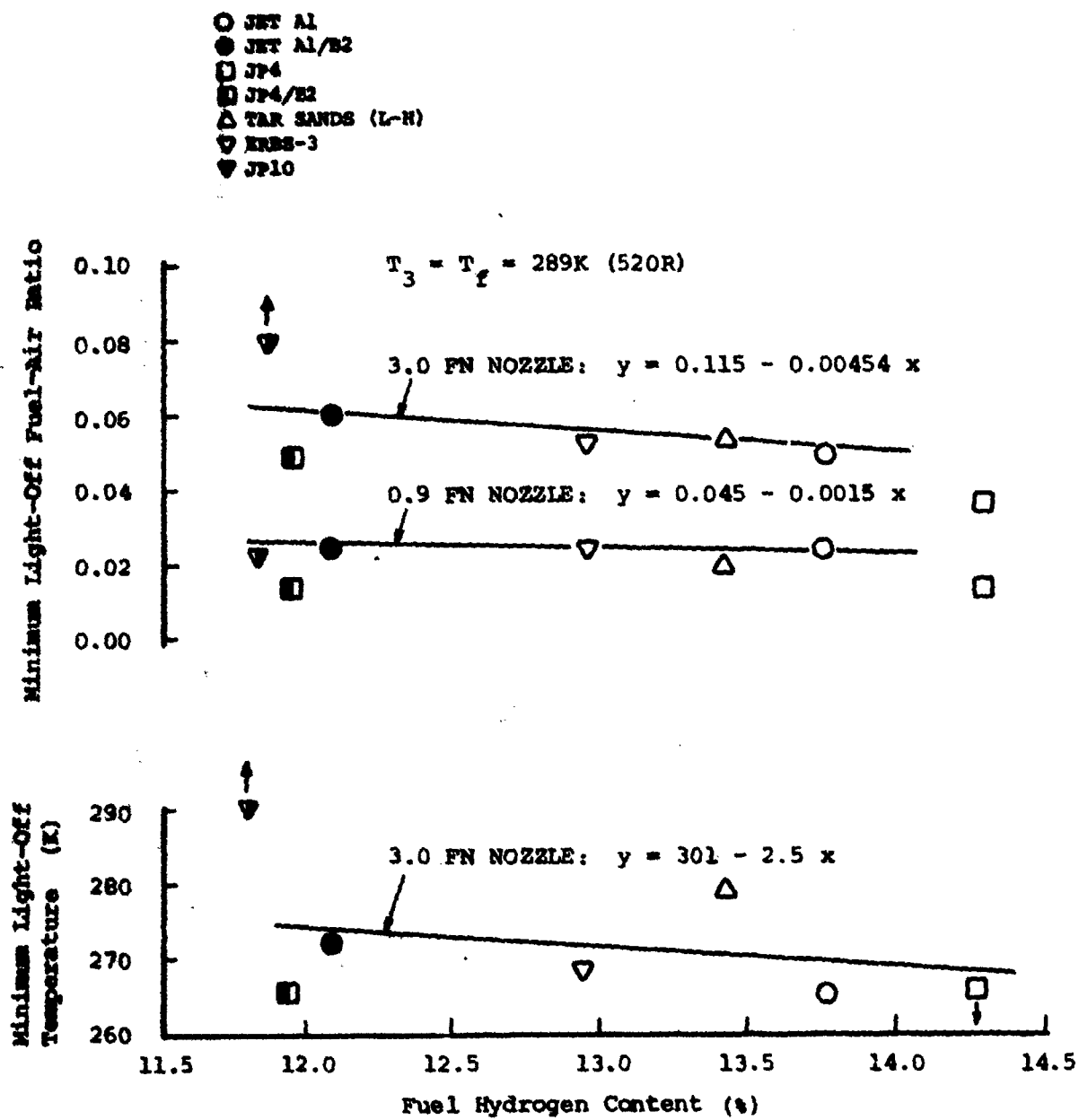
Figure 6.11:   Effect of Fuel Hydrogen Content on Light-Up
Characteristics

-114 -
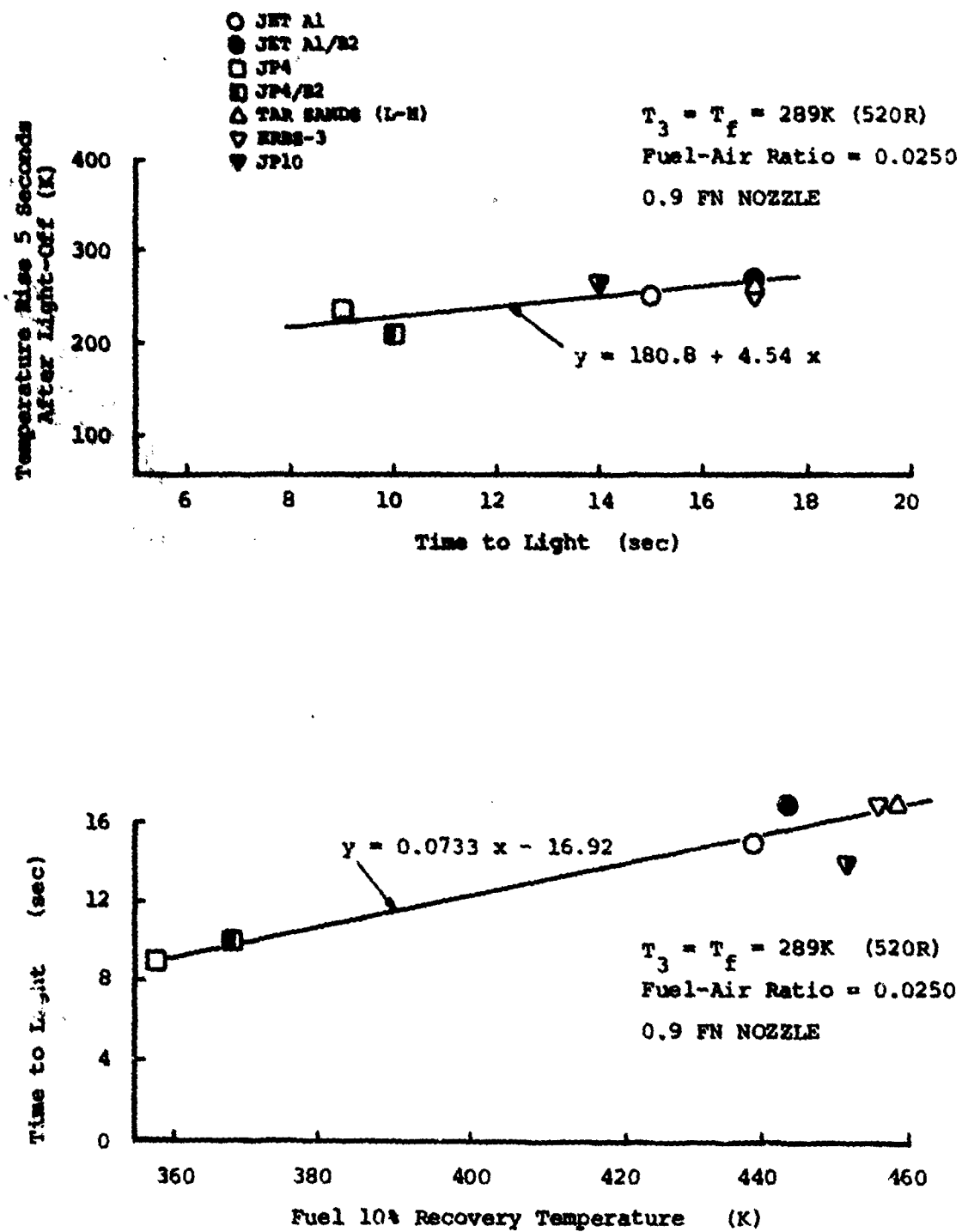
Figure 6.12:   Effect of Fuel Volatility on Time to Light and
Temperature Rise after Ignition
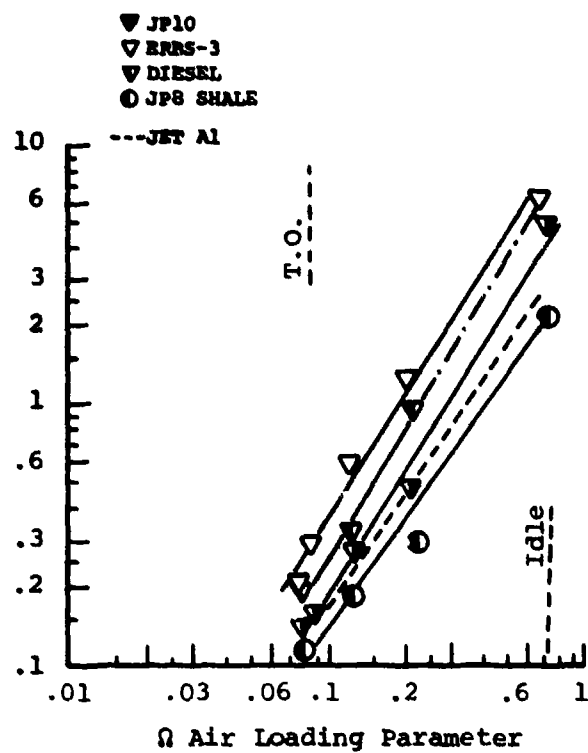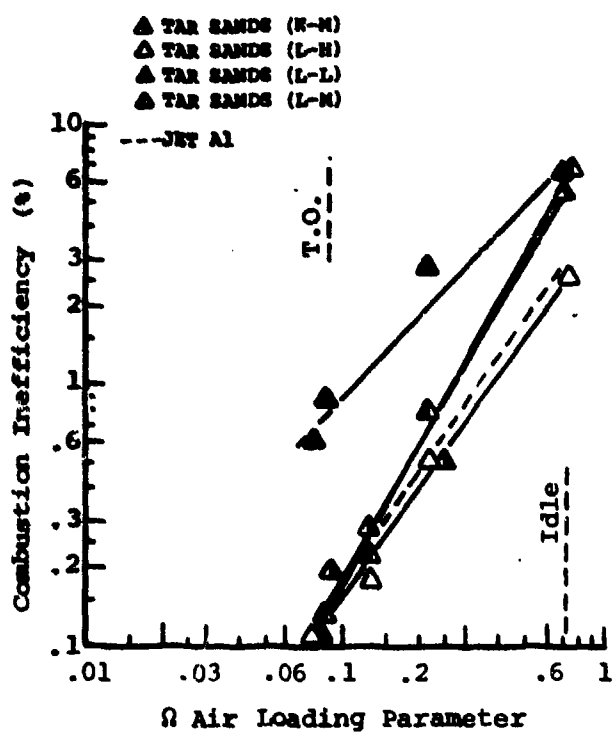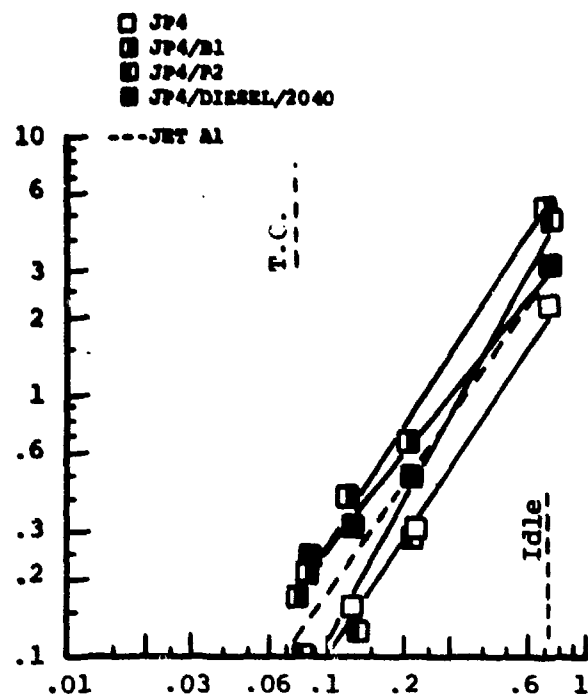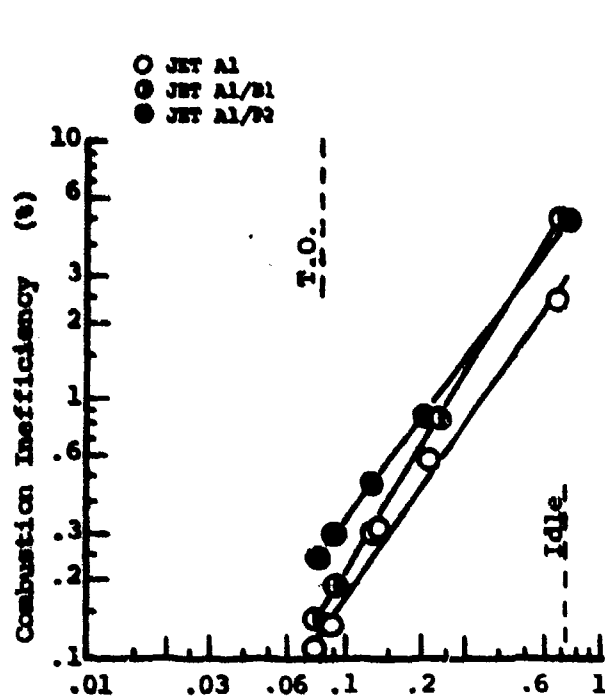
Figure 6.13: Combustion Efficiency Comparison
(Thrust Level Tests, Simplex Nozzle)
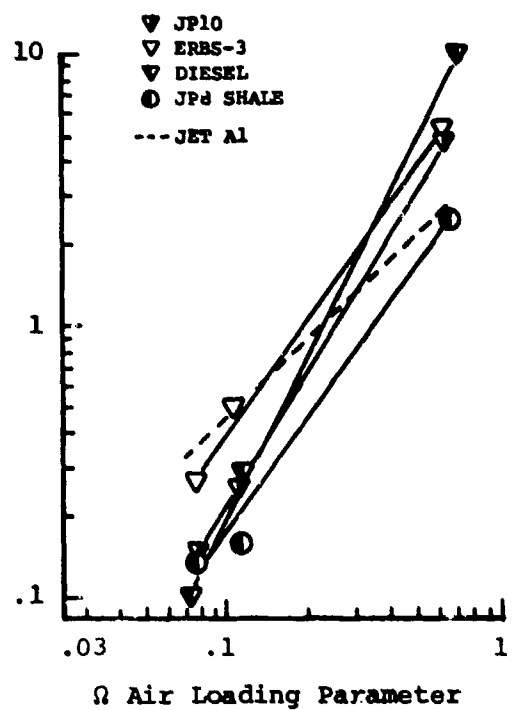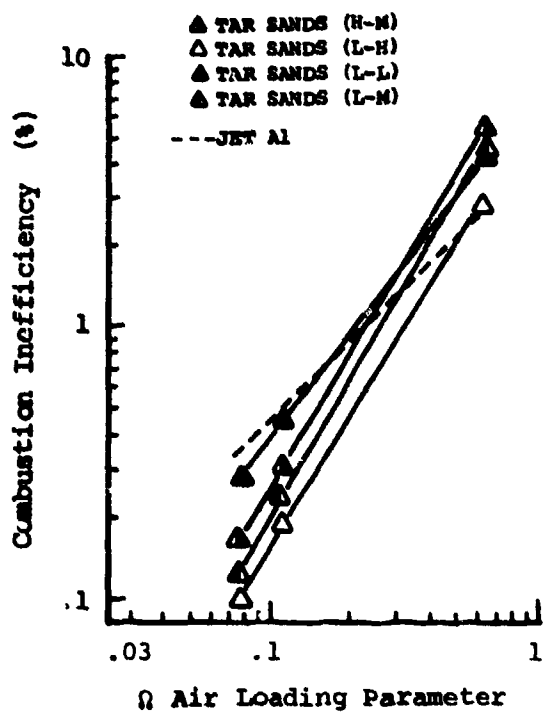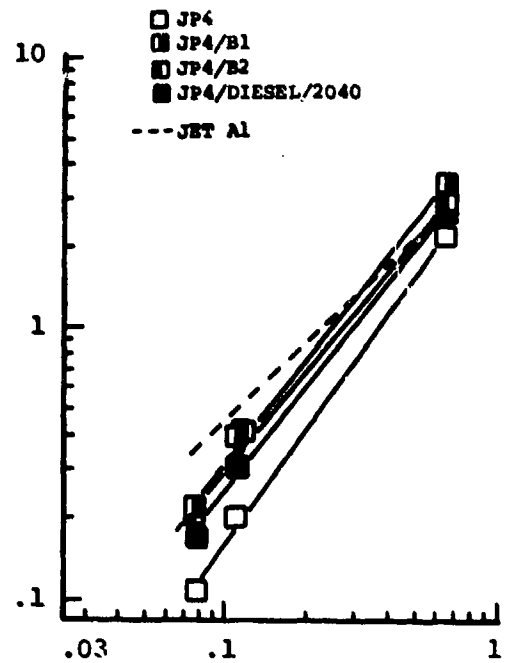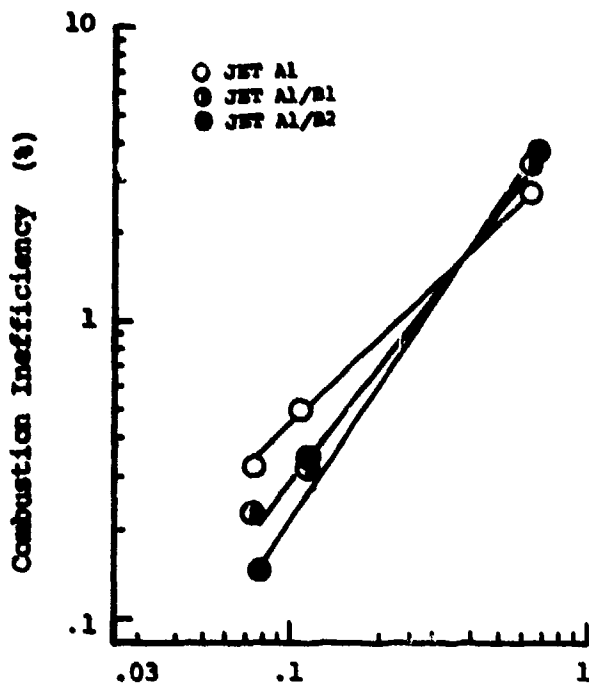
Figure 6.14: Combustion Efficiency Comparison
(Power Level Tests, Simplex Nozzle)
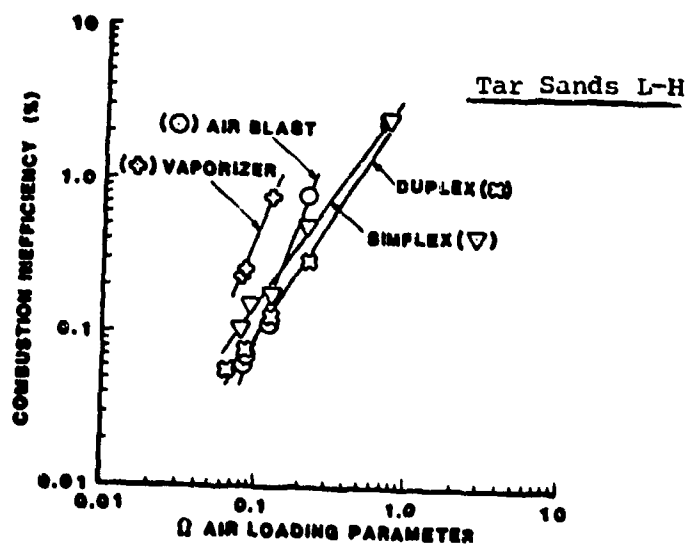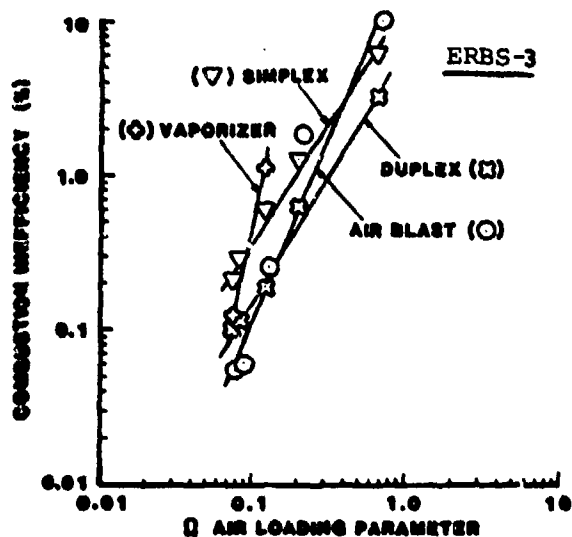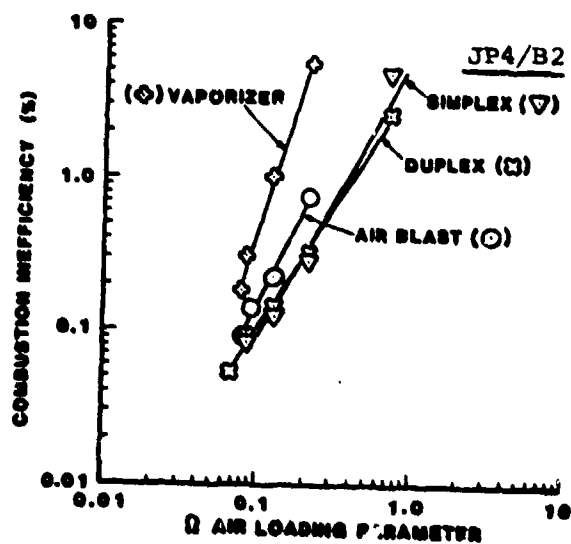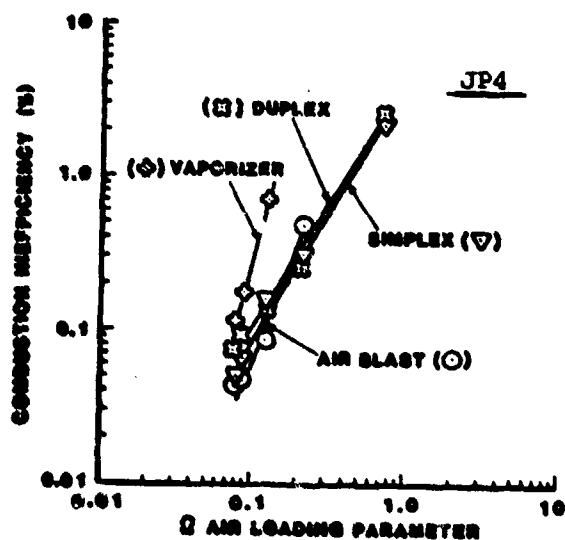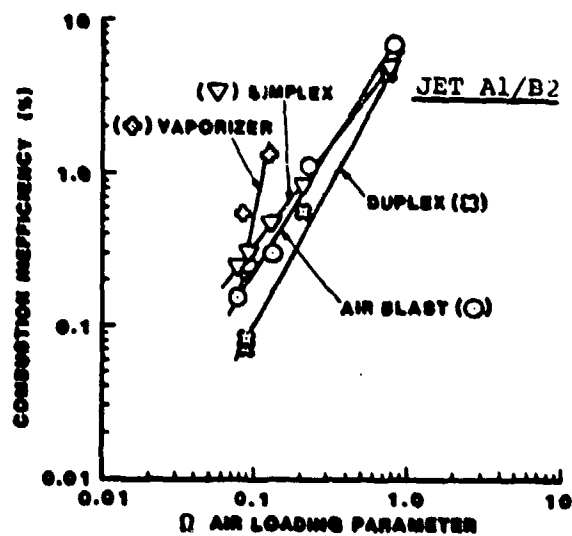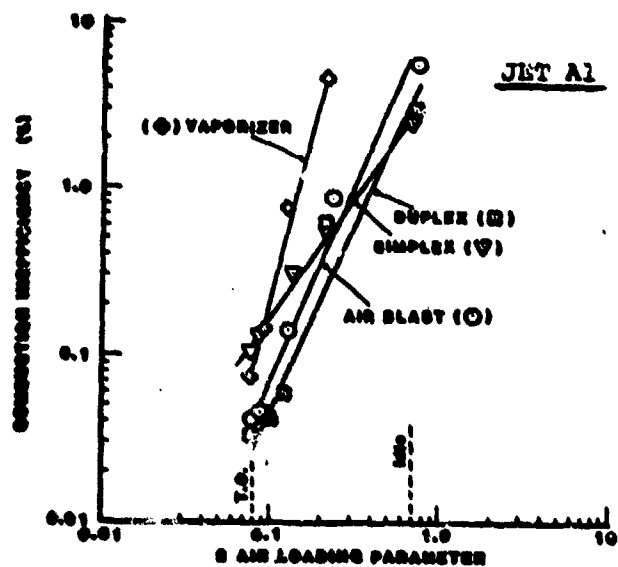
Figure 6.15: Nozzle Comparison (Thrust Level Tests)
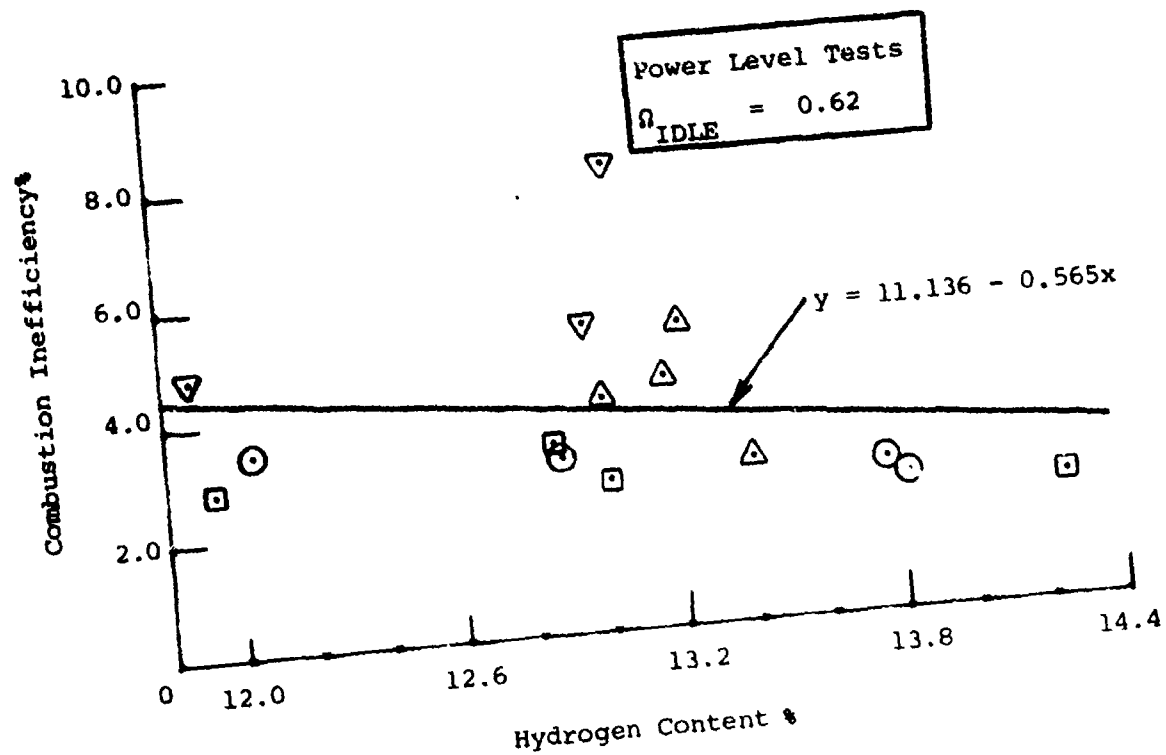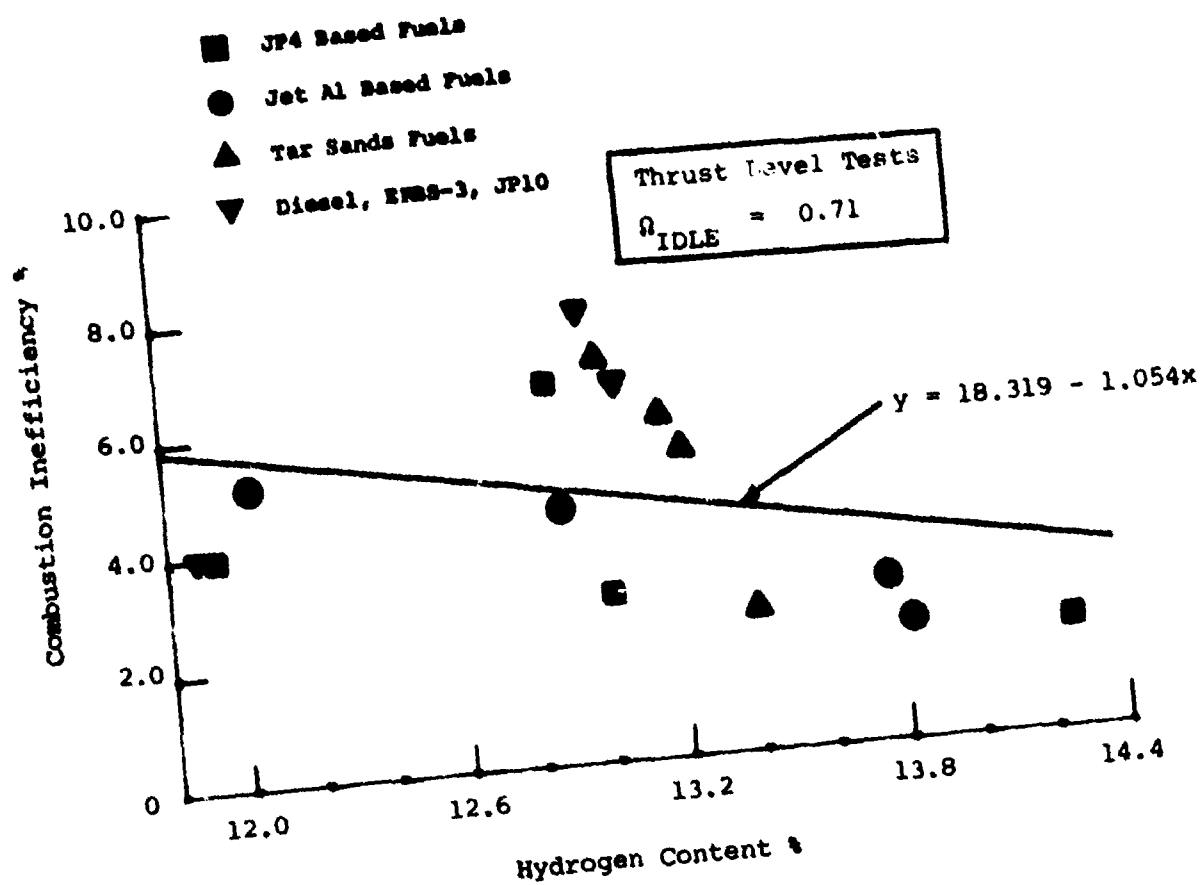
Figure 6.16: Effect of Hydrogen Content on Idle Combustion Inefficiency, Simplex Nozzle
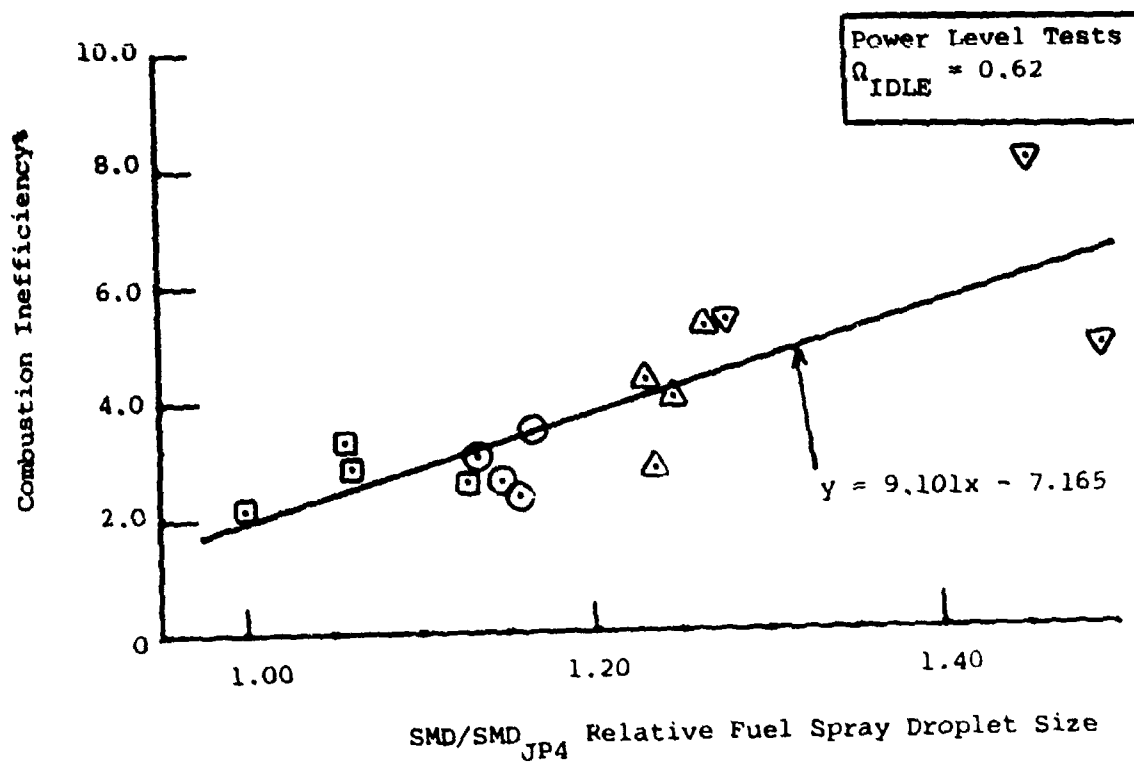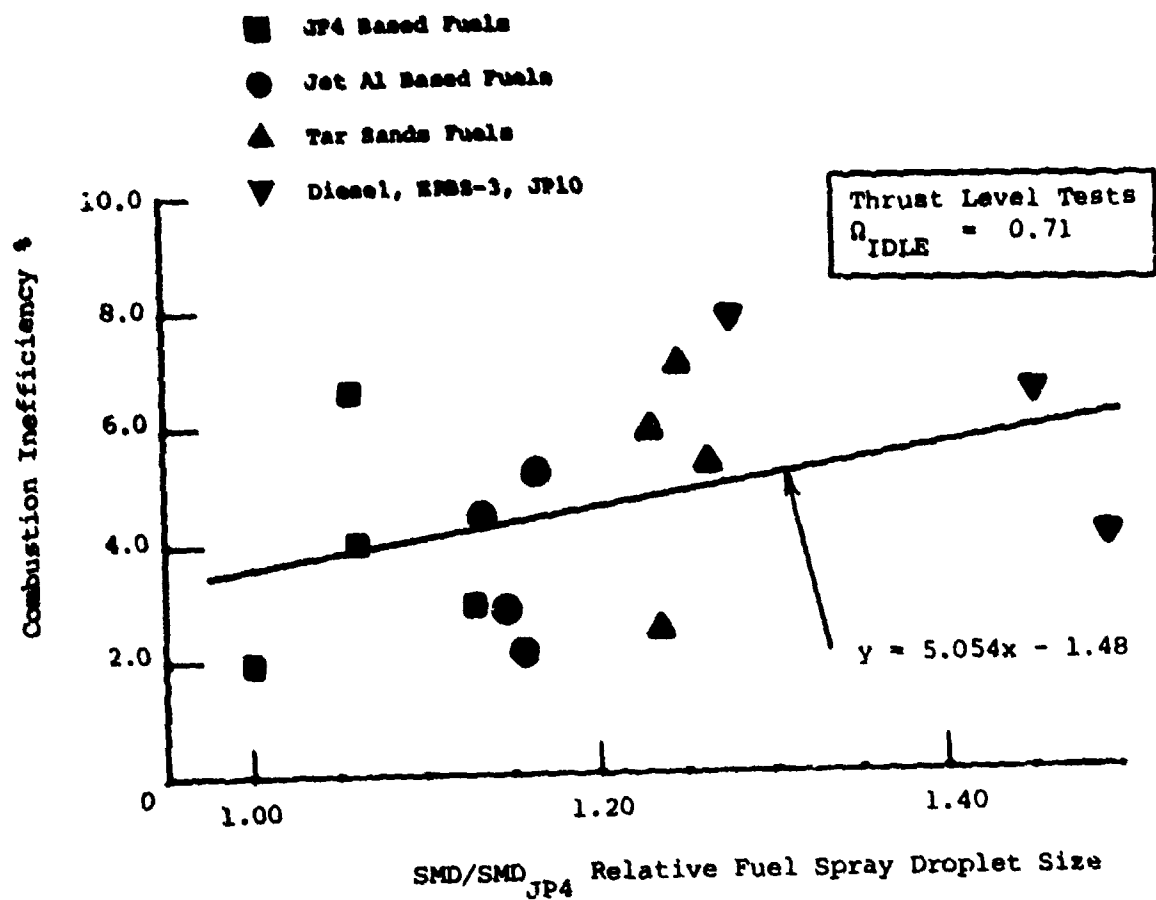
Figure 6.17:   Effect of Spray Quality on Idle Combustion Inefficiency,
              Simplex Nozzle
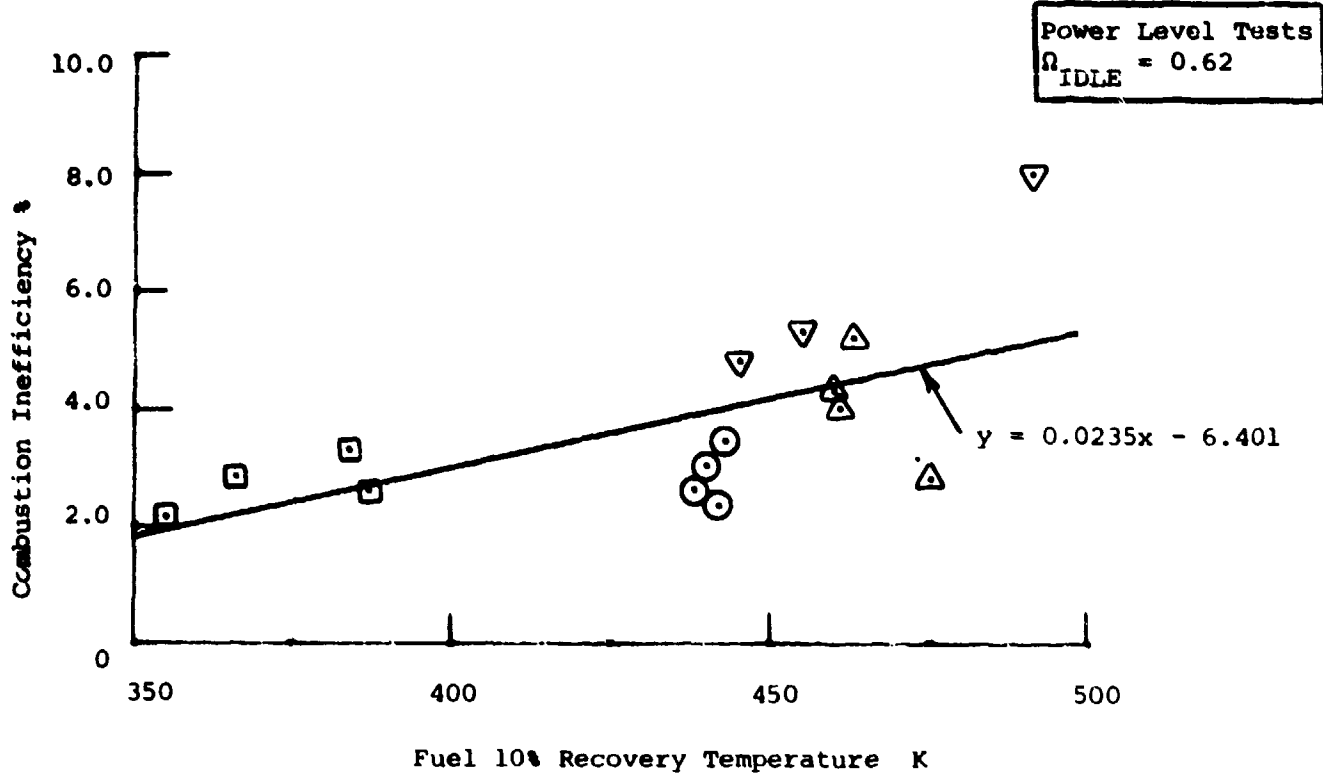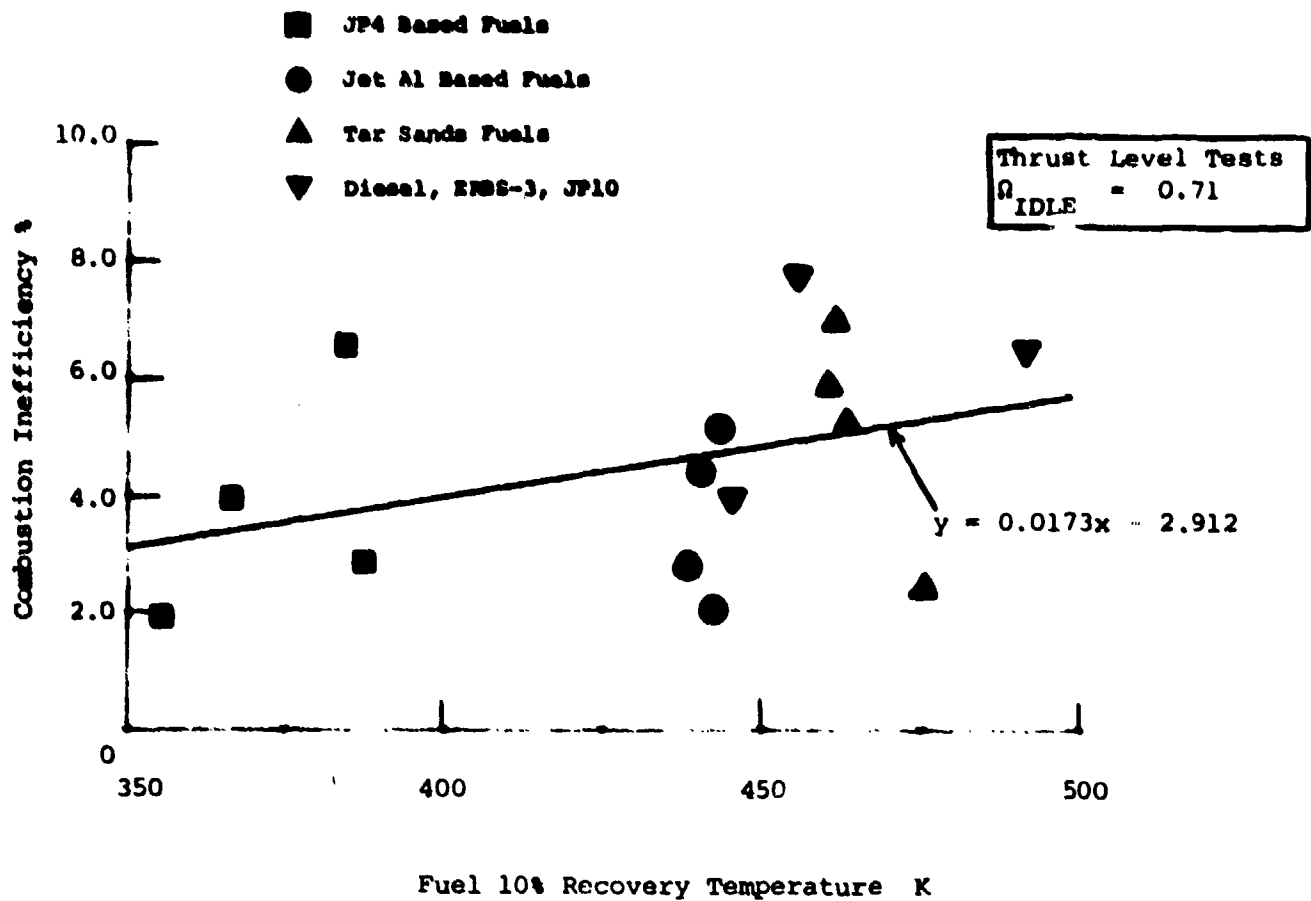
Figure 6.18: Effect of Fuel Volatility on Idle Combustion Inefficiency, Simplex Nozzle
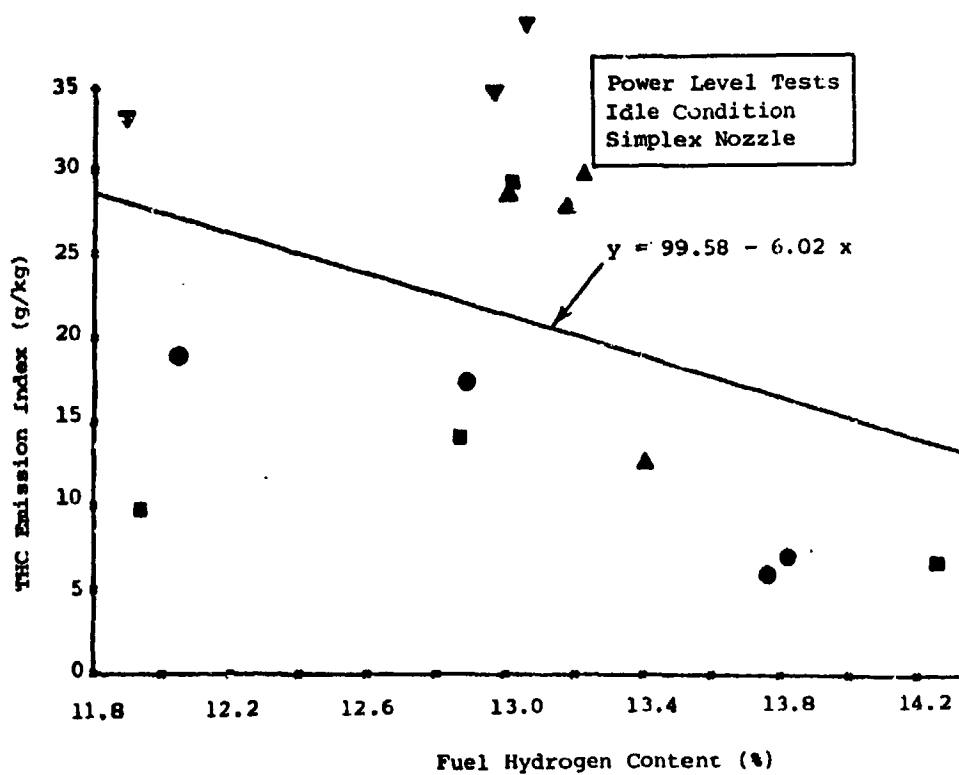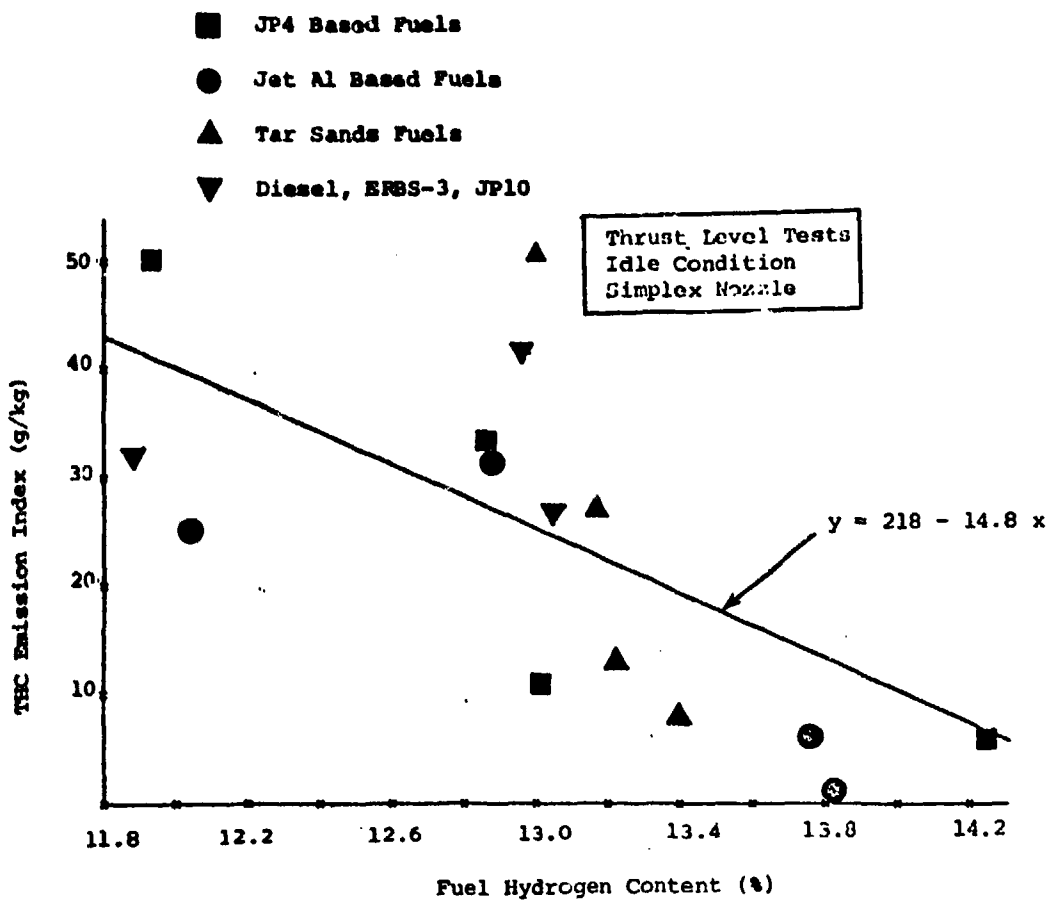
Figure 6.19: Effect of Hydrogen Content on THC Emissions
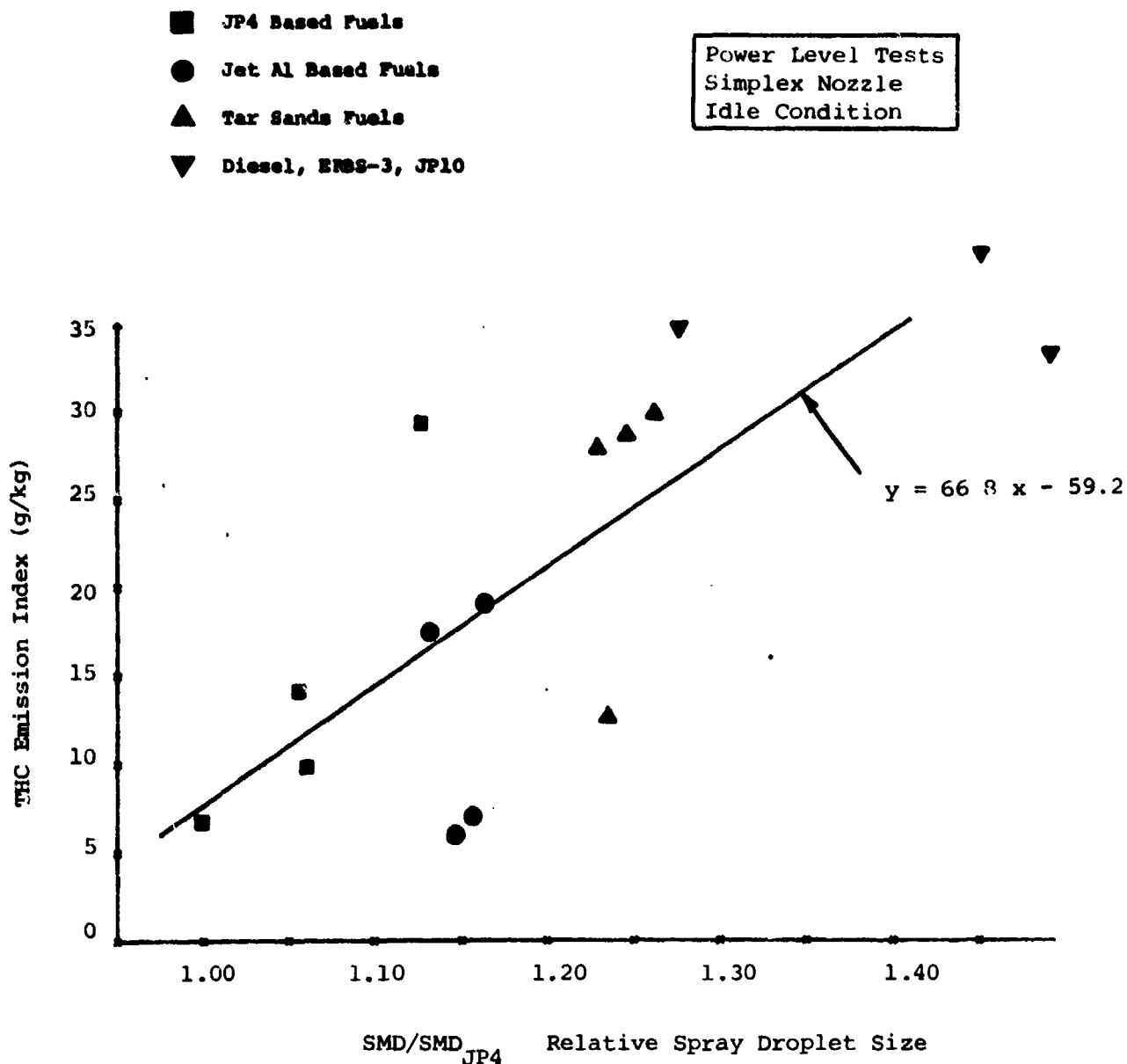
Figure 6.20:   Effect of Fuel Spray Characteristics on THC Emissions
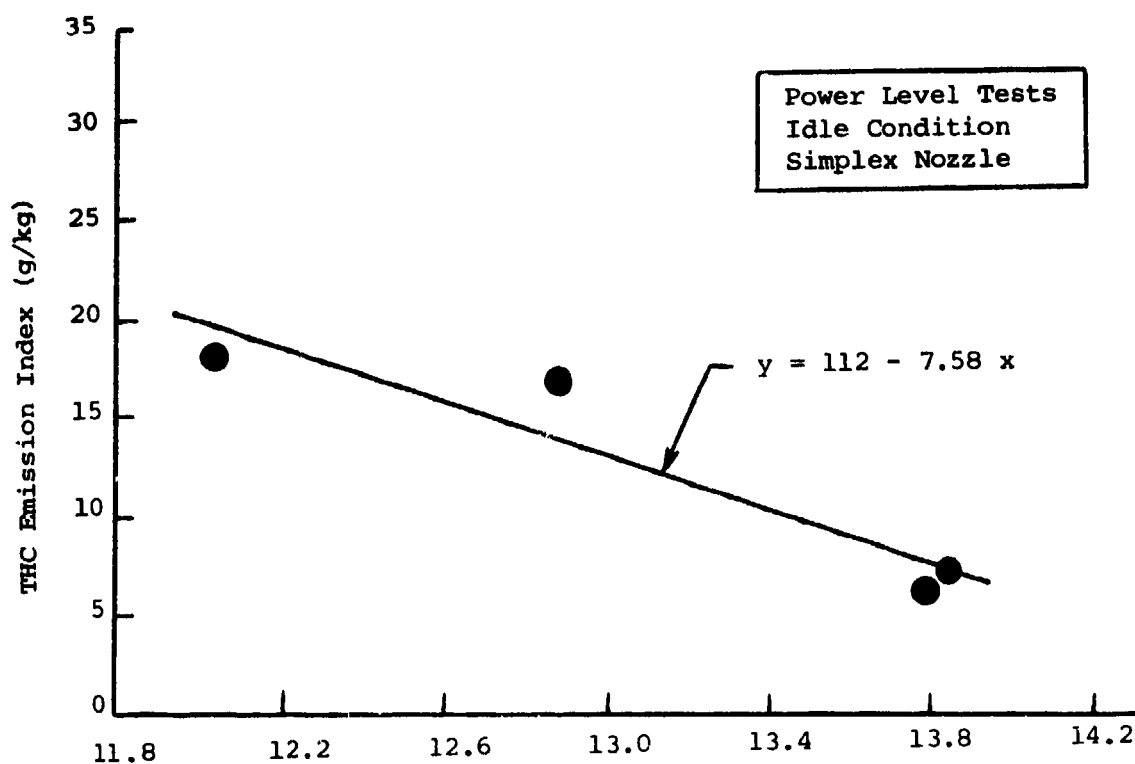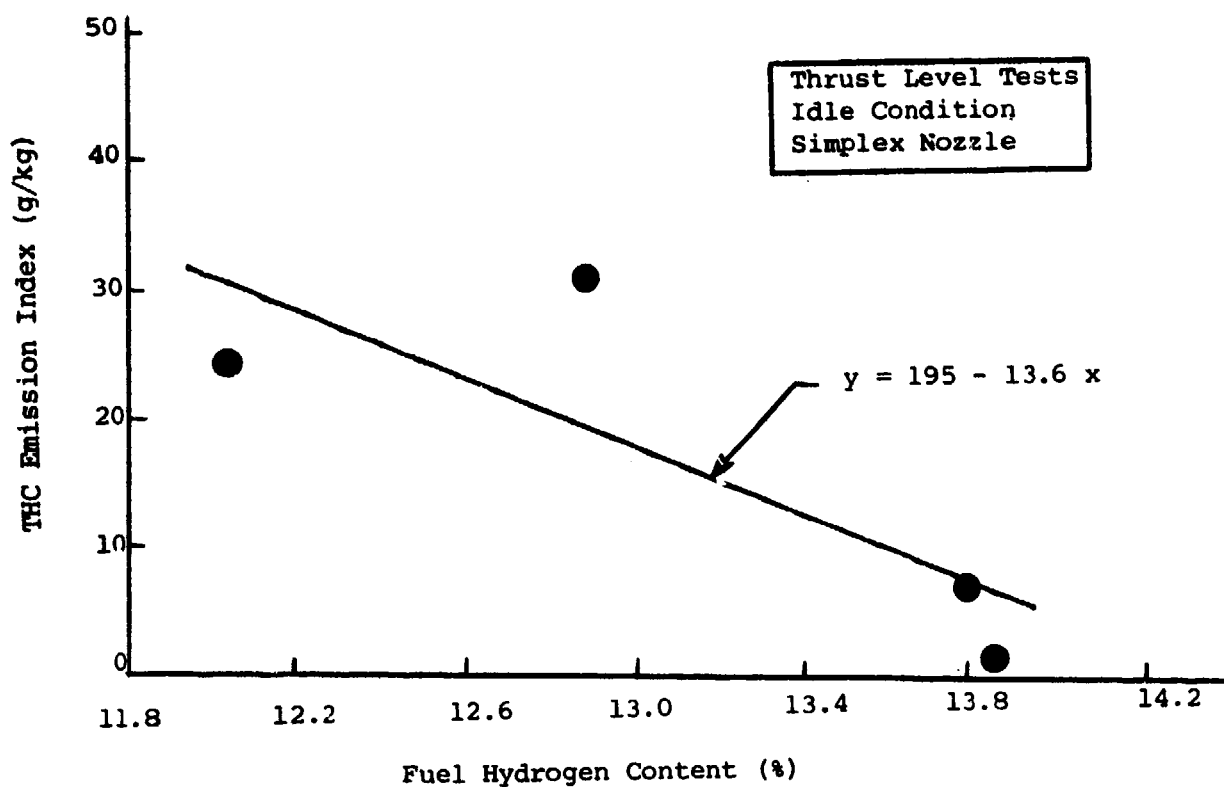
Figure 6.21: Effect of Hydrogen Content on THC Emissions (JET Al Based Fuels)
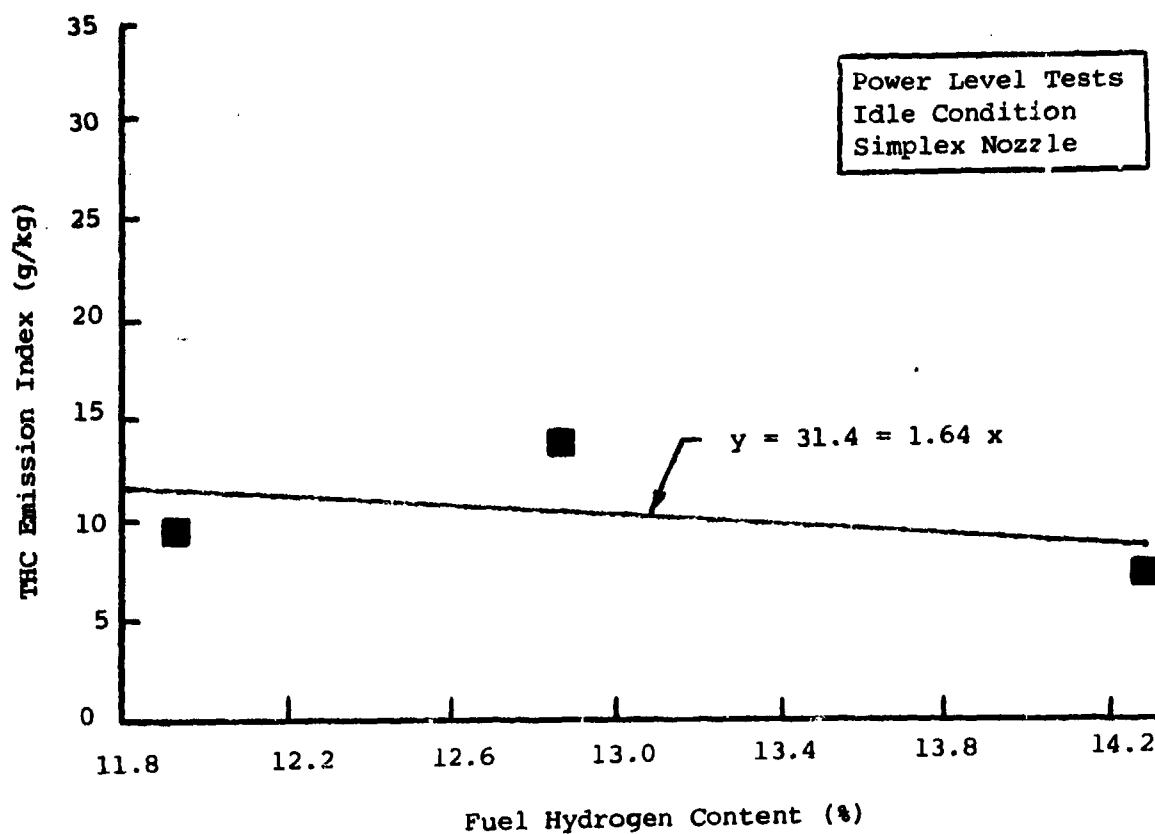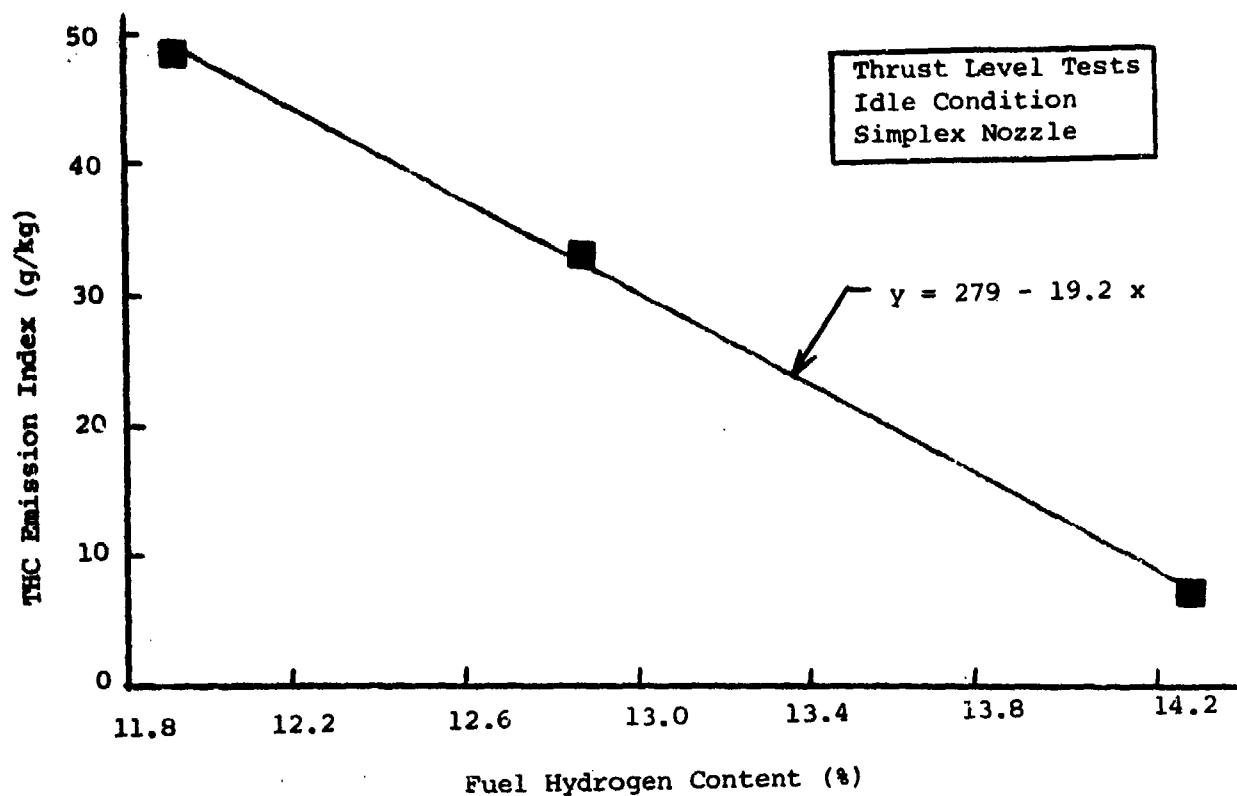
Figure 6.22: Effect of Fuel Hydrogen Content on THC Emissions
(JP4, JP4/B1, JP4/B2 Fuels)
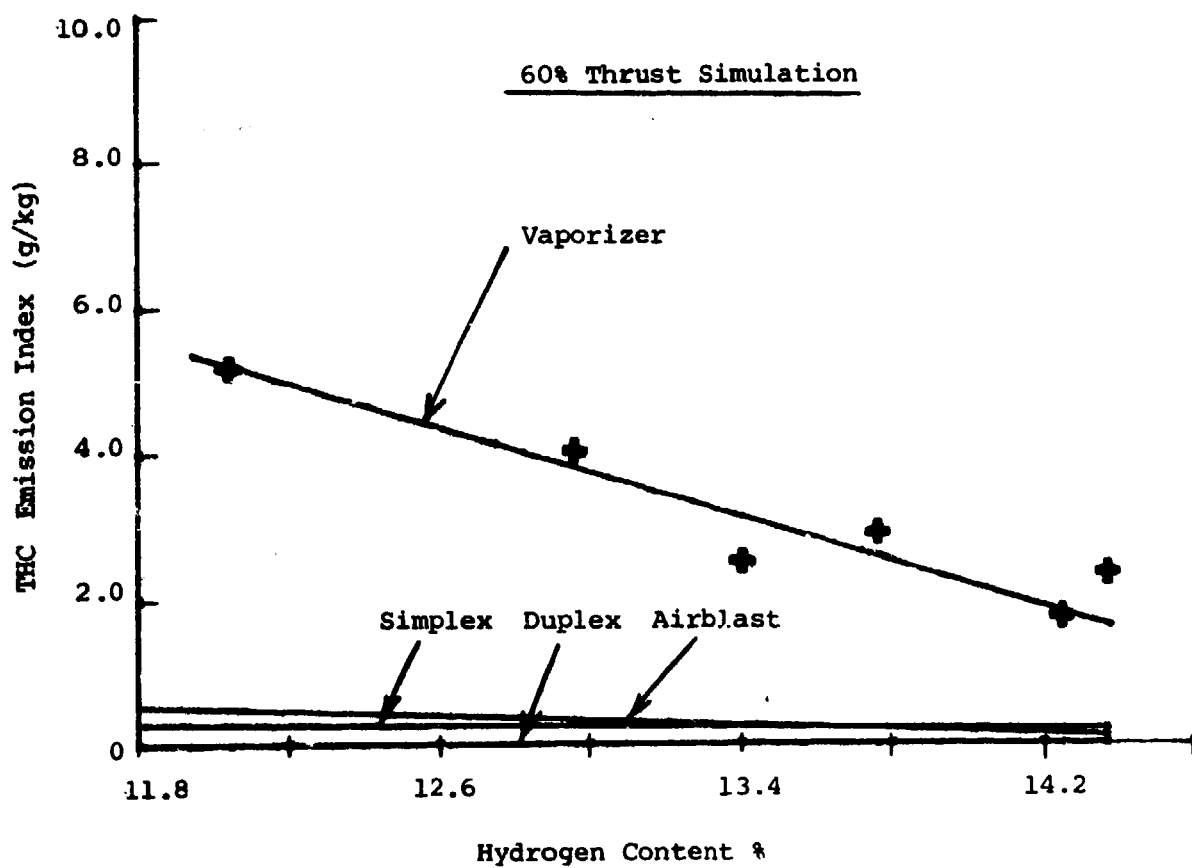
Figure 6.23: Effect of Hydrogen Content on THC Emissions (Nozzle Comparison)
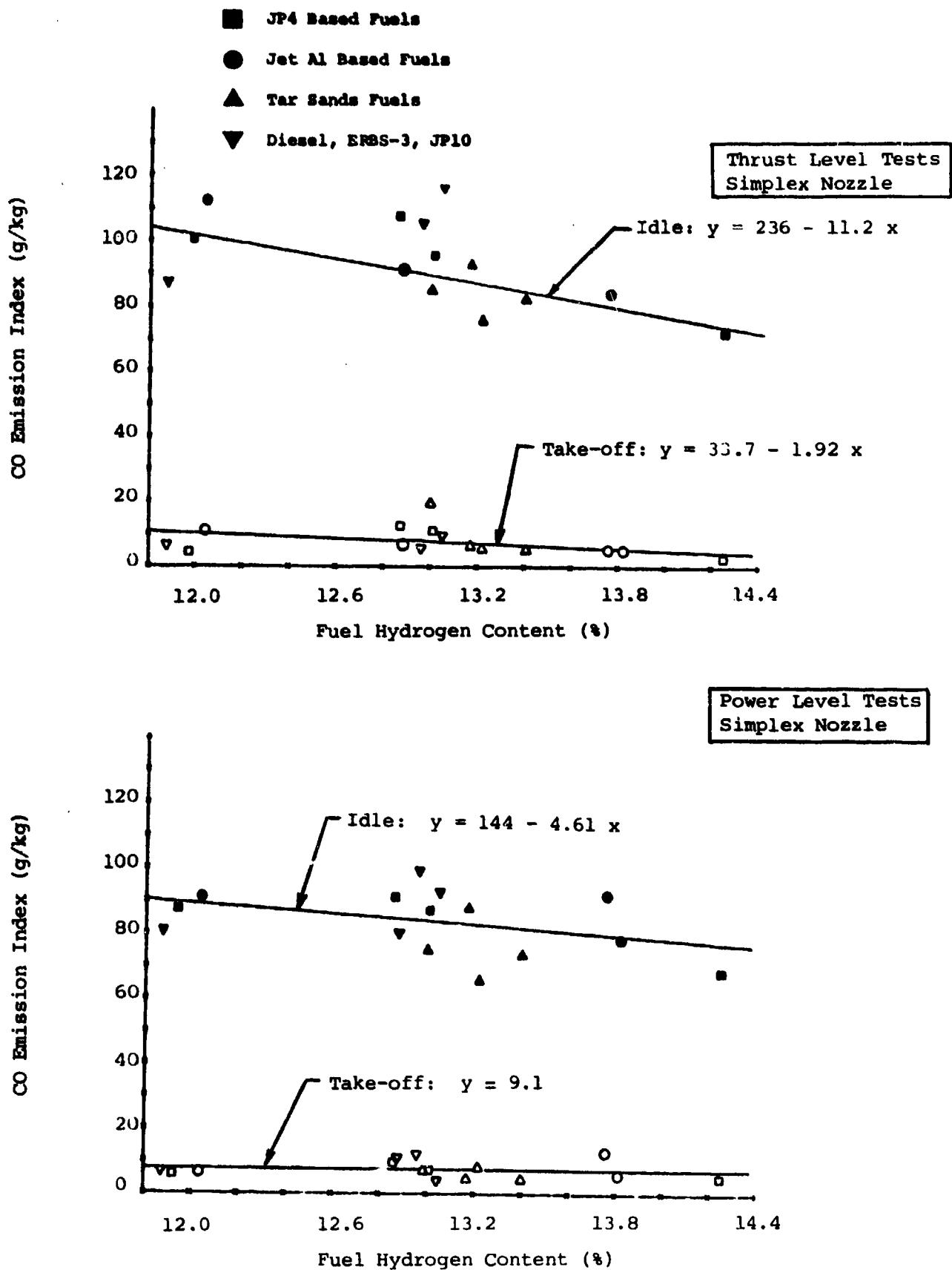
Figure 6.24: Effect of Fuel Hydrogen Content on CO Emissions

- 127 -

Figure 6.25: Effect of Fuel Spray Quality on CO Emissions
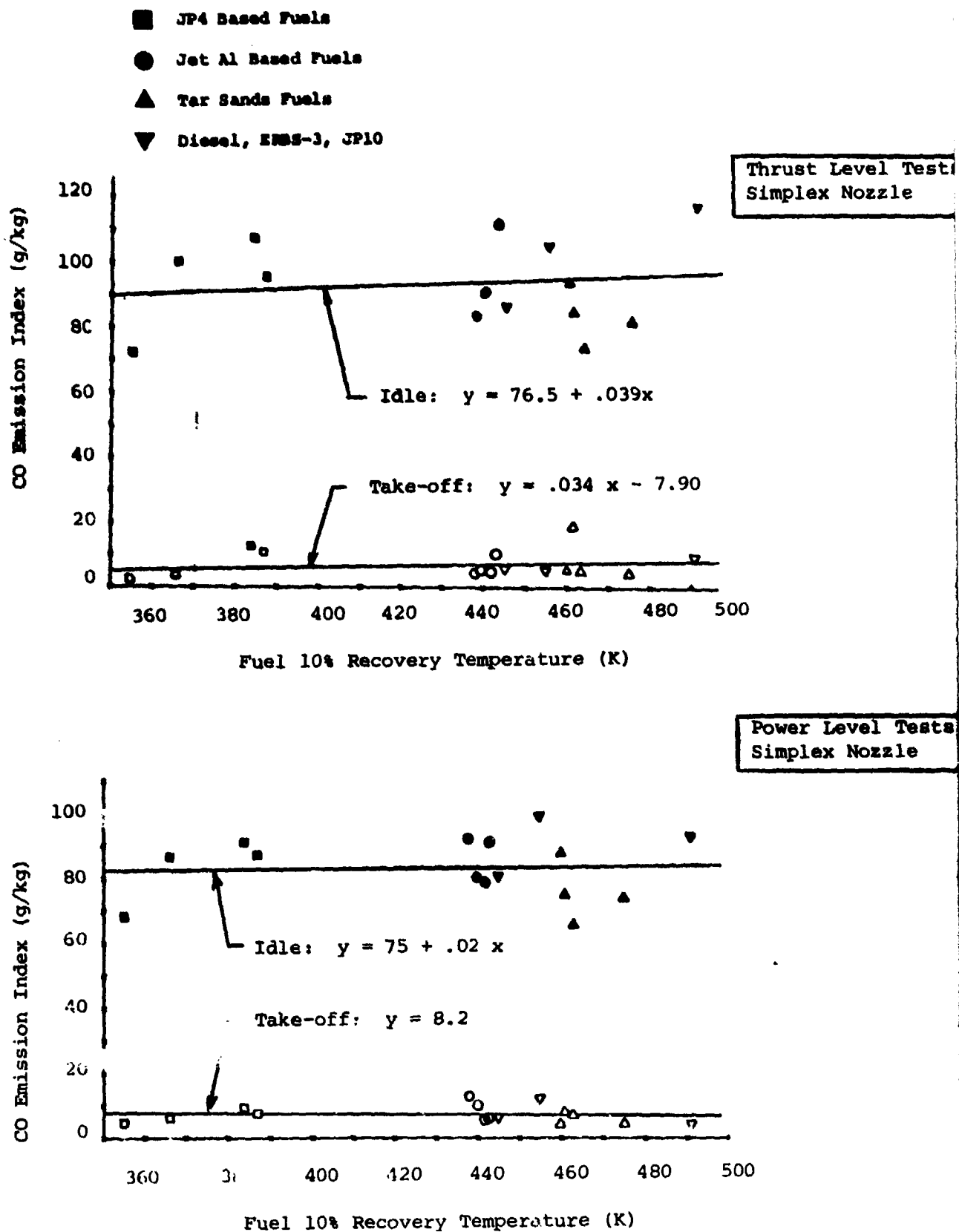
Figure 6.26: Effect of Volatility on CO Emissions
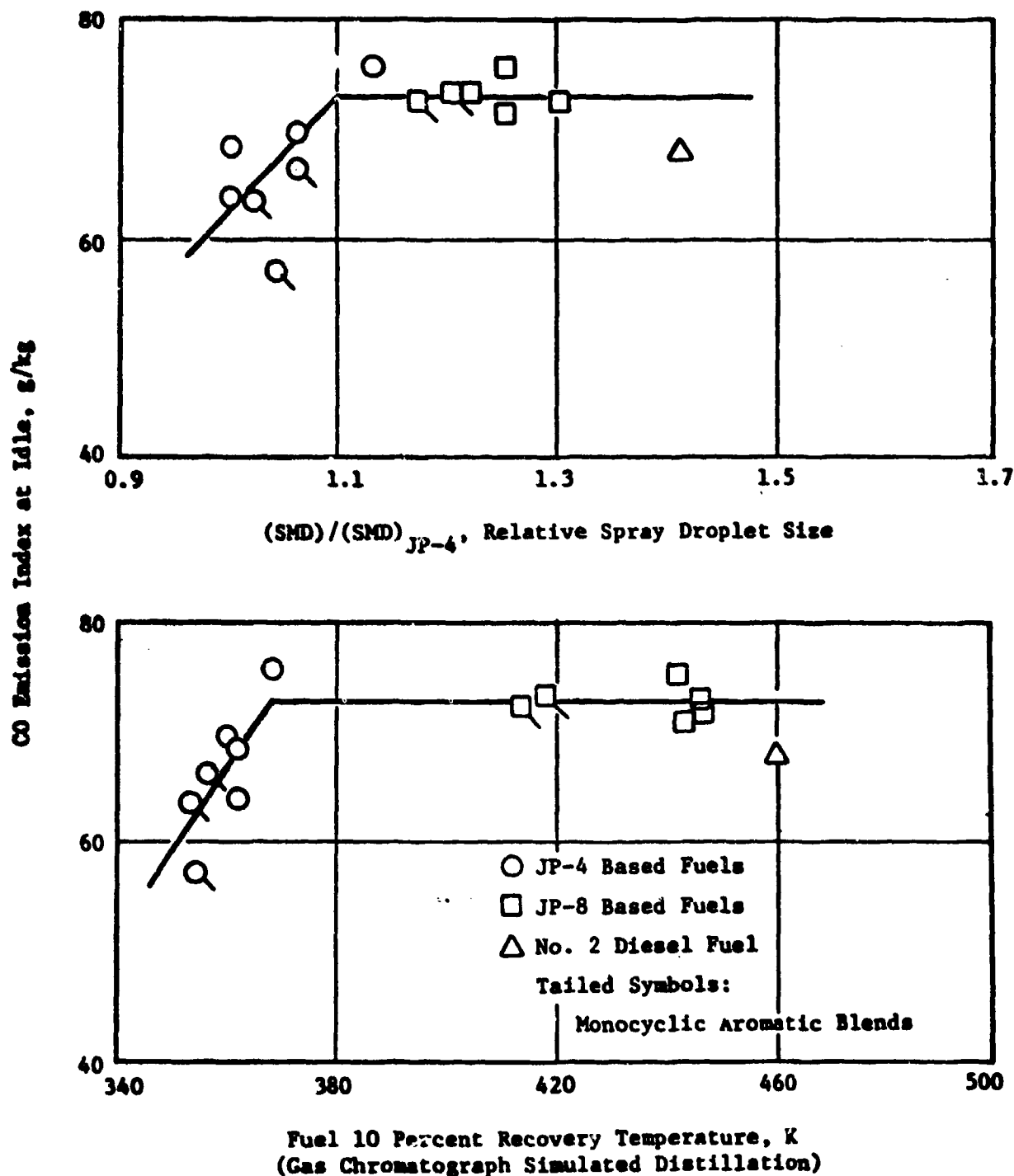
Figure 6.27: Effect of Fuel Atomization and Volatility on Idle CO Emission Levels. (J79 Data)[3]
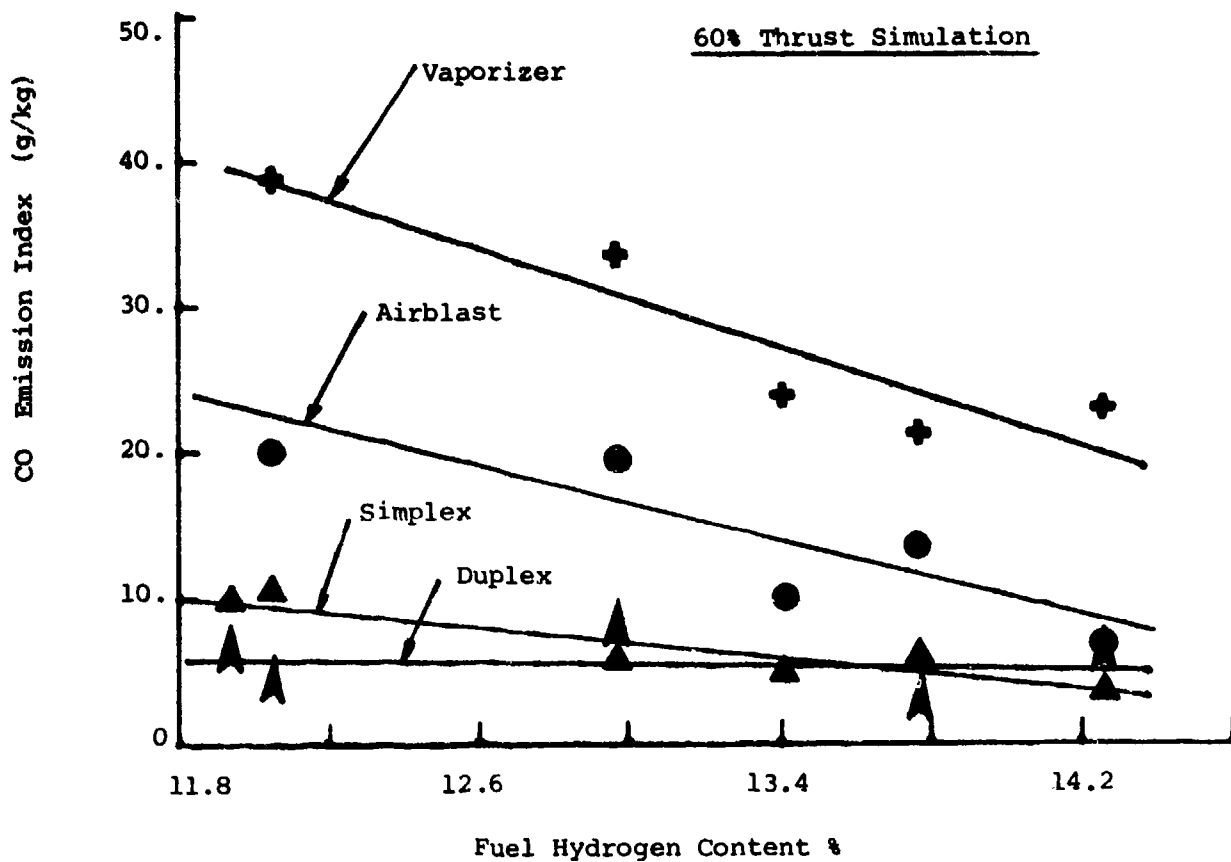
Figure 6.28: Effect of Hydrogen Content on CO Emissions
(Nozzle Comparison)
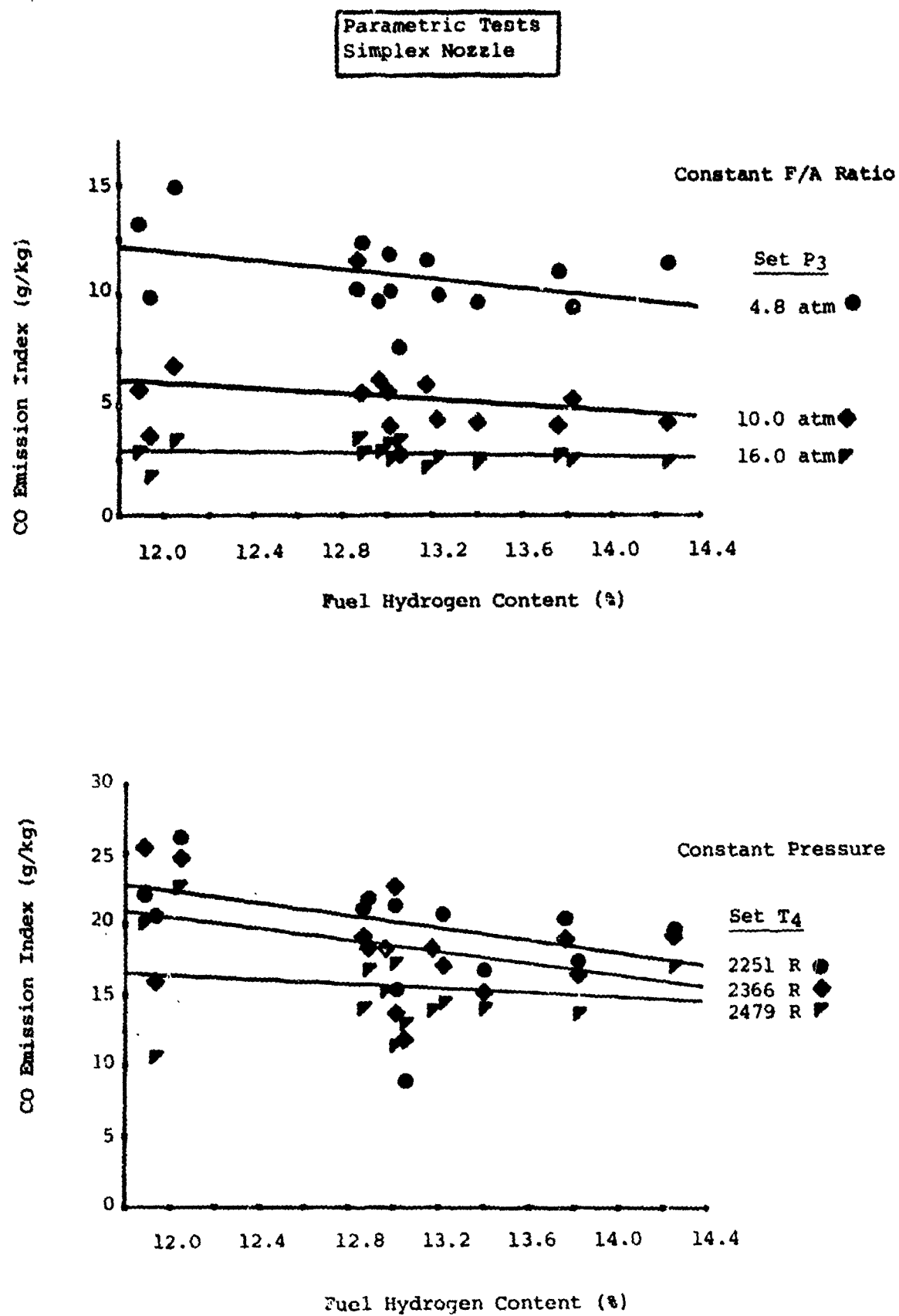
Figure 6.29: Effects of Pressure and Fuel-Air Ratio on CO Emissions
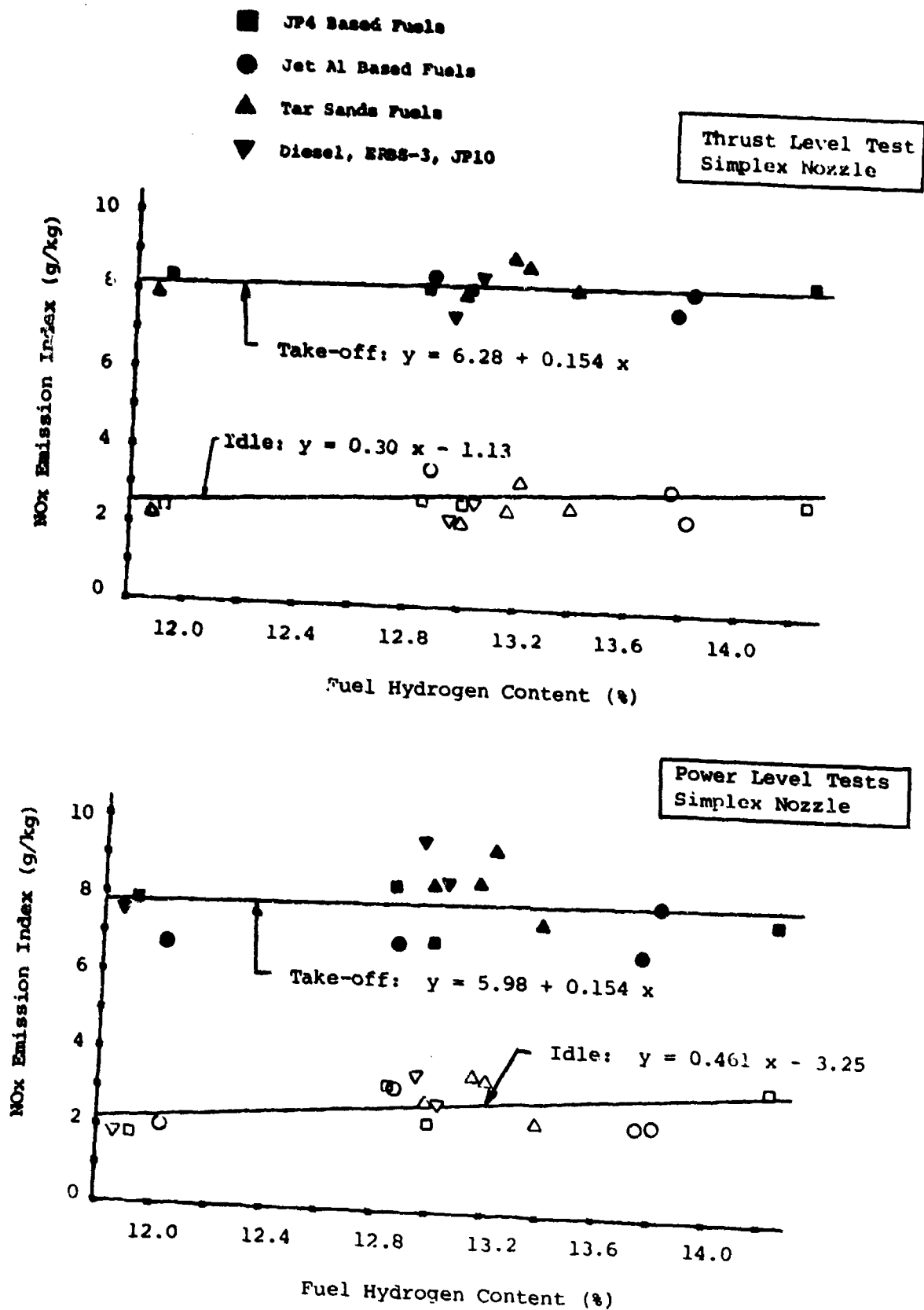
Figure 6.30: Effect of Hydrogen Content on NOx Emissions
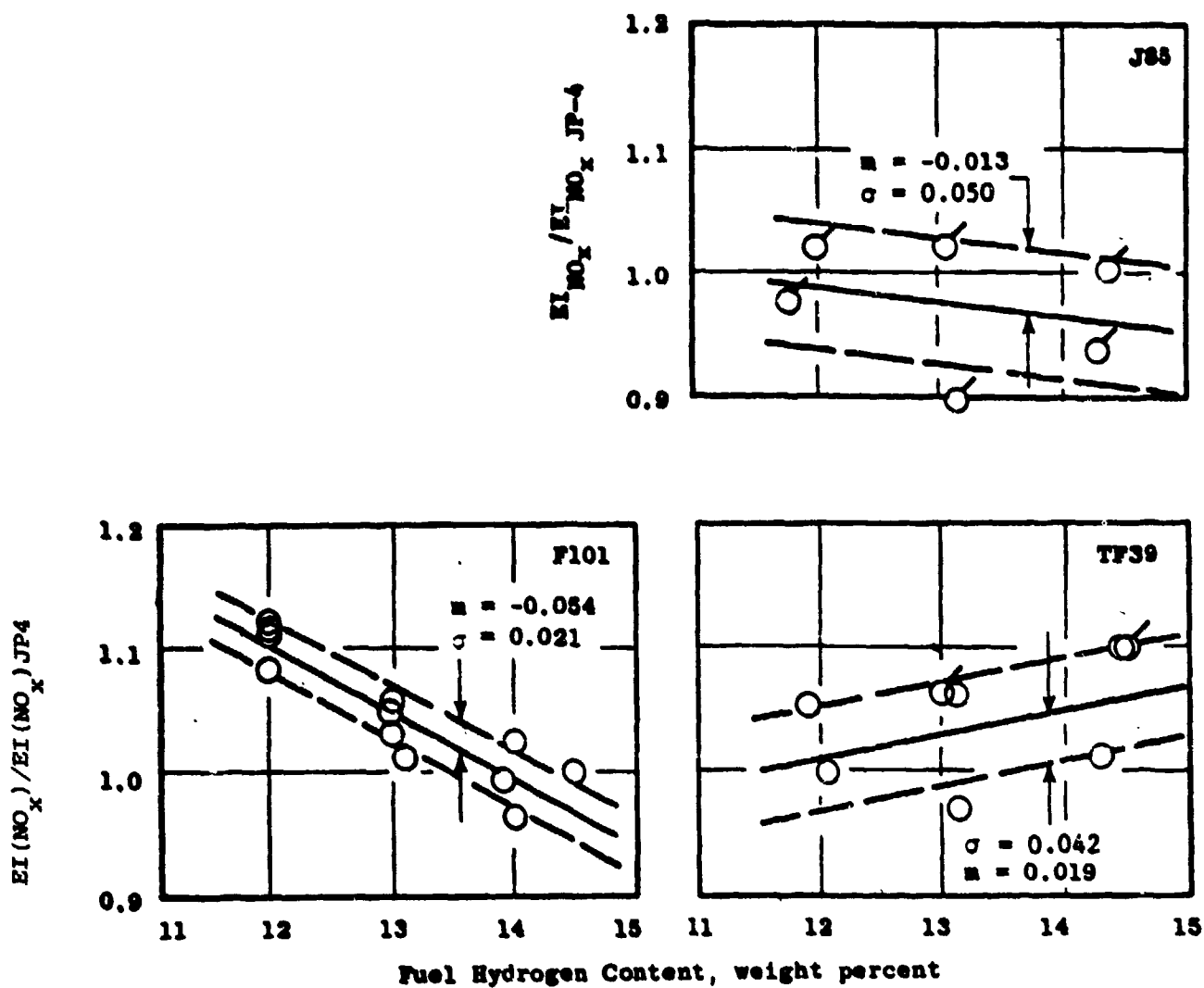
Figure 6.31: Engine Data for NO_x Correlations with Respect to Fuel Hydrogen Content [4]
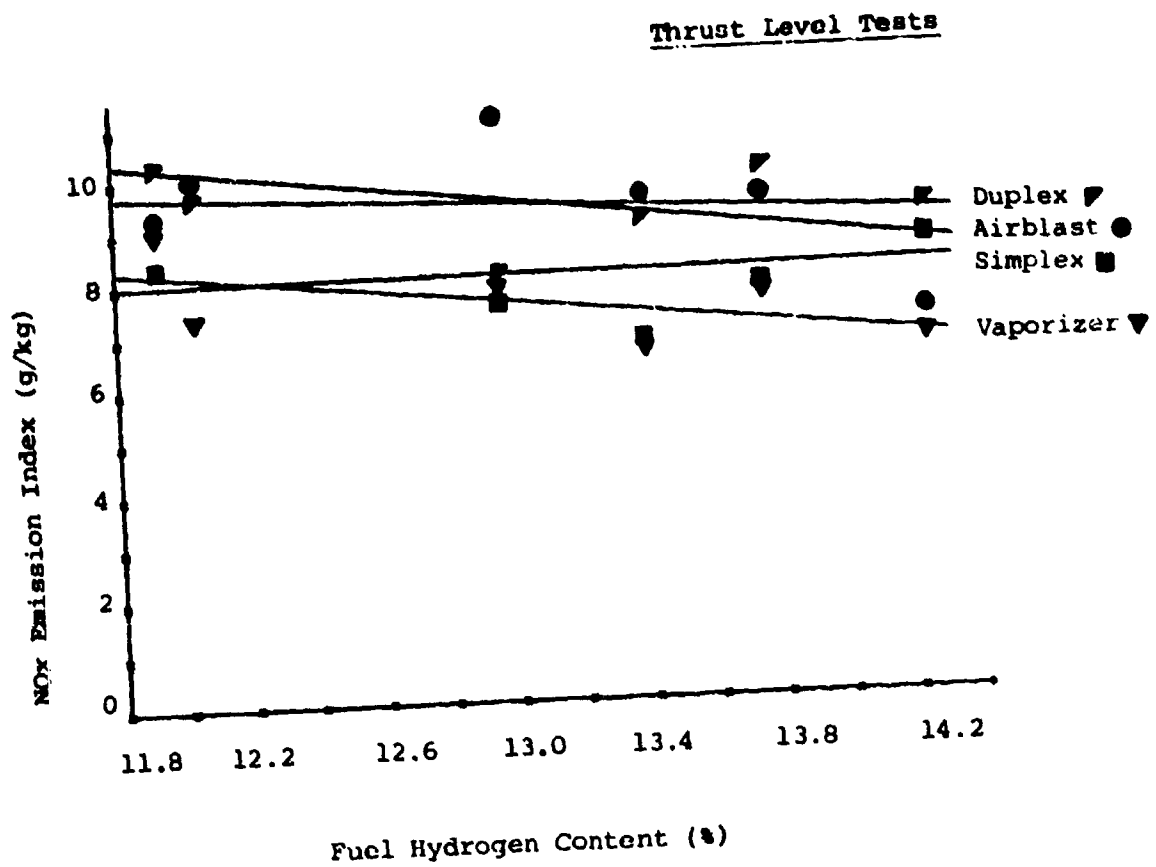
Figure 6.32: Comparison of Nozzle Performance with Respect to NOx Emissions
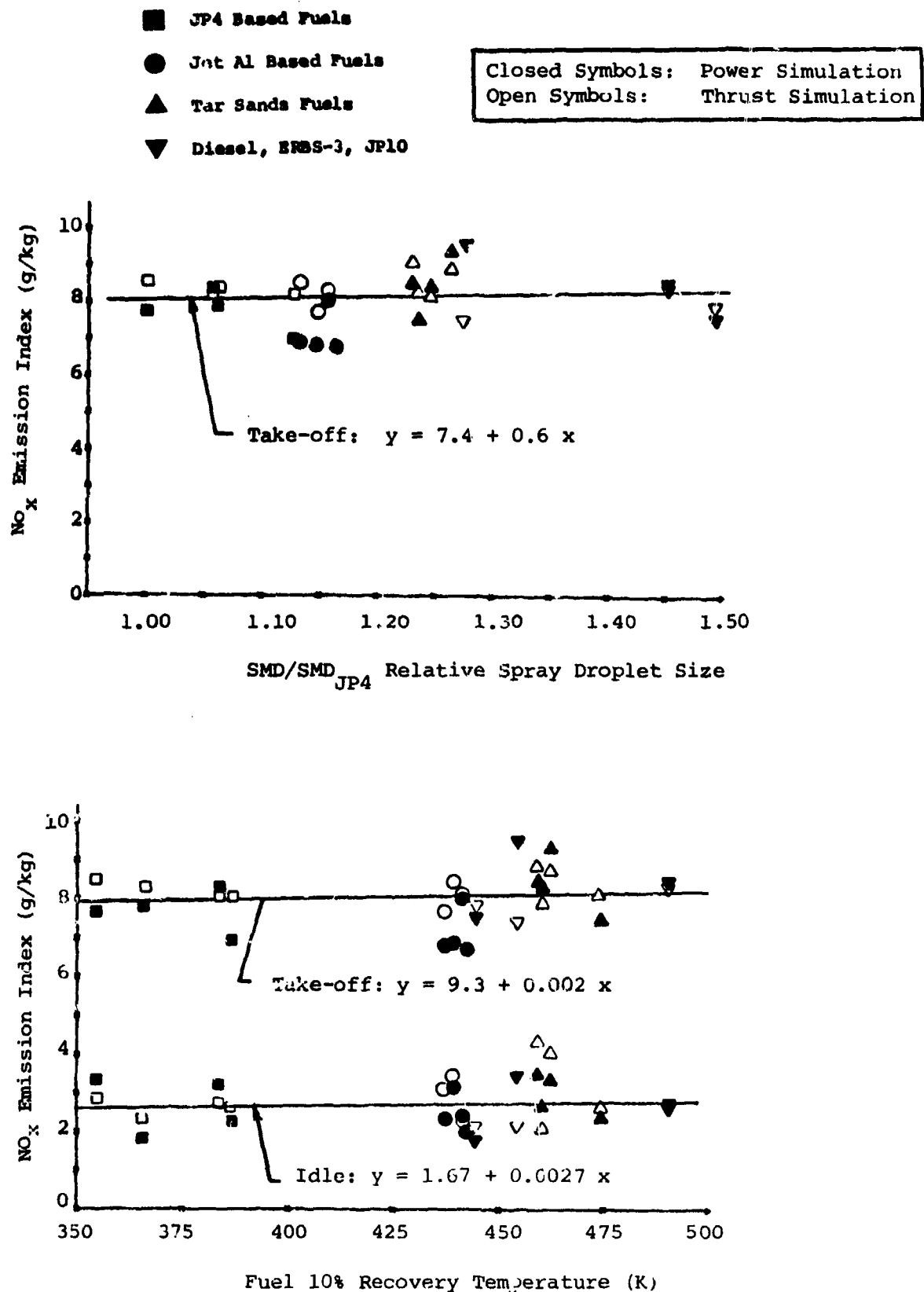
Figure 6.33: Effect of Fuel Properties on NOx Emissions, Simplex Nozzle
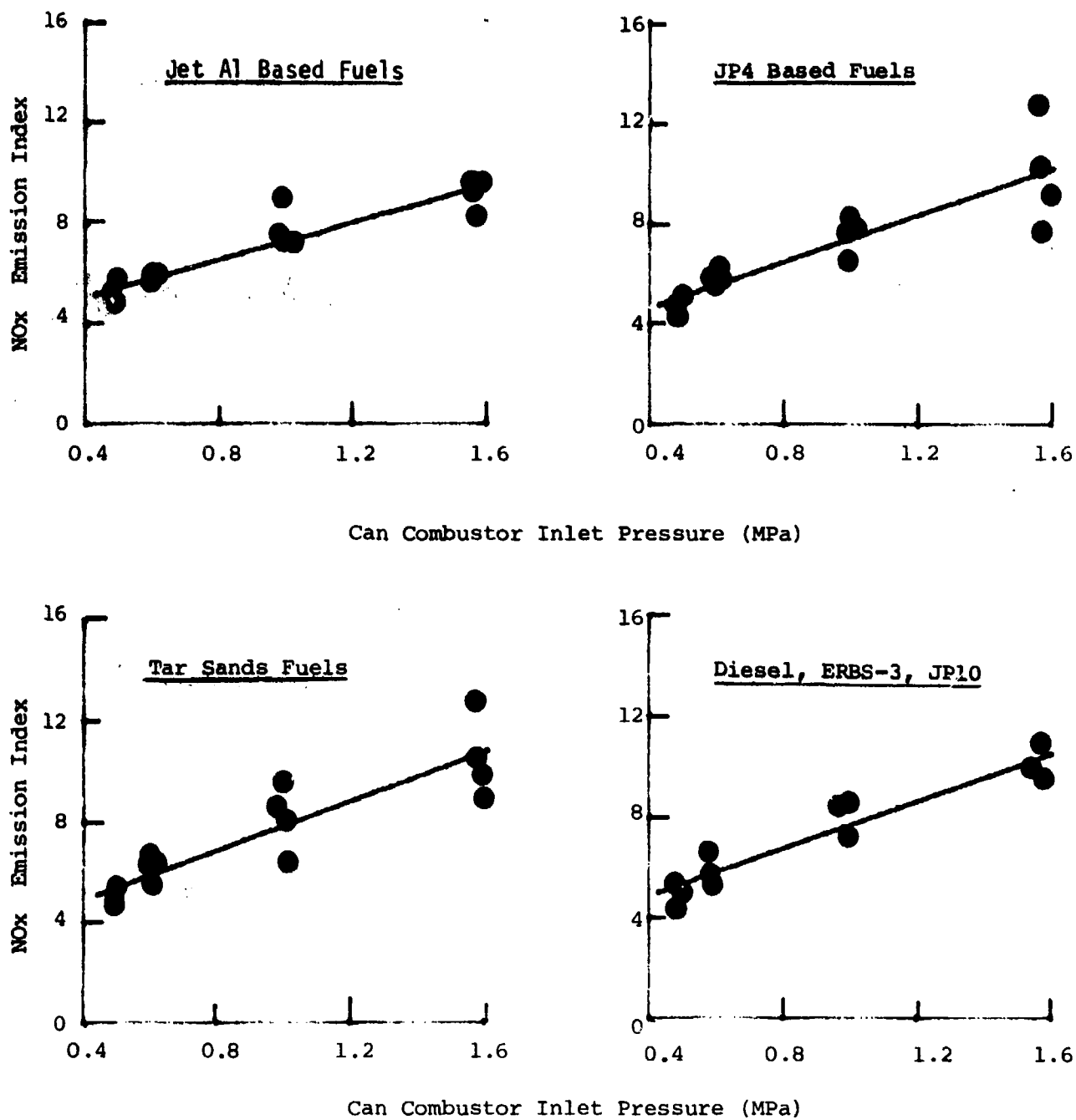
Figure 6.34: Effect of Pressure on NOx Emissions
(Parametric Tests , Simplex Nozzle)
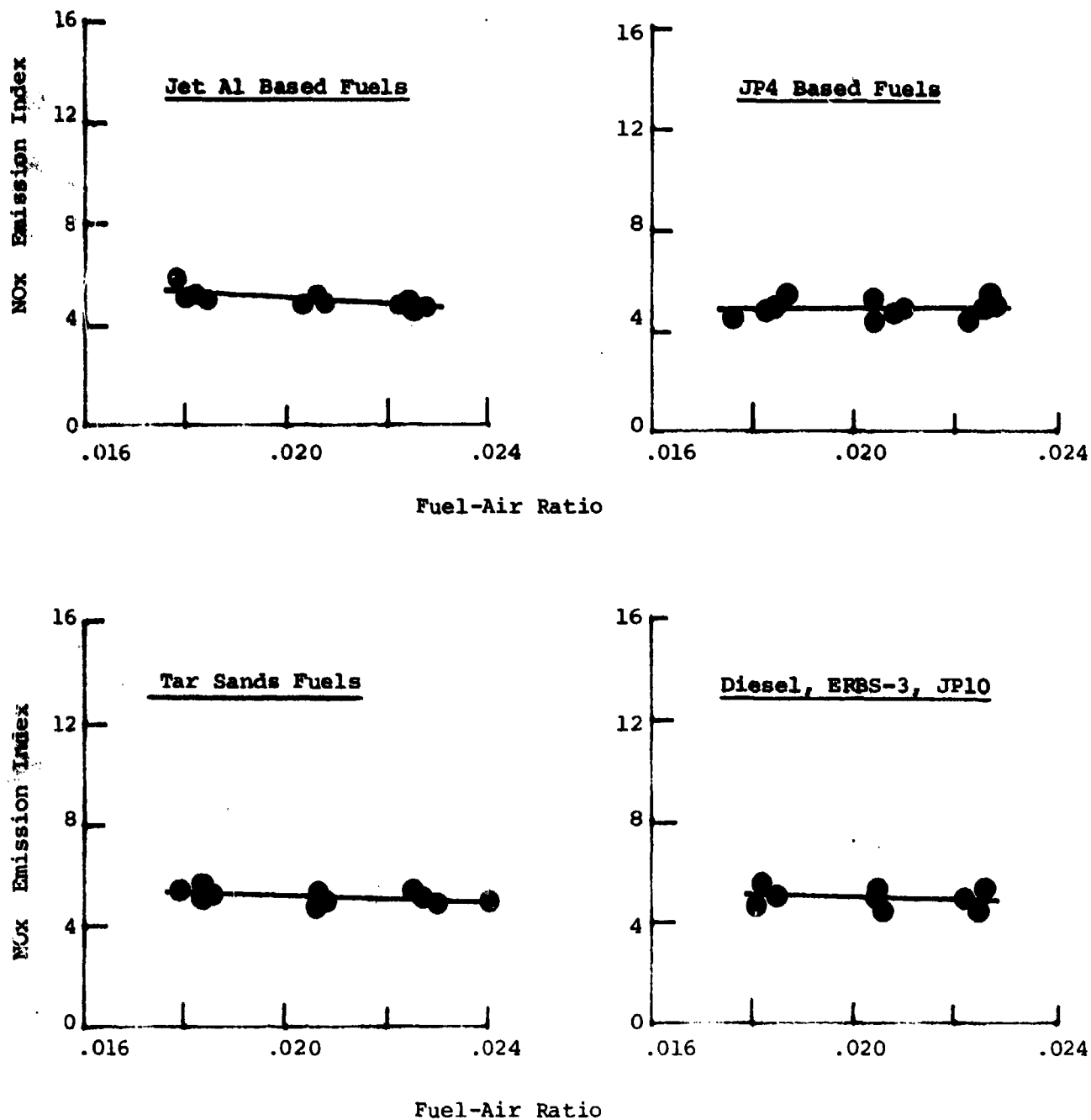
Figure 6.35: Effect of Fuel-Air Ratio on NOx Emissions
(Parametric Tests, Simplex Nozzle)
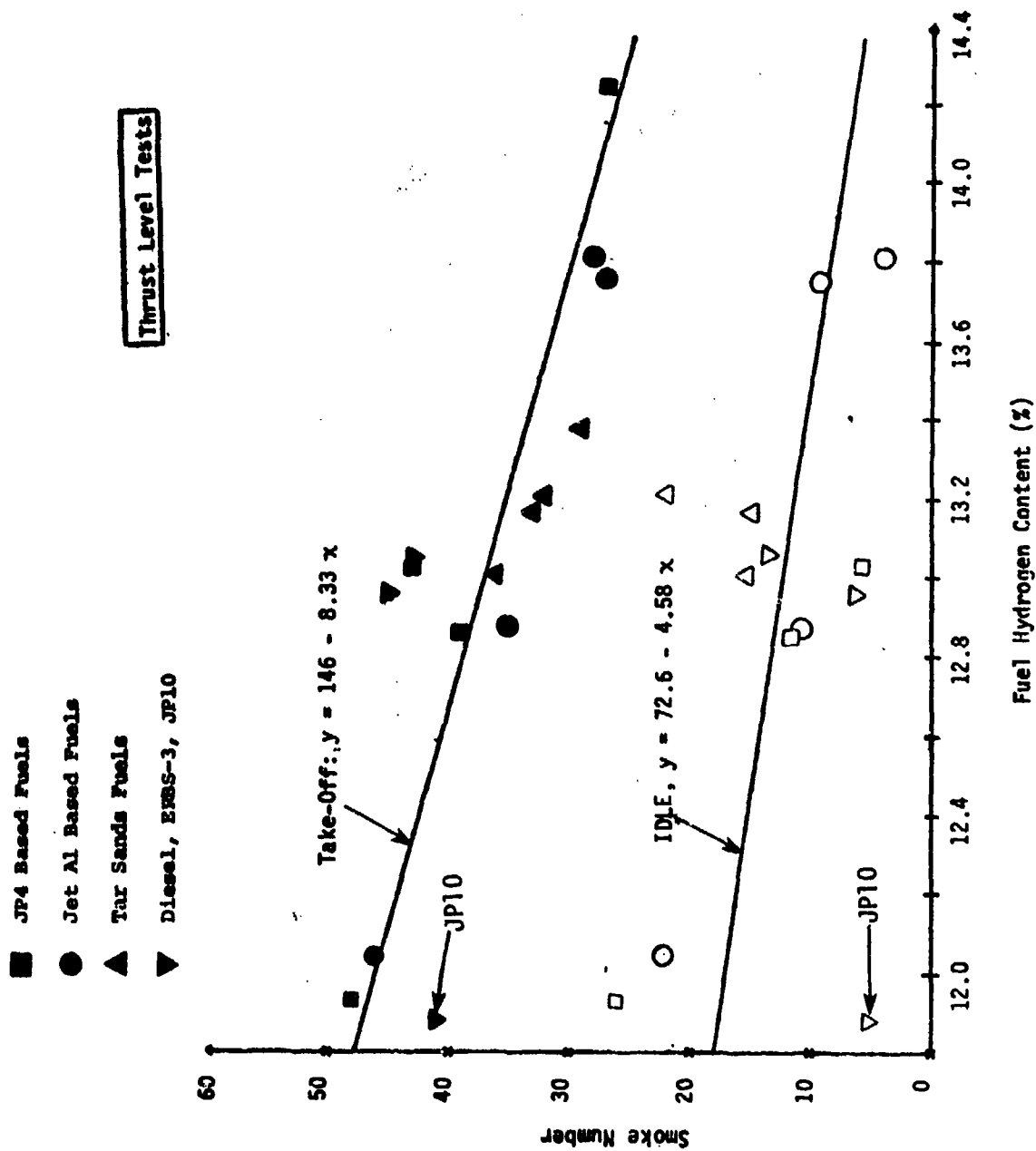
Figure 6.36: Effect of Hydrogen Content on Smoke Emissions, Simplex Nozzle

Top chart equation:

$$y = 175 - 10.8\, x$$

Labels: Thrust Level Tests / Jet A1 Based Fuels

Bottom chart equation:

$$y = 168 - 10.0\, x$$

Labels: Thrust Level Tests / JP4 Based Fuels

X-axis: Hydrogen Content %

Y-axis: Smoke Number
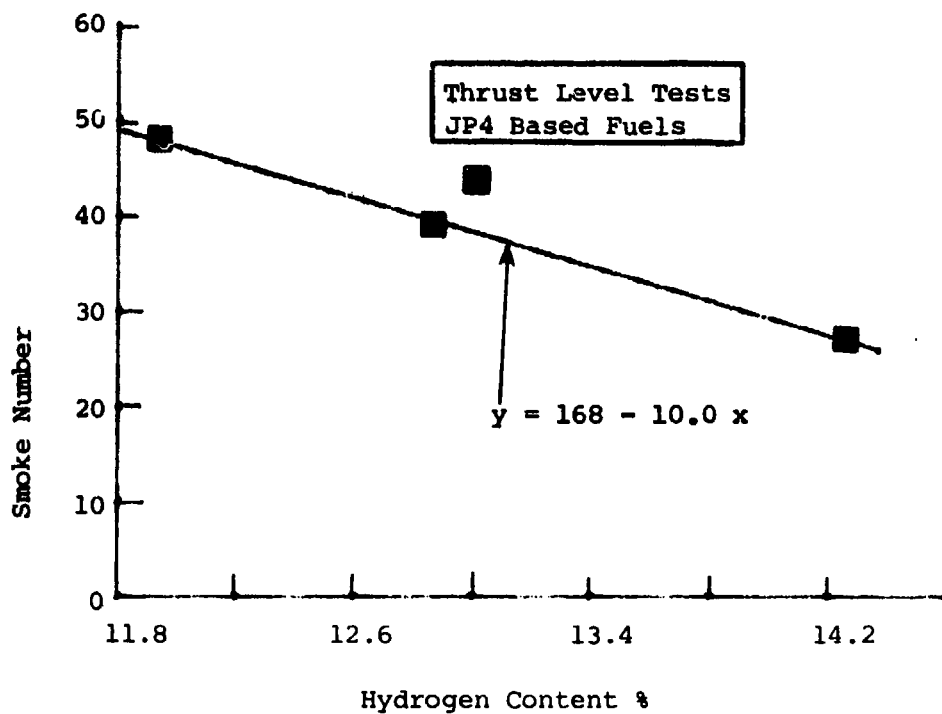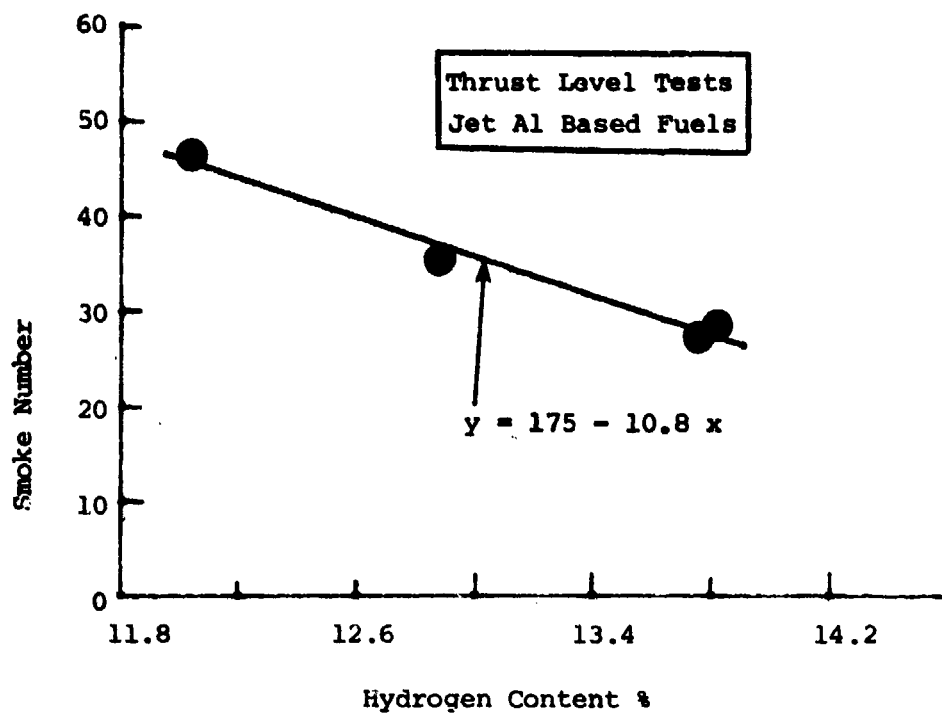
Figure 6.37:   Effect of Hydrogen Content on Smoke Emissions
(Jet A1 and JP4 Based Fuels, Simplex Nozzle)
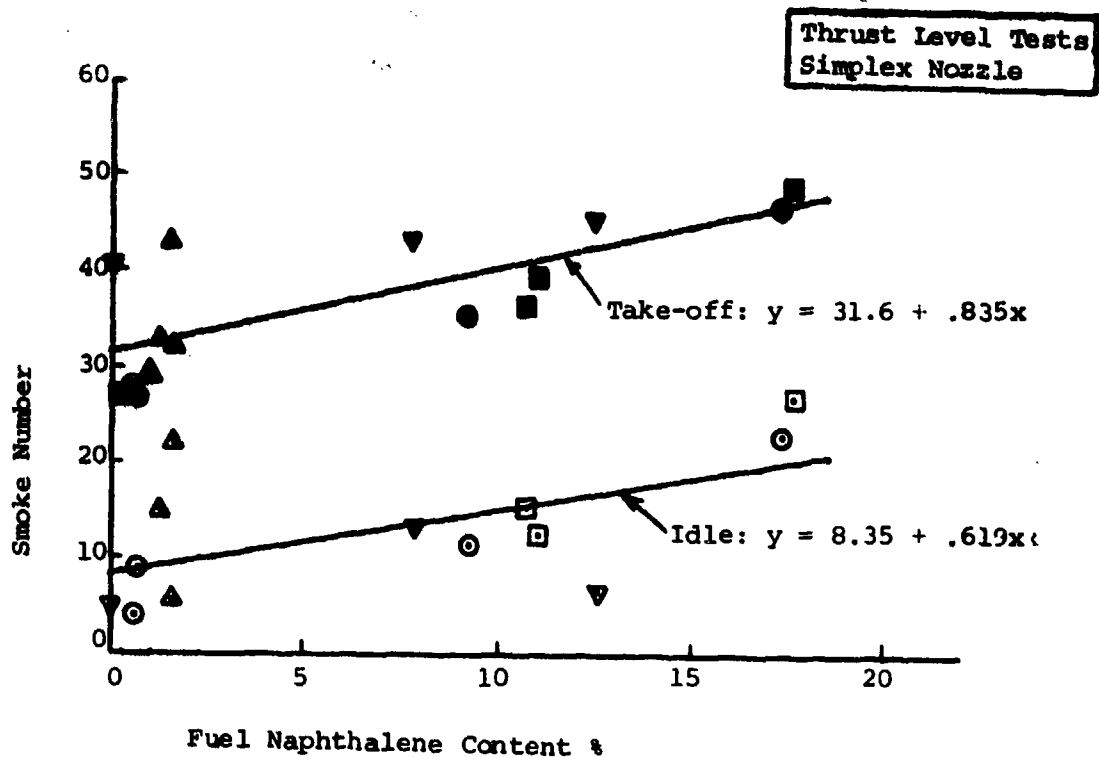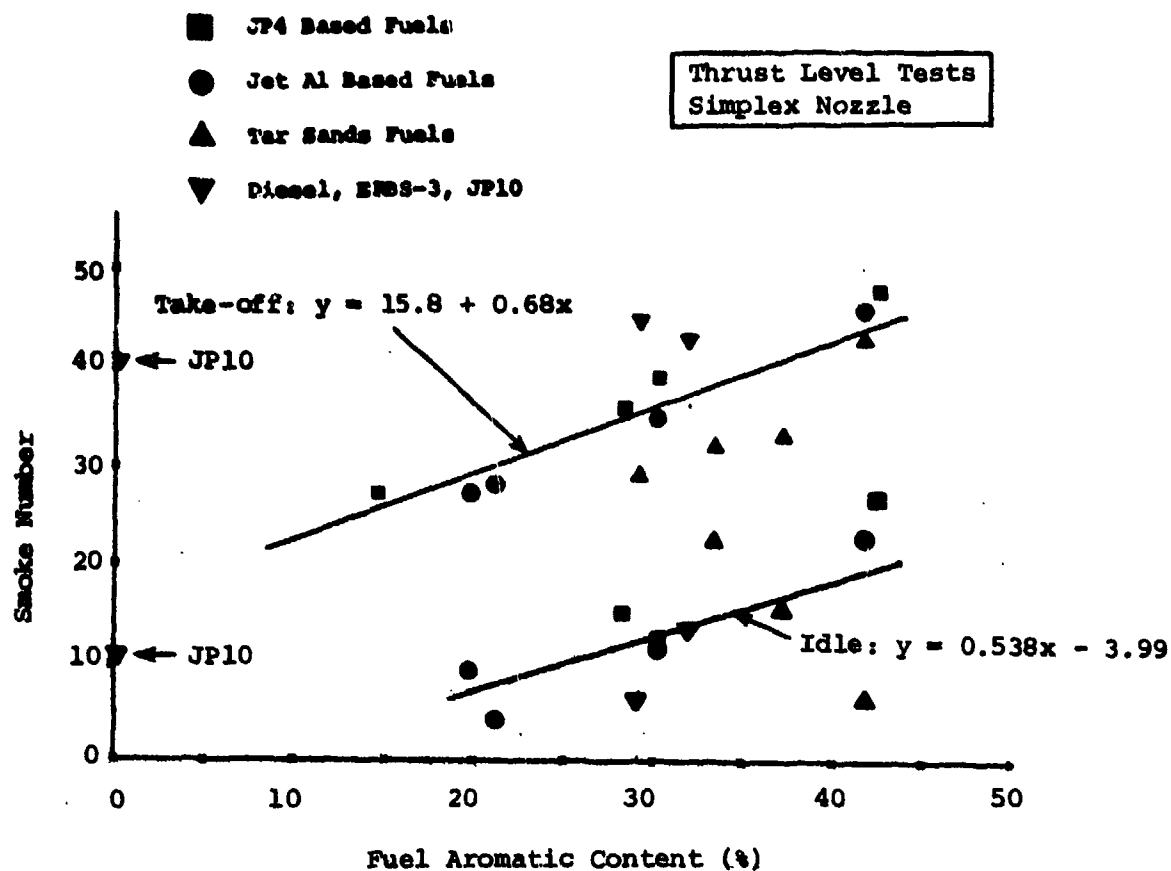
Figure 6.38: Effects of Aromatics and Naphthalene Contents on Smoke Emissions
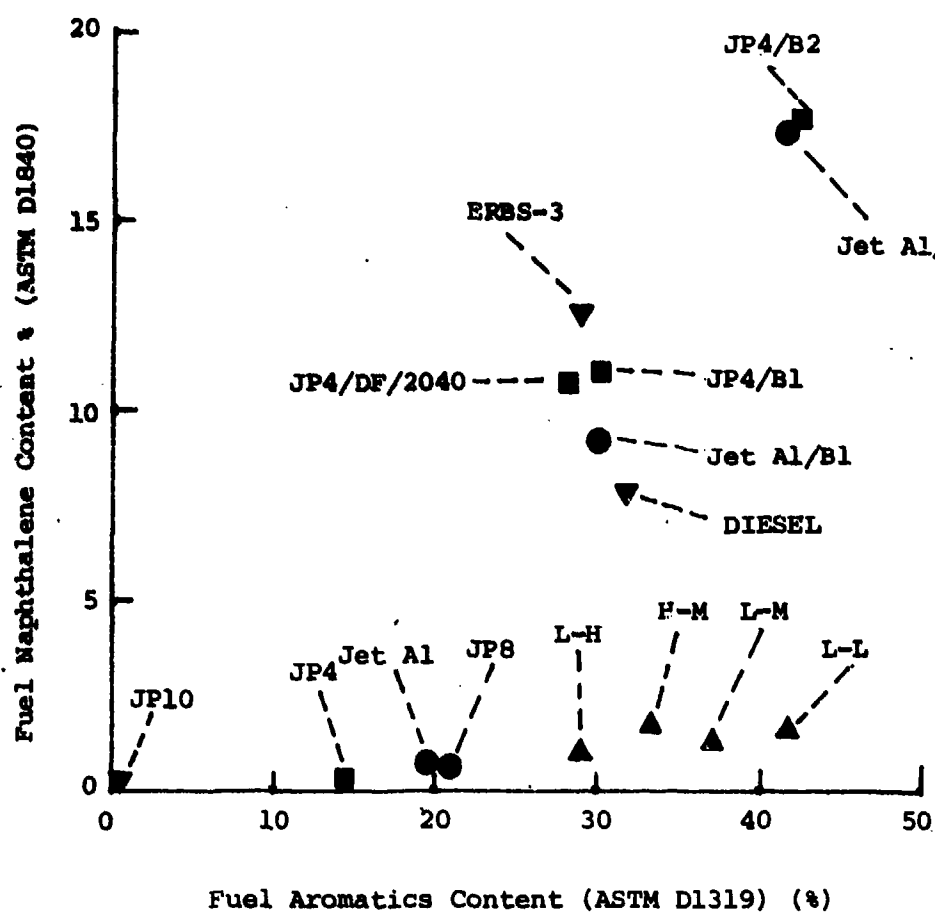
Figure 6.39:   Effect of Aromatics Content on Naphthalene Content
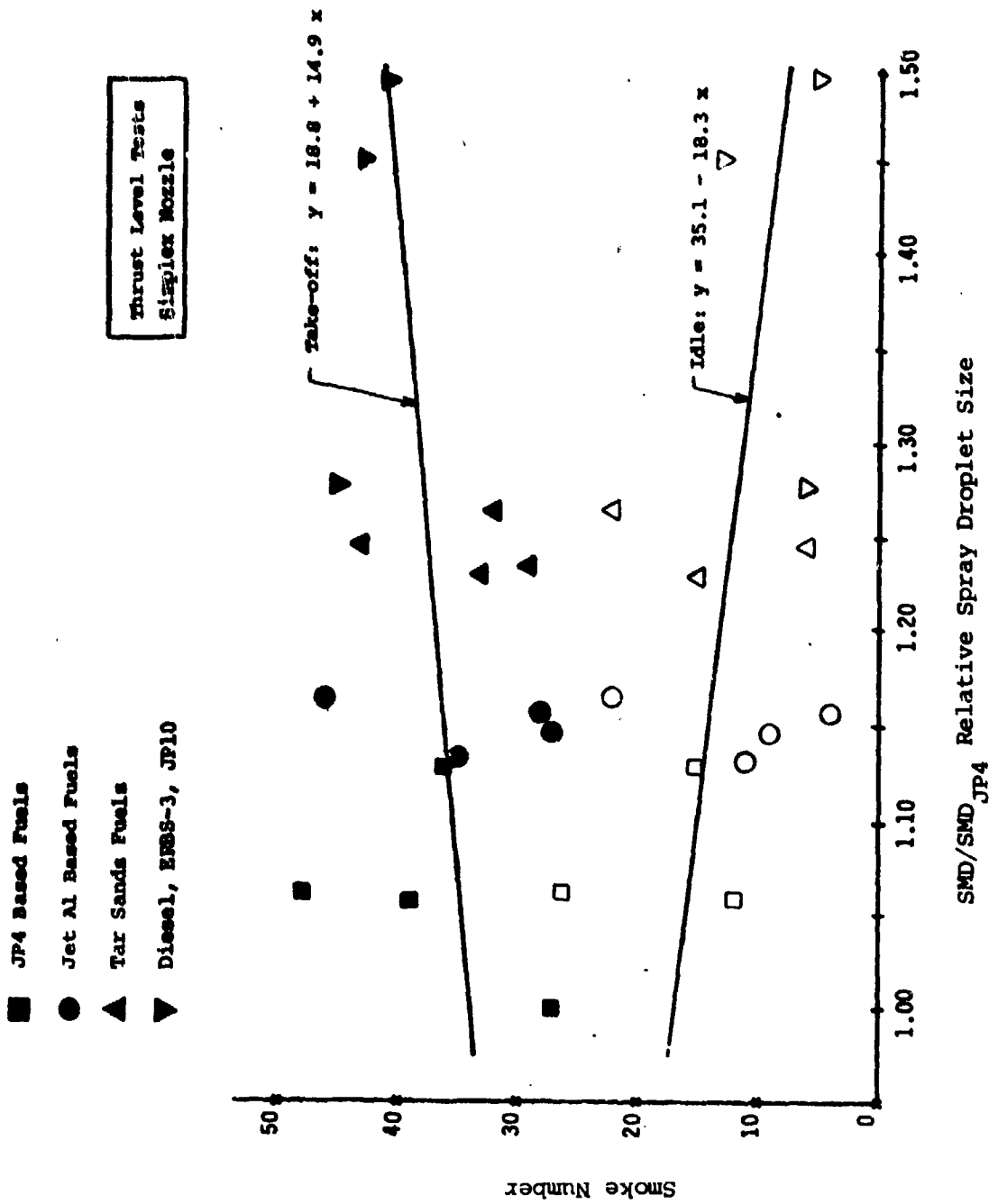
Figure 6.40: Effect of Fuel Spray Quality on Smoke Emissions
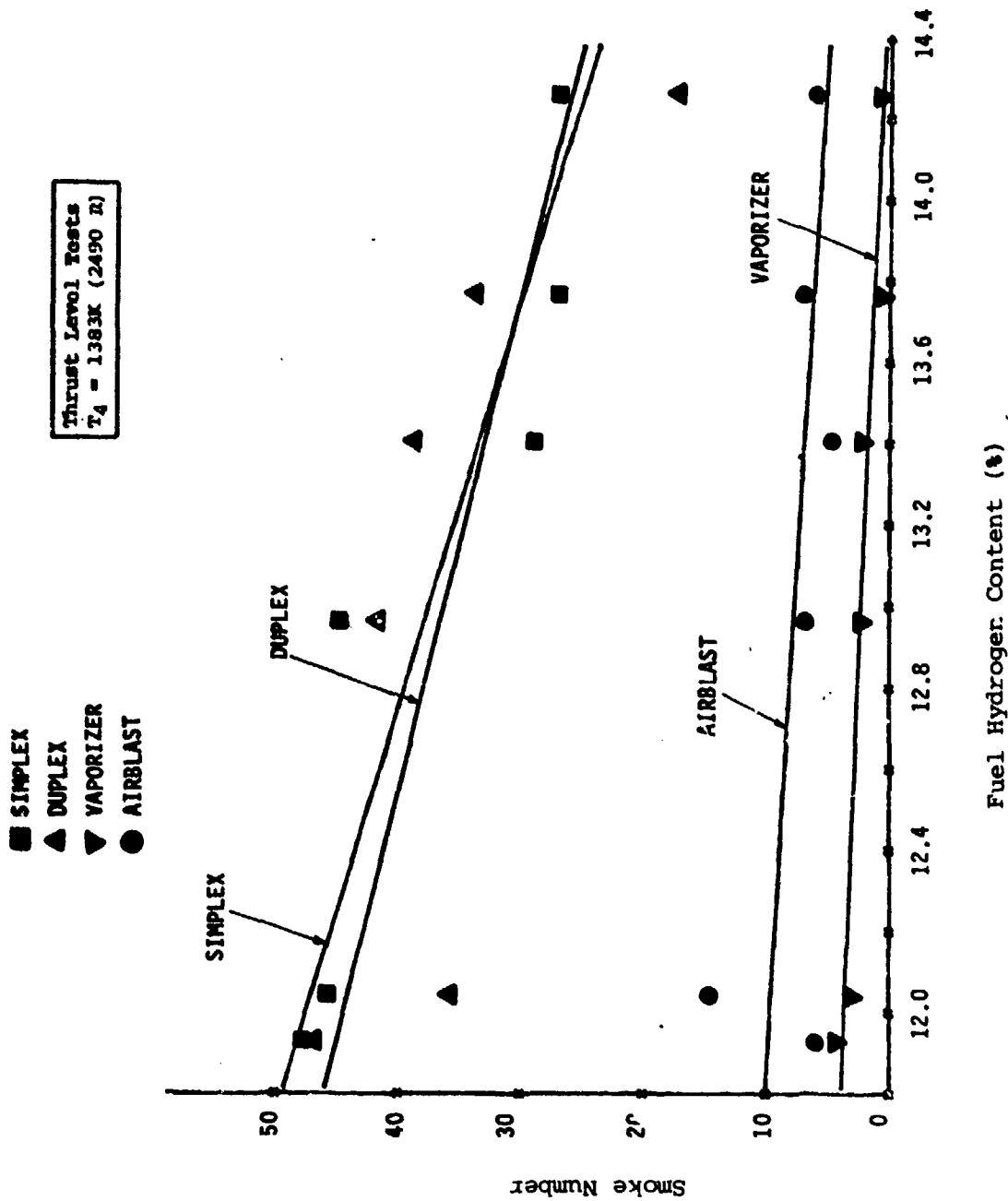
Figure 6.41: Effect of Hydrogen Content on Smoke Emissions (Nozzle Comparison)
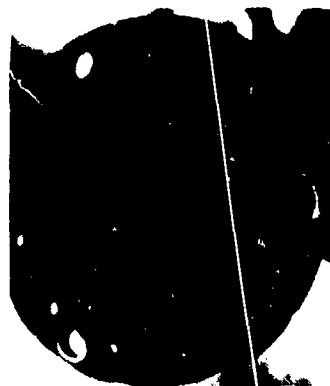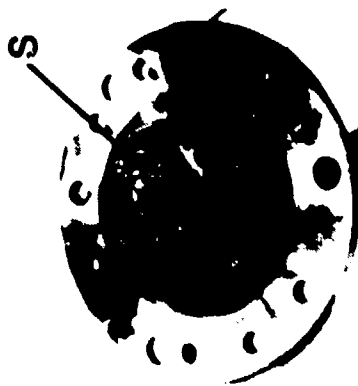
Figure 6.42: Results of Carbon Check Runs, Thrust Cycle Simulation (Simplex Pressure Atomizer)
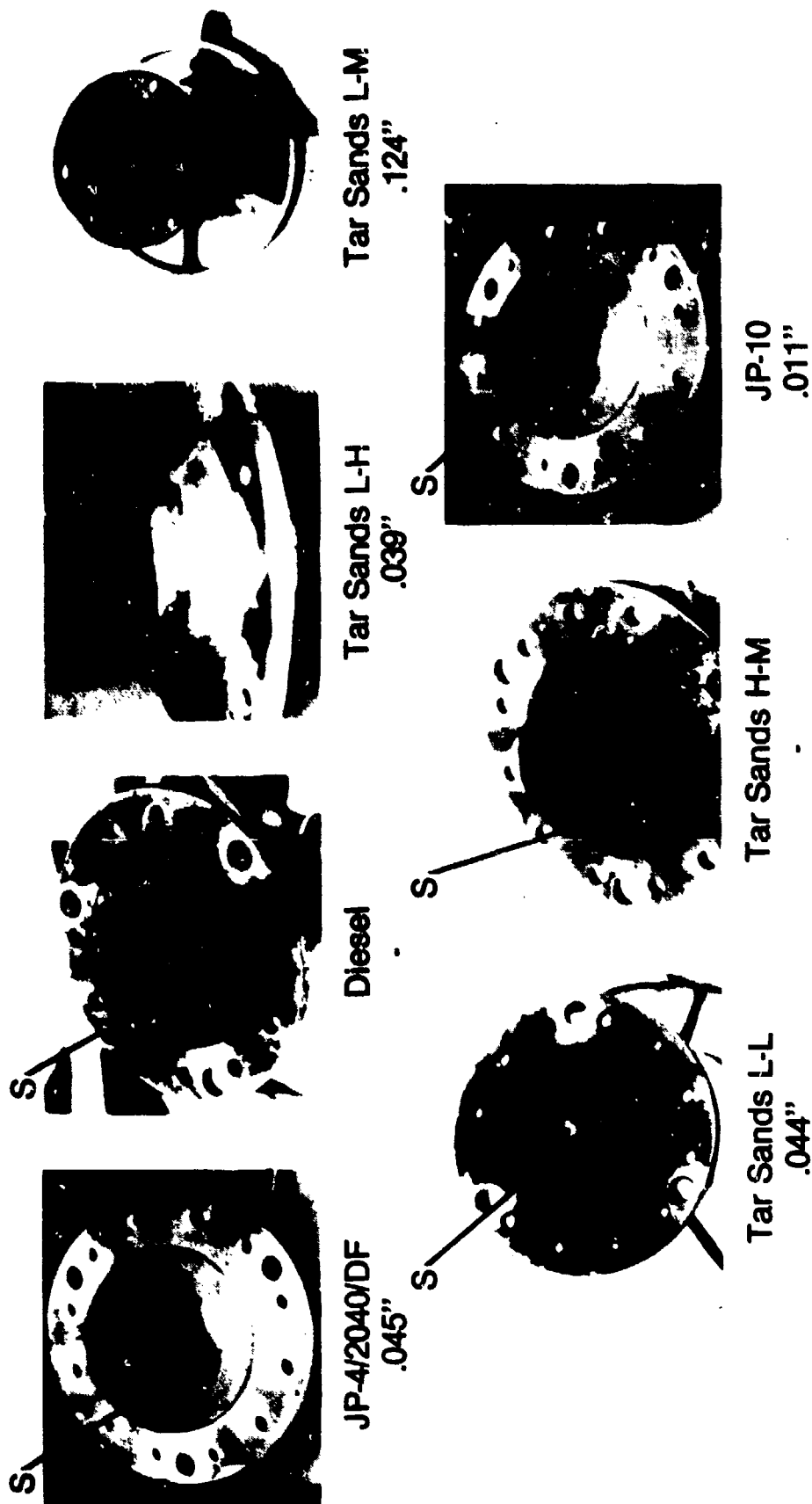
Figure 6.43: Results of Carbon Check Runs, Thrust Cycle Simulation (Simplex Pressure Atomizer)
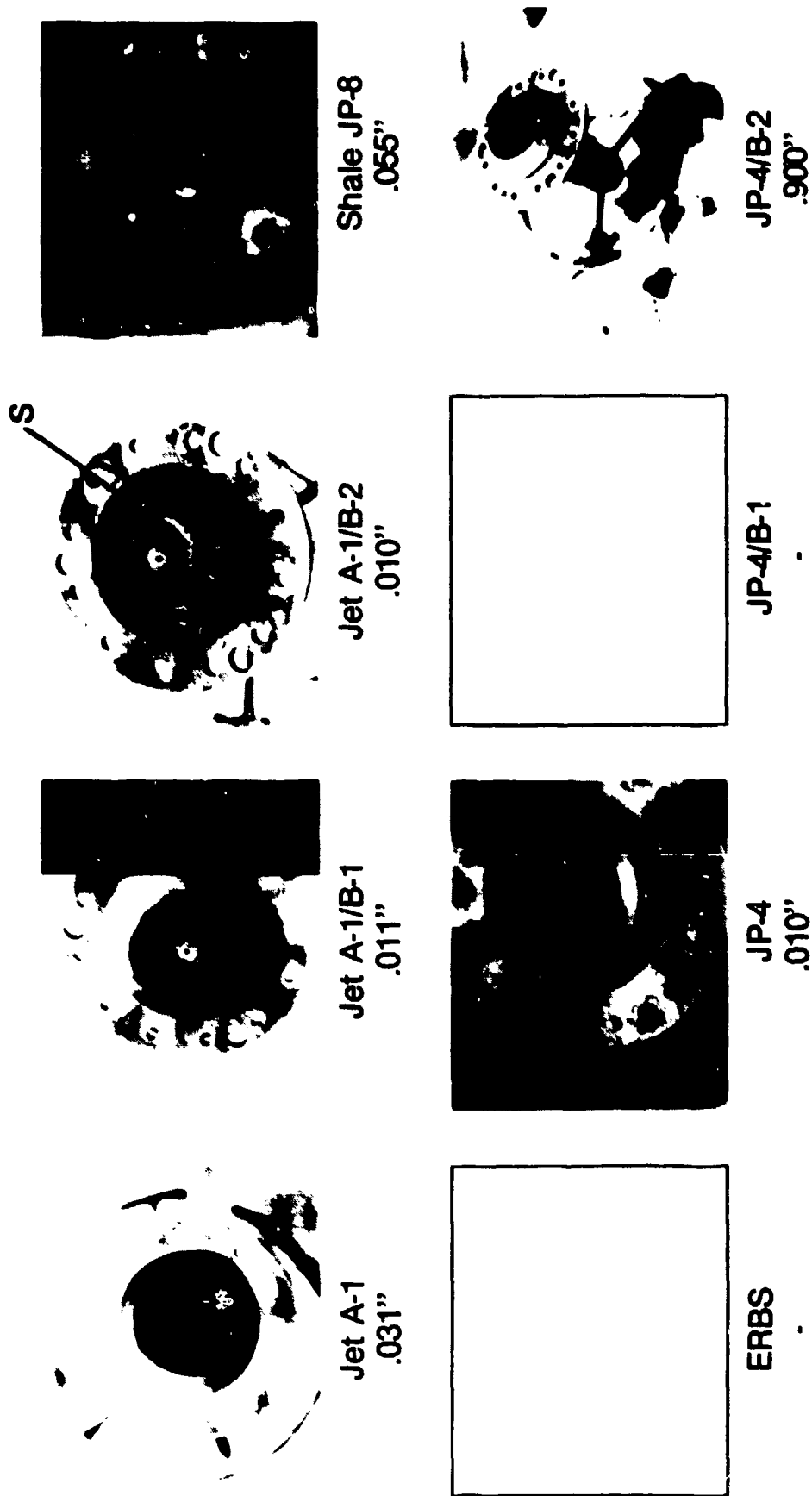
Figure 6.44: Results of Carbon Check Runs, Power Cycle Stimulation (Simplex Pressure Atomizer)

Tar Sands L-M
.846"

Tar Sands L-H
.033"

JP-10
.060"

Diesel
.084"

Tar Sands H-M
.030"

JP-4/2040/DF
.025"

Tar Sands L-L
.052"
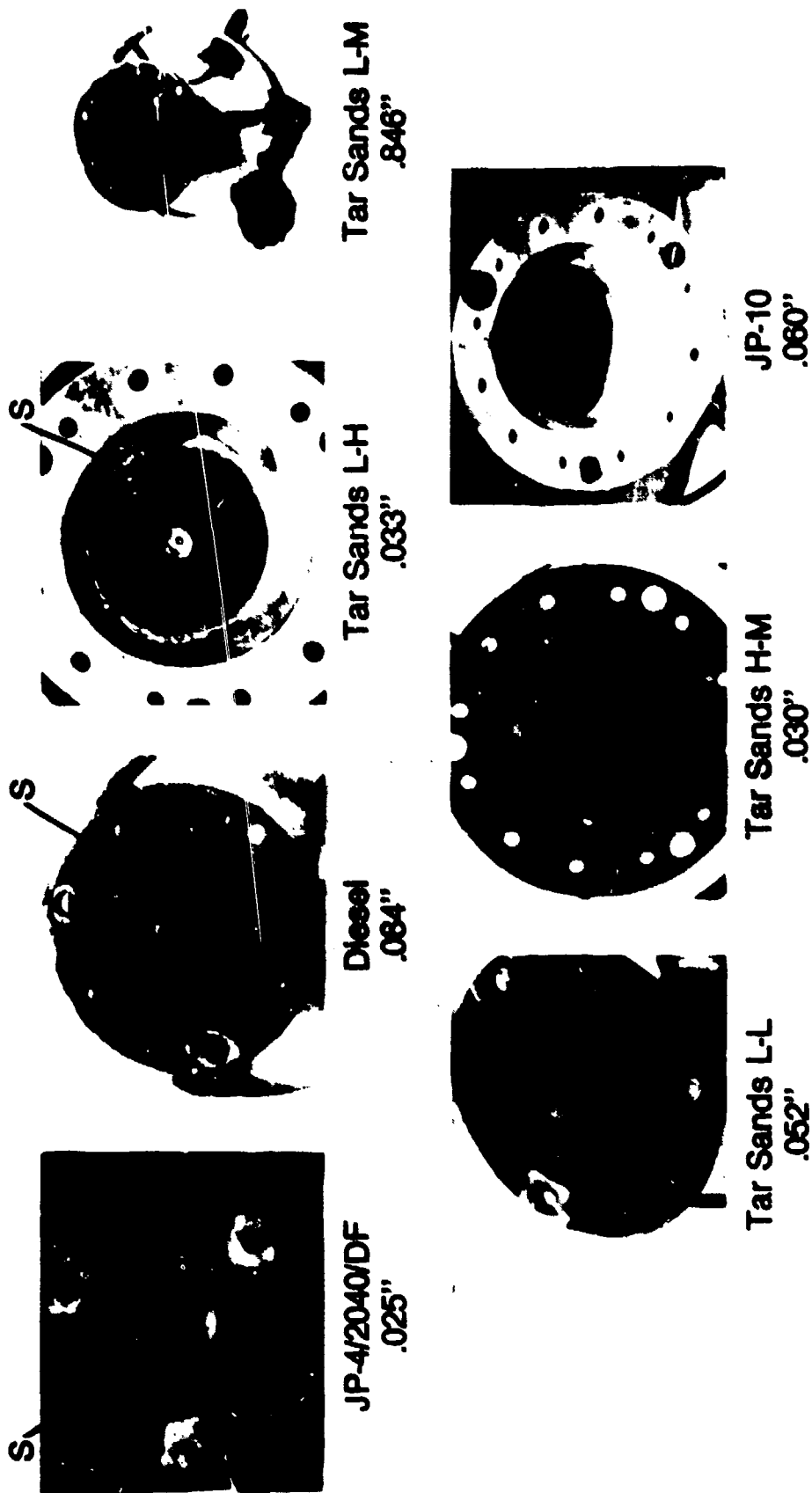
Figure 6.45: Results of Carbon Check Runs, Power Cycle Simulation (Simplex Pressure Atomizer)

- 148 -
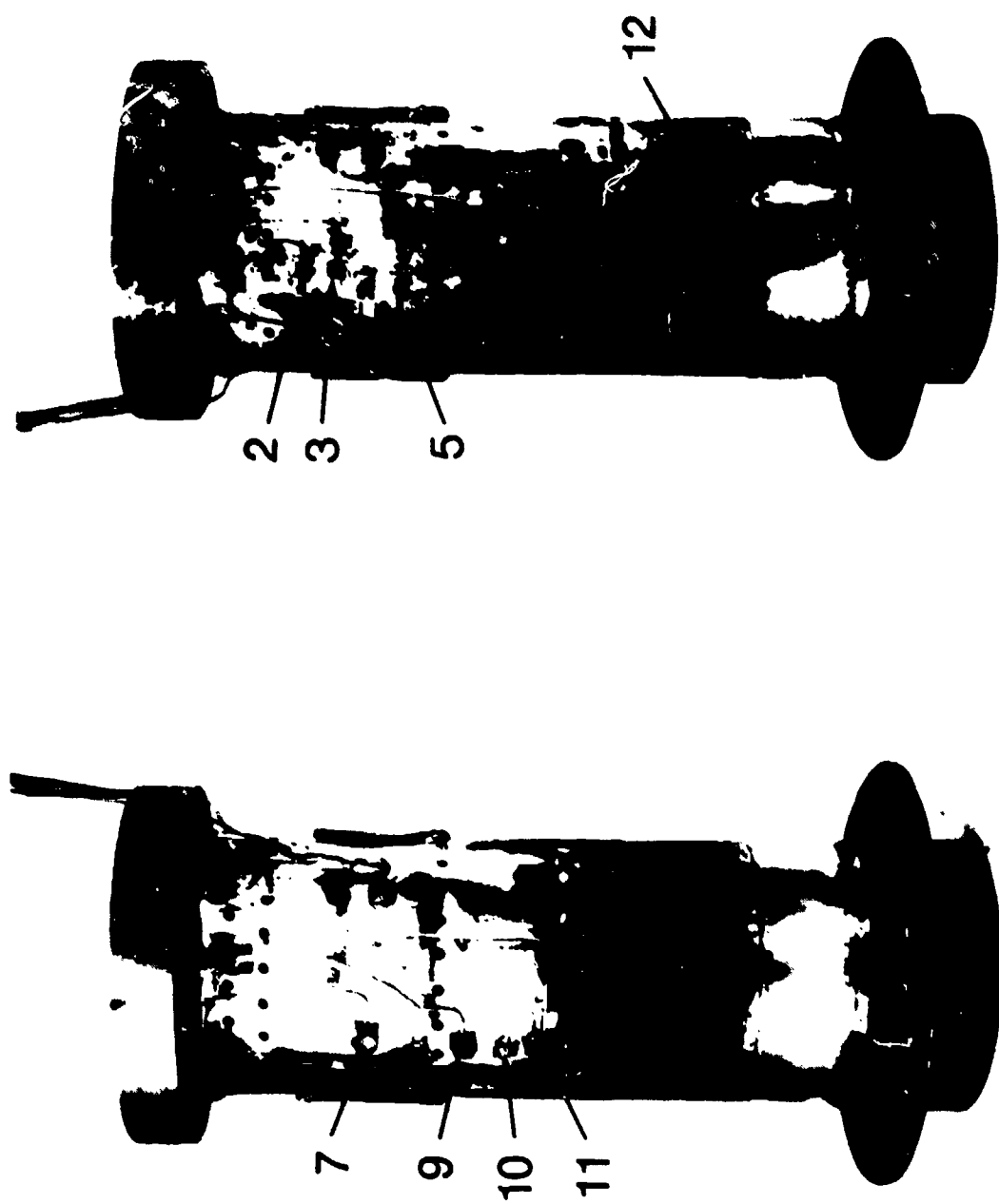
Figure 6.46: Thermocouples Used in Average Liner Temperature Calculations
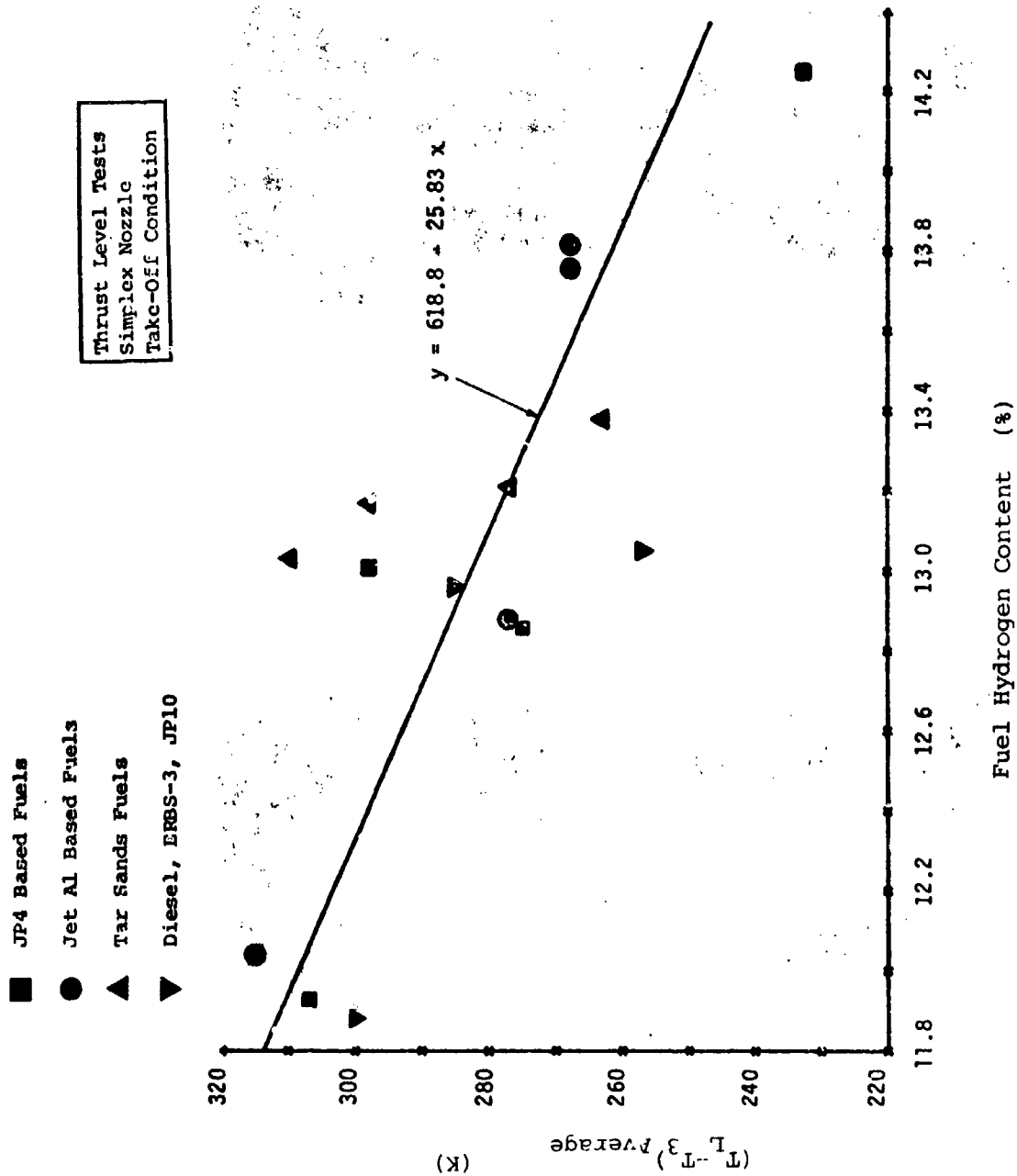
Figure 6.47: Effect of Hydrogen Content on Liner Temperatures
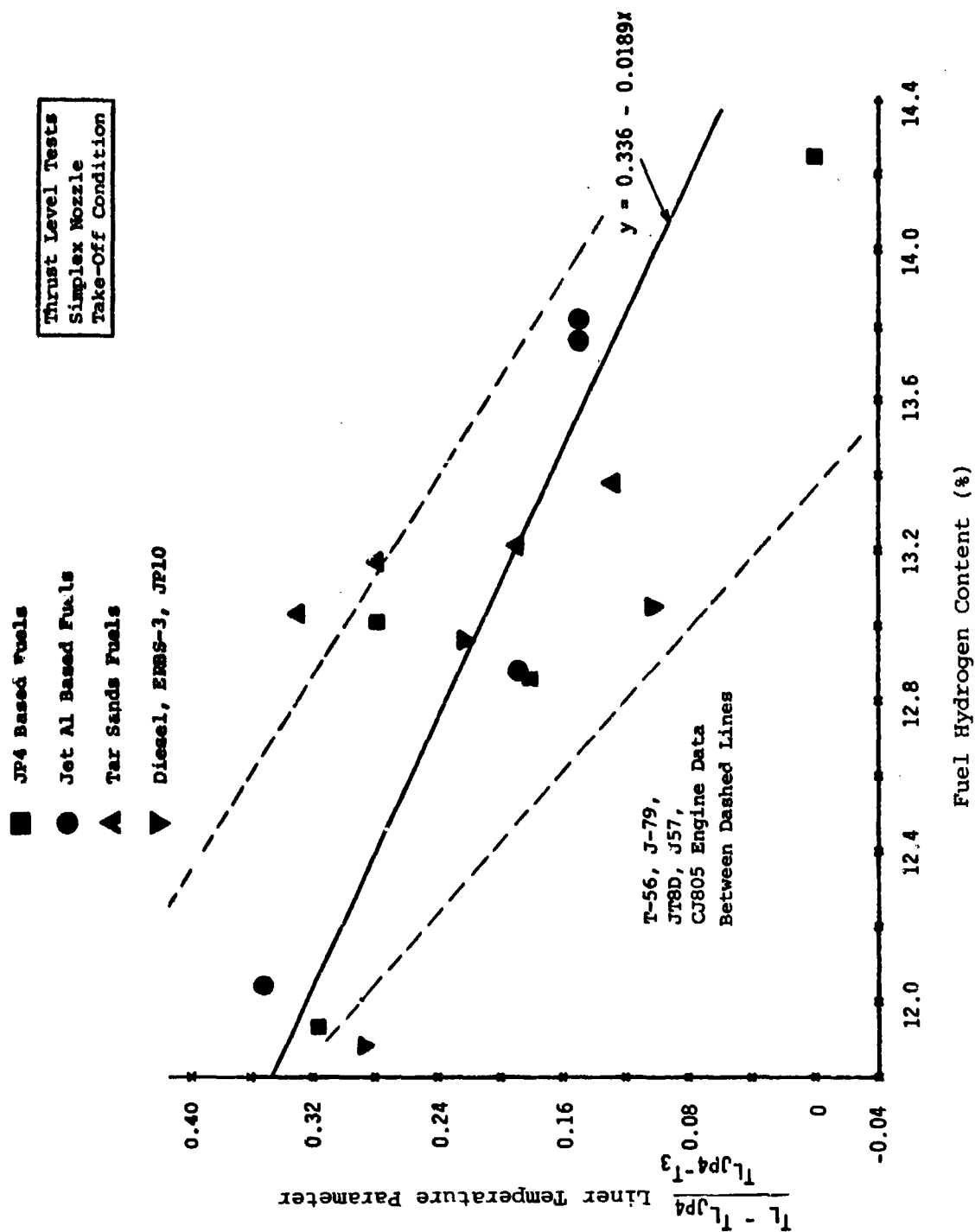
Figure 6.48: Effect of Hydrogen Content on Liner Temperatures
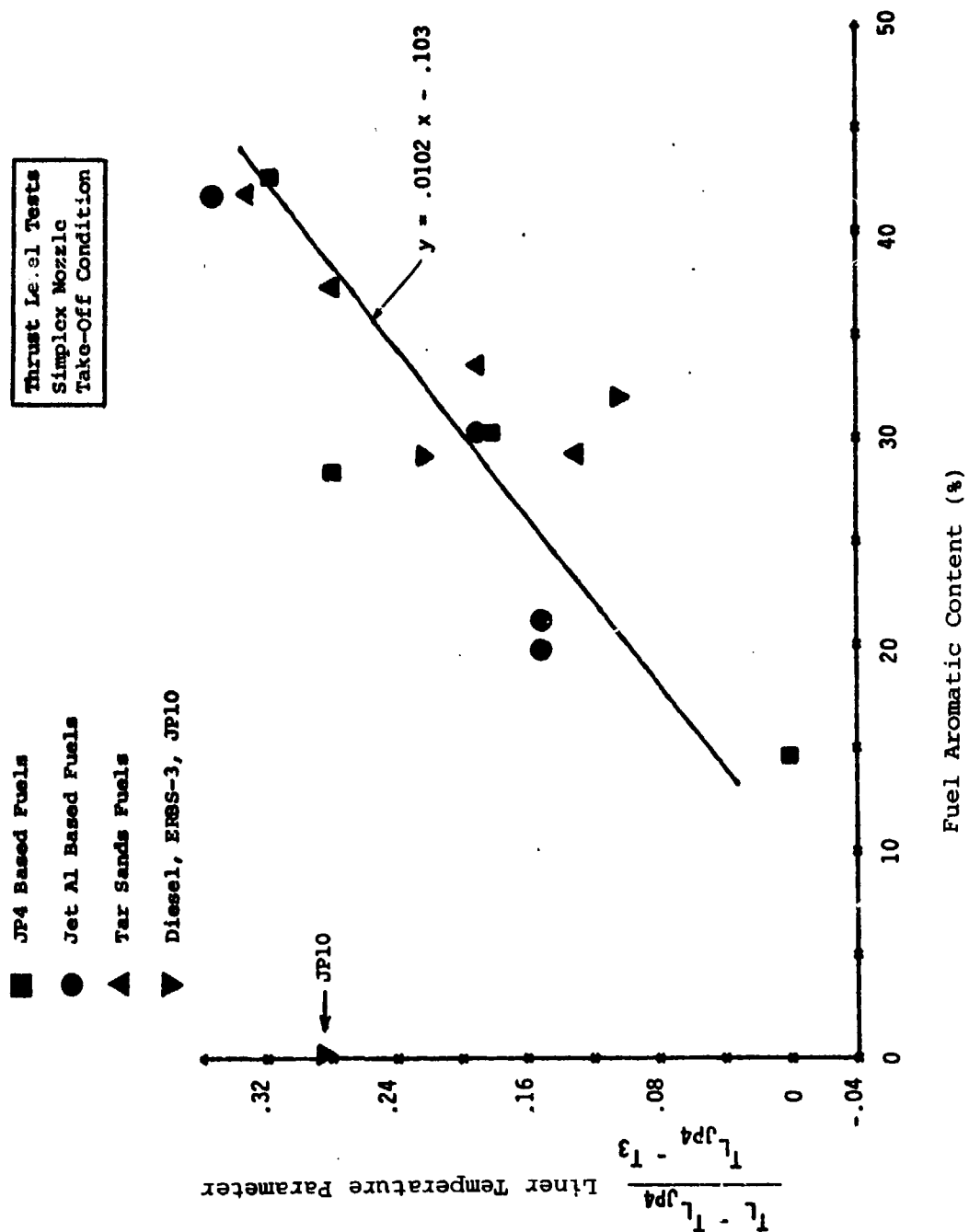
Figure 6.49: Effect of Aromatics Content on Liner Temperatures
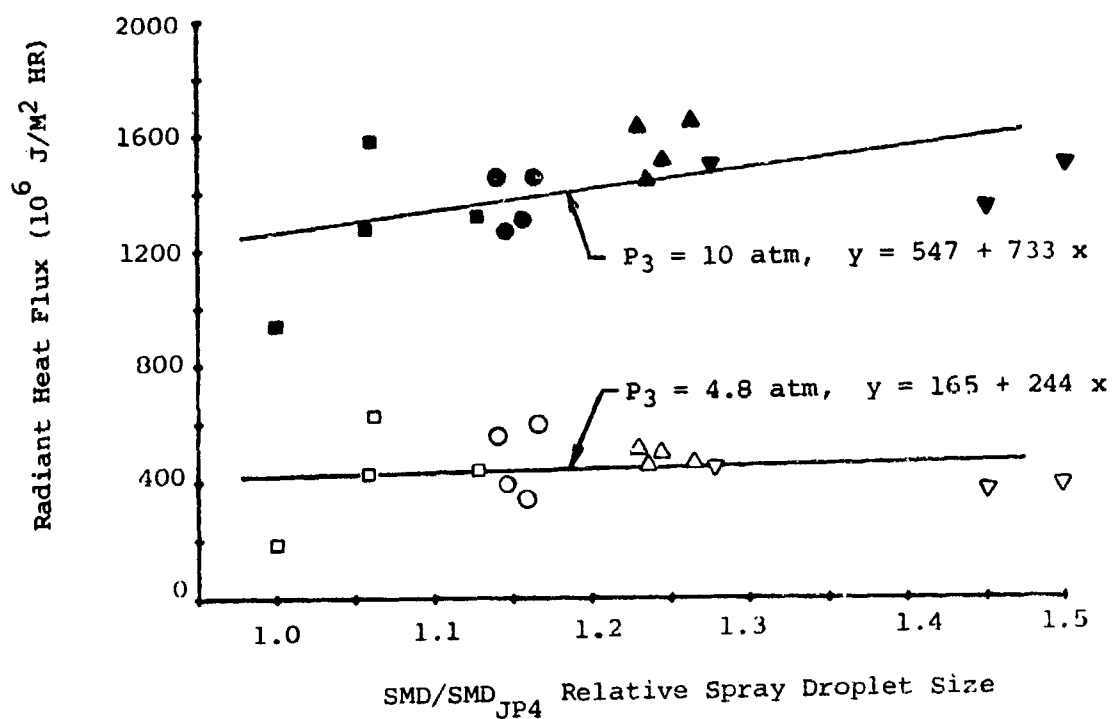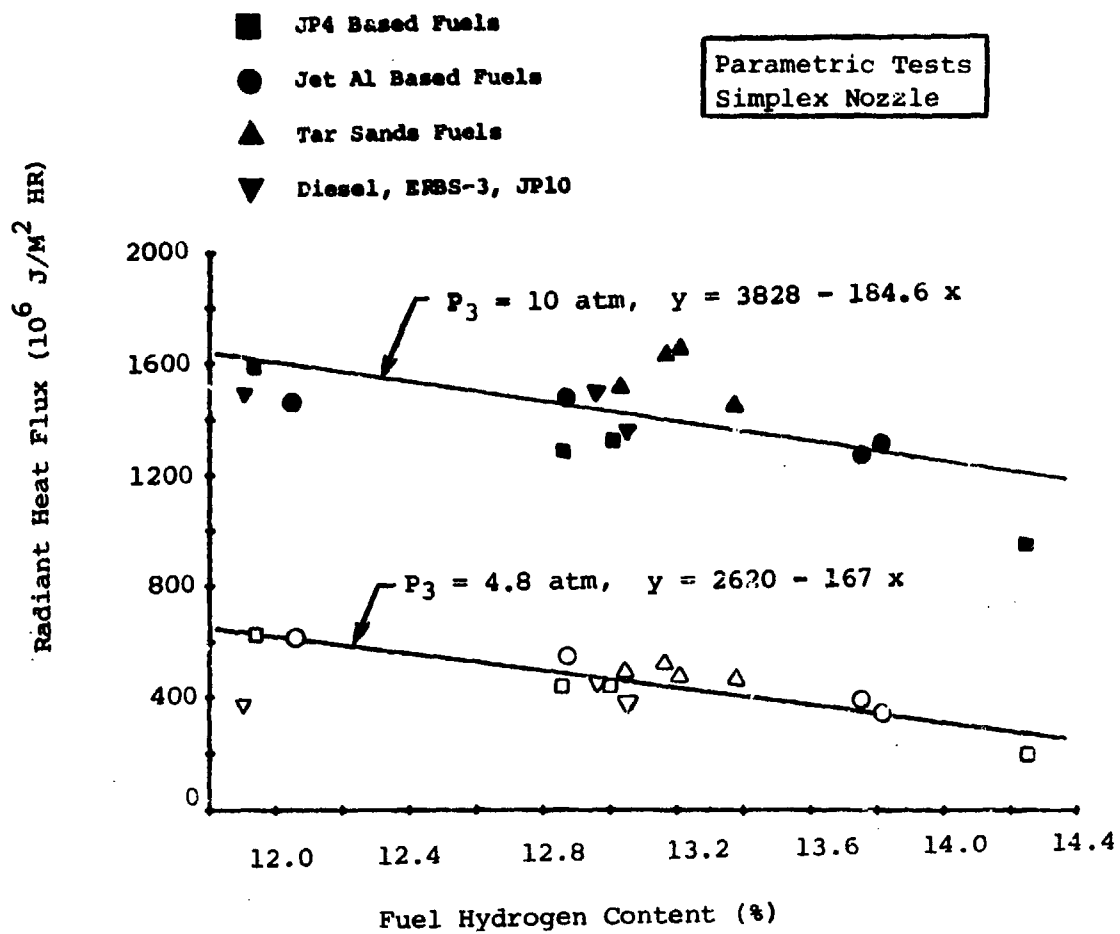
Figure 6.50: Effect of Hydrogen Content and Spray Quality on Radiation
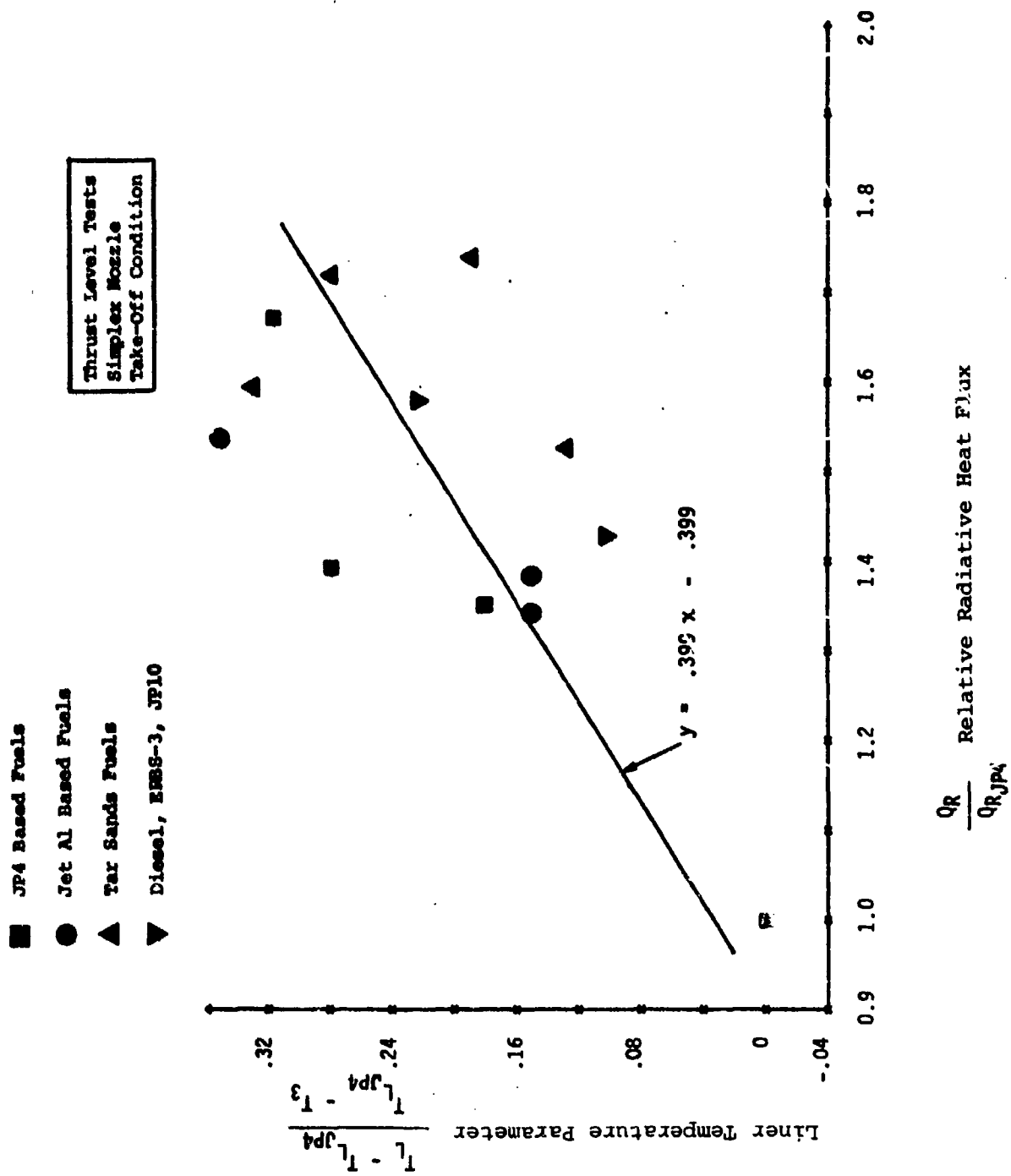
Figure 6.51: Effect of Measured Radiative Flux on Liner Temperatures

- 154 -
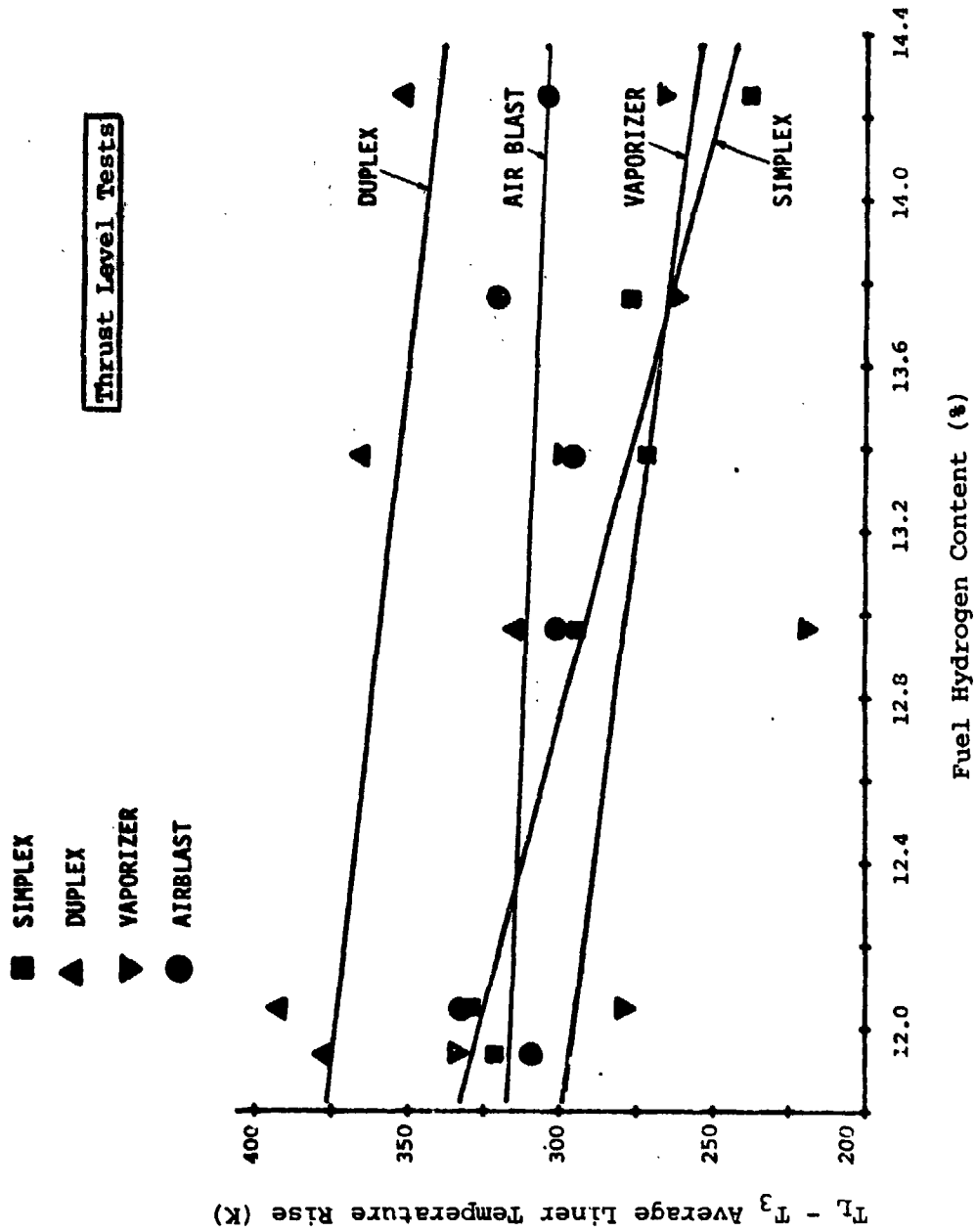
Figure 6.52: Effect of Hydrogen Content on Liner Temperatures (Nozzle Comparison)
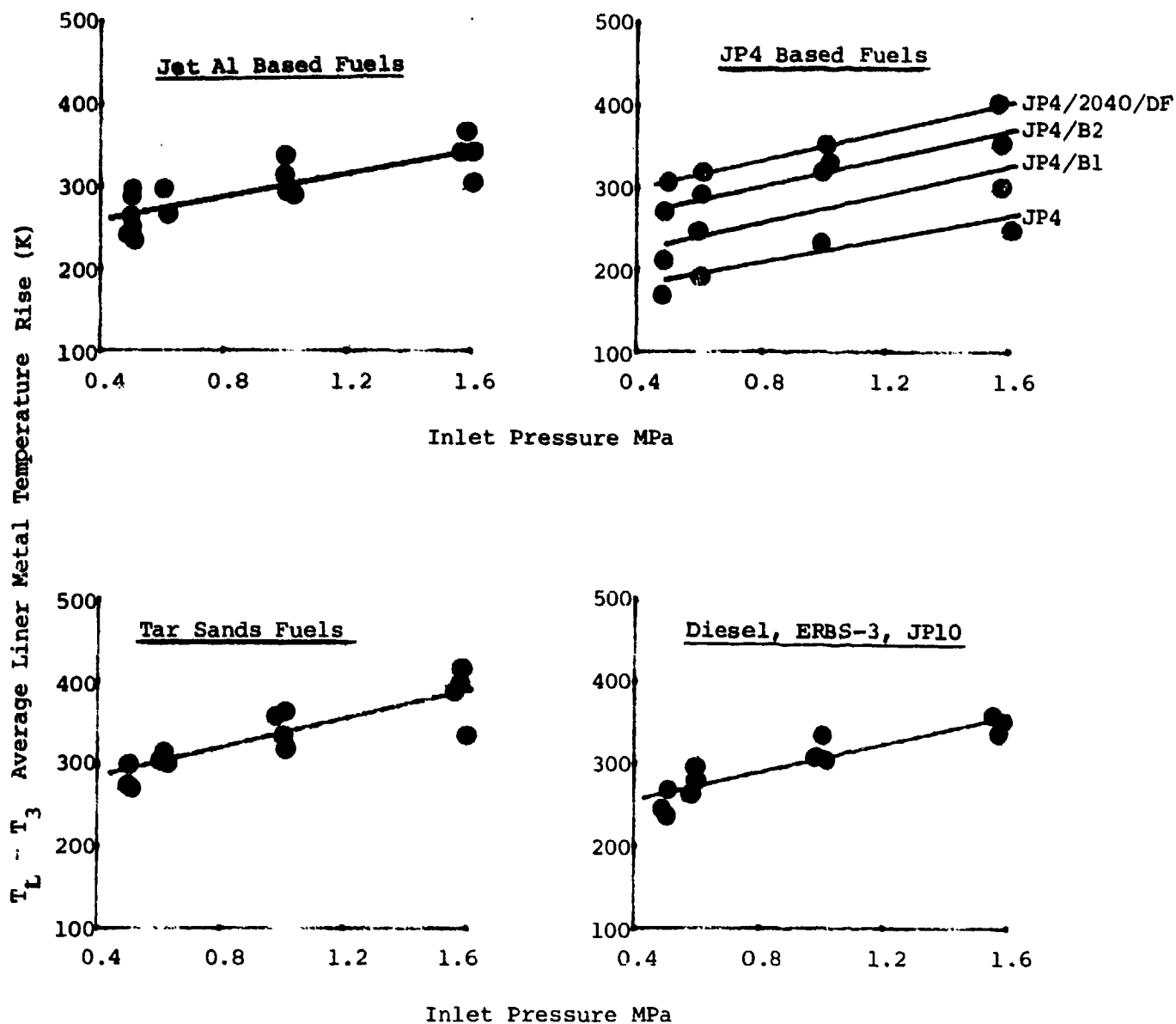
Figure 6.53: Effect of Inlet Pressure on Metal Temperatures
(Parametric Tests, Simplex Nozzle)
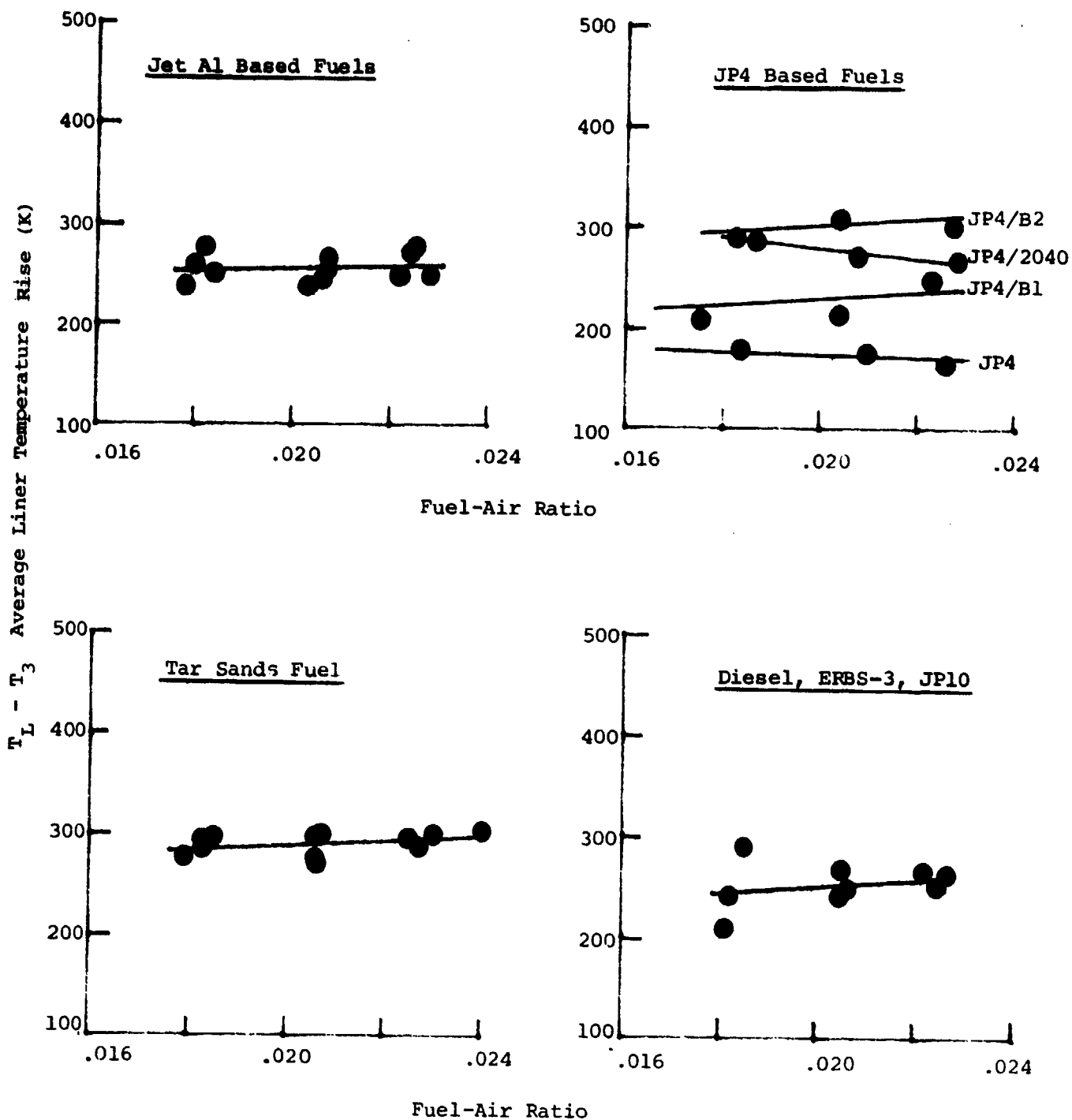
Figure 6.54: Effect of Fuel-Air Ratio on Liner Temperatures
(Parametric Tests, Simplex Nozzle)
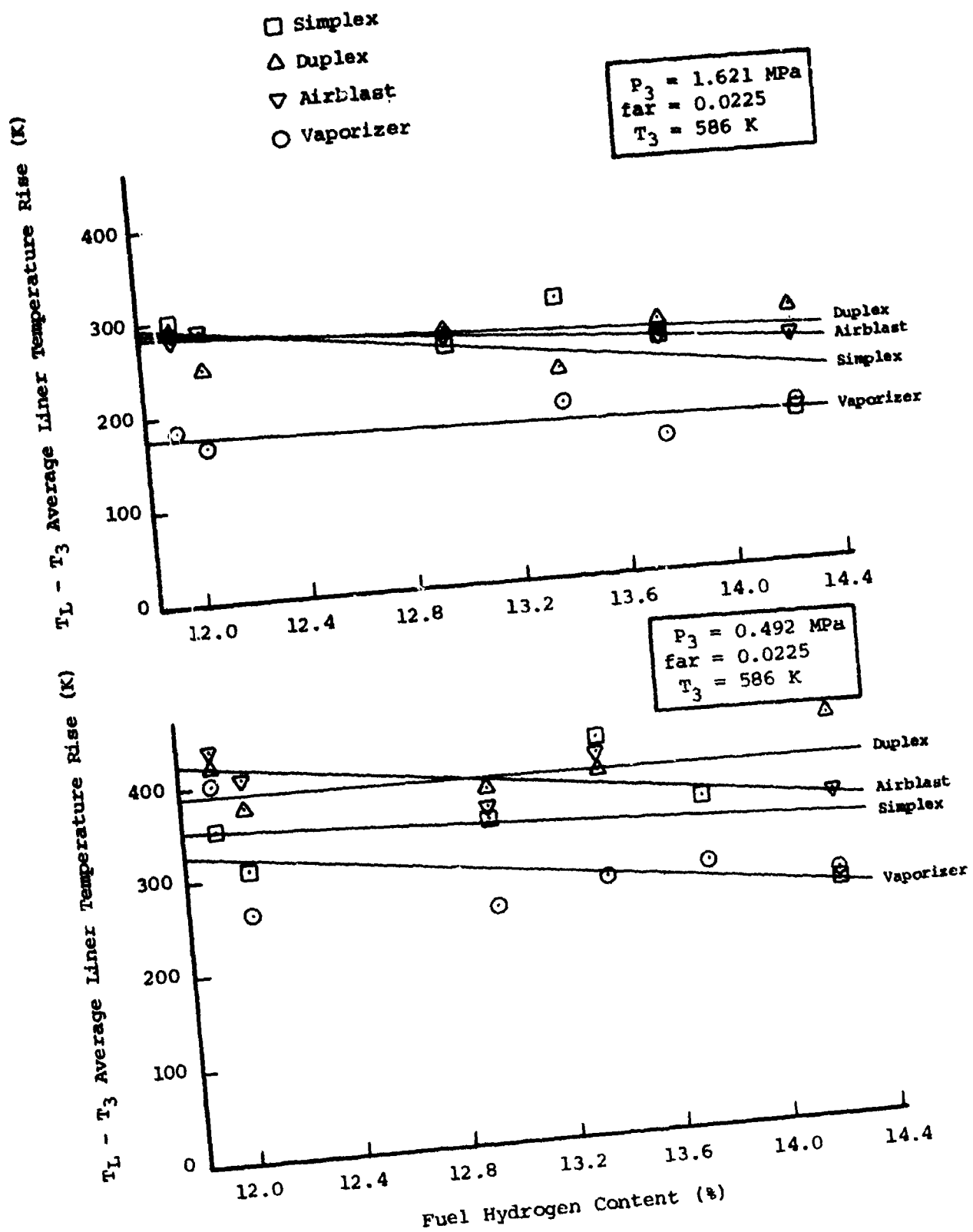
Figure 6.55: Effect of Hydrogen Content on Liner Temperatures (Nozzle Comparison, Parametric Tests)

SECTION VII

CONCLUSIONS AND RECOMMENDATIONS

Based on the rig tests with the can combustor, together with other reported data on fuel effects, several conclusions and recommendations are presented.

7.1 CONCLUSIONS

(a) The Can Combustor proved to be a satisfactory tool for evaluating combustion characteristics of the candidate fuels while simulating performance of small turboprop and turbofan combustion systems. The data base has been used to determine test requirements for reverse flow annular combustion systems with selected fuels.

(b) Lean Blow Out Stability is strongly influenced by fuel hydrogen content and by spray quality. Volatility effects are mixed: For JP4 based fuels volatility appears to have little influence on lean blow out performance, whereas for other fuels volatility has a stronger effect. Airblast and vaporizer nozzles have worse lean blow out limits than pressure atomizing nozzles.

(c) Cold Start Tests indicate that minimum light off fuel-air ratio and minimum light up temperature are strongly influenced by volatality and by properties affecting fuel atomization. Fuel hydrogen content appears to have a weak influence on light-up characteristics.

(d) Steady State Performance Tests indicate that low end combustion efficiencies are significantly influenced by fuel properties; CO emissions are strongly influenced by fuel hydrogen content and weakly by relative droplet size and volatility; THC emissions are strongly influenced by fuel hydrogen content and relative droplet size. Fuel effects on NO_x emissions at take-off are small and within range of repeatability; at idle NO_x emissions appear to be influenced by combustion efficiency which affects reaction zone gas temperatures. Smoke levels are strongly influenced by fuel hydrogen content, aromatic content and atomizer design. The nature of the aromatics appear to influence the smoke emissions as well.

(e) Carbon Check Tests in some cases were inconclusive possibly because of carbon shedding with several test fuels; there was no liner carbon or soot with any of the test fuels. Carbon on the pressure atomizer swirler sheath was relatively heavy with JP4/B2, L-M tar sands and diesel. There was no fuel nozzle carbon with either airblast or vaporizing nozzles. No fuel spray deterioration was observed with any of the nozzles or test fuels.

(f) Radiation Heat Loads and Liner Temperatures are strongly influenced by fuel hydrogen content and by properties affecting fuel atomization characteristics.

- 159 -

(g) Consistent trends have been observed between baseline fuels (i.e. Jet A and JP4) and their corresponding blends. Therefore, reverse-flow annular combustor tests can be confined to the baseline and one deviate fuel. L-H and L-L fuels appear to represent extremes of the tar sand family and ERBS-3 is a good representative of broadened specification fuels.

7.2 RECOMMENDATIONS

The following test plan is recommended for Phase III testing with PT6 and JT15D reverse-flow annular combustion systems.

7.2.1 **TEST FUELS:** The test fuels for the program are:

- PT6 Atmospheric Tests: Jet A1, Jet A1/B1, Jet A1/B2, JP4, JP4/B1, JP4/B2, JP4/DF/2040, ERBS-3, Shale JP8, L-L Tar Sands, L-H Tar Sands and JP-10 (12 fuels).

- PT6 Full Pressure and Cold Start Tests: Jet A1, Jet A1/B2, JP4, JP4/B2, ERBS-3, Shale JP-8, L-L, L-H Tar Sands, JP-10 and RJ-6 (10 fuels).

- JT15D Atmospheric Tests: Shale JP8, JP4, ERBS-3 and JP10 (4 fuels).

7.2.2 PT6 ATMOSPHERIC COMBUSTOR TESTS:

- Combustor Configuration   —   2 (Bill of Material and Lean Front End)

- Fuel Nozzle   —   2 (Simplex With Different Flow Numbers)

- Operating Cycle   —   To Simulate PT6A-65

- Test Matrix   —   Data Points

Thermal Paint	2
Temperature Traversing Steady State Performance	240
Stability (Lean Limit)	96
	338

7.2.3 JT15D ATMOSPHERIC COMBUSTOR TESTS:

- Combustor Configurations   —   2 (Bill of Material and Rich Front End)

- Fuel Nozzle Types   —   2 (Simplex and Airblast)

- Operating Cycle   –   To simulate JT15D-5

- Test Matrix   –   <u>Data Points</u>

	Data Points
Thermal Paint	2
Temperature Traversing Steady State Performance	80
Stability (Lean Limit)	<u>24</u>
	106

7.2.4 COLD START TESTS:

- Test Vehicle   –   PT6A-65 Engine

- Test Facility   –   National Research Council, Ottawa

- Combustor Configuration   –   PT6A-65 Bill of Materials

- Fuel Nozzles   –   PT6A-65 Bill of Materials

- Minimum Temperature   –   -50°F (228K)

- Data Points   –   230

7.2.5 PT6 FULL PRESSURE TESTS:

- Test Vehicle   –   PT6A-65 Gas Generator

- Stoichiometry Variations   –   2 (Bill of Material and 5% Cabin Bleed Corresponding to Rich Front End)

- Combustion Configuration   –   PT6A-65 Bill of Material

- Fuel Nozzle Types   2 (Simplex with different Flow Numbers)

- Operating Cycle   –   PT6A-65

- Test Parameters   –   Metal Temperatures, Emissions, Smoke, Pattern Factor and Pressure Drop etc.

- Data Points   –   200

SECTION VIII

BIBLIOGRAPHY

1. Allan, F.J., Sampath, P., Alternate Fuels Combustion Research Test Plan for Phase II, Eng. R 1074 submitted to AFWAL and CDND, Sept. 1980.

2. Jackson, T.A., "The Evaluation of Fuel Property Effects in Air Force Gas Turbine Engines - Program Genesis", prepared for ASME, 1980.

3. Gleason, C.C., et al., "Evaluation of Fuel Character Effects on J79 Engine Combustion System", General Electric Company, AFAPL-TR-79-2015, CEEDO-TR-79-07, June 1979.

4. Gleason, C.C., et al., "Evaluation of Fuel Character Effects on F101 Engine Combustion System", General Electric Company, AFAPL-TR-79-2018, CEEDO-TR-79-07, June 1979.

5. Jackson, T.A., Blazowski, W.S., "Fuel Hydrogen Content as an Indicator of Radiative Heat Transfer in an Aircraft Gas Turbine Combustor, Gas Turbine Combustion and Fuels Technology", ASME, 1977.

6. Lohmann, R.P. Szetela, E.J., Vranos, A., "Analytical Evaluation of the Impact of Broad Specification Fuels on High Bypass Turbofan Engine Combustors", United Technologies Corporation, Pratt and Whitney Aircraft Group, Commercial Products Division, NASA CR-159454, PWA 5564-15, December 1978.

7. "Low NO_x Emission Combustor for Automobile Gas Turbine Engines", APTD-1457.

8. Demitri, E.P., Topping, R.F., Wilson, R.P., "Study of Research and Development Requirements of Small Gas Turbine Combustors", NASA CR-159796, ADL 83381-1, January 1980.

9. Odgers, J., Kretschmer, D., "Alternative Fuels, Experimental Values of Flash Point, Vapor Pressure and Surface Tension", Report J.O. 104, Laval University, April 1982.

10. "Control of Air Pollution from Aircraft and Aircraft Engines", Environmental Protection Agency, U.S. Federal Register, March 24, 1978.

11. Blazowski, W.S., "Combustion Considerations for Future Jet Fuels", Proceedings of Sixteenth International Symposium on Combustion, August 1976.

APPENDIX A
Lean Limit Test Data

NOZZLE	FUEL	SET P_3 (MPa)	SET T_3 (°K)	SET W_c (kg/s)	LL far
SIMPLEX	JET A1	0.408	372.8	0.113	0.0041
		0.414	372.2	0.158	0.0042
		0.408	371.1	0.208	0.0048
		0.412	371.6	0.241	0.0056
SIMPLEX	JET A1/B1	0.400	373.8	0.111	0.0045
		0.397	370.5	0.159	0.0044
		0.400	375.5	0.203	0.0060
		0.397	375.5	0.230	0.0071
		0.400	375.5	0.113	0.0043
SIMPLEX	JET A1/B2	0.404	373.9	0.113	0.0046
		0.405	376.1	0.160	0.0061
		0.413	376.1	0.205	0.0062
		0.406	373.9	0.230	0.0068
		0.402	377.8	0.108	0.0056
SIMPLEX	JP8 Shale	0.416	375.5	0.115	0.0040
		0.414	375.5	0.161	0.0040
		0.417	375.0	0.207	0.0045
		0.408	374.4	0.238	0.0053
SIMPLEX	ERBS-3	0.408	371.1	0.111	0.0065
		0.420	373.3	0.165	0.0061
		0.414	373.8	0.206	0.0063
		0.411	374.4	0.245	0.0067
SIMPLEX	Diesel	0.412	376.6	0.109	0.0077
		0.408	375.0	0.160	0.0068
		0.407	375.0	0.206	0.0062
		0.413	375.0	0.230	0.0062
SIMPLEX	JP10	0.408	377.2	0.111	0.0072
		0.416	378.3	0.162	0.0073
		0.417	378.3	0.207	0.0122
		0.414	375.0	0.227	0.0129
SIMPLEX	Tar Sands L-H	0.396	375.0	0.110	0.0056
		0.400	371.6	0.111	0.0056
		0.393	374.4	0.159	0.0050
		0.400	373.3	0.202	0.0052
		0.400	375.0	0.227	0.0052
SIMPLEX	Tar Sands H-M	0.404	370.0	0.113	0.0057
		0.407	375.0	0.162	0.0051
		0.407	375.0	0.209	0.0050
		0.404	375.0	0.231	0.0058
		0.400	373.3	0.113	0.0055

NOZZLE	FUEL	SET P_3 (MPa)	SET T_3 (°K)	SET W_c (kg/s)	LL far
SIMPLEX	Tar Sands L-M	0.402	375.5	0.115	0.0051
		0.401	372.7	0.158	0.0049
		0.399	375.5	0.204	0.0051
		0.398	374.4	0.232	0.0056
		0.407	373.8	0.117	0.0052
SIMPLEX	Tar Sands L-L	0.400	376.1	0.112	0.0065
		0.396	376.6	0.109	0.0062
		0.403	376.1	0.158	0.0067
		0.398	375.5	0.208	0.0078
		0.400	376.1	0.231	0.0094
SIMPLEX	JP4	0.409	377.7	0.115	0.0034
		0.419	376.6	0.167	0.0037
		0.406	376.6	0.200	0.0046
		0.419	374.4	0.234	0.0062
		0.408	378.3	0.109	0.0036
SIMPLEX	JP4'B1	0.412	376.1	0.107	0.0042
		0.408	377.2	0.112	0.0039
		0.407	376.6	0.161	0.0044
		0.413	375.5	0.211	0.0054
		0.414	375.5	0.235	0.0063
SIMPLEX	JP4/B2	0.408	377.7	0.115	0.0042
		0.406	375.0	0.157	0.0054
		0.416	377.7	0.206	0.0088
		0.405	377.7	0.222	0.0100
		0.405	378.8	0.220	0.0042
SIMPLEX	JP4/2040/DF	0.387	376.1	0.108	0.0046
		0.395	376.6	0.109	0.0043
		0.402	375.5	0.160	0.0051
		0.393	376.1	0.204	0.0063
		0.393	376.1	0.232	0.0072
DUPLEX	JET A1	0.413	376.6	0.106	0.0059
		0.408	377.7	0.161	0.0051
		0.422	375.5	0.208	0.0055
		0.419	376.6	0.232	0.0066
		0.405	377.2	0.112	0.0058
DUPLEX	ERBS-3	0.408	374.4	0.113	0.0057
		0.409	373.9	0.156	0.0050
		0.409	375.0	0.209	0.0065
		0.404	375.0	0.224	0.0075

NOZZLE	FUEL	SET P_3 (MP$_a$)	SET T_3 (°K)	SET W_c (kg/s)	LL far
DUPLEX	Tar Sands L-H	0.396	370.5	0.112	0.0066
		0.398	375.0	0.112	0.0067
		0.400	372.7	0.159	0.0061
		0.398	373.3	0.204	0.0068
		0.400	374.4	0.228	0.0076
DUPLEX	JP4	0.408	376.1	0.114	0.0029
		0.410	377.2	0.157	0.0045
		0.415	376.6	0.205	0.0062
		0.416	377.7	0.228	0.0063
		0.404	377.7	0.110	0.0031
DUPLEX	JP4/B2	0.412	373.3	0.104	0.0039
		0.409	374.4	0.162	0.0055
		0.420	373.3	0.228	0.0073
		0.412	377.2	0.112	0.0037
		0.405	375.5	0.201	0.0063
AIRBLAST	JET A1	0.418	375.0	0.113	0.0103
		0.412	376.6	0.157	0.0094
		0.405	376.6	0.208	0.0093
		0.405	376.6	0.231	0.0101
AIRBLAST	JET A1/B2	0.405	377.2	0.102	0.0113
		0.401	378.8	0.100	0.0111
		0.406	378.3	0.157	0.0099
		0.408	376.6	0.205	0.0095
		0.413	377.2	0.226	0.0112
AIRBLAST	ERBS	0.417	373.8	0.115	0.0118
		0.399	373.8	0.159	0.0115
		0.412	372.7	0.207	0.0104
		0.413	372.2	0.230	0.0103
AIRBLAST	Tar Sands L-H	0.397	371.6	0.112	0.0104
		0.397	371.6	0.112	0.0121
		0.404	374.4	0.158	0.0101
		0.400	373.3	0.208	0.0099
		0.397	372.2	0.234	0.0105
AIRBLAST	JP4	0.402	376.6	0.113	0.0087
		0.403	376.6	0.160	0.0082
		0.405	376.6	0.203	0.0088
		0.404	375.5	0.228	0.0085
		0.406	376.1	0.113	0.0087
AIRBLAST	JP4/B2	0.406	368.8	0.116	0.0090
		0.411	370.0	0.162	0.0088
		0.416	371.1	0.211	0.0085
		0.416	368.8	0.236	0.0087

NOZZLE	FUEL	SET P_3 (MPa)	SET T_3 (°K)	SET W_c (kg/s)	LL far
VAPORIZER	JET A1	0.404	373.3	0.115	0.0107
		0.415	377.2	0.159	0.0113
		0.398	374.4	0.180	0.0148
		0.404	375.5	0.206	0.0198
VAPORIZER	JET A1/B2	0.402	377.2	0.114	0.0064
		0.408	378.3	0.115	0.0089
		0.408	377.2	0.157	0.0098
		0.412	374.4	0.182	0.0126
		0.418	376.6	0.218	0.0141
VAPORIZER	ERBS	0.406	375.5	0.115	0.0127
		0.415	374.4	0.158	0.0129
		0.406	375.0	0.186	0.0170
		.0.415	375.0	0.202	0.0152
VAPORIZER	Tar Sands L-H	·0.397	373.8	0.116	0.0098
		·0.404	373.8	0.160	0.0131
		0.40	375.	0.180	UNSTABLE
		0.40	375.	0.210	UNSTABLE
VAPORIZER	JP4	0.405	376.6	0.112	0.0090
		0.400	377.2	0.163	0.0124
		0.400	376.6	0.185	0.0127
		0.411	375.0	0.213	0.0152
		0.403	377.7	0.112	0.0092
VAPORIZER	JP4/B2	0.404	375.5	0.114	0.0070
		0.407	377.2	0.159	0.0088
		0.408	377.2	0.183	0.0119
		0.405	376.6	0.206	0.0155
		0.409	378.3	0.109	0.0069

NOZZLE	FUEL	W_c (kg/s)	far	T_f ($^\circ$K)	T_3 ($^\circ$K)	TTL (sec)
SIMPLEX 0.9	JET A1	0.0231	0.0253	289	288	15
		0.0231	0.0248	289	289	19
		0.0231	0.0219	256	256	10
		0.0231	0.0208	256	256	9
		0.0231	0.0190	256	256	25
		0.0280	0.0173	257	256	15
		0.0231	0.0172	256	256	13
		0.0231	0.0167	257	256	NO
		0.0231	0.0155	256	256	NO
		0.0231	0.0026	243	241	12
		0.0231	0.0218	243	241	10
		0.0231	0.0231	243	241	NO
SIMPLEX 0.9	JET A1/B2	0.0231	0.0285	288	289	7
		0.0231	0.0249	287	289	17
		0.0231	0.0243	287	288	10
		0.0133	0.0219	288	288	NO
		0.0231	0.0212	288	288	NO
		0.0231	0.0182	288	288	NO
		0.0231	0.0371	285	284	4
		0.0233	0.0314	285	283	18
		0.0134	0.0283	285	283	NO
		0.0281	0.0280	285	283	21
		0.0234	0.0247	285	283	NO
		0.0237	0.0238	285	284	NO
		0.0233	0.0441	272	271	5
		0.0234	0.0311	274	272	11
		0.0233	0.0294	273	272	28
		0.0234	0.0262	274	273	NO
		0.0231	0.0300	255	255	15
		0.0233	0.0243	257	255	17
		0.0233	0.0243	256	256	20
		0.0234	0.0229	255	255	NO
		0.0231	0.0225	255	256	NO
		0.0233	0.0218	257	257	NO
		0.0234	0.0242	250	251	28
		0.0234	0.0217	249	250	NO
		0.0231	0.0259	242	242	8
		0.0233	0.0237	242	242	6
		0.0231	0.0228	242	241	NO

NOZZLE	FUEL	W_c (kg/s)	far	T_f (°K)	T_3 (°K)	TTL (sec)
SIMPLEX 0.9	JP4	0.0234	0.0278	289	289	4
		0.0234	0.0275	289	289	7
		0.0234	0.0223	290	290	19
		0.0233	0.0213	289	290	17
		0.0235	0.0192	290	290	14
		0.0235	0.0182	290	290	25
		0.0235	0.0179	290	290	NO
		0.0231	0.0268	272	273	9
		0.0231	0.0245	273	272	8
		0.0233	0.0216	274	273	6
		0.0233	0.0200	272	273	NC
		0.0235	0.0176	272	273	NO
		0.0235	0.0230	357	255	13
		0.0233	0.0220	257	257	20
		0.0233	0.0197	257	257	22
		0.0233	0.0180	257	257	NO
		0.0230	0.0210	240	204	13
		0.0232	0.0289	240	240	10
		0.0232	0.0172	241	241	9
		0.0231	0.0161	242	242	NO
		0.0233	0.0269	244	253	5
		0.0234	0.0182	244	254	20
		0.0234	0.0159	250	255	NO
SIMPLEX 0.9	JP4/B2	0.0231	0.0251	289	289	10
		0.0231	0.0197	289	289	14
		0.0231	0.0173	289	289	18
		0.0231	0.0144	289	289	19
		0.0132	0.0125	289	289	22
		0.0231	0.0114	289	289	NO
		0.0232	0.0219	272	272	17
		0.0232	0.0216	272	272	7
		0.0232	0.0205	272	273	NO
		0.0231	0.0240	258	258	12
		0.0231	0.0203	257	257	15
		0.0231	0.0174	257	257	16
		0.0231	0.0159	257	257	NO
		0.0231	0.0243	241	240	10
		0.0231	0.0219	241	240	12
		0.0231	0.0201	242	242	17
		0.0230	0.0200	242	241	10
		0.0232	0.0174	242	242	14
		0.0231	0.0156	242	241	NO

NOZZLE	FUEL	W_c (kg/s)	far	T_f ($^\circ$K)	T_3 ($^\circ$K)	TTL (sec)
SIMPLEX 0.9	Tar Sands L-H	0.0212	0.0256	291	290	17
		0.0231	0.0229	291	290	9
		0.0232	0.0224	291	290	28
		0.0232	0.0290	291	290	26
		0.0233	0.0205	291	290	NO
		0.0233	0.0194	291	290	NO
		0.0229	0.0231	274	274	15
		0.0231	0.0228	274	274	20
		0.0230	0.0214	274	274	NO
		0.0231	0.0207	274	274	NO
		0.0231	0.0240	255	257	18
		0.0231	0.0231	255	257	10
		0.0230	0.0217	255	257	NO
		0.0232	0.0257	245	247	5
		0.0232	0.0242	245	247	NO
		0.0232	0.0230	246	248	NO
		0.0232	0.0224	246	248	NO
		.0231	0.0262	242	242	12
		.0232	0.0242	240	241	15
		.0231	0.0237	242	242	NO
		.0231	0.0226	241	241	NO
		.0233	0.0265	241	248	NO
		.0232	0.0249	240	248	7
		.0231	0.0234	240	248	3
SIMPLEX 0.9	ERBS	0.0231	0.0250	288	289	17
		0.0231	0.0248	289	288	16
		.0232	0.0246	290	288	21
		.0231	0.0241	288	289	NO
		.0231	0.0226	288	288	NO
		.0231	0.0280	273	272	9
		.0231	0.0274	273	272	5
		.0231	0.0250	273	272	NO
		.0232	0.0290	255	255	23
		.0232	0.0280	257	257	9
		.0232	0.0265	256	256	NO
		.0231	0.0307	241	242	9
		.0231	0.0295	241	241	24
		.0232	0.0268	242	242	10
		.0231	0.0256	243	242	10
		.0231	0.0244	243	241	NO
		.0231	0.0226	242	240	NO

NOZZLE	FUEL	W_c (kg/s)	far	T_f (°K)	T_3 (°K)	TTL (sec)
SIMPLEX 0.9	JP10	.0232	0.0286	290	288	12
		.0231	0.0253	290	288	14
		.0232	0.0226	289	288	22
		.0231	0.0201	288	288	NO
		.0231	0.0161	288	288	NO
		.0232	0.0282	273	273	9
		.0231	0.0270	273	272	13
		.0230	0.0254	273	273	NO
		.0232	0.0252	273	273	NO
		.0231	0.0280	256	256	13
		.0231	0.0247	257	257	14
		.0235	0.0236	257	256	8
		.0228	0.0222	257	256	10
		.0231	0.0211	254	255	NO
		.0231	0.0189	256	255	NO
		.0231	0.0164	255	255	NO
		.0231	0.0249	242	242	7
		.0229	0.0243	242	241	NO
		.0231	0.0241	242	242	12
		.0231	0.0227	242	242	7
		.0231	0.0220	242	242	NO
SIMPLEX 3.0	JET A1	.0230	0.0518	290	288	11
		.0230	0.0500	290	288	8
		.0231	0.0485	290	288	NO
		.0230	0.0481	290	288	NO
		.0230	0.0475	290	288	NO
		.0231	0.0473	290	288	NO
		.0231	0.0581	273	274	6
		.0231	0.0581	273	274	9
		.0231	0.0569	273	275	NO
		.0231	0.0556	273	274	NO
		.0231	0.0545	273	274	18
		.0231	0.0545	273	274	NO
		.0231	0.0539	273	274	NO
		.0231	0.0528	273	274	NO
		.0231	0.0510	273	274	NO
		.0231	0.0651	261	261	8
		.0231	0.0628	261	261	NO
		.0231	0.0627	261	262	24
		.0231	0.0616	261	262	24
		.0231	0.0690	260	260	4
		.0231	0.0606	260	260	NO
		.0231	0.0600	262	262	NO
		.0231	0.0591	261	261	NO
		.0231	0.0568	260	260	NO

NOZZLE	FUEL	W_c (kg/s)	far	T_f ($^\circ$K)	T_3 ($^\circ$K)	TTL (sec)
SIMPLEX 3.0	JET A1/B2	.0231	0.0604	288	288	7
		.0231	0.0591	288	288	NO
		.0231	0.0578	289	288	NO
		.0231	0.0554	289	288	NO
		.0.'31	0.0527	290	288	NO
		.0232	0.0610	272	273	3
		.0232	0.0594	272	273	4
		.0232	0.0551	272	273	4
		.0232	0.0551	272	273	NO
		.0232	0.0527	272	272	NO
		.0233	0.0397	273	272	NO
		.0233	0.0330	273	272	NO
		.0231	0.0673	269	269	3
		.0231	0.0673	268	269	14
		.0231	0.0657	269	268	NO
		.0234	0.0651	264	264	NO
		.0234	0.0649	264	264	NO
		.0233	0.0718	261	261	NO
		.0233	0.9697	261	261	NO
		.0232	0.0703	256	257	13
		.0233	0.0700	255	256	19
		.0233	0.0669	255	256	NO
		.0232	0.0634	256	256	NO
		.0233	0.0595	255	256	NO
SIMPLEX 3.0	JP4	.0233	0.0381	289	288	9
		.0233	0.0362	288	289	13
		.0235	0.0354	288	290	8
		.0234	0.0331	289	289	NO
		.0234	0.0293	289	288	NO
		.0233	0.0504	273	273	3
		.0232	0.0478	273	273	4
		.0232	0.0456	274	274	5
		.0232	0.0428	274	274	6
		.0232	0.0422	273	274	1
		.0232	0.0406	273	274	NO
		.0232	0.0389	273	274	NO
		.0233	0.0360	274	274	NO
		.0233	0.0470	262	262	5
		.0233	0.0462	257	258	22
		.0232	0.0453	257	258	21
		.0233	0.0423	255	257	NO

NOZZLE	FUEL	W_c (kg/s)	far	T_f ($^\circ$K)	T_3 ($^\circ$K)	TTL (sec)
		.0232	0.0498	242	241	7
		.0230	0.0439	242	241	NO
		.0231	0.0437	241	240	17
		.0231	0.0432	242	241	NO
		.0231	0.0426	242	240	NO
SIMPLEX 3.0	JP4/B2	.0231	0.0496	289	288	10
		.0231	0.0454	289	288	8
		.0231	0.0418	288	288	NO
		.0231	0.0418	289	288	NO
		.0231	0.0522	273	270	4
		.0231	0.0503	272	274	11
		.0231	0.0491	272	271	NO
		.0231	0.0479	272	273	NO
		.0231	0.0692	261	271	13
		.0232	0.0653	261	261	18
		.0232	0.0598	261	261	11
		.0230	0.0586	261	261	NO
		.0231	0.0582	261	262	
		.0231	0.0695	257	257	24
		.0231	0.0677	257	257	12
		.0231	0.0658	255	256	NO
		.0231	0.0627	258	256	NO
		.0231	0.0584	255	256	NO
		.0231	0.0535	255	256	NO
SIMPLEX 3.0	Tar Sands L-H	.0231	0.0581	290	288	7
		.0230	0.0554	290	288	20
		.0230	0.0541	290	288	16
		.0230	0.0529	290	288	NO
		.0230	0.0487	290	288	NC
		.0230	0.0439	290	289	NO
		.0231	0.0384	290	289	NO
		.0231	0.0652	278	278	8
		.0231	0.0635	278	278	9
		.0232	0.0626	278	278	NO
		.0231	0.0669	272	274	28
		.0231	0.0650	272	274	NO
		.0231	0.0632	272	274	NO
		.0231	0.0608	272	274	NO
		.0231	0.0584	272	274	NO
		.0231	0.0565	272	274	NO
		.0231	0.0541	272	274	NO

NOZZLE	FUEL	W_c (kg/s)	far	T_f ($^\circ$K)	T_3 ($^\circ$K)	TTL (sec)
SIMPLEX 3.0	ERBS	.0232	0.0647	288	290	3
		.0231	0.0577	290	289	3
		.0231	0.0553	289	290	9
		.0232	0.0551	288	289	NO
		.0232	0.0533	288	290	12
		.0232	0.0491	289	289	NO
		.0232	0.0443	289	289	NO
		.0231	0.0661	274	273	3
		.0231	0.0646	273	273	NO
		.0231	0.0621	273	273	NO
		.0231	0.0579	272	273	NO
		.0231	0.0679	269	269	7
		.0232	0.0649	269	270	11
		.0232	0.0651	265	265	20
		.0230	0.0518	264	2b5	NO
		.0231	0.0515	264	265	NO
		.0230	0.0661	261	261	21
		.0231	0.0653	262	262	NO
SIMPLEX 3.0	JP10	.0231	0.0724	288	289	14
		.0231	0.0661	289	290	NO
		.0232	0.0658	289	289	NO
		.0232	0.05(9	289	289	NO
		.0231	0.0507	289	289	NO

APPENDIX C
Combustor Pressure Drop Data

NOZZLE	W_c (kg/s)	T_3 (°K)	P_3 (MP$_a$)	P (KP$_a$)	$\frac{P}{P_3}$ (%)	$\frac{W_c \sqrt{T_3}}{P_3}$
SIMPLEX 3.0	0.126	500	0.455	11.68	2.569	6.20
	0.182	375	0.340	25.50	7.492	10.36
	0.206	572	0.684	24.46	3.575	7.20
	0.283	617	0.904	37.11	4.106	7.79
	0.297	633	0.976	38.21	3.916	7.65
DUPLEX	0.131	499	0.461	12.36	2.791	6.38
	0.187	375	0.351	26.30	7.494	10.34
	0.204	570	0.685	24.62	3.595	7.12
	0.279	619	0.902	38.43	4.261	7.71
	0.322	632	0.971	44.38	4.571	8.33
AIRBLAST	0.122	500	0.436	11.54	2.643	6.28
	0.183	374	0.357	22.63	6.334	9.92
	0.206	569	0.695	20.65	2.970	7.07
	0.280	620	0.916	31.08	3.394	7.60
	0.282	631	0.971	30.57	3.148	7.31
VAPORIZER	0.204	571	0.691	20.57	2.976	7.07
	0.277	618	0.909	23.22	2.555	7.57
	0.307	633	0.957	36.74	3.839	8.08

APPENDIX D
Thrust Level Simulation Data

NOZZLE	FUEL	CONDITION	HC (EI)	CO (EI)	NO_x (EI)	SMOKE NUMBER	T_L-T_3 (°K)	100-η (%)
SIMPLEX	JET A1	IDLE	5.75	84.0	3.20	9	161	2.85
		T.O.	0	4.62	7.75	27	268	0.11
	JET A1/B1	IDLE	31.1	91.2	3.55	11	127	4.45
		T.O.	0	5.99	8.50	35	277	0.14
	JET A1/B2	IDLE	24.9	112.	N/A	22	137	5.20
		T.O.	0	10.4	N/A	46	315	0.24
	SHALE JP8	IDLE	N/A	N/A	2.40	4	145	2.10
		T.O.	0	4.9	8.25	28	268	0.10
	DIESEL	IDLE	26.5	118.	2.70	13	160	6.50
		T.O.	0	9.08	8.50	43	257	0.17
	ERBS-3	IDLE	41.4	105.	2.25	6	110	7.80
		T.O.	1.0	5.2	7.50	45	285	0.21
	L-H	IDLE	7.5	82.2	2.65	N/A	125	2.45
		T.O.	0	4.6	8.25	29	263	0.11
	H-M	IDLE	12.6	74.7	4.20	22	174	5.30
		T.O.	0	4.7	8.80	32	277	0.12
	L-M	IDLE	26.7	94.2	4.45	15	177	5.90
		T.O.	0	4.7	9.00	33	298	0.11
	L-L	IDLE	50.2	85.1	2.15	6	128	7.00
		T.O.	1.8	18.9	3.10	43	310	0.68
	JP4	IDLE	5.6	72.1	2.90	N/A	175	1.95
		T.O.	0	2.1	8.55	27	233	0.05
	JP4/B1	IDLE	0	107.	2.70	12	148	6.60
		T.O.	0	13.2	8.20	39	275	0.17
	JP4/B2	IDLE	50.0	100.	2.40	26	115	4.00
		T.O.	0	4.1	8.35	48	307	0.10
	JP4/204G/DF	IDLE	10.6	95.6	2.65	15	156	2.90
		T.O.	0	10.4	8.15	36	298	0.19
	JP10	IDLE	31.8	87.0	2.20	5	100	4.00
		T.O.	0	6.0	7.90	41	300	0.14
DUPLEX	JET A1	IDLE						3.005
		60%	0	2.51				
		T.O.			10.0	34	N/A	0.033
	JET A1/B2	IDLE						4.520
		60%	0	3.90				
		T.O.			9.70	36	370	0.112
	ERBS-3	IDLE						3.177
		60%	0	7.78				
		T.O.			8.10	42	301	0.102
	L-H	IDLE						2.591
		60%	0	5.41				
		T.O.			9.05	39	347	0.057

NOZZLE	FUEL	CONDITION	HC (EI)	CO (EI)	NO$_x$ (EI)	SMOKE NUMBER	T_L-T_3 (°K)	100-η (%)
DUPLEX	JP4	IDLE						2.182
		60%	0	5.70				
		T.O.			9.20	17	334	0.049
	JP4/B2	IDLE						7.409
		60%	0	6.31				
		T.O.			10.3	47	357	0.095
AIRBLAST	JET A1	IDLE						5.641
		60%	0	6.11				
		T.O.			9.45	7	307	0.041
	JET A1/B2	IDLE						6.883
		60%	0.6	10.3				
		T.O.			10.0	15	316	0.153
	ERBS-3	IDLE						10.05
		60%	1.4	5.47				
		T.O.			11.0	7	291	0.057
	TAR SANDS L-H	30%						0.800
		60%	0	4.61				
		T.O.			9.50	5	289	0.060
	JP4	30%						0.471
		60%	0	3.63				
		T.O.			7.20	2	292	0.043
	JP4/B2	30%						0.751
		60%	0	9.52				
		T.O.			9.30	6	297	0.091
VAPORIZER	JET A1	60%	2.91	21.07				0.754
		T.O.			7.60	1	255	0.077
	JET A1/B2	60%	5.17	38.71				1.377
		T.O.			7.35	3	270	0.545
	ERBS-3	60%	4.01	33.38				1.148
		T.O.			7.80	2	217	0.125
	TAR SANDS L-H	60%	2.48	23.68				0.787
		T.O.			6.50	2	289	0.258
	JP4	60%	1.74	22.85				0.097
		T.O.			6.70	1	259	0.119
	JP4/B2	60%	N.A.	N.A.				1.999
		T.O.			7.		2.9	

APPENDIX E
Power Level Simulation Data

NOZZLE	FUEL	CONDITION	HC (EI)	CO (EI)	NO_x (EI)	SMOKE NUMBER	T_L-T_3 (°K)	$100-\eta$ (%)
SIMPLEX	JET A1	IDLE	5.97	91.70	2.40	25	141	2.62
		T.O.	0.36	12.64	6.80	47	258	0.352
	JET A1/B1	IDLE	17.34	79.72	3.20	24	166	3.03
		T.O.	0	9.80	6.90	49	241	0.205
	JET A1/B2	IDLE	18.90	90.72	2.05	28	129	3.45
		T.O.	0	6.26	6.75	50	305	0.149
	JP8 SHALE	IDLE	7.01	78.64	2.45	N/A	120	2.35
		T.O.	0	5.77	8.00	N/A	288	0.125
	DIESEL	IDLE	42.18	92.28	2.78	9	146	8.00
		T.O.	0	3.60	8.50	28	308	0.118
	ERBS-3	IDLE	34.64	98.62	3.50	9	62	5.30
		T.O.	0	11.55	9.55	39	252	0.280
	L-H	IDLE	12.53	73.42	2.40	N/A	91	2.80
		T.O.	0	4.11	7.50	N/A	297	0.105
	H-M	IDLE	29.73	65.11	3.40	18	104	5.20
		T.O.	0	7.21	9.35	35	273	0.168
	L-M	IDLE	27.78	87.40	3.55	13	164	4.30
		T.O.	0.37	4.00	8.50	27	272	0.130
	L-L	IDLE	28.50	74.65	2.75	9	124	4.00
		T.O.	1.34	7.21	8.40	23	305	0.278
	JP4	IDLE	6.69	68.18	3.40	7	182	2.15
		T.O.	0	4.55	7.70	28	302	0.113
	JP4/B1	IDLE	14.02	90.81	3.25	23	166	3.30
		T.O.	0	9.29	8.35	N/A	281	0.230
	JP4/B2	IDLE	9.77	86.41	1.85	28	155	2.85
		T.O.	0.59	6.29	7.85	34	314	0.220
	JP4/2040/DF	IDLE	29.24	86.9	2.30	14	139	2.60
		T.O.F	0	7.29	6.95	39	289	0.180
	JP10	IDLE	33.06	80.39	1.80	11	N/A	4.80
		T.O.	0	6.26	7.55	28	294	0.145

NOZZLE	FUEL	P_3 (MP$_a$)	far	Q_{rad} (MJ/m^{2}hr)	CO (EI)	NO$_x$ (EI)	SMOKE NUMBER	T_1-T_3 (°K)	100-η (%)
SIMPLEX	JET A1	.480	.0184		20.3	5.0	3.6	250	.471
		.480	.0206	391	19.0	5.1	2.2	241	.441
		.491	.0228		19.1	4.6	2.4	146	.444
		.605	.0206		11.0	5.7	5.9	284	.256
		1.01	.0207	1272	4.1	9.0	25.9	338	.096
		1.61	.0213		2.7	9.3	20.3	344	.064
	JET A1/B1	.489	.0182		21.6	5.1	9.3	275	.502
		.489	.0207	549	18.3	4.9	11.1	264	.426
		.491	.0225		16.7	4.7	13.0	272	.389
		.601	.0210		12.3	5.8	22.1	297	.285
		1.01	.0210	1450	5.6	7.6	42.8	315	.129
		1.61	.0209		2.9	9.5	30.8	343	.067
	JET A1/B2	.499	.1078		26.0	5.8	17.0	235	.712
		.499	.0203	603	24.6	4.8	24.8	236	.572
		.496	.0222		22.6	4.7	30.3	247	.524
		.617	.0205		14.9	5.9	35.5	268	.347
		1.04	.0205	1459	6.8	7.3	32.5	292	.158
		1.64	.0200		3.4	9.6	37.1	307	.080
	SHALE JP8	.501	.0180		17.3	5.1	7.1	257	.402
		.492	.0207	344	16.4	4.9	2.8	251	.382
		.496	.0224		13.7	4.9	2.8	269	.320
		.601	.0204		9.4	6.0	13.8	298	.218
		1.02	.0204	1312	5.3	7.4	14.2	293	.122
		1.62	.0203		2.6	8.3	30.3	368	.060
	DIESEL	.482	.0185		8.7	5.0	6.4	290	.203
		.506	.0205	376	11.7	5.1	9.7	267	.271
		.506	.0222		12.9	4.9	4.6	265	.300
		.599	.0209		7.6	5.6	7.6	297	.176
		1.02	.0208	1354	2.8	8.6	27.6	334	.065
		1.63	.0207		3.4	9.5	37.5	350	.079
	ERBS-3	.483	.0181		31.4	4.6	9.9	208	.730
		.487	.0206	453	18.2	4.3	10.7	246	.423
		.497	.0225		15.2	4.3	14.1	253	.353
		.604	.0209		9.7	5.3	26.6	280	.226
		1.02	.0207	1496	6.1	7.2	55.9	308	.142
		1.62	.0204		2.9	10.9	49.6	340	.067
	L-H	.481	.0183		16.6	5.1	0.7	291	.387
		.500	.0207	454	15.1	5.0	9.3	301	.351
		.512	.0225		14.0	5.3	4.5	295	.325
		.619	.0205		9.6	6.4	18.2	316	.223

NOZZLE	FUEL	P_3 (MP$_a$)	far	Q_{rad} (MJ/m^{2}hr)	CO (EI)	NO$_x$ (EI)	SMOKE NUMBER	T_L-T_3 (°K)	100-η (%)
SIMPLEX	L-H	.998	.0212	1446	4.2	8.6	34.5	358	.098
		1.62	.0206		2.4	12.7	38.0	416	.005
	H-M	.492	.0185		20.6	5.2	28.9	297	.479
		.496	.0206	462	17.0	4.8	9.4	299	.396
		.504	.0240		14.4	6.3	6.3	304	.335
		.606	.0210		9.9	8.1	16.7	306	.231
		1.03	.0214	1649	4.3	8.1	43.2	364	.101
		1.64	.0216		2.7	9.8	37.9	391	.063
	L-M	.509	.0179		17.8	5.4	7.9	277	.413
		.495	.0206	513	18.2	4.7	8.1	275	.424
		.498	.0280		13.9	4.8	12.7	300	.323
		.612	.0206		11.6	5.5	17.8	306	.268
		1.03	.0208	1631	6.0	6.4	35.9	317	.138
		1.62	.0216		2.2	10.5	43.7	398	.051
	L-L	.490	.0183		21.2	5.6	13.9	285	.494
		.500	.0206	500	22.6	5.2	11.3	272	.524
		.494	.0227		17.2	5.0	14.9	287	.401
		.612	.0209		11.8	6.5	26.6	302	.275
		1.02	.0212	1513	5.7	9.6	33.1	334	.132
		1.64	.0216		3.3	9.0	31.2	336	.076
	JP4	.511	.0184		19.5	4.8	0	175	.454
		.487	.0210	193	19.4	4.7	0.7	170	.451
		.505	.0226		17.0	4.8	0	160	.396
		.613	.0214		11.4	5.7	0.9	191	.264
		1.02	.0217	947	4.2	7.6	13.0	231	.098
		1.65	.0213		2.5	9.1	35.2	246	.101
	JP4/B1	.512	.0176		21.0	4.4	10.5	205	.488
		.491	.0204	432	19.0	4.2	5.5	210	.442
		.496	.0223		14.0	4.3	1.4	244	.326
		.603	.0203		10.2	5.8	3.9	248	.236
		1.02	.0207	1280	11.5	6.5	52.9	318	.267
		1.62	.0203		3.5	7.7	46.9	299	.082
	JP4/B2	.492	.0187		20.4	5.4	28.8	282	.474
		.503	.0104	624	15.8	5.1	37.8	305	.366
		.506	.0227		10.6	5.3	36.3	299	.247
		.616	.0211		9.9	6.2	35.7	320	.229
		1.04	.0218	1586	3.6	7.8	47.5	332	.084
		1.62	.0216		1.8	10.2	30.4	352	.042
	JP4/2040/DF	.509	.0183		15.2	4.8	6.4	286	.353
		.491	.0208	442	13.6	4.6	8.5	269	.316
		.502	.0228		11.5	4.8	10.1	263	.267
		.612	.0211		10.1	5.7	24.8	292	.235

NOZZLE	FUEL	P_3 (MPa)	far	Q_{rad} (MJ/m²hr)	CO (EI)	NO_x (EI)	SMOKE NUMBER	T_L-T_3 (°K)	$100-\eta$ (%)
SIMPLEX	JP4/2040/DF	1.03	.0208	1320	4.0	8.2	34.9	352	.093
		1.61	.0208		2.6	12.7	18.2	400	.061
	JP10	.483	.0182		21.9	5.6	17.7	240	.510
		.496	.0205	386	25.2	5.3	14.7	242	.587
		.493	.0226		20.0	5.3	16.5	255	.465
		.589	.0228		13.2	6.6	28.4	263	.307
		.996	.0209	1475	5.7	8.5	36.1	308	.132
		1.60	.0212		2.9	9.9	30.4	358	.068
DUPLEX	JET A1	.485	.0182		19.7	5.1	2.0	N/A	.458
		.492	.0206		13.2	5.6	0.8	290	.306
		.493	.0225		14.5	5.3	2.0	265	.337
		.610	.0206		9.1	6.5	5.3	268	.212
		1.02	.0209		3.6	8.5	?8.0	304	.085
		1.62	.0209		2.2	10.1	24.8	342	.051
	JET A1/B2	.503	.0179		23.1	4.6	20.4	N/A	.537
		.503	.0204		20.3	4.7	17.8	N/A	.471
		.503	.0221		18.8	4.6	20.6	N/A	.437
		.620	.0203		12.9	5.3	37.5	275	.298
		1.03	.0207		5.0	7.7	35.9	320	.116
		1.65	.0215		2.7	8.9	33.3	374	.062
	ERBS-3	.494	.0181		13.0	5.9	6.3	249	.301
		.498	.0207		10.3	5.9	5.9	256	.239
		.498	.0226		9.4	5.6	5.9	271	.219
		.618	.0205		8.4	7.3	10.7	313	.195
		1.02	.0213		2.8	10.2	23.4	381	.066
		1.62	.0215		1.6	12.1	40.8	372	.038
	TAR SANDS L-H	.501	.0179		7.4	6.5	34.7	275	.171
		.487	.0208		4.2	8.2	19.9	233	.096
		.497	.0221		2.2	10.9	17.9	221	.052
		.611	.0210		14.0	5.3	11.8	331	.325
		1.01	.0215		13.9	4.7	20.1	369	.323
		1.58	.0226		10.9	5.1	40.2	380	.254
	JP4	.495	.0176		N/A	N/A	13.9	236	N/A
		.495	.0200		N/A	N/A	10.8	246	N/A
		.492	.0238		16.4	3.8	4.3	269	.381
		.600	.0218		8.3	5.2	2.8	299	.194
		1.03	.0220		3.3	7.0	19.9	384	.077
		1.62	.0221		3.2	7.2	25.6	419	.074
	JP4/B2	.510	.0185		15.9	5.9	17.5	353	.370
		.497	.0210		14.1	5.1	9.3	324	.327
		.509	.0231		10 5	5.0	19.9	294	.246
		.613	.0214		7.3	6.8	11.6	322	.170

NOZZLE	FUEL	P_3 (MP$_a$)	far	Q_{rad} (MJ/m^{2}hr)	CO (EI)	NO$_x$ (EI)	SMOKE NUMBER	T_L-T_3 (°K)	100-η (%)
DUPLEX	JP4/B2	1.03	.0214		4.3	8.1	48.2	400	.099
		1.63	.0216		2.6	9.8	25.3	418	.061
AIRBLAST	JET A1	.492	.0180		26.7	4.6	5.7	256	.619
		.492	.0205		20.5	4.7	3.2	250	.475
		.491	.0226		18.6	4.6	2.6	245	.432
		.605	.0206		11.8	5.8	2.8	254	.273
		1.02	.0208		3.8	8.2	10.7	278	.089
		1.64	.0209		1.6	10.7	18.2	343	.036
	JET A1/B2	.503	.0180		23.1	4.6	9.8	247	.537
		.503	.0202		20.3	4.7	6.0	266	.471
		.503	.0220		18.8	4.6	8.4	289	.437
		.620	.0205		12.9	5.3	12.0	300	.298
		1.03	.0208		5.1	7.7	18.3	312	.116
		1.65	.0203		2.6	8.9	24.1	404	.062
	ERBS-3	.497	.0179		25.6	5.4	5.7	217	.595
		.492	.0202		19.8	5.8	6.5	235	.459
		.490	.0220		12.5	5.7	4.9	266	.289
		.601	.0205		8.2	6.6	5.5	278	.191
		1.01	.0204		2.6	9.1	16.5	296	.061
		1.63	.0213		1.2	11.3	30.9	353	.029
	TAR SANDS	.601	.0212		6.4	6.4	3.7	260	.148
	L-H	1.01	.0211		2.1	10.3	6.2	302	.048
		1.64	.0214		1.5	12.5	20.5	400	.034
	JP4	.495	.0185		27.3	4.4	0	203	.635
		.492	.0213		N/A	N/A	1.2	229	N/A
		.498	.0232		21.1	4.5	0	240	.489
		.603	.0218		11.2	5.5	0.5	247	.261
		1.01	.0216		3.3	8.5	4.2	301	.076
		1.62	.0219		1.6	11.1	15.3	338	.036
	JP4/32	.509	.0135		17.6	6.2	7.6	268	.409
		.495	.0214		15.7	5.5	5.9	279	.365
		.495	.0234		12.9	5.6	5.2	279	.300
		.606	.0216		6.8	6.8	6.7	296	.158
		.999	.0217		2.6	12.1	10.2	407	.061
		1.61	.0218		1.9	14.6	18.1	436	.044
VAPORIZER	JET A1	.492	.0182		124.	2.1	1.4	150	7.24
		.481	.0207		116.	2.5	0.8	143	5.54
		.489	.0226		103	2.7	0.2	141	4.14
		.599	.0207		56.3	3.8	1.4	205	2.10
		.999	.0214		7.8	7.3	0	292	.182
		1.65	.0227		2.4	11.2	4.8	275	.056

NOZZLE	FUEL	P_3 (MPa)	far	Q_{rad} (MJ/m²hr)	CO (EI)	NO_x (EI)	SMOKE NUMBER	T_1-T_3 (°K)	$100-\eta$ (%)
VAPORIZER	JET A1/B2	.488	.0179		163	1.7	4.5	142	11.47
		.498	.0206		123	2.2	2.6	170	6.22
		.502	.0224		108	2.7	2.0	164	4.55
		.615	.0204		53.0	3.8	2.2	229	1.87
		1.02	.0207		9.3	7.2	2.8	314	.259
		1.62	.0195		4.2	10.5	6.2	260	.099
	EkbS-3	.497	.0178		15.6	2.1	1.4	N/A	.417
		.487	.0206		13.4	2.3	1.8	N/A	.345
		.490	.0226		12.0	2.9	1.6	N/A	.303
		.597	.0209		N/A	N/A	1.8	N/A	N/A
		1.01	.0208		9.9	7.1	1.6	232	.238
		1.63	.0208		2.6	10.1	6.9	246	.059
	TAR SANDS L-H	.498	.0179		144	1.2	4.4	144	9.83
		.495	.0205		114	2.0	1.2	162	5.61
		.499	.0226		93.3	2.6	1.4	183	4.16
		.619	.0209		50.7	3.4	1.0	238	1.81
		1.02	.0213		5.3	7.1	0.6	263	.124
		1.58	.0206		1.5	9.2	0.6	267	.073
	JP4	.495	.0175		72.6	1.7	0.4	140	3.51
		.499	.0212		62.4	2.9	0.6	155	1.80
		.502	.0230		62.8	3.3	0	167	1.78
		.606	.0218		23.7	4.7	0	243	.591
		1.02	.0217		7.4	7.3	0.4	267	.172
		1.63	.0217		2.8	10.1	1.3	256	.066
	JP4/B2	.495	.0186		122.	1.7	1.8	151	6.00
		.516	.0207		76.4	2.4	2.2	189	2.61
		.502	.0235		67.8	2.9	2.4	182	2.02
		.613*	.0215		14.1	4.1	0.8	275	.363
		1.02*	.0216		3.3	7.7	1.2	374	.095
		1.63*	.0210		0.2	17.4	2.2	400	.005

*Suspect conditions (T_3 not set properly).